

The PADMET Platform – Pharmacokinetic Characterization of Carbohydrate Mimetics

Inauguraldissertation

zur

Erlangung der Würde eines Doktors der Philosophie
vorgelegt der
Philosophisch-Naturwissenschaftlichen Fakultät
der Universität Basel

von

Matthias Beat Wittwer

Aus Trub, BE, Schweiz

Basel, 2012

Genehmigt von der Philosophisch-Naturwissenschaftlichen Fakultät auf Antrag von

Prof. Dr. Beat Ernst, Institute of Molecular Pharmacy, University of Basel

Dr. Manfred Kansy, F. Hoffmann-La Roche, Basel

Basel, den 21. September 2010

Prof. Dr. Martin Spiess

Dekan

Acknowledgements

Acknowledgements

This thesis would not have been possible without the support and help of many people to whom I am greatly thankful.

First, I would like to thank Prof. Beat Ernst for having had the courage to initiate this project and entering into the field of pharmacokinetics that was new to his laboratory. I am grateful that he entrusted me with the buildup of the PADMET platform and for his support and encouragement during my thesis. Several people from the laboratory deserve special thanks including Dr. Brian Cutting for familiarizing me with the realm of NMR, Dr. Daniela Stokmaier for introducing me to the art of cell culture, Dr. Martin Smiesko for his advice and collaboration with respect to molecular modeling, and Dr. Steven Knecht for helpful discussions and support concerning the HPLC and other analytical techniques. Furthermore, I am thankful to Dr. Jonas Egger and Dr. Stefanie Mesch for answering chemistry-related questions, synthesizing molecules for testing, and for teaching me how to do rock climbing. Many thanks go to my master students Erich Gubler and Jacqueline Bezençon for their invaluable help and enthusiasm in creating the PADMET platform. Moreover, I would like to express my gratitude to Simon Kleeb for having been willing to take over the project and continue it, for countless fruitful discussions, interesting questions, criticism, good solutions, and for his company in the laboratory as well as in the opera. I wish Simon and Jacqueline all the best and many interesting discoveries on the PADMET platform. Finally, I would like to thank all other members, past and present, of the Institute of Molecular Pharmacy and the Institute of Molecular Modeling for their help, friendship, interesting discussions, splendid coffee breaks, collaborative efforts, and for keeping me going.

I am indebted to Dr. Manfred Kansy for his constant help in terms of both knowledge and materials, for giving me access to his laboratory, for many valuable contacts, and for serving as co-referee on my thesis-committee. I am grateful to many people from Dr. Kansy's group, especially Frank Senner and Severin Wendelspiess for their help with the PAMPA and CMC assays, Björn Wagner for pK_a and logD determinations and everything associated with it, and Stefanie Bendels and Holger Fischer for fruitful discussions and important hints. At Roche I am furthermore thankful to Christoph Funk, Renée Portmann, Volkmar Starke, and Florian Klammers for their help with transporter-, metabolism, and PPB-associated questions and assays.

Acknowledgements

Moreover, I am grateful to Prof. G. Imanidis and Dr. Marcel Schneider for providing the Caco-2 cells and their knowledge associated with this assay. Without their help this project would have taken longer to complete.

Finally, I would like to thank four people in particular: My father for his constant support and understanding, my mother for all her warmth and nice words, and my brother for being my best friend. And finally, Morena for all the happiness and joy she has brought into my life and for sharing many great adventures, big and small.

Preface

Preface

The work described in this thesis was conducted from May 2007 until September 2010 at the Institute of Molecular Pharmacy at the University of Basel under the guidance of Prof. Dr. Beat Ernst.

Parts of this thesis have already been published in or submitted to peer reviewed journals. These manuscripts are included in the respective paragraphs. References in these sections are independent from the rest of this PhD thesis. Prior to each manuscript, the contribution of the author of this thesis to the respective section is mentioned.

Manuscripts published in or submitted to peer-reviewed journals:

- Mesch, S.; Moser, D.; Strasser, D. S.; Kelm, A.; Cutting, B.; Rossato, G.; Vedani, A.; Koliwer-Brandl, H.; Wittwer, M.; Rabbani, S.; Schwardt, O.; Kelm, S.; Ernst, B. Low Molecular Weight Antagonists of the Myelin-Associated Glycoprotein: Synthesis, Docking, and Biological Evaluation *J. Med. Chem.* **2010**, *53*, 1597-1615.
- Klein, T.; Abgottspon, D.; Wittwer, M.; Rabbani, S.; Herold, J.; Jiang, X.; Kleeb, S.; Lüthi, C.; Scharenberg, M.; Bezençon, J.; Gubler, E.; Pang, L.; Smiesko, M.; Cutting, B.; Schwardt, O.; Ernst, B. FimH Antagonists for the Oral Treatment of Urinary Tract Infections: From Design and Synthesis to *In Vitro* and *In Vivo* Evaluation *J. Med. Chem.* **2010**, *53*, 8627-8641.
- Wittwer, M.; Kleeb, S.; Bezençon, J.; Gubler, E.; Cutting, B.; Ernst, B. The PADMET Platform – Early Pharmacokinetic Characterization in *Academia Bioorg. Med. Chem., in preparation.*
- Wittwer, M.; Bezençon, J.; Cutting, B.; Wagner, B.; Kansy, M.; Ernst, B. pK_a determination by ¹H-NMR spectroscopy – An old methodology revisited *ChemMedChem, in preparation.*
- Wittwer, M.; Smiesko, M.; Ernst, B. Sweet previsions: Modeling the permeation of carbohydrate mimetics *J. Med. Chem., in preparation.*

Preface

Parts of this thesis were presented at conferences:

Oral presentation

- Wittwer, M.; Mesch, S.; Gubler, E.; Cutting, B.; Ernst, B. The PADMET Platform. *Annual Research Meeting of the Department of Pharmaceutical Sciences*, February 13th **2009**, Basel, Switzerland

Posters

- Wittwer, M.; Mesch, S.; Gubler, E.; Cutting, B.; Ernst, B. The PADMET Platform – Pharmacokinetic Profiling of Glycomimetics. *logP2009 Symposium*, **2009**, Zurich, Switzerland.
- Wittwer, M.; Bezençon, J.; Cutting, B.; Wagner, B.; Kansy, M.; Ernst, B. pK_a determination by ¹H-NMR spectroscopy – An old methodology revisited. *Swiss Pharma Science Day*, September 9th **2010**, Bern, Switzerland.
- Wittwer, M.; Kleeb, S.; Bezençon, J.; Gubler, E.; Cutting, B.; Ernst, B. PADMET Platform: Pharmacokinetic Profiling of Glycomimetics. *Swiss Pharma Science Day*, September 9th **2010**, Bern, Switzerland.
- Wittwer, M.; Smiesko, M.; Ernst, B. Sweet Previsions: Modeling the Permeation of Carbohydrate Antagonists. *Fall Meeting of the Swiss Chemical Society*, September 16th **2010**, Zurich, Switzerland.

Abstract

Abstract

More than two decades ago it was realized that drug discovery and development strategies focusing exclusively on affinity enhancement and potency are unsuccessful. Instead, simultaneous optimization of pharmacodynamic and pharmacokinetic properties has been proposed and implemented. As a result, new assays for pharmacokinetic characterization were required and existing assays were modified to fulfill high-throughput requirements. These assays, typically used at early stages of drug discovery and development, were modified and employed during this doctoral thesis to determine pharmacokinetic parameters of carbohydrate mimetics. The project was termed PADMET platform, with PADMET standing for **p**hysicochemical properties, **a**bsorption, **d**istribution, **m**etabolism, **e**limination, and **t**oxicity. The aims of the platform were on the one hand the elucidation of the pharmacokinetic behavior of carbohydrate mimetics and on the other hand the development of such compounds with improved drug-likeness.

While building up the PADMET platform, the need for an inexpensive and uncomplicated pK_a determination method became apparent. A methodology based on $^1\text{H-NMR}$ spectroscopy was chosen for this purpose and scope and limitations of this approach were explored. An excellent correlation to reference data was achieved.

The components of the platform were used to characterize 93 carbohydrate mimetics regarding several pharmacokinetic parameters. The results were used in different projects of which two are discussed in detail in this thesis. First, one of the primary goals of the FimH antagonist project was the synthesis of orally available compounds with fast renal excretion. By the aid of various assays, molecules with a promising profile could be identified. Indeed, *in vivo* mouse studies confirmed the intended properties. The permeability values gathered during this project were correlated to calculated descriptors and to experimental lipophilicity values in order to identify the driving force of the permeation of carbohydrate mimetics. Calculated lipophilicity values as single descriptor proved to be superior to other descriptors and to combinations thereof.

Second, during the MAG project compounds with maintained local concentrations in the cerebrospinal fluid were envisioned. Permeation through artificial blood-brain barrier and stability in artificial cerebrospinal fluid were thus determined.

Abbreviations

Abbreviations

| | |
|--------------|---|
| aCSF | artificial cerebrospinal fluid |
| ADME | absorption, distribution, metabolism, elimination |
| AUC | area under the curve |
| BBB | blood-brain barrier |
| BBB-PAMPA | blood-brain barrier parallel artificial membrane permeation assay |
| Caco-2 cells | Caucasian colon adenocarcinoma cells |
| CE | capillary electrophoresis |
| CES | carboxylesterase |
| CFU | colony forming units |
| CHO cells | Chinese hamster ovary cells |
| ClAc | 2-chloroacetyl |
| CMC | critical micelle concentration |
| CNS | central nervous system |
| CRD | carbohydrate recognition domain |
| CSF | cerebrospinal fluid |
| CYP | cytochrome P450 |
| D | distribution coefficient |
| DCE | 1,2-dichloroethane |
| DCM | dichloromethane |
| DMAP | 4-dimethylamino-pyridine |
| DMF | <i>N,N</i> -dimethylformamide |
| DMSO | dimethyl sulfoxide |
| DC-SIGN | dendritic cell-specific intercellular adhesion molecule-3-grabbing non-integrin |
| DMEM | Dulbecco's Modified Eagle's Medium |
| DMSO | dimethyl sulfoxide |
| EPD | electropotentiometric determination |
| FAc | 2-fluoroacetyl |
| f_b | fraction bound |
| FBS | fetal bovine serum |
| GADD45a | growth arrest and DNA damage gene |
| Gal | galactose |

Abbreviations

| | |
|------------------|---|
| GalNAc | <i>N</i> -acetylglucosamine |
| GFP | green fluorescent protein |
| GPE | guinea pig erythrocytes |
| HB | hydrogen bond |
| hERG | human ether-a-go-go-related gene |
| HPLC | high-performance liquid chromatography |
| IAM | immobilized artificial membrane |
| IC ₅₀ | half maximal inhibitory concentration |
| IgG | immunoglobulin G |
| <i>i</i> PrOH | 2-propanol |
| i.v. | intravenous |
| K _D | dissociation constant |
| k _{off} | dissociation rate constant |
| k _{on} | association rate constant |
| LC-MS | liquid chromatography-mass spectroscopy |
| LDH | lactate dehydrogenase |
| MAG | myelin-associated glycoprotein |
| Man | mannose |
| MBP | mannose-binding protein |
| MDCK | Madin-Darby canine kidney cells |
| MeCN | acetonitrile |
| MOG | myelin oligodendrocyte glycoprotein |
| MS | mass spectrometry or molecular sieve |
| MTT | 3-[4,5-dimethylthiazol-2-yl]-2,5-diphenyltetrazolium bromide |
| Neu5Ac | <i>N</i> -acetylneuraminic acid |
| NGFR | nerve growth factor receptor |
| NgR | Nogo receptor |
| NIS | <i>N</i> -iodosuccinimide |
| NMR | nuclear magnetic resonance |
| nosyl | 2-nitrobenzylsulfonyl |
| OAT | organic anion transporter |
| P | partitioning coefficient |
| PADMET | physicochemical properties, absorption, distribution, metabolism, elimination, toxicity |

Abbreviations

| | |
|--------------|--|
| PAMPA | parallel artificial membrane permeation assay |
| P_{app} | apparent permeability |
| PDB | Protein Data Bank |
| P_e | effective permeation |
| PEPT | peptide transporter |
| P-gp | P-glycoprotein |
| PK | pharmacokinetics |
| pK_a | negative common logarithm of the dissociation constant K_a |
| PNS | peripheral nervous system |
| p.o. | peroral |
| PPB | plasma protein binding |
| PSA | polar surface area |
| <i>p</i> -Ts | <i>p</i> -tolylsulfonyl |
| QSAR | quantitative structure-activity relationships |
| QSPR | quantitative structure-property relationships |
| RhoA-ROCK | Rho-associated, coiled coil-containing protein kinase |
| RP | reversed phase |
| RTN4 | reticulon 4 |
| S | solubility |
| SAR | structure-activity relationships |
| SASA | solvent accessible surface area |
| SGA | spectral gradient analysis |
| SGAG | sulphated glycosaminoglycans |
| sGF | simulated gastric fluid |
| sIF | simulated intestinal fluid |
| SPR | structure-property relationships |
| STD NMR | saturation transfer difference NMR |
| TEER | transepithelial resistance |
| TfOH | trifluoroacetic acid |
| THF | tetrahydrofurane |
| TMS | trimethylsilyl |
| trNOE | transfer nuclear Overhauser enhancement |
| UDPGT | uridine diphosphate-glucuronosyltransferase |
| UPEC | uropathogenic <i>E. coli</i> |

Abbreviations

| | |
|--------|--|
| UTI | urinary tract infection |
| UV | ultraviolet |
| VCCLAB | virtual computational chemistry laboratory |

Table of contents

Table of contents

| | | |
|-------|---|-----|
| 1 | Introduction..... | 11 |
| 1.1 | Pharmacokinetic characterization today | 11 |
| 1.1.1 | Physicochemical parameters..... | 11 |
| 1.1.2 | Absorption | 13 |
| 1.1.3 | Distribution..... | 14 |
| 1.1.4 | Metabolism | 15 |
| 1.1.5 | Elimination | 16 |
| 1.1.6 | Toxicity..... | 18 |
| 1.1.7 | Status quo and future perspectives..... | 19 |
| 1.2 | Carbohydrates as drug targets | 20 |
| 1.2.1 | Introduction to carbohydrates in biology and as drug target..... | 20 |
| 1.2.2 | C-type lectins as drug targets..... | 22 |
| 1.2.3 | I-type lectins as drug target | 23 |
| 1.2.4 | Bacterial and viral lectins as drug targets..... | 23 |
| 1.2.5 | Future perspectives..... | 25 |
| 1.3 | Carbohydrate antagonists and pharmacokinetics | 26 |
| 1.3.1 | General considerations | 26 |
| 1.3.2 | Examples of successful pharmacokinetic amelioration of carbohydrates..... | 27 |
| 1.4 | Aims of this thesis | 27 |
| 2 | Methods and assays | 29 |
| 2.1 | The PADMET platform – an overview..... | 29 |
| 2.2 | One method in detail: pK_a determination by NMR | 48 |
| 3 | Results and discussion | 61 |
| 3.1 | Pharmacokinetic properties of FimH antagonists with biphenyl-moiety | 61 |
| 3.2 | Factors influencing the permeation properties of carbohydrate mimetics..... | 76 |
| 3.3 | Pharmacokinetic behavior of MAG antagonists..... | 93 |
| 4 | Summary and outlook..... | 113 |
| 5 | References..... | 120 |

1.1 Pharmacokinetic characterization today

1 Introduction

1.1 Pharmacokinetic characterization today

Initially, the focus of the drug discovery and development process was primarily set on increasing affinity and establishing structure-activity relationships (SAR).¹ However, it was realized that this strategy did not yield the necessary success, since many compounds that showed promising *in vitro*-results exhibited lacking *in vivo*-activity. When looking at the underlying cause, pharmacokinetic (PK) liabilities were suspected to be responsible for 39% of failures in phase I clinical trials.² This high number, however, has often been misinterpreted, since the data set used in this study comprised a high percentage of antibiotics. With the revised data set only, 7 percent of failures were due to problematic PK behavior thus being only the fourth most important cause after lacking efficacy, animal toxicity, and adverse effects in man.³ Nevertheless, the stage was set for a new approach that focused not only on SAR but also on structure-properties relationships (SPR).⁴ As a consequence, a wealth of new experiments were implemented and combined with activity assays during early stages of drug discovery and development.⁵ Therefore, promising candidates for clinical testing could be identified that not only showed high activity at the target site but also reached it unaltered, within the intended time, and at sufficient concentrations. Today, besides various methodologies assessing absorption, distribution, metabolism, and excretion (ADME) properties, compounds are also characterized with respect to their physicochemical parameters which are often underlying descriptors for the other processes. Furthermore, toxicity is a key issue for successful drug discovery and development and is hence addressed already at early stages. In the following section, the most common parameters and the corresponding *in vitro* assays are briefly described. An excellent overview of these concepts can be gained by reading Kerns and Di⁶ who are presenting additional information concerning *in silico* and *in vivo* approaches.

1.1.1 Physicochemical parameters

pK_a: The negative logarithm of the dissociation constant (pK_a) of an acid or base describes at which pH a compound reaches its equilibrium between ionized and unionized form. For many ADME parameters this information is of crucial importance, since they can vary considerably

1 Introduction

depending on which protonation state is predominant. Absorption, plasma protein binding, and excretion, amongst others, are known to be constrained by the pK_a value.^{6,7}

The most common determination methods include spectral gradient analysis (SGA) based on changes of the UV-spectrum upon ionization,⁸ potentiometric titration assessing the pH-change after adding acid or base,⁹ and capillary electrophoresis measuring the migration time through a capillary with different pH-buffers as eluent.^{10, 11} Furthermore, NMR-based approaches can be utilized.¹²⁻¹⁴

logP/logD: Lipophilicity has been used for many years as an easily accessible surrogate marker for various biological processes including membrane permeation, plasma protein binding, and *in vivo* pharmacological and toxic effects. The field has been comprehensively summarized by Waring.¹⁵ Lipophilicity is commonly assessed as partitioning (logP) or distribution coefficient (logD). The first describes the ratio of the concentrations of the uncharged form of a compound in two immiscible solvents (usually octanol and water), the latter the ratio of summarized concentrations of uncharged and charged forms in the corresponding phases. logD thus depends on the $pK_a(s)$ of a compound. The gold standard for determination is the so-called shake-flask approach where the compound of interest is dissolved in buffer followed by the addition of octanol, then the mixture is shaken. After separation of the two phases, concentrations are assessed and the coefficient is calculated.^{16, 17} Other commonly used determination methods include reversed-phase HPLC,¹⁸⁻²¹ capillary electrophoresis,²² and pH-metric approaches.²³

Solubility: Solubility is a key property, since low values might falsify assay results and oral availability might be seriously hampered.^{24, 25} Two different solubility definitions need to be distinguished, namely thermodynamic and kinetic solubility. The first is the solubility of a compound in buffered solution and is usually determined by the shake-flask procedure. The buffer is saturated with analyte and the solution is shaken. Then, the suspension is allowed to reach equilibrium between dissolved and precipitated compound. After filtration the concentration is determined.^{6, 26} Another option is the determination by potentiometric titration.²⁷ Unlike the shake flask procedure, this approach requires an ionizable center in the molecule of interest. Thermodynamic solubility is mostly relevant for formulation and oral application studies. In contrast, kinetic solubility is measured starting from a DMSO stock solution. Besides the already mentioned pH-metric approach, that can also be applied for the determination of the kinetic solubility,²⁷ three analytical methods are commonly used. First,

1.1 Pharmacokinetic characterization today

the UV method developed by Avdeef that measures the concentration of a compound after filtration against a single point standard.²⁸ The compound addition as DMSO stock solution and concentration determination by UV-spectroscopy yields high-throughput compatibility. Second, nephelometric solubility determination can be used.²⁹ Hereby, a serial dilution in buffer with constant DMSO concentration is performed and precipitation is detected by the scattering of a laser beam. Third, a turbidimetric approach has been described where constant amounts of DMSO stock solution are sequentially added to a stirred buffer solution in a cuvette.²⁴ Upon precipitation, a diminished UV-transmission is observed. The results are of relevance for *in vitro* assays, since they are often based on compounds dissolved in DMSO.

Critical micelle concentration (CMC): The CMC can be used for the prediction of ADME parameters (e.g., blood-brain barrier permeation)³⁰⁻³² and toxicological effects (most prominently phospholipidosis)³³ as well as for the explanation of unexpected assay results. In the latter case, when micelles are formed the actual free concentration is lower than anticipated leading to a right-shift of the concentration-effect curve. Furthermore, micelle formation is of importance for formulation development.^{34, 35} Determination methods include direct (via the surface tension)³⁶⁻⁴⁰ and indirect approaches. The latter are based on UV-⁴¹ or fluorescence-spectroscopy,⁴² NMR,^{43, 44} isothermal calorimetry (ITC),⁴⁵⁻⁴⁸ and capillary electrophoresis.⁴⁹

1.1.2 Absorption

Oral availability is a highly desirable property for most indications, since it offers the possibility of applying a medication perorally, considered to be the most convenient treatment for patients. Besides sufficient solubility and metabolic stability, permeation through biological membranes is the most important prerequisite for oral availability.⁵⁰ The assessment of this parameter already at early stages of drug discovery and development is thus of major interest and can be determined with three methods.

Immobilized artificial membrane (IAM) HPLC: The principle of this method is the same as for HPLC-based techniques. A compound in the mobile phase is exposed to a stationary phase with bonded phospholipids and the retention time is compared to calibration compounds with known permeation properties.⁵¹⁻⁵⁴ Even though the method is fast (when run with a gradient method),⁵⁵ requires little material, and is insensitive to impurities, it is less

1 Introduction

predictive than other methods. This is probably due to the fact that only physicochemical interactions with phospholipids can be studied and specific processes important for permeation through bilayers (molecular volume, polarity transitions) remain unvalued.⁶

Parallel artificial membrane permeation assay (PAMPA): Ever since Kansy and coworkers introduced a methodology based on artificial membranes, permeation assessment has been greatly simplified and could be performed at high-throughput scale.⁵⁶ In brief, filter supports of a sandwich-plate are impregnated with a phospholipid-solvent mixture. Then, buffer with the dissolved sample is placed in the lower (donor) while blank buffer is placed in the upper (acceptor) compartment. The two plates are then assembled and diffusion through the membrane is allowed to happen. Since its development, the assay has undergone various modifications with the aim to better mimic the physiological conditions and to speed up the procedure. For example, pH-gradients between the donor and acceptor compartment are applied, surfactant is added to the acceptor buffer in order to simulate plasma protein binding, and stirring plates are placed in the donor compartments in order to reduce the unstirred water layer.⁵⁷⁻⁵⁹ In general, PAMPA is a fast and relatively inexpensive tool for the assessment of membrane permeation by passive diffusion. However, neither active transport processes nor gastrointestinal metabolic degradation can be studied.

Cell-based approaches: A more labor-intensive and complex approach for the determination of permeation is based on cell-monolayers. These are cultivated on filter-support inlets of 6- to 96-well plates. The flux of a compound in apical to basal direction or *vice versa* can be studied, giving indications on the expected *in vivo* behavior. Furthermore, active transport processes and to a limited extent also metabolic degradation can be studied.⁶⁰ Commonly used cell lines are human colorectal adenocarcinoma cells (Caco-2)⁶¹⁻⁶³ and Madin-Darby canine kidney cells (MDCK).⁶⁴ Combined approaches using PAMPA and Caco-2 results have been described.⁶⁵

1.1.3 Distribution

Distribution, in general assessed by the volume of distribution, is a parameter not easily accessible by *in vitro* testing. Often modeling based on various input parameters, such as lipophilicity and pK_a , is required for prediction.^{66, 67} Another highly important descriptor is plasma protein binding (PPB), since evasion into deeper compartments of the body, *e.g.*, fatty

1.1 Pharmacokinetic characterization today

tissue or musculature, can only happen if a compound is not bound to blood components and can thus leave the circulation.⁶⁸ Furthermore, PPB also strongly influences metabolism and excretion since in accordance with the “free drug” hypothesis only unbound drug is accessible to these processes.^{69,70} Finally, high PPB is a risk factor for drug-drug interactions.

Plasma protein binding (PPB): As illustrated above, PPB is important for the pharmacokinetic behavior of a compound and hence is determined by *in vitro* assays either prospectively or after suspicious *in vivo* experimental results. Various procedures have been established. Most commonly, PPB is determined by equilibrium dialysis. Briefly, a compartment containing plasma is separated by a semipermeable membrane from a buffer compartment. The compound of interest is added to the plasma compartment and the system is allowed to reach equilibrium. Then, the concentrations are determined in both compartments and the fraction bound to plasma proteins can be calculated. The approach has been miniaturized and is available on a 96-well scale.^{71, 72} Other procedures include plasmon surface resonance- (Biacore[®]) or nuclear magnetic resonance (NMR)-based approaches as well as ultrafiltration/ultracentrifugation, immobilized-protein HPLC-columns or microcalorimetry methods, amongst others.⁶ Concerns have been raised on whether PPB as single parameter is significant, since it has been shown that pharmacodynamic and pharmacokinetic behavior can also be influenced by binding kinetics, *i.e.*, association and dissociation constants (k_{on} and k_{off}).⁷³⁻⁷⁵ Therefore, these parameters together with PPB might provide a better understanding of a compound's *in vivo* behavior than PPB alone.

1.1.4 Metabolism

Even though stability in various biological matrices, such as gastrointestinal fluids, plasma or cerebrospinal fluid, but also under assay conditions might be problematic, the main focus during the drug discovery and development process is often put on hepatic metabolism.⁶ This is mainly due to two factors. First, hepatic metabolic stability is a critical parameter, since the metabolites of a drug might be less active, inactive or even toxic. Characterization of metabolic pathways and the corresponding products is thus essential. Second, proneness to metabolic degradation bears the risk of causing drug-drug interactions and hence triggering adverse drug reactions.⁷⁶

In general, two phases of hepatic metabolism can be distinguished. Phase I metabolism is dependent on monooxygenases, so called cytochromes, that functionalize xenobiotics by

1 Introduction

oxidation. Contrastingly, phase II metabolic reactions involve the conjugation with polar groups such as glucuronic acid, sulfate or glycine in order to facilitate renal excretion.⁷⁷

Determination of hepatic metabolic degradation: Different experimental approaches for the determination of metabolic degradation exist and are, ranked by raising complexity, based on liver microsomes, S9 fractions, hepatocyte cultures, and liver slices. Liver microsomes are prepared by differential centrifugation of homogenized liver tissue and contain membrane-bound enzymes such as cytochromes P450 and UDP-glucuronosyltransferases (UDPGT). They are most commonly used for fast, preliminary hepatic stability screening of a large number of compounds.^{78, 79} If phase II metabolic degradation is of interest, either hepatocyte cytosol or S9 (supernatant of strained liver tissue homogenate) can be used.⁸⁰ In contrast to cytosol, S9 also contains cytochromes P450 even though at lower concentration than in liver microsomes. Typically, these kinds of studies are performed at a later stage of drug discovery and development with selected compounds where phase II metabolism is suspected to play an important role. When the interplay of phase I and phase II metabolism together with cellular uptake by both active and passive mechanisms is of interest, hepatocytes are employed as test system.^{80, 81} They can be grown on supports or be used in suspension. The most complex system are high-precision rat liver slices which allow to study the passage through the liver including uptake by transporters, metabolic alteration, and biliary excretion.⁸² Both hepatocytes and liver slices represent sophisticated test systems and are therefore used at late stages of drug discovery and development for a complete metabolic characterization of selected compounds.

Additionally to the approaches mentioned above, assays with recombinant human cytochromes are usually used for the elucidation of the contribution of one enzyme to total degradation.⁸³ Furthermore, this allows a risk-assessment of drug-drug interactions and the planning of the corresponding clinical studies. In general, it is beneficial to have three or more enzymes involved in metabolic degradation, since this enables so-called metabolic switching, *i.e.*, metabolic degradation by other enzymes in case one pathway is blocked.⁶

1.1.5 Elimination

A drug's journey through the body ends with its elimination which is mainly dominated by two processes, namely hepatobiliar and renal excretion. While hydrophilic compounds and metabolites are usually excreted renally, lipophilic compounds that are not prone to metabolic

1.1 Pharmacokinetic characterization today

alterations are eliminated via the bile to the gastrointestinal tract.⁷⁷ Both processes involve elimination from the blood stream. The difference, however, is that the uptake into hepatocytes can be due to active transport or passive permeation whereas excretion into the urinary tract system is first based on filtration in the glomeruli of the kidneys and only at later stages influenced by the processes mentioned above. The blood-urine barrier acts as selective filter for compounds with molecular weights below 60 kD that do not bear extensively negative charges.^{77, 84} Albumine and many other plasma proteins are thus barely filtered and remain in circulation while electrolytes, carbohydrates, and other small molecules, amongst them most xenobiotics, are readily filtered into the primary urine. From there reabsorption is possible by both transporter mediation and passive diffusion. In addition, active secretion can be a major component of overall renal clearance and can be identified by comparing a compound's elimination to the creatinine clearance.⁷⁷ Similarly, active transport processes are also of high importance for the extrusion of both unaltered xenobiotics and metabolites thereof from the hepatocytes into the bile. Due to the enormous importance active transport processes can play, various approaches to assess them have been developed.⁸⁵

Experimental procedures to study active transport: Four major determination methods are currently employed: the cell layer permeability method, the uptake method, the inverted vesicle assay, and the ATPase assay.

The cell layer permeability method is based on a monolayer that is confluent grown on the filter of an inlet to a well plate. The permeation of a compound from the apical to the basolateral ($P_{A>B}$) and from the basolateral to the apical ($P_{B>A}$) compartment is assessed. If the transport from the apical to the basolateral compartment is bigger than in the other direction and the uptake ratio ($P_{A>B} / P_{B>A}$) is more or equal to 2, active uptake is probable. If on the other hand the transport from the basolateral to the apical compartment is bigger than in the other direction and the efflux ratio ($P_{B>A} / P_{A>B}$) is more or equal to 2, active efflux is probable.⁶ Besides Caco-2 and MDCK cells, transfected cell lines are often used for these experiments.

The uptake method is based on cells that are transfected with specific transporters. These are exposed to a compound of interest, then uptake is stopped and the cells are washed. After lysis, the concentrations of both transfected and non-transfected (control) cells lysates are determined.⁸⁶ The assay is rather simple and used as early screening tool. Common cell types include Chinese hamster ovary (CHO) cells and *Xenopus* oocytes.⁸⁷

1 Introduction

Inverted vesicles are based on the insertion of transporter genes into insect cells (*Spodoptera frugiperda*) which then produce vesicles containing these transporters. The vesicles are then inverted and expose their intracellular membrane to the outside. When they are added to solutions with compounds that are substrates for these efflux transporters, an intracellular accumulation results that can be detected after washing and lysis.⁸⁸

As last possibility, transporters of the ATP binding cassette family (e.g., P-gp) need energy in order to mediate substrate permeation through membranes. The required conversion of ATP to ADP and inorganic phosphate can be indirectly assessed by reacting the phosphate with ammonium molybdate. The intense color of this complex can be quantified by a UV-Vis plate reader.⁸⁹

1.1.6 Toxicity

Toxicity is a tremendously important but complex area of drug discovery and development. Besides insufficient efficacy, toxicity is the most important cause for compound attrition in clinical trials and can lead to market withdrawal even after several years of successful application in therapy.⁹⁰ Therefore, early *in vitro* studies to identify toxic structures are of crucial importance for the efficacy of a development program. The main focus lies on the determination of reactive metabolites and on off-target effects but also toxic effects due to agonism or antagonism at the therapeutic target have to be considered. At later stages of development, animal studies are unavoidable for a thorough elucidation of dose-toxicity relationships as well as for acute and chronic toxicity information. Based on these results, the doses for human phase I clinical trials can be determined.

Due to spectacular market withdrawals caused by QT-prolongations and torsade des pointes-arrhythmias in patients, a relatively new form of toxicity has been put into focus. Investigations revealed that these effects were caused by blocking specific cardiac potassium channels, so-called hERG channels, encoded by the human ether-a-go-go related gene. Even though the symptoms of hERG blocking are also depending on physiological and genetic factors⁹¹ and are in general a rare event (e.g., an incidence of arrhythmia in patients taking terfenadine of 1:50'000 was observed),⁹² it is of critical importance to avoid blocking due to the potentially fatal outcome.

Early toxicity assays: Screening for hERG blocking has gained increasing importance. In general, either high throughput methods or in-depth, low throughput methods can be applied.

1.1 Pharmacokinetic characterization today

High-throughput experiments are performed with cells transfected with hERG and are based on membrane potential-sensitive dyes,⁹³ radioactive ligand binding⁹⁴ or rubidium efflux.⁹⁵ Furthermore, methods based on the patch-clamp approach that directly measure the membrane potential have been developed in high- and low-throughput applications.⁹⁶

Various screens for mutagenicity and genotoxicity have been developed and two types can be distinguished. These are on the one hand, assays looking at the direct influence of a test compound on DNA and chromosomes, *e.g.*, in the micronucleus,⁹⁷ chromosomal aberration⁹⁸ or comet assay⁹⁹ and on the other hand, assays focusing on the mutation rate of different systems as indicator for mutagenicity, *e.g.*, in the Ames test (bacteria),¹⁰⁰ thymidine kinase mouse lymphoma cell¹⁰¹ (animal cells) or GADD45a-GFP¹⁰² (human cells) genotoxicity assay.

In order to evaluate the cytotoxicity of a compound, several assays have been developed that assess normal cell function and membrane integrity. The MTT (3-(4,5-Dimethylthiazol-2-yl)-2,5-diphenyltetrazolium bromide) human hepatotoxicity assay is based on the reduction of yellow-colored MTT to purple-colored formazan by mitochondria in healthy hepatocytes. Absorption at 550 nm of control cells and of cells exposed to a compound are compared, with lower absorption indicating cell toxicity.¹⁰³ Another assay format exploits the uptake and accumulation of neutral red in lysosomes of healthy hepatocytes. Reduced accumulation suggests cytotoxic effects.¹⁰⁴ Alternatively, the release of intracellular lactate dehydrogenase (LDH) due to membrane lysis of dead cells can be assessed. The principle is the LDH-catalyzed production of formazan that can be quantified photospectroscopically.¹⁰⁵

Another important toxicological concern is the formation of reactive metabolites that would form adducts with biomolecules and consequently trigger cell damage or allergic reactions. Usually, reactive metabolites can be detected by adding glutathione to the same incubation mixtures as used for metabolic stability assays. With this method also the reactive site of the molecule can be determined.¹⁰⁶

1.1.7 Status quo and future perspectives

As a result of these efforts, according to Kola and Landis, terminations of development caused by poor PK performance could be reduced.¹⁰⁷ It needs to be noted, however, that other authors disagree with that view and could not find any amelioration, with toxicity and lack of efficacy as major problems.⁹⁰ This latter study denominated pharmacokinetic liabilities to be responsible for 11% of development terminations while toxicity issues accounted for 33% of

1 Introduction

terminations. Indeed, based on these numbers no major change is observable compared to Kennedy's study³ which found pharmacokinetic reasons and toxicity in man and animals to be responsible for 7% and 33% of development terminations, respectively. It remains to be seen, to what extent toxicity and lack of efficacy are correlated with pharmacokinetic liabilities which might thus be the underlying cause.

Therefore, further work is still required to ameliorate both the pharmacokinetic as well as toxicological evaluation. Kerns and Di consider prediction accuracy, lacking data for model development, and missing high-throughput methods for various areas (*e.g.*, CYP induction, renal clearance, key toxic mechanisms) as critical fields with potential for improvement.¹ Furthermore, the need for development of fast, reliable, and inexpensive methods is highlighted. Balbach and Korn hint to the combination of tight schedules and little material synthesized in early drug discovery and development and conclude that fast assay procedures with low compound consumption are crucial prerequisites for successful projects.¹⁰⁸ Van de Waterbeemd emphasizes the importance of exploiting existing databases for matched-pair analysis and as basis to reliably deduce structure-property relationships in order to make knowledge-based decisions.¹⁰⁹ The same author together with Smith, Beaumont, and Walker stresses that attrition rates of drug candidates are still too high and they argue that better understanding of transporter-mediated processes will greatly contribute to better PK predictions. Furthermore, they state that better understanding of descriptors in combination with larger databases containing oral absorption and bioavailability results are required.¹¹⁰ This is in line with the opinions of other authors that there is a great need for better prediction tools.^{109, 111} In addition, prediction of effectiveness needs to be improved further, since a lack thereof is the most important cause for the attrition of drug development projects.⁹⁰

1.2 Carbohydrates as drug targets

1.2.1 Introduction to carbohydrates in biology and as drug target

An excellent overview on carbohydrates as drug targets was written by Ernst and Magnani and basic information as well as many examples in this section have been taken from this review.¹¹² In general, carbohydrates are the most abundant natural products. Every cell is coated by a layer of complex carbohydrates, so-called glycans, that form the glycocalyx.¹¹³ Glycans include proteoglycans, glycoproteins, glycolipids, as well as

1.2 Carbohydrates as drug targets

glycophosphatidylinositol-linked proteins and exhibit a broad diversity which originates from four factors. First, they are assembled from various monosaccharide building blocks which can, second, be linked in different positions. Third, every sugar can be linked severalfold leading to branched structures. Finally, the possibility of α - or β -linkage on the anomeric center further increases the structural complexity.

The information of such highly complex surface structures is decoded by carbohydrate-binding proteins that are involved in a wealth of important physiological and pathophysiological events. Currently, more than 80 such proteins are known and for many thereof binding specificity has been elucidated. Large screening programs with glycoarrays are performed to identify missing glycan-binding epitopes and together with existing information lead to new carbohydrate-related targets. This enables the synthesis of new chemical entities that mimic bioactive carbohydrates and thus form a new class of therapeutics.

Even though carbohydrates are highly important for a plethora of biological processes, not many carbohydrates and carbohydrate-derived drugs have made their way into clinical application and a considerable number of pathophysiological important carbohydrate-protein interactions remain to be exploited therapeutically.¹¹² Besides synthetic considerations (complex, multiple step-reactions; many stereocenters), pharmacokinetic liabilities might be responsible for this observation. The latter problem will be discussed in more depth in chapter 1.3 of the introduction.

Nevertheless, several carbohydrates or mimetics thereof have been successfully introduced to the market. Examples are found for various indications such as anticoagulation (fondaparinux,¹¹⁴ dalteparin,¹¹⁵ ardeparin,¹¹⁵ nardoparin,¹¹⁵ enoxaparin¹¹⁵), diabetes (voglibose,¹¹⁶ miglitol,¹¹⁷ acarbose¹¹⁸), epilepsy (topiramate),¹¹⁹ osteoarthritis (sodium hyaluronate),¹²⁰ and Gaucher's disease (miglustat).¹²¹ The most prominent examples, though, are probably the two drugs against influenza, zanamivir¹²² and oseltamivir.¹²³

In addition to these already marketed drugs, reams of new chemical entities are in preclinical or clinical evaluation. The main targets of these compounds are carbohydrate-binding proteins of the lectin family, since they are more homogeneous, better classified, and more selective than the sulphated glycosaminoglycans (SGAG) binding proteins.^{124, 125} The lectin family of vertebrates can be further divided into intracellular lectins (e.g., calnexin, L-type and P-type lectins) that are involved in glycoprotein processing and quality control by binding to core oligosaccharide structures and extracellular lectins (e.g., galectins, C-type, I-type, and R-type lectins) that recognize terminal carbohydrate epitopes of other cells and pathogens. The

1 Introduction

extracellular lectins generally represent better accessible and more interesting molecular targets and are thus accounting for most carbohydrate drug discovery programs.

1.2.2 C-type lectins as drug targets

C-type lectins include two important research areas, namely antagonists against selectins and DC-Sign. The latter is discussed in the review paper mentioned at the beginning of this chapter¹¹² and shall not be subject of this introduction.

Selectins are probably the most intensely studied mammalian carbohydrate-binding proteins. Since their discovery in 1989,¹²⁶⁻¹²⁸ much progress has been made in the understanding of their function as adhesion-molecules.¹²⁹ Three members of the family are known (E-, P-, and L-selectin) which all contain a Ca^{2+} -dependent carbohydrate recognition domain (CRD) that recognizes a common carbohydrate epitope shared by sialyl $\text{Le}^{\text{a/x}}$ (sialyl Lewis^a and sialyl Lewis^x).¹³⁰ Selectins represent an attractive therapeutic target in diseases where cell adhesion, extravasation of cells from the bloodstream or the migration of specific lymphocytes is important for the pathology.

As an example, E- and P-selectins have been shown to mediate the acute adhesion and aggregation of leukocytes and erythrocytes during a vaso-occlusive crisis in a mouse model of sickle cell disease.^{131,132} Furthermore, aberrant extravasation of cells from the bloodstream is crucial for various inflammatory diseases (such as asthma, colitis, arthritis and psoriasis) as well as cancer. Tumor cells use the selectin pathway to extravasate out of the bloodstream in order to metastasize. A broad variety of solid tumors and adenocarcinomas, such as gastrointestinal,¹³³ pancreatic,¹³⁴ breast,¹³⁵ lung,¹³⁶ and prostate cancers,¹³⁷ express high levels of sLe^{x} and sLe^{a} . Patients expressing these selectin ligands on gastric and colon tumor cells¹³⁸ have poorer chances of survival.¹³⁹ Selectins and their ligands have also been reported to be important for the dissemination of hematological cancers¹⁴⁰ and the homing of leukemic stem cells to microdomains within the bone marrow.¹⁴¹ Potent selectin antagonists therefore present new therapeutic opportunities for treating these diseases. Various compounds have entered clinical trials, amongst them bimosiamose against psoriasis and asthma (Phase IIa),¹⁴² GMI-1070 for the treatment of acute sickle cell crisis (Phase II),¹⁴³ and PSI-697 against atherothrombotic and venous thrombotic diseases (Phase I).¹⁴⁴

1.2 Carbohydrates as drug targets

1.2.3 I-type lectins as drug target

The family of I-type lectins consists of carbohydrate-binding proteins in the immunoglobulin superfamily and include the Siglecs.¹⁴⁵ The Siglecs are primarily expressed on leukocytes that mediate acquired and innate immune functions and act as cell signalling co-receptors. The variable cytoplasmic regulatory elements and diverse specificity for their sialoside ligands enable Siglecs to carry out unique roles at the cell surface. The best studied Siglecs are Siglec 2, a regulatory protein that prevents the overactivation of the immune system and the development of autoimmune diseases, and **MAG**, a protein that blocks regeneration of the central nervous system (CNS) after injury.¹⁴⁶ In contrast to the peripheral nervous system (PNS), the injured adult CNS is not capable of axon regeneration. Even though neurite outgrowth is possible in principal, it is prevented by inhibitor proteins expressed on residual myelin and on astrocytes that are recruited to the site of injury. Three major inhibitor proteins have been identified up to date: reticulon 4 (RTN4; also known as nogo A),¹⁴⁷ myelin oligodendrocyte glycoprotein (MOG),¹⁴⁸ and MAG.¹⁴⁹ These three proteins activate the RTN4 receptor, which then forms a complex with the nerve growth factor receptor (NGFR; also known as p75NTR). This leads to the activation of the RhoA–ROCK (Rho-associated, coiled coil-containing protein kinase) cascade resulting in growth cone collapse.¹⁵⁰ MAG is further validated as therapeutic target by the high correlation between the degree of neurite outgrowth and the binding affinities of antagonists against this target, suggesting that potent glycan inhibitors of MAG can potentially enhance axon regeneration.¹⁵¹ Due to further refinements of the SAR profile, MAG antagonists that have improved affinities and, at least in some cases, remarkably simple structures have been identified.¹⁵²⁻¹⁵⁷ Unfortunately, owing to the use of different assay formats, it has been difficult to compare the reported affinities of these compounds for various ligands.

1.2.4 Bacterial and viral lectins as drug targets

Enteric, oral and respiratory bacteria require adhesion to the host's tissue for colonization and subsequent development of an infectious disease. This enables them to avoid clearance and killing by immune factors, bacteriolytic enzymes and antibiotics. Moreover, after adhesion bacteria are better able to acquire nutrients, further enhancing their ability to survive and infect the host. As a consequence, compounds that prevent the adhesion of pathogens to host tissues may offer a novel strategy to combat infectious diseases.¹⁵⁸ Furthermore, because anti-adhesive agents are not bactericidal, they are less likely to promote the propagation of

1 Introduction

resistant strains than conventional bactericidal agents such as antibiotics. The strategy therefore seems promising for the reduction of the currently prevailing drug-resistance problem.¹⁵⁹ Carbohydrate epitopes on the surface of host cells which are used by bacteria and viruses for colonization and infection represent the starting point of the search for glycomimetic entry inhibitors. However, that fact that most pathogens possess genes encoding several types of adhesins is a challenge for anti-adhesion therapy, since they may express different types, thus evading elimination by adhesion-blocking. Fortunately, glycomimetic antagonists that are designed to inhibit multiple adhesins are feasible to develop.

Urinary tract infections (UTIs) are among the most prevalent inflammatory diseases that are caused by pathogens.^{160,161} The predominant pathogen in UTIs is uropathogenic *Escherichia coli* (UPEC), which causes more than 80% of all infections in otherwise healthy people (uncomplicated UTI). In healthy individuals, most uropathogens originate from the rectal microbiota and enter the normally sterile urinary bladder through the urethra, where they trigger the infection (cystitis). Once in the urinary tract, bacteria attach to the urinary tract epithelium through fimbrial adhesion molecules to avoid the host's defence mechanisms. Once bound, the bacteria are presumably internalized in an active process that is similar to phagocytosis.¹⁶²

Uncomplicated UTI can be effectively treated with oral antibiotics such as fluoroquinolones, cotrimoxazol or amoxicillin and clavulanate, depending on the susceptibility of the pathogen involved. However, recurrent infections and subsequent antibiotic exposure can result in the emergence of antimicrobial resistance, which often leads to treatment failure and reduces the range of therapeutic options. So, there is an urgent need for efficient, cost-effective and safe non-antibiotic therapy to prevent and treat UTIs without facilitating antimicrobial resistance. Inhibition of type 1 fimbriae-mediated bacterial attachment to the bladder epithelium is a promising approach to achieve this goal.¹⁶³ Studies showed that α -mannosides are the primary bladder cell ligands for UPEC and that the attachment event requires the highly conserved **FimH** lectins, which are located at the tip of the bacterial fimbriae. A structure–function analysis showed that the residues of the FimH mannose binding pocket are invariant across 200 UPEC strains.¹⁶⁴ More than two decades ago, various oligomannosides¹⁶⁵ and aromatic α -mannosides¹⁶⁶ that antagonize type 1 fimbriae-mediated bacterial adhesion were identified. Two approaches have been taken to improve their affinity: the rational design of ligands guided by information obtained from the crystal structure of FimH, and the multivalent presentation of the α -mannoside epitope. The crystal structure of the FimH receptor-binding domain was solved in 1999¹⁶⁷ and the corresponding complex with oligomannoside-3 has

1.2 Carbohydrates as drug targets

recently become available.¹⁶⁸ Despite this detailed knowledge of the binding event, few attempts to translate this information into low-molecular-mass antagonists have been reported.^{166, 169, 170} The reference compound, methyl α -D-mannoside binds in the millimolar range,¹⁷¹ but the most potent monovalent antagonist reported so far binds with nanomolar affinity.¹⁷⁰ Although monovalent and oligovalent antagonists with nanomolar affinity have been reported, there are no data available regarding their pharmacokinetic properties. However, for the treatment of UTI, oral bioavailability and fast renal excretion to reach the targets in the urinary tract are prerequisites for therapeutic success.

Another popular research field in the area of bacterial lectins is the quest for new treatments against *Pseudomonas aeruginosa*. This topic is discussed *in extensio* in the review article mentioned at the beginning of this chapter¹¹² and is not deepened further here.

1.2.5 Future perspectives

The knowledge and understanding of the involvement of carbohydrates has risen considerably over the past decades. Besides ongoing research for the identification of new carbohydrate-related targets, major improvements concerning both activity and specificity could be achieved. Advancements in NMR spectroscopy^{172,173} and X-ray crystallography¹⁷⁴ formed the basis for this development by providing structure-based information and understanding native interactions.¹⁷⁵⁻¹⁷⁸ Nevertheless, various shortcomings when working with carbohydrates and mimetics thereof prevail and need to be addressed better. Besides pharmacodynamic problems (*e.g.*, enhancing binding affinity and simultaneously maintaining selectivity), pharmacokinetic liabilities are major drawbacks. To circumvent these problems, knowledge about negligible and replaceable functional groups is crucial and will be benefited by improved analytical approaches enabling better access to structural information. In addition, early-ADMET assays are intended to address the problem of drug-likeness at an earlier stage and thus contribute significantly to successful drug discovery programs.

1 Introduction

1.3 Carbohydrate antagonists and pharmacokinetics

1.3.1 General considerations

Unfortunately, not much information has been published concerning the pharmacokinetic behavior of carbohydrates and mimetics thereof. For example, since Lipinski's seminal paper²⁴ it is known that absorption from the gastrointestinal tract depends on lipophilicity, molecular weight, and number of hydrogen bond donors and acceptors. Various other publications found as well a significant dependence of permeation on these parameters and on polar surface area with low values generally being beneficial (except for logP).¹⁷⁹⁻¹⁸⁶ When looking at typical structural features of carbohydrates (such as rather high molecular weights, polarity, number of rotatable bonds, and number of hydrogen bond acceptors and donors) it becomes apparent that they contrast with the requirements for oral bioavailability. Furthermore, the low distribution coefficients (logD) as a result of the numerous hydroxy functions suggest low plasma protein binding, low volume of distribution, and low rates of metabolism.¹⁵ Together with the expected fast renal elimination,¹⁸⁷ carbohydrates are prone to very short half-life times in plasma and would thus require frequent application. Furthermore, carbohydrates often show only high micromolar to even millimolar IC₅₀ values. Consequently, without modifications to improve both the pharmacodynamic and the pharmacokinetic behavior carbohydrates are rather unattractive as drugs.

Several strategies are used to address the above-mentioned problems. For the amelioration of permeation, omitting nonessential functional groups can prove useful. Moreover, a prodrug-approach¹⁸⁸ or the biosteric replacement of crucial groups¹⁸⁹ could benefit oral availability. These modifications bear the additional advantage of enhancing the lipophilicity of the compounds and thus might enhance plasma protein binding, leading to longer plasma half-life times.⁷⁰ On the other hand, metabolic alteration gets more probable with increasing lipophilicity and the property should thus be carefully balanced.¹⁵

In addition to the above-mentioned considerations, active transport might be envisioned in case sufficiently high passive diffusion for oral absorption and arrival at the site of action is not achieved. There are numerous examples of marketed drugs for which active transportation is exploited, *e.g.*, β -lactam antibiotics, heart glycosides, and fungicides. The possibility of active transportation can also be incorporated in rational design strategies. Transporters play furthermore an important role during the elimination process of carbohydrates concerning both active re-uptake and secretion.

1.4 Aims of this thesis

The considerations discussed above found practical applications in the development of carbohydrates as exemplified in the next paragraph.

1.3.2 Examples of successful pharmacokinetic amelioration of carbohydrates

The most successful carbohydrate mimetic currently on the market is oseltamivir. With a carbohydrate lead structure as starting point, lead likeness was reached by eliminating unrequired polar groups and metabolic soft spots. By the use of an ester prodrug-approach, an orally available neuraminidase-inhibitor was obtained.¹²³ After absorption, the ester is cleaved liberating the active metabolite RO64-0802.¹⁹⁰ With this strategy, an absolute bioavailability of the orally applied prodrug of 80% was achieved. Within 30 minutes the active metabolite is detectable in plasma and maximal concentrations are reached after 3 to 4 hours.¹⁹¹

The antiviral drug valacyclovir is a good example for the successful exploitation of active transport processes. By adding the amino acid L-valine to the parent compound acyclovir, the oral availability could be increased fivefold due to active transport through the gastrointestinal mucosa by the peptide transporters 1 and 2 (PEPT1 and PEPT2).¹⁹² As a result, the structural requirements for transportation by PEPT1 were elucidated and extensively studied.¹⁹³ These efforts are expected to find broad application for various compounds with problematic bioavailability.

Active transport can also be a disadvantage when the process is involved in excretion and elimination. Again, oseltamivir is a prominent example, since its active metabolite RO64-0802 is actively excreted by organic anion transporters (OAT).¹⁹⁴ Indeed, when oseltamivir is co-administered together with probenecid, a competitive inhibitor of OAT1, the serum half-life of the active metabolite is prolonged.¹⁹⁵ A better understanding of the role transporters play for pharmacokinetic processes will offer new opportunities or prevent failures due to inappropriate pharmacokinetic behavior.

1.4 Aims of this thesis

As exemplified in the previous chapter, not much is known about the pharmacokinetic behavior of carbohydrates and mimetics thereof. One aim of this thesis was therefore to provide additional information to better understand the factors influencing ADME processes and to expand the knowledge on the pharmacokinetic behavior of carbohydrates. Furthermore,

1 Introduction

various assays were used to characterize carbohydrate mimetics with respect to their expected pharmacokinetic behavior.

2.1 The PADMET platform – an overview

2 Methods and assays

2.1 The PADMET platform – an overview

In order to analyze the pharmacokinetic behavior of the carbohydrate mimetics synthesized in the research group of Prof. B. Ernst at the University of Basel, various assays were built up and adapted to the requirements of this specific compound class.

The first author was responsible for the building up of all assays, including their evaluation and adaptation to carbohydrate mimetics, and wrote the manuscript.

This manuscript is in preparation for *Bioorganic Medicinal Chemistry*.

2 Methods and assays

The PADMET Platform – Early Pharmacokinetic Characterization in Academia

Matthias Wittwer, Simon Kleeb, Jacqueline Bezençon, Erich Gubler, Brian Cutting, Beat Ernst*

Institute of Molecular Pharmacy, Pharmacenter, University of Basel, Klingelbergstrasse 50, 4056 Basel, Switzerland.

* *Correspondence:* Prof. Dr. Beat Ernst

Institute of Molecular Pharmacy

University of Basel

Klingelbergstrasse 50

CH-4056 Basel

Tel.: +41 61 267 1551,

Fax: +41 61 267 1552

Keywords: ADME, pharmacokinetic characterization, in vitro assays, academic reserach

Abbreviations: aCSF, artificial cerebrospinal fluid; ADME, absorption, distribution, metabolism, elimination; BBB-PAMPA, blood-brain barrier parallel artificial membrane permeation assay; Caco-2 cells, Caucasian colon adenocarcinoma cells; CMC, critical micelle concentration; CNS, central nervous system; CSF, cerebrospinal fluid; DMEM, Dulbecco's Modified Eagle's Medium; DMSO, dimethyl sulfoxide; f_b , fraction bound; FBS, fetal bovine serum; HPLC, high-performance liquid chromatography; LC-MS, liquid chromatography-mass spectroscopy; MDCK, Madin-Darby canine kidney cells; NMR, nuclear magnetic resonance; PADMET, physicochemical properties, absorption, distribution, metabolism, elimination, toxicity; PAMPA, parallel artificial membrane permeation assay; PK, pharmacokinetics; SAR, structure-activity relationships; sGF, simulated gastric fluid; sIF, simulated intestinal fluid; (Q)SPR, (quantitative) structure-property relationships; TEER, transepithelial resistance.

2.1 The PADMET platform – an overview

Abstract

After researcher realized the importance of pharmacokinetic characterization for successful drug development and discovery, the focus was set on optimizing concomitantly pharmacodynamic and pharmacokinetic properties. Therefore, structure-activity relationships were complemented by structure-property relationships. For this purpose, properties of large data sets needed to be measured and consequently a wealth of new assays meeting high-throughput requirements became necessary. As a result of these efforts, development failures due to pharmacokinetic liabilities could be reduced even though they remain responsible for 11% of failures.

Generally, it is striking that pharmacokinetic characterization seems to be restricted to company research and that only in isolated cases academic groups assess the according parameters. Instead, *in silico* tools or rules of thumb are frequently applied which are often developed based on known compound families. Therefore, their application to unknown, new chemical entities might be problematic.

A possible explanation for the uncommonness of pharmacokinetic characterization in academic research might be the belief that the according assays are both complicated as well as expensive and that the efforts do not pay out.

In this communication the feasibility of such assays in an academic environment is demonstrated. Furthermore, detailed experimental procedures with information about costs, required equipment and time consumption are given. Finally, the benefits for academic research projects are exemplified by the impact on three projects.

2 Methods and assays

1. Introduction

Towards the end of the last century, the importance of pharmacokinetic (PK) characterization during drug development has been recognized.^{1,2} As a consequence, *in vitro* assays were used already at early stages of drug discovery for a reliable prediction of ADME properties of a given compound, *i.e.* its absorption, distribution, metabolism, and elimination.^{3,4} Thus, the intestinal absorption of a new compound can be characterized by a number of physicochemical parameters, such as pK_a ,⁵ solubility,⁶ and with limitations the distribution coefficient ($\log D$).⁷⁻¹⁰ Additional evidence can be gained based on its permeation through an artificial membrane (parallel artificial membrane permeability assay, PAMPA)¹¹ or on the cell level with monolayers of Caco-2 (colorectal adenocarcinoma cells)¹² or MDCK cells (Madin-Darby canine kidney cells)¹³. Finally, a comparison of results obtained from PAMPA and Caco-2 cells allows the estimation of the contribution of active transport to the uptake mechanism.

Convenient methods for the assessment of numerous additional pharmacokinetic parameters, including plasma protein binding^{14,15} and metabolic stability (liver microsomes, cytochrome assays),¹⁶ are available. This led to an early engagement in the elucidation of structure-property relationships (SPR), especially also quantitative structure-pharmacokinetic relationships (QSPR),¹⁷⁻¹⁹ in contrast to the exclusive focus on structure-activity relationships (SAR) that was prevalent previously. Responding to a growing interest, property-based lead optimization in order to ameliorate the pharmacokinetic properties of a lead came to the fore.²⁰ Furthermore, ever since Lipinski *et al.* have shown in their seminal paper⁶ that also calculated descriptors such as molecular weight, ClogP, and the number of hydrogen donors and acceptors can be predictive for successful drug development, the importance of *in silico* prediction has been more and more recognized.^{21,22} An excellent overview on assays and concepts applied in modern ADME optimization was recently published by Kerns and Li.⁹

As a result of these efforts, late-stage failure in the drug discovery and development process due to PK liabilities has been reduced.^{23,24} Nevertheless, problems related to the pharmacokinetic behavior of a compound remain responsible for on average 11% of development terminations during clinical phases I to III, a percentage that did not basically change over recent years.²⁵

2.1 The PADMET platform – an overview

In general, it is striking that ADME characterization is almost exclusively restricted to company research (for examples see these references)^{26, 27} and that only in isolated cases medicinal chemistry groups in academia routinely assess pharmacokinetic parameters or profiles *in vitro*. For reaching drug-likeness, *in silico* methods or rules of thumb are applied. While these approaches might be useful for known compound families, they are not likely to be successful for new chemical entities, since computer-based prediction tools need to be trained for new compound series.^{28, 29} One explanation for the current status might be the misconception that the establishment of assays is both expensive and labor-intensive and that these efforts can be avoided by more inexpensive *in silico* approaches.

As our group is developing carbohydrate mimetics, prediction tools for PK properties most probably not developed or not trained with molecules from this compound class turned out to be unreliable. In addition, since only a few examples of carbohydrate mimetic drugs were introduced to the market, only limited knowledge on ADME properties for this compound class exist.³⁰ As a consequence of this lack of knowledge, we decided to build up a PADMET platform (physicochemical parameters, absorption, distribution, metabolism, elimination and toxicity) consisting of various assays for PK characterization of carbohydrate mimetics.

In this communication, the feasibility of the project in an academic environment is demonstrated. All assays implemented in the PADMET platform are described with detailed experimental procedures. Finally, the benefits for various projects are demonstrated.

2. Methods and assay description

Protocols for different pharmacokinetic assays are presented to demonstrate their feasibility in an academic environment and to stimulate the buildup of PADMET platforms in other research groups. A short rationale for the interest in the according assay is given at the beginning of each section. At the end of every method description costs for consumables, time consumption, and required equipment are summarized (see also overview in Table 1). For most assays a LC-MS for concentration determinations (HPLC might also be possible depending on the compound's properties) and a temperature-controlled shaker are required. The methodologies do not rely on robotic equipment, even though many protocols could be adapted accordingly.

2 Methods and assays

Table 1. Overview of time consumption and costs for different assays. Time consumption (including preparation of consumables and of experiment, excluding time for periods that do not require control, i.e. during shaking or concentration determination): + up to 3 hours, ++ 3 to 6 hours, +++ a whole day. Costs for consumables and special devices required for the experiments (excluding LC-MS, UV-spectrophotometer, NMR, shakers, centrifuge, incubator, and laminar flow): + inexpensive, ++ expensive but no major investment, +++ expensive and major investments required.

| Assay | Time | Costs |
|---|------|-------|
| logP/D (partition/distribution coefficient) | ++ | + |
| pKa | + | + |
| logS (solubility) | + | + |
| PAMPA (parallel artificial membrane permeation assay) | ++ | +++ |
| Caco 2 cell-based assay | +++ | +++ |
| PPB (plasma protein binding) | ++ | ++ |
| Stability in the GIT | + | + |
| Stability in the CNS | + | + |

Materials

Dimethyl sulfoxide (DMSO), 1-octanol, pepsin, pancreatin, and Dulbecco's Modified Eagle's Medium (DMEM) high glucose were purchased from Sigma-Aldrich (Sigma-Aldrich, St. Louis MI, USA). PAMPA System Solution, GIT-0 Lipid Solution, and Acceptor Sink Buffer were ordered from pIon (pIon, Woburn MA, USA). L-glutamine-200 mM (100X) solution, MEM non-essential amino acid (MEM-NEAA) solution, fetal bovine serum (FBS), and DMEM without sodium pyruvate and phenol red were bought from Invitrogen (Invitrogen, Carlsbad CA, USA). Human plasma was bought from Biopredic (Biopredic, Rennes, France) and acetonitrile (MeCN) from Acros (Acros Organics, Geel, Belgium). The Caco-2 cells were kindly provided by Prof G. Imanidis, FHNW, Muttentz, and originated from the American Type Culture Collection (Rockville MD, USA).

2.1 The PADMET platform – an overview

logD_{7.4} determination

Background: The distribution coefficient logD_{7.4} as a measure of lipophilicity enables predictions concerning various parameters (e.g., permeation, metabolism, plasma protein binding) [10].

Method: The *in silico* prediction tool ALOGPS³¹⁻³³ was used to estimate the logP values of the compounds. Depending on these values, the compounds were classified into three categories: hydrophilic compounds (logP below zero), moderately lipophilic compounds (logP between zero and one) and lipophilic compounds (logP above one). For each category, two different ratios (volume of 1-octanol to volume of buffer) were defined as experimental parameters:

| Compound type | logP | Ratios (1-octanol: buffer) |
|-----------------------|-------|----------------------------|
| hydrophilic | < 0 | 30:140, 40:130 |
| moderately lipophilic | 0 - 1 | 70:110, 110:70 |
| lipophilic | > 1 | 3:180, 4:180 |

Equal amounts of phosphate buffer (0.1 M, pH 7.4) and 1-octanol were mixed and shaken vigorously for 5 min to saturate the phases. The mixture was left until separation of the two phases occurred, and the buffer was retrieved. Stock solutions of the test compounds were diluted with buffer to a concentration of 1 μM. For each compound, six determinations, i.e., three determinations per 1-octanol:buffer ratio, were performed in different wells of a 96-well plate. The respective volumes of buffer containing analyte (1 μM) were pipetted to the wells and covered by saturated 1-octanol according to the chosen volume ratio. The plate was sealed with aluminium foil, shaken (1350 rpm, 25 °C, 2 h) on a Heidolph Titramax 1000 plate-shaker (Heidolph Instruments GmbH & Co. KG, Schwabach, Germany) and centrifuged (2000 rpm, 25 °C, 5 min, 5804 R Eppendorf centrifuge, Hamburg, Germany). The aqueous phase was transferred to a 96-well plate for analysis by liquid chromatography-mass spectrometry (LC-MS).

logD_{7.4} was calculated from the 1-octanol:buffer ratio (o:b), the initial concentration of the analyte in buffer (1 μM), and the concentration of the analyte in buffer (c_B) with equilibration:

$$\log D_{7.4} = \frac{1\mu\text{M} - c_B}{c_B} \times \frac{1}{o:b}$$

2 Methods and assays

The average of the three $\log D_{7.4}$ values per 1-octanol:buffer ratio was calculated. If the two mean values obtained for a compound did not differ by more than 0.1 unit, the results were accepted.

Time: About 6 hours, possibility to determine 16 compounds in parallel in a 96-well plate.

Costs: Inexpensive consumables (octanol, phosphate buffer, plate, sealing foil).

Equipment: Plate shaker, pipettes (and optionally Hamilton syringe), centrifuge (ideally with insert for 96-well plate, otherwise transfer to tubes required), HPLC or LC-MS.

pK_a determination

Background: pK_a values are of crucial importance for many processes involved in a compounds passage through the body, including absorption, metabolism, distribution, excretion, and activity at the target.⁹

Method: The pK_a values were determined as described elsewhere.³⁴ Briefly, the pH of a sample solution is gradually changed and the chemical shift of protons adjacent to ionizable moieties is monitored. If the shift is plotted against pH a sigmoidal curve results whose inflection point confers to the pK_a value.

Time: About 3 hours are required if the pH needs to be gradually changed for one or two samples. If more compound is available and the NMR spectrometer has a automated sample handler series of 9 to ten samples can be prepared and measured over night. For this method only 1.5 hours are required.

Costs: For the method described above the only requirements are D₂O and NMR tubes and hence costs are very low

Equipment: This determination method is simple and feasible in every chemistry lab, since it relies only on a pH-meter and NMR-access.

Thermodynamic solubility determination

Background: Solubility is a crucial parameter for drug discovery projects. Insufficient solubility will affect oral absorption,⁴ will lead to problems for i.v. applications and has the potential to negatively influence assay results.⁹

Method: Microanalysis tubes (Labo-Tech J. Stofer LTS AG, Muttenz, Switzerland) were charged with 1 mg of solid substance and 250 μ L of phosphate buffer (50 mM, pH 6.5). The samples were briefly shaken by hand, then sonicated for 15 min and vigorously shaken (600 rpm, 25 °C, 2 h) on a Eppendorf Thermomixer comfort (Eppendorf, Hamburg, Germany). Afterwards, the samples were left undisturbed for 24 h. After measuring the pH, the saturated

2.1 The PADMET platform – an overview

solutions were filtered through a filtration plate (MultiScreen® HTS, Millipore, Billerica MA, USA) by centrifugation (1500 rpm, 25 °C, 3 min). Prior to concentration determination by LC-MS, the filtrates were diluted (1:1, 1:10 and 1:100 or, if the results were outside of the calibration range, 1:1000 and 1:10000). The calibration was based on six values ranging from 0.1 to 10 µg/mL. Concentrations were determined by LC-MS. The upper limit for a reliable determination with this method is a maximum solubility of 3000 µg/ml.

Time: About 3 hours, possibility to determine numerous compounds in parallel

Costs: Inexpensive consumables (glass vials, 96-well plates, buffer components) except for the filtration plates (a package of ten suffices for 960 determinations, though).

Equipment: Ultrasonic bath, shaker, pipettes, centrifuge (with insert for 96-well plate, otherwise different filtration device required), pH-meter, HPLC or LC-MS.

Parallel artificial membrane permeation assay (PAMPA)

Background: Oral availability is a desired property for drugs due to the ease of application. As a basis therefore, a compound needs to be able to permeate through biological membranes. A simple, high-throughput determination method to assess permeation through membranes is the PAMPA assay¹¹ that uses a 96-well format with artificial membranes.

Method: logP_e was determined in a 96-well format with the PAMPA permeation assay. For each compound, measurements were performed at three pH values (5.0, 6.2, 7.4) in quadruplicates. For this purpose, 12 wells of a deep well plate, i.e., four wells per pH-value, were filled with 650 µL System Solution. Samples (150 µL) were withdrawn from each well to determine the blank spectra by UV-spectroscopy (SpectraMax 190, Molecular Devices, Silicon Valley Ca, USA). Then, analyte dissolved in DMSO was added to the remaining System Solution to yield 50 µM solutions. To exclude precipitation, the optical density was measured at 650 nm, with 0.01 being the threshold value. Solutions exceeding this threshold were filtrated. Afterwards, samples (150 µL) were withdrawn to determine the reference spectra. Further 200 µL were transferred to each well of the donor plate of the PAMPA sandwich (pIon, Woburn MA, USA, P/N 110 163). The filter membranes at the bottom of the acceptor plate were impregnated with 5 µL of GIT-0 Lipid Solution and 200 µL of Acceptor Sink Buffer were filled into each acceptor well. The sandwich was assembled, placed in the GutBox™, and left undisturbed for 16 h. Then, it was disassembled and samples (150 µL) were transferred from each donor and acceptor well to UV-plates. Quantification was performed by both UV-spectroscopy and LC-MS. logP_e-values were calculated with the aid of the PAMPA Explorer Software (pIon, version 3.5). logP_e values above -6.3 or membrane

2 Methods and assays

retention of more than 80% were considered as threshold for oral availability (given no metabolic degradation occurs).³⁵ For compounds with weak chromophores LC-MS detection is highly recommended. In this case, we made good experiences with diluting the acceptor medium with acetonitrile 1:1 (to break up the micelles) and to measure each reference well directly after the according donor well (less variability). Furthermore, both donor and reference samples need to be diluted not to exceed the linear concentration range of triple quadrupole-MS instruments.

Time: For the protocol described above, about 6 hours distributed on two days (due to the overnight permeation period) are required. 7 compounds at three pH values or 21 compounds at one pH value in quadruplicates can be measured in one assay. Other protocols exist with shorter assay durations (i.e. 4 hours or 30 minutes) and the choice of the appropriate conditions depends on compound properties (mainly lipophilicity).

Costs: Both expensive (buffers, PAMPA sandwiches, lipid mixture, UV-plates) and inexpensive (deep well plate) consumables are required. Since many transfer steps are needed, pipette tip consumption needs to be taken into account as cost factor. Furthermore, the PAMPA Explorer software needs to be purchased (major cost factor). Nevertheless, compared to cell-based assays PAMPA is easy to perform, requires little additional instruments and exhibits an excellent reproducibility of results.

Equipment: 96-well UV-spectrophotometer, multichannel pipette, pipettes, pH-meter (for pH adjustment of buffers), LC-MS. Optionally, a GutBox[®] is required if the assay is performed under stirring conditions.

Caco 2 cell assay

Background: In contrast to the PAMPA, Caco-2 cell-based absorption assays¹² also yield information about active transport processes and to a limited extent about metabolism. They are considered as surrogate cell-line for human small intestine cells and are thus used as model for gastrointestinal permeation.

Method: The cells were cultivated in tissue culture flasks (BD Biosciences, Franklin Lakes NJ, USA) with DMEM high glucose medium, containing 1% L-glutamine solution, 1% MEM-NEAA solution, and 10% FBS. The cells were kept at 37 °C in humidified air, containing 8% CO₂ and the medium was changed every second to third day. When approximately 90% confluence was reached, the cells were split in a 1:10 ratio and distributed to new tissue culture flasks. At passage numbers between 60 and 65, they were seeded at a density of 5.33×10^5 cells per well to Transwell[®] 6-well plates (Corning Inc., Corning NY,

2.1 The PADMET platform – an overview

USA) with 2.5 mL of culture medium in the basolateral compartment and 1.5 mL (days 1 to 10) or 1.8 mL (from day 10 on) in the basolateral compartment. The medium was renewed on alternate days. Experiments were performed between days 19 and 21 post-seeding. DMEM without sodium pyruvate and phenol red was used as transport medium for experiments. Previous to the experiment, the integrity of the Caco-2 monolayers was evaluated by measuring the transepithelial resistance (TEER) in transport medium (37 °C) with an Endohm tissue resistance instrument (World Precision Instruments Inc., Sarasota FL, USA). Only wells with TEER values higher than 300 Ωcm^2 were used. Experiments were performed in triplicates. Transport medium (10 μL) from the apical compartments of three wells were replaced by the same volume of compound stock solutions (10 mM). The Transwell® plate was then shaken (250 rpm) in the incubator. Samples (100 μL) were withdrawn after 5, 15, 30, 60, and 120 min from the basolateral compartment and concentrations were analyzed by HPLC. Apparent permeability coefficients (P_{app}) were calculated according to the following equation

$$P_{\text{app}} = \frac{dQ}{dt} \times \frac{1}{A \times c_0}$$

where dQ/dt is the permeability rate, A the surface area of the monolayer, and c_0 the initial concentration in the donor compartment.¹² After the experiment, TEER values were assessed again for every well and results from wells with values below 300 Ωcm^2 were discarded.

Time: About one day is required for the assay preparation and its execution. It needs to be considered, however, that also cell cultivation requires considerable time (medium changes, splitting, freezing of backup samples).

Costs: Cells and consumables (media, cell culture flasks, pipettes, Transwell® plates) are rather costly. Furthermore, the required infrastructure needed for work with cells (laminar flow bench, incubator) is a major cost factor.

Equipment: Incubator, laminar flow bench, tissue resistance measurement instrument, plate shaker with temperature control (saturated atmosphere required, can be achieved by placing water container in shaker; alternatively, a normal shaker can be placed in the incubator), HPLC or LC-MS. Remark: Experience regarding the work with cell cultures is a precondition.

Plasma protein binding (PPB)

Background: Trainor nicely summarized the importance of plasma protein binding in a recently published review.¹⁴ In brief, it is assumed that only the unbound fraction of a compound can interact with a target, be metabolized, and be excreted (“free drug hypothesis”)

2 Methods and assays

even though limitations may apply.⁹ Therefore, knowing the amount of unbound drug is of crucial importance.

Method: The dialysis membranes (HTDialysis LCC, Gales Ferry, USA; MWCO 12-14 K) were prepared according to company instructions. The human plasma was centrifuged (5800 rpm, 25 °C, 10 min), the pH of the centrifugate (without floating plasma lipids) was adjusted to 7.5, and analyte was added to yield 10 µM solutions. Equal volumes (150 µL) of phosphate buffer (0.1 M, pH 7.5) and analyte-containing plasma were transferred to the separated compartments of the assembled 96-well high throughput dialysis block (HTDialysis LCC, Gales Ferry, USA). Measurements were performed in triplicates. The plate was covered with a sealing film and incubated (5 h, 37 °C). Buffer and plasma compartment were processed separately. From the buffer compartments, 90 µL were withdrawn and 10 µL blank plasma were added. From the plasma compartments, 10 µL were withdrawn and 90 µL of blank buffer were added. After protein precipitation with 300 µL ice-cooled MeCN, the solutions were mixed, centrifuged (3600 rpm, 4 °C, 11 min), and 50 µL of the supernatant were retrieved. Analyte concentrations were determined by LC-MS. The fraction bound (f_b) was calculated as follows:

$$f_b = 1 - \frac{c_b}{c_p}$$

where c_b is the concentration in the buffer and c_p the concentration in the plasma compartment. Values were accepted if the recovery of analyte was between 80 and 120%.

Time: About 6 hours, possibility to determine 36 compounds in parallel (as triplicates) even though without robotic liquid handling 12 compounds are better feasible.

Costs: The major cost factor for this assay is the purchase of plasma. Besides this, once the dialysis block has been purchased little additional costs will arise (for membranes and sealing films) since consumables are inexpensive.

Equipment: Dialysis block, pipettes, multichannel pipette (not indispensable but comfortable for liquid handling in parallel), centrifuge, HPLC or LC-MS.

Stability in simulated gastrointestinal fluids

Background: Stability in the gastrointestinal tract is a precondition for absorption of a compound and can be a major obstacle in drug development.³⁶ The according fluids can be simulated and a compound's stability therein can be assessed.

Method: Simulated gastric fluid (sGF) and simulated intestinal fluid (sIF) were prepared according to the United States Pharmacopeia (USP 28). sGF contained sodium chloride (200

2.1 The PADMET platform – an overview

mg), pepsin (320 mg) and 37% aq HCl (0.7 mL) in bidistilled water (100 mL). sIF consisted of monopotassium phosphate (680 mg), 0.2 M NaOH (7.7 mL), and pancreatin (1 g) in bidistilled water (100 mL). sIF was adjusted to pH 6 by adding 0.2 M NaOH. sGF and sIF were preheated (37 °C) and the compounds were added to yield 10 µM solutions. Incubations were performed on a Eppendorf Thermomixer comfort (500 rpm, 37 °C). Before starting the experiment (t = 0 min) and after an incubation time of 15, 30, 60, and 120 min samples (20 µL) were withdrawn, precipitated with ice-cooled MeCN, and centrifuged (3600 rpm, 4 °C, 10 min). The concentrations of analyte in the supernatant were analyzed by LC-MS. Stability was expressed as percentage remaining compound relative to the initial concentration. The concentrations of analyte in the supernatant were analyzed by HPLC or LC-MS.

Time: About 3 hours, possibility to determine numerous compounds in parallel.

Costs: Inexpensive consumables (simulated fluid components, tubes).

Equipment: Temperature-controlled shaker, centrifuge, HPLC or LC-MS.

Stability in aCSF (artificial cerebrospinal fluid)

Background: For specific projects with compounds that are applied directly to the central nervous system or that are supposed to interact with targets therein, stability in cerebrospinal fluid might be a critical factor. Consequently, this parameter is of interest for such projects and can be assessed in artificial cerebrospinal fluid.

Method: Artificial cerebrospinal fluid was prepared according to published results with additionally 0.4% V/V human plasma.^{37, 38} The concentrations of electrolytes (in mmol/L) were the following: sodium 140, chlorine 125, hydrogen carbonate 22.5, potassium 2.9, calcium 1.15, magnesium 1, urea 4.16, and glucose 3.2. Solutions of analyte (100 µM) were prepared in this aCSF and incubated at 37 °C and 300 rpm on a Eppendorf Thermomixer comfort. 20 µL-samples were withdrawn after at the beginning of the experiment and after 30, 60, 120, 180 minutes, and 24 hours and concentrations were analyzed by HPLC.

Time: About 3 hours, possibility to determine numerous compounds in parallel

Costs: Inexpensive consumables (simulated fluid components, tubes).

Equipment: Temperature-controlled shaker, HPLC or LC-MS.

LC-MS measurements

Analyses were performed using a 1100/1200 Series HPLC System coupled to a 6410 Triple Quadrupole mass detector (Agilent Technologies, Inc., Santa Clara CA, USA) equipped with electrospray ionization. The system was controlled with the Agilent MassHunter Workstation

2 Methods and assays

Data Acquisition software (version B.01.04). The column used was an Atlantis[®] T3 C18 column (2.1 x 50 m) with a 3- μ m particle size (Waters Corp., Milford MA, USA). The mobile phase consisted of two eluents: solvent A (H₂O, containing 0.1% formic acid, v/v) and solvent B (acetonitrile, containing 0.1% formic acid, v/v), both delivered at 0.6 mL/min. The gradient was ramped from 95% A/5% B to 5% A/95% B over 1 min, and then hold at 5% A/95% B for 0.1 min. The system was then brought back to 95% A/5% B, resulting in a total duration of 4 min. MS parameters such as fragmentor voltage, collision energy, polarity were optimized individually for each drug, and the molecular ion was followed for each compound in the multiple reaction monitoring mode. The concentrations of the analytes were quantified by the Agilent Mass Hunter Quantitative Analysis software (version B.01.04).

3. Application to current research projects

In this section, the usefulness of the determination of pharmacokinetic properties shall be highlighted with a special focus on cross-validation by different assays.

MAG project: In a recently published paper,³⁹ nanomolar antagonists against the myelin-associated glycoprotein (MAG) were presented. The question was raised whether the concentration of a locally applied antagonist can be expected to be maintained over time. An answer could be given by the aid of three assays, namely for the determination of $\log D_{7.3}$, BBB-PAMPA (blood-brain barrier parallel artificial membrane permeation assay), and stability in artificial cerebrospinal fluid. Even though low distribution coefficients at pH 7.3 ($\log D_{7.3}$) in the range of -0.27 to 0.87 already suggested an evasion of antagonists from the cerebrospinal compartment by passive diffusion to be unlikely, this assumption was controlled by subjecting the compounds to a BBB-PAMPA (blood-brain barrier PAMPA). This assay is used to assess permeation through the blood-brain barrier and is basically a variation of the normal PAMPA with modifications in the lipid composition to better reflect the more lipophilic membrane of the blood-brain barrier. As expected, no permeation could be observed. Furthermore, the stability of the compounds in artificial cerebrospinal fluid was examined and no degradation over 24h occurred. In conclusion, both the high stability and the low potential for passive permeation make the maintenance of the local concentration for the synthesized compounds highly probable.

FimH project: The aim of this project was to find an orally available, potent antibiotic agent with fast renal excretion to treat infections of the urinary tract. Indeed, compounds fulfilling

2.1 The PADMET platform – an overview

these requirements could be synthesized.⁴⁰ The first generation showed desirable properties concerning renal excretion, i.e. low $\log D_{7.4}$ values and pK_a values yielding ionized molecules.⁴¹ Nevertheless, these findings were contradictive to oral availability and indeed no permeation could be observed in the PAMPA. Therefore, a prodrug-approach was envisioned. The carboxy-moiety contained in the first-generation molecules was esterified to address the problem of insignificant membrane permeation by passive diffusion. As a consequence of this modification, PAMPA results were significantly ameliorated and in vivo oral bioavailability could be anticipated. However, in order to still profit of the desired properties of the first-generation compounds rapid liberation of the active principle was a crucial precondition. Indeed, fast and specific ester-cleavage could be demonstrated. In addition, moderate in vitro-plasma protein binding was observed which is in general a desirable finding if fast renal excretion is intended. Animal studies confirmed the properties expected after in vitro studies. In conclusion, the first orally available FimH antagonists could be achieved based on the systematic use of in vitro-ADME tools. The main remaining problem, namely the insufficient solubility of the compounds, is expected to negatively influence both absorption and applicability. Further publications will demonstrate the pharmacokinetic amelioration of the antagonists based on the findings of the first compound series.

Selectine project: The above-mentioned assays were also applied to a third research area, namely to the selectine antagonist project. The most promising antagonists with the lowest IC_{50} values were characterized concerning their pharmacokinetic behavior. PAMPA, $\log D_{7.4}$, plasma protein binding, and critical micelle concentration (CMC) were determined. Especially the determination of the CMC was of critical importance, since micelle formation explained inconsistent assay results.

General observations: Experimental determination often resulted in unexpected outcomes when compared to calculated data. This observation was especially valid for pK_a and $\log D_{7.4}$ determinations and can be attributed to the special compound class of carbohydrate mimetics that are most probably not used for the training of prediction tools. Given the inexpensive and fast determination protocols for both parameters presented above, it is suggested to apply these procedures also in other academic research institutions for a better insight into the expected pharmacokinetic behavior.

2 Methods and assays

4. Summary and conclusions

In this communication, the feasibility of pharmacokinetic compound characterization in an academic environment was demonstrated. An overview of various assays for the determination of physicochemical properties as well as the expected absorption, distribution, metabolism, and elimination behavior was given. Furthermore, detailed experimental procedures for every assay and information about the respective costs and required time were presented.

In general, the different tools of the PADMET platform proved to be useful and stimulating for three different research projects. The predicted behavior could be confirmed in one case with animal studies. Differences between calculated and experimentally determined values were frequently observed. In conclusion, it seems thus reasonable to use various assays in order to identify the most promising compound with both satisfactory pharmacodynamic and pharmacokinetic behavior for in vivo testing.

Acknowledgements

The authors would like to express their gratitude to Dr. Manfred Kansy, Dr. Christoph Funk, Frank Senner, Björn Wagner, and Florian Klammers from F. Hoffmann-La Roche AG for their help and support during the building-up of the PADMET platform.

Bibliography

1. Prentis, R. A.; Lis, Y.; Walker, S. R. Pharmaceutical innovation by the seven UK-owned pharmaceutical companies (1964-1985). *British Journal of Clinical Pharmacology* **1988**, 25, 387-396.
2. Kennedy, T. Managing the drug discovery/development interface. *Drug Discovery Today* **1997**, 2, 436-444.
3. Tang, W.; Lu, A. Drug metabolism and pharmacokinetics in support of drug design. *Curr Pharm Des* **2009**, 15, 2170-83.

2.1 The PADMET platform – an overview

- Lipinski, C. A. Drug-like properties and the causes of poor solubility and poor permeability. *Journal of Pharmacological and Toxicological Methods* **2000**, 44, 235-249.
- Horter, D.; Dressman, J. B. Influence of physicochemical properties on dissolution of drugs in the gastrointestinal tract. *Advanced Drug Delivery Reviews* **2001**, 46, 75-87.
- Lipinski, C. A.; Lombardo, F.; Dominy, B. W.; Feeney, P. J. Experimental and computational approaches to estimate solubility and permeability in drug discovery and development settings. *Advanced Drug Delivery Reviews* **1997**, 23, 3-25.
- Hansch, C.; Leo, A. *Substituent constants for correlation analysis in chemistry and biology*. Wiley: New York, 1979.
- Corti, G.; Maestrelli, F.; Cirri, M.; Zerrouk, N.; Mura, P. Development and evaluation of an in vitro method for prediction of human drug absorption - II. Demonstration of the method suitability. *European Journal of Pharmaceutical Sciences* **2006**, 27, 354-362.
- Kerns, E. H.; Di, L. *Drug-like properties : concepts, structure design and methods : from ADME to toxicity optimization*. Academic Press: Amsterdam ; London, 2008; p xix, 526 p., [2] p. of plates.
- Waring, M. J. Lipophilicity in drug discovery. *Expert Opinion on Drug Discovery* **2010**, 5, 235-248.
- Kansy, M.; Senner, F.; Gubernator, K. Physicochemical high throughput screening: Parallel artificial membrane permeation assay in the description of passive absorption processes. *J. Med. Chem.* **1998**, 41, 1007-1010.
- Artursson, P.; Karlsson, J. Correlation between Oral-Drug Absorption in Humans and Apparent Drug Permeability Coefficients in Human Intestinal Epithelial (Caco-2) Cells. *Biochem. Biophys. Res. Commun.* **1991**, 175, 880-885.
- Irvine, J. D.; Takahashi, L.; Lockhart, K.; Cheong, J.; Tolan, J. W.; Selick, H. E.; Grove, J. R. MDCK (Madin-Darby canine kidney) cells: A tool for membrane permeability screening. *Journal of Pharmaceutical Sciences* **1999**, 88, 28-33.
- Trainor, G. L. The importance of plasma protein binding in drug discovery. *Expert Opinion on Drug Discovery* **2007**, 2, 51-64.
- Oravcová, J.; Böhs, B.; Lindner, W. Drug-protein binding sites. New trends in analytical and experimental methodology. *J Chromatogr B Biomed Appl* **1996**, 677, 1-28.
- Mohutsky, M. A.; Chien, J. Y.; Ring, B. J.; Wrighton, S. A. Predictions of the in vivo clearance of drugs from rate of loss using human liver microsomes for phase I and phase II biotransformations. *Pharmaceutical Research* **2006**, 23, 654-662.

2 Methods and assays

17. Pickett, S. D.; McLay, I. M.; Clark, D. E. Enhancing the hit-to-lead properties of lead optimization libraries. *Journal of Chemical Information and Computer Sciences* **2000**, *40*, 263-272.
18. Mayer, J. M.; Vandewaterbeemd, H. Development of Quantitative Structure Pharmacokinetic Relationships. *Environmental Health Perspectives* **1985**, *61*, 295-306.
19. Mager, D. E. Quantitative structure-pharmacokinetic/pharmacodynamic relationships. *Advanced Drug Delivery Reviews* **2006**, *58*, 1326-1356.
20. van de Waterbeemd, H.; Smith, D. A.; Beaumont, K.; Walker, D. K. Property-based design: Optimization of drug absorption and pharmacokinetics. *J. Med. Chem.* **2001**, *44*, 1313-1333.
21. Michielan, L.; Moro, S. Pharmaceutical Perspectives of Nonlinear QSAR Strategies. *Journal of Chemical Information and Modeling* **2010**, *50*, 961-978.
22. Darvas, F.; Dorman, G.; Papp, A. Diversity measures for enhancing ADME admissibility of combinatorial libraries. *Journal of Chemical Information and Computer Sciences* **2000**, *40*, 314-322.
23. Keseru, G. M.; Makara, G. M. The influence of lead discovery strategies on the properties of drug candidates. *Nature Reviews Drug Discovery* **2009**, *8*, 203-212.
24. Kola, I.; Landis, J. Can the pharmaceutical industry reduce attrition rates? *Nature Reviews Drug Discovery* **2004**, *3*, 711-715.
25. Schuster, D.; Laggner, C.; Langer, T. Why drugs fail-a study on side effects in new chemical entities. *Curr Pharm Des* **2005**, *11*, 3545-59.
26. Kerns, E. H.; Di, L. Pharmaceutical profiling in drug discovery. *Drug Discovery Today* **2003**, *8*, 316-323.
27. Balbach, S.; Korn, C. Pharmaceutical evaluation of early development candidates "the 100 mg-approach". *International Journal of Pharmaceutics* **2004**, *275*, 1-12.
28. Lee, A. C.; Crippen, G. M. Predicting pK_a . *Journal of Chemical Information and Modeling* **2009**, *49*, 2013-2033.
29. van de Waterbeemd, H.; Gifford, E. ADMET in silico modelling: Towards prediction paradise? *Nature Reviews Drug Discovery* **2003**, *2*, 192-204.
30. Ernst, B.; Magnani, J. L. From carbohydrate leads to glycomimetic drugs. *Nature Reviews Drug Discovery* **2009**, *8*, 661-677.
31. Tetko, I. V.; Poda, G. I. Application of ALOGPS 2.1 to predict log D distribution coefficient for Pfizer proprietary compounds. *Journal of Medicinal Chemistry* **2004**, *47*, 5601-5604.

2.1 The PADMET platform – an overview

32. Tetko, I. V.; Gasteiger, J.; Todeschini, R.; Mauri, A.; Livingstone, D.; Ertl, P.; Palyulin, V.; Radchenko, E.; Zefirov, N. S.; Makarenko, A. S.; Tanchuk, V. Y.; Prokopenko, V. V. Virtual computational chemistry laboratory - design and description. *Journal of Computer-Aided Molecular Design* **2005**, 19, 453-463.
33. ALOGPS. <http://www.vcclab.org/lab/alogps/start.html>.
34. Wittwer, M.; Bezencon, J.; Cutting, B.; Wagner, B.; Kansy, M.; Ernst, B. pK_a determination by ¹H-NMR spectroscopy - An old methodology revisited. Submitted to *Bioorg. Med. Chem.*
35. Avdeef, A.; Bendels, S.; Di, L.; Faller, B.; Kansy, M.; Sugano, K.; Yamauchi, Y. PAMPA - Critical factors for better predictions of absorption. *J. Pharm. Sci.* **2007**, 96, 2893-2909.
36. Dressman, J. B.; Thelen, K.; Jantratid, E. Towards quantitative prediction of oral drug absorption. *Clinical Pharmacokinetics* **2008**, 47, 655-667.
37. Mitchell, R. A.; Herbert, D. A.; Carman, C. T. Acid-Base Constants and Temperature Coefficients for Cerebrospinal Fluid. *J Appl Physiol* **1965**, 20, 27-30.
38. *Wissenschaftliche Tabellen Geigy*. 8th Edition, 2nd reprint ed.; Ciba-Geigy Limited: Basel, Switzerland, 1981; p 290.
39. Mesch, S.; Moser, D.; Strasser, D. S.; Kelm, A.; Cutting, B.; Rossato, G.; Vedani, A.; Koliwer-Brandl, H.; Wittwer, M.; Rabbani, S.; Schwaradt, O.; Kelm, S.; Ernst, B. Low Molecular Weight Antagonists of the Myelin-Associated Glycoprotein: Synthesis, Docking, and Biological Evaluation. *Journal of Medicinal Chemistry* **2010**, 53, 1597-1615.
40. Klein, T.; Abgottspon, D.; Wittwer, M.; Rabbani, S.; Herold, J.; Jiang, X.; Kleeb, S.; Lüthi, C.; Scharenberg, M.; Bezencon, J.; Gubler, E.; Pang, L.; Smiesko, M.; Cutting, B.; Schwaradt, O.; Ernst, B. FimH Antagonists for the Oral Treatment of Urinary Tract Infections: From Design and Synthesis to *In Vitro* and *In Vivo* Evaluation. Submitted to *J. Med. Chem.*
41. Varma, M. V. S.; Feng, B.; Obach, R. S.; Troutman, M. D.; Chupka, J.; Miller, H. R.; El-Kattan, A. Physicochemical Determinants of Human Renal Clearance. *Journal of Medicinal Chemistry* **2009**, 52, 4844-4852.

2 Methods and assays

2.2 One method in detail: pK_a determination by NMR

A detailed method description for the pK_a determination by NMR is presented in this chapter. Even though the methodology is not new, it is the first time that its scope and limitations were explored. The numerous advantages of this approach make it a valid tool for pK_a determination in an academic environment.

The first author was responsible for the building up of the assay, including its evaluation, and he performed or supervised all measurements and evaluations. Furthermore, he wrote the manuscript.

This manuscript is in preparation for *ChemMedChem*.

2.2 One method in detail: pK_a determination by NMR

pK_a determination by ¹H-NMR spectroscopy - An old methodology revisited

Matthias Wittwer^a, Jacqueline Bezençon^a, Brian Cutting^a, Bjoern Wagner^b, Manfred Kansy^b,
Beat Ernst^{a,*}

^a Institute of Molecular Pharmacy, Pharmacenter, University of Basel, Klingelbergstrasse 50,
4056 Basel, Switzerland.

^b Pharmaceuticals Division, Non-Clinical Safety, F. Hoffmann-La Roche Ltd., 4070 Basel,
Switzerland.

* *Correspondence:* Prof. Dr. Beat Ernst

Institute of Molecular Pharmacy

University of Basel

Klingelbergstrasse 50

CH-4056 Basel

Tel.: +41 61 267 1551,

Fax: +41 61 267 1552

Keywords: pK_a determination, ¹H-NMR spectroscopy, physicochemical properties,
dissociation constant

Abbreviations: pK_a negative common logarithm of the dissociation constant K_a, NMR
nuclear magnetic resonance, UV ultraviolet, SGA spectral gradient analysis, CE capillary
electrophoresis, EPD electropotentiometric determination.

2 Methods and assays

Abstract

pK_a values of acids and bases have an essential impact on organic synthesis, medicinal chemistry as well as material and food sciences. Especially in drug discovery and development, pK_a values are of utmost importance for the prediction of pharmacokinetic and pharmacodynamic properties, for example permeation through biological barriers, interactions with targets or induction of side effects

To date, different methods for the determination of pK_a s are available, including potentiometric, UV-spectroscopic, and capillary electrophoresis techniques. An additional option is provided by nuclear magnetic resonance (NMR) spectroscopy. The underlying principle is the alteration of chemical shifts of magnetic nuclei (^{13}C and ^1H) depending on the protonation state of an adjacent acidic or basic site. When these chemical shifts are plotted against the pH, the inflection point of the resulting sigmoidal curve defines the pK_a .

Although pK_a determinations by ^1H -NMR spectroscopy are reported for numerous, but mostly isolated cases, the potential of this approach is not yet fully evaluated. We therefore revisited this method with a diverse set of test compounds covering a broad range of pK_a values (pK_a 1 to 14). The much higher natural abundance and gyromagnetic ratio of ^1H compared to ^{13}C leads to higher sensitivity and therefore a reduction of sample consumption and measuring time. A comparison with values obtained by an UV spectroscopic method and with reference values from electropotentiometric determination revealed an excellent correlation and confirmed the reliability and utility of the ^1H -NMR approach. Furthermore, a comparison with computed results showed that the NMR-based approach yielded pK_a values with a lower maximal deviation. Overall, a fast access to pK_a values can prove to be extremely beneficial in organic synthesis as well as in medicinal chemistry.

2.2 One method in detail: pK_a determination by NMR

1. Introduction

pK_a values of acids and bases have an essential impact on organic synthesis, medicinal chemistry as well as material and food sciences. Especially in drug discovery and development, pK_a values are of utmost importance for the prediction of pharmacokinetic and pharmacodynamic properties, for example permeation through biological barriers, interactions with targets or induction of side effects.¹ It is therefore indispensable to have access to this parameter at an early stage of medicinal chemistry program.

For the determination of pK_a values, various experimental approaches based on different analytical methods are commonly used. First, protonation and deprotonation can be followed by spectrophotometric methods.² This approach, the so-called spectral gradient analysis (SGA), offers the advantage of being highly compatible with automation and therefore medium to high-throughput applications. Moreover, pK_as at low and high pHs with overlapping values, and with an appropriate co-solvent for hardly soluble compounds, can be determined. However, the spectrophotometric approach relies on chromophores in proximity to the ionizable centers. Furthermore, depending on the spectroscopic properties, sample concentrations larger than the typically used 50 μM, might be necessary. Finally, sample impurities can lead to distortions of the results.

An alternative approach is based on potentiometric measurements, also called the pH-metric approach, where the pH-change caused by the addition of acid or base enables the determination of pK_a values.³ The advantages are identical to those of the UV-spectroscopic determination. A further benefit is that chromophores are no longer required. However, the impurities remain critical and the method is rather slow. Nevertheless, the pH-metric method is considered the gold standard.⁴

With capillary electrophoresis (CE), a third method for pK_a determination is available.⁵⁻⁹ As the migration time through a capillary depends on the fraction of charged compound, the pK_a value is obtained from the inflection point of the sigmoidal curve obtained when the retention time is plotted against the pH of the buffer. The CE approach is highly flexible, since different determination methods, such as spectroscopy or nitrogen detection, can be employed. Furthermore, it is compatible with high-throughput requirements and sample consumption is very low with about 0.2 ng per injection.¹⁰ Unlike in the previously described methods,

2 Methods and assays

sample impurities usually do not influence the results, since CE is a separation technique. One drawback is the requirement of 50 μM solutions, which could cause problems with compounds of low solubility.

Finally, in silico $\text{p}K_{\text{a}}$ prediction is fast and inexpensive. Nevertheless, commercial software needs to be validated and trained when applied to a new class of compounds.¹¹

Overall, $\text{p}K_{\text{a}}$ determinations depend on expensive, automated instrumentation or on laborious and time-consuming manual titration experiments. Furthermore, sample consumption is often critical. Since typically only milligram amounts of test compounds are available and the investment in expensive equipment is not justifiable for single $\text{p}K_{\text{a}}$ determinations, alternative approaches are still required.

NMR offers an interesting alternative. Although specific approaches based on ^{15}N -, ^{11}B - or ^{19}F -NMR spectroscopy are reported,¹²⁻¹⁴ the pH-dependence of chemical shifts of ^{13}C nuclei adjacent to ionizable functions is a more general approach for $\text{p}K_{\text{a}}$ determinations¹⁵ and has successfully been employed for the determination of both $\text{p}K_{\text{a}}$ s of acids¹⁶⁻²⁰ and bases.^{12,21} Additionally, ^{13}C -NMR spectroscopy (often in combination with ^1H - or ^{15}N -NMR) allows the determination of $\text{p}K_{\text{a}}$ values in isotopically enriched proteins. The applicability has been demonstrated with *Bacillus circulans* Xylanase²² or calmodulin.²³ Furthermore, pH-implications on structure^{24,25} and functionality^{26,27} can be investigated as well. However, without isotope enrichment, the low natural abundance of ^{13}C nuclei (1.11%) results in prolonged measurement times, a substantial drawback of $\text{p}K_{\text{a}}$ -determination by ^{13}C -NMR spectroscopy.

Beneficial effects, such as low sample consumption and short measurement times, which result from the higher abundance of ^1H , lead to an improvement of sensitivity by a factor of 3200²⁸ and favor $\text{p}K_{\text{a}}$ determination by ^1H -NMR. Various applications, i.e. $\text{p}K_{\text{a}}$ determination of amino acids,²⁹ residues in peptides,³⁰ and whole proteins such as human hemoglobin,³¹ myoglobin,³² protein tyrosine phosphatase,³³ thiosubtilisin,³⁴ hen and turkey lysozymes,³⁵ human thioredoxin,³⁶ and *Myobacterium tuberculosis* RecA intein³⁷ have been reported. Moreover, the $\text{p}K_{\text{a}}$ values for single compounds^{38,39} and for small, restricted datasets⁴⁰⁻⁴² were also determined. Finally, the method can be used to determine the micro-speciation of compounds,^{43,44} i.e. the site-specific $\text{p}K_{\text{a}}$ values in multiprotic compounds that might overlap

2.2 One method in detail: pK_a determination by NMR

and hence lead to only one measurable macro-pK_a. It has been shown that micro-pK_a values can have important implications on pharmacokinetic behavior.⁴⁵ However, to our knowledge, the broad applicability of the method in drug discovery has not been demonstrated. We therefore explored scope and limitation of the ¹H-NMR approach for pK_a determination regarding measurement time and sample consumption.

2. Material and methods

Nuclear magnetic resonance spectroscopy was performed on a Bruker Avance III Ultra Shield at 500 MHz (¹H-NMR) spectrometer. Chemical shifts are given in ppm. Presaturation experiments were performed in order to clearly see the diluted ligand without complications due to the larger H-O-D signal.⁴⁶

Deuterium oxide and deuterated d₆-dimethyl sulfoxide were purchased from Armar Chemicals. Dimethyl sulfoxide, N-acetylneuraminic acid, diazepam, phenol, papaverin, propranolol, paracetamol, neocuproine, 5-nitro-1,10-phenanthroline, 4,7-dimethoxy-1,10-phenanthroline, 4-phenylbutylamine, serotonin, benzoic acid, aniline, phenobarbital, diltiazem, promethazine, sucrose, and uracil were purchased from Sigma. Imidazole was purchased from Acros Organics. Dioxane was obtained from Fluka. 1,10-phenanthroline and 2,2'-bipyridine were purchased from Riedel-de Haën. Codeine phosphate, acetylsalicylic acid, benzocaine, and phenazone were purchased from Siegfried AG. 4-Aminopyridine-2-carboxylic acid was purchased from Apollo Scientific. 2-Amino-1,10-phenanthroline was purchased from Specs.

For an optimal planning of the experiments, the software CS ChemBioDraw[®] Ultra (version 11.0.1) was used to predict ¹H-NMR spectra of the compounds in the various ionization states.

For the measurement, a 10⁻⁴ M solution of the analyte in D₂O was prepared (primary solution) and dioxane was added as an internal standard to obtain a 50 μM solution. When DMSO stock solutions were used, DMSO was used as internal standard. The primary solution was aliquoted into 8 to 15 samples and the pH values of the samples were adjusted (close to the predicted pK_a, at the pK_a itself, and at two extreme pH values, e.g. 1 and 13.5) with 0.5 M or 8 M NaOH and 0.5 M or 4 M HCl, respectively. Aliquots (500 μl) of samples at each pH value

2 Methods and assays

were transferred to NMR tubes and the recorded spectra were analyzed with the software MestReNova (Mestrelab research, version 5.2.5-4119). The resulting chemical shifts of a specific proton close to the ionizable function were plotted against the pH value resulting in a sigmoidal curve (software Prism[®], GraphPad, version 5.0b). The pK_a was determined from the inflection point (Figure 1). Alternatively, it was recently shown that Excel[®] can be used for the same purpose.⁴⁷ Since the measurements were performed in D₂O, 0.41 needs to be subtracted from the result to yield the values for a water environment.³⁰

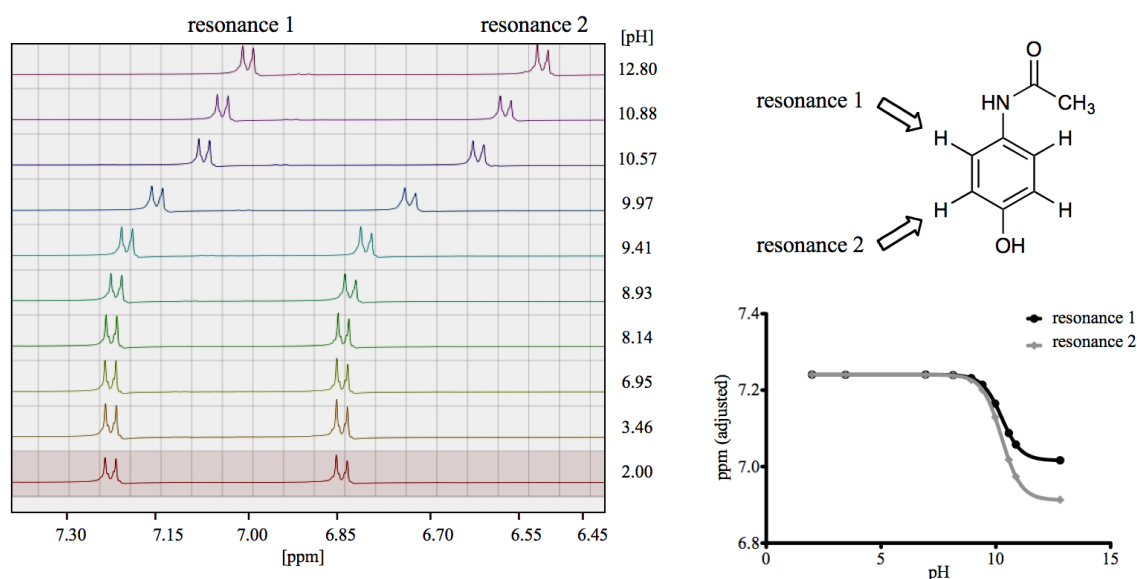


Figure 1: Chemical shift dependence on the ionization state of the analyte paracetamol. When plotted against the corresponding pH values, the pK_a value corresponds to the inflection point of the resulting sigmoidal curve. The downfield doublet is the resonance for the protons in *meta*-position to the hydroxy-moiety whereas the upfield one belongs to those in *ortho*-position.

3. Results and discussion

In previously reports, e.g.,^{15,29} pK_a values were determined by measuring chemical shifts using typically more than 15, and only in some isolated cases, e.g.,³⁹ 9 data points. To determine an optimal compromise between data quality on the one and sample and time consumption on the other hand the number of data points was optimized. Table 1 shows that 9 data points yield in general excellent results for pK_a over eleven orders of magnitude (pK_a values from 1.44 to 12.6). However, for compounds with extremely low or high pK_a values such as uracil, the number of data points had to be increased, expanding the applicability range by almost another order of magnitude (pK_a s up to 13.3).

2.2 One method in detail: pK_a determination by NMR

The ¹H-NMR approach allows pK_a determinations either with low sample consumption or short measurement time. For the first case, 50 μM solutions at 9 pH-values are usually sufficient. The approach is also of utility for compounds with low solubility. In addition, the required amount of a sample can be further reduced by using Shigemi NMR tubes, requiring as little as 200 μL per sample. When only very limited sample amounts are available, one sample with a progressional pH change is used. By this approach, as little as 6.25 μg of a compound with a molecular weight of 500 are required or even less (2.5 μg) when a Shigemi tube is used. As a consequence, the pK_a value of compounds with a solubility of as little as 12.5 ng/mL can still be assigned. Furthermore, since NMR is a non-destructive method, the analyte can be recovered provided no pH-dependent decomposition occurred. Finally, when a fast determination is required, samples with higher concentrations can be used. The overall measurement time is typically in the range of less than 5 minutes and thereby reduced by a factor of 10 compared to ¹³C-NMR spectroscopy.

For the validation of the approach a homogeneous data set is required. When not indicated otherwise, the reference values obtained by potentiometry were therefore taken from one reference.¹⁰ For comparison, pK_a-values for a small set of phenanthrolines were determined by UV spectrophotometry (SGA) on a Sirius instrument. The results are in excellent agreement with both values obtained by ¹H-NMR spectroscopy and by reference values of potentiometric titrations (Table 1). By contrast, *in silico* predictions of pK_a-values calculated by EPIK⁴⁸ show a much higher maximal deviation (3.83 pH-units) than ¹H-NMR-based results (0.51 pH-units).

pK_a values determined by ¹H-NMR differ typically by +/- 0.3 units from literature data (Table 1). Only for five compounds these limits were exceeded, with a difference of maximally -0.48 to +0.51. The reliability of the approach is also highlighted in Figure 2, which shows the excellent correlation to reference values over 12 orders of magnitude reflected by an R² value of 0.99.

A clear advantage of the NMR method is the possibility to start from a DMSO stock solution as usually prepared for biological testing. In this case, the DMSO peak (at 2.71 ppm)⁴⁹ is used as internal standard. A possible disadvantage is the superposition of a resonance of interest of the test compound with the DMSO resonance. In contrast to earlier publications, e.g.,³⁰ HCl

2 Methods and assays

and NaOH can be used instead of DCl and NaOD for the adjustment of the pHs of the samples. The small amounts of added base or acid do not generate spectral disturbances when the H₂O signal is suppressed, e.g..^{29,42}

Table 1: p*K*_a values obtained by NMR-spectroscopic and spectrophotometry compared to published data,¹⁰ unless indicated otherwise, with deviations. EPD: electropotentiometric determination, * deviation from spectrophotometrically determined values.

| Compound | NMR | p <i>K</i> _a by spectro-photometry | published p <i>K</i> _a (EPD) ¹⁰ | Deviation from published p <i>K</i> _a [p <i>H</i> units] | Computed p <i>K</i> _a (Epik) ⁴⁸ |
|-----------------------------------|--------------|---|---|---|---|
| Phenazone | 0.94 | | 1.44 | 0.5 | 4.92 |
| Benzocaine | 2.45 | | 2.39 | -0.06 | 5.52 |
| Neuraminic acid | 2.49 | | 2.60 | 0.11 | 5.6 |
| Diazepam | 3.07 | | 3.35 | 0.28 | 3.88 |
| Acetyl salicylic acid | 3.24 | | 3.50 | 0.26 | 5.08 |
| Benzoic acid | 4.02 | | 3.98 | -0.04 | 5.41 |
| Aniline | 4.38 | | 4.60 ⁵⁰ | 0.22 | 4.5 |
| Papaverine | 6.1 | | 6.39 | 0.29 | 9.32 |
| Imidazol | 6.95 | | 6.95 ⁵¹ | 0 | 6.67 |
| Phenobarbital | 7.26 | | 7.49 | 0.23 | 6.64 |
| Codeine | 8.15 | | 8.22 | 0.07 | 9.42 |
| Diltiazem | 8.5 | | 8.02 | -0.48 | 9.16 |
| Promethazine | 9.21 | | 9.00 | -0.21 | 8.75 |
| Propranolol | 9.38 | | 9.53 | 0.15 | 9.09 |
| Paracetamol | 9.84 | | 9.63 | -0.21 | 10.05 |
| Phenol | 9.97 | | 10.01 | 0.04 | 9.92 |
| 4-Phenylbutylamine | 10.53 | | 10.50 | -0.03 | 9.94 |
| Serotonin | 10.92, 10.08 | | 10.91, 9.97 | -0.01, -0.11 | 9.84, 9.73 |
| Sucrose | 12.93 | | 12.60 | -0.33 | 13.08 |
| Uracil | 13.72, 9.34 | | 13.28, 9.21 | -0.44, -0.31 | 9.45, 9.1 |
| 1,10-Phenanthroline | 4.73 | 5.00 | 4.80 ⁵² | 0.27* | 4.92 |
| 2-Amino-1,10-phenanthroline | 6.56 | 6.73 | | 0.17 | 5.52 |
| 4,7-Dimethoxy-1,10-phenanthroline | 6.42 | 6.69 | | 0.27 | 5.6 |
| 5-Nitro-1,10-phenanthroline | 3.15 | 3.66 | 3.57 ⁵² | 0.51* | 3.88 |
| 5-Amino-1,10-phenanthroline | 5.37 | 5.57 | 5.78 ⁵³ | 0.2* | 5.08 |
| Neocuproin | 5.63 | 5.74 | 6.15 ⁵⁴ | 0.11* | 5.41 |
| 2,2-Bipyridine | 4.54 | 4.54 | 4.44 ⁵⁴ | 0* | 4.5 |
| 4-Aminopyridine-2-carboxylic acid | 9.57, 1.01 | 9.43 | | -0.14 | 9.32, 0.78 |

2.2 One method in detail: pK_a determination by NMR

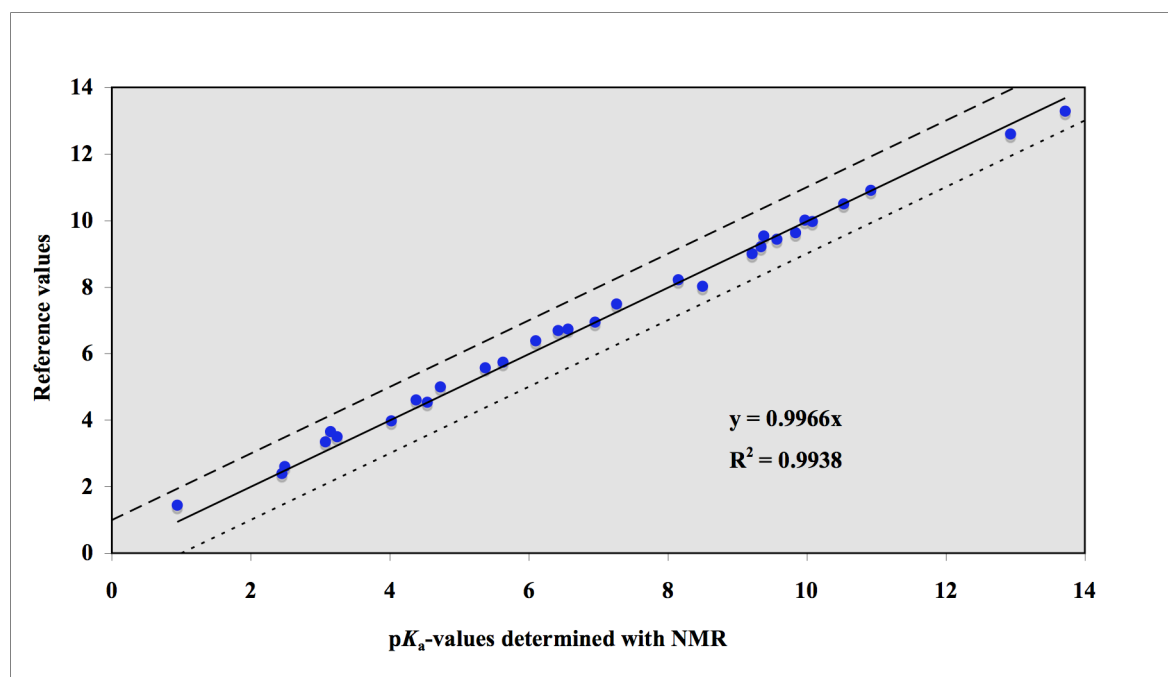


Figure 2: Comparison of published data with values obtained by the presented ¹H-NMR method.

The presented ¹H-NMR method is suited to obtain a reasonable estimate of pK_a values rather than high-precision data. Therefore, spectra at merely 8 to 15 pH values per compound are recorded compared to the much higher number of data points required for other methods. Furthermore, the ionic strength of the solution was not considered and the determination in D₂O is only a surrogate for the determination in H₂O. Nevertheless, despite these constraints, accurate results, which are reproducible over time, were obtained.

However, there are also some limitations with the presented method, e.g. when the chemical shift of protons adjacent to ionizable centers are not resolved. In these cases, other NMR methods, including ¹³C-, ¹⁵N- or ¹⁹F-NMR spectroscopy or 2D-methods, such as HSQC, can be applied. The latter approach allows to determine the protonation site, an information not always evident in other approaches. Furthermore, by the use of different solvents (e.g. deuterated methanol), the pK_a values of sparsely soluble compounds can be determined. In those cases measurements have to be performed at different water/organic solvent ratios, to allow correction for the influence of the organic solvent on pK_a, by applying e.g. Yasuda-Shedlovsky extrapolations.^{55,56}

2 Methods and assays

4. Conclusion

In conclusion, a $^1\text{H-NMR}$ method was revisited, which allows a fast, sensitive and reliable determination of pK_a values over a broad pH-range. In comparison to other methods, such as potentiometric titration or capillary electrophoresis, the sample consumption is low. In addition, since an NMR instrument is available in nearly every synthetic chemistry lab, investment in additional equipment is not necessary.

Acknowledgements

The authors gratefully acknowledge the financial support by the Swiss National Science Foundation (grant no. 200020120628) and thank Dr. M. Smiesko for the calculation of the pK_a values with EPIK.

References

1. Hörter, D.; Dressman, J. B. *Adv. Drug Deliv. Rev.* **2001**, *46*, 75-87.
2. Box, K.; Bevan, C.; Comer, J.; Hill, A.; Allen, R.; Reynolds, D. *Anal. Chem.* **2003**, *75*, 883-892.
3. Avdeef, A. *J. Pharm. Sci.* **1993**, *82*, 183-190.
4. Kerns, E. H.; Di, L. *Drug-like Properties: Concepts, Structure Design and Methods*; Academic Press: Burlington, 2008, p. 275.
5. Ishihama, Y.; Nakamura, M.; Miwa, T.; Kajima, T.; Asakawa, N. *J. Pharm. Sci.* **2002**, *91*, 933-942.
6. Cleveland, J. A., Jr.; Benko, M. H.; Gluck, S. J.; Walbroehl, Y. M. *J. Chromatogr.* **1993**, *652*, 301-308.
7. Gluck, S. J.; Cleveland, J. A., Jr. *J. Chromatogr. A* **1994**, *680*, 43-48.
8. Gluck, S. J.; Cleveland, J. A., Jr. *J. Chromatogr. A* **1994**, *680*, 49-56.
9. Beckers, J. L.; Everaerts, F. M.; Ackermans, M. T. *J. Chromatogr.* **1991**, *537*, 407-428.
10. Avdeef, A. "Absorption and Drug Development: Solubility, Permeability and Charge State", Wiley-Interscience, New Jersey, **2003**, p. 32.
11. Lee, A. C.; Crippen, G. M. *J. Chem. Inf. Model.* **2009**, *49*, 2013-2033.
12. Paschal, J. W.; Dorman, D. E. *Org. Magn. Res.* **1978**, *11*, 632-634.
13. Tossell, J. A. *Geochim. Cosmochim. Acta* **2005**, *69*, 5647-5658.

2.2 One method in detail: pKa determination by NMR

14. Taft, R. W.; Levins, P. L. *Anal. Chem.* **1962**, *34*, 436-437.
15. Berger, S.; Braun, S. 200 and more NMR Experiments: A Practical Course; Wiley-Interscience: New Jersey, 2004, p. 290.
16. Cistola, D. P.; Small, D. M.; Hamilton, J. A. *J. Lipid Res.* **1982**, *23*, 795-799.
17. London, R. E. *J. Magn. Reson.* **1980**, *38*, 173-177.
18. Holmes, D. L.; Lightner, D. A. *Tetrahedron* **1996**, *52*, 5319-5338.
19. Farcasiu, D.; Ghenciu, A. *J. Prog. Nucl. Magn. Reson. Spectrosc.* **1996**, *29*, 129-168.
20. Reniero, F.; Guillou, C.; Calabi, L.; Paleari, L.; Biondi, L.; De Miranda, M.; Ghelli, S. *Anal. Biochem.* **2003**, *319*, 195-205.
21. Delfini, M.; Segre, A. L.; Conti, F.; Barbucci, R.; Barone, V.; Ferruti, P. *J. Chem. Soc., Perkin Trans. 2* **1980**, 900-903.
22. McIntosh, L. P.; Hand, G.; Johnson, P. E.; Joshi, M. D.; Körner, M.; Plesniak, L. A.; Ziser, L.; Wakarchuk, W. W.; Withers, S. G. *Biochemistry* **1996**, *35*, 9958-9966.
23. Zhang, M.; Vogel, H. J. *J. Biol. Chem.* **1993**, *268*, 22420-22428.
24. Clark, A. T.; Smith, K.; Muhandiram, R.; Edmondson, S. P.; Shriver, J. W. *J. Mol. Biol.* **2007**, *372*, 992-1008.
25. Forsyth, W. R.; Antosiewicz, J. M.; Robertson, A. D. *Proteins*, **2002**, *48*, 388-403.
26. Spink, E.; Cosgrove, S.; Rogers, L.; Hewage, C.; Malthouse, J. P. G. *J. Biol. Chem.* **2007**, *282*, 7852-7861.
27. O'Sullivan, D. B.; O'Connell, T. P.; Mahon, M. M.; Koenig, A.; Milne, J. J.; Fitzpatrick, T. B.; Malthouse, J. P. G. *Biochemistry* **1999**, *38*, 6187-6194.
28. Levitt, M. H. Spin Dynamics: Basics of Nuclear Magnetic Resonance; Wiley and Sons: New York, 2001, p. 416.
29. Rabenstein, D. L.; Sayer, T. L. *Anal. Chem.* **1976**, *48*, 1141-1146.
30. Krezel, A.; Bal, W. *J. Inorg. Biochem.* **2004**, *98*, 161-166.
31. Perutz, M. F.; Gronenborn, A. M.; Clore, G. M.; Fogg, J. H.; Shih, D. T.-b. *J. Mol. Biol.* **1985**, *183*, 491-498.
32. Bashford, D.; Case, D. A.; Dalvit, C.; Tennant, L.; Wright, P. E. *Biochemistry* **1993**, *32*, 8045-8056.
33. Tishmack, P. A.; Bashford, D.; Harms, E.; Van Etten, R. L. *Biochemistry* **1997**, *36*, 11984-11994.
34. Kahyaoglu, A.; Jordan, F. *Prot. Sci.* **2002**, *11*, 965-973.
35. Bartlik, K.; Redfield, C.; Dobson, C. M. *Biophys. J.* **1994**, *66*, 1180-1184.

2 Methods and assays

36. Quijada, J.; Lopez, G.; Versace, R.; Ramirez, L.; Tasayco, M. L. *Biophys. Chem.* **2007**, *129*, 242-250.
37. Du, Z.; Shemella, P. T.; Liu, Y.; McCallum, S. A.; Pereira, B.; Nayak, S. K.; Belfort, G.; Belfort, M.; Wang, C. *J. Am. Chem. Soc.* **2009**, *131*, 11581-11589.
38. Orfi, L.; Larive, C. K.; LeVine, S. M. *Lipids* **1997**, *32*, 1035-1040.
39. Szakács, Z.; Béni, S.; Varga, Z.; Örfi, L.; Kéri, G.; Noszál, B. *J. Med. Chem.* **2005**, *48*, 249-255.
40. Handloser, C. S.; Chakrabarty, M. R.; Mosher, M. W. *J. Chem. Educ.* **1973**, *50*, 510-511.
41. Szakács, Z.; Hägele, G. *Talanta* **2004**, *62*, 819-825.
42. Grycova, L.; Dommissse, R.; Pieters, L.; Marek, R. *Magn. Reson. Chem.* **2009**, *47*, 977-981.
43. Tanokura, M. *Biochim. Biophys. Acta* **1983**, *742*, 576-585.
44. Box, K. J.; Donkor, R. E.; Jupp, P. A.; Leader, I. P.; Trew, D. F.; Turner, C. H. *J. Pharm. Biomed. Anal.* **2008**, *47*, 303-311.
45. Marosi, A.; Kovacs, Z.; Béni, S.; Kökösi, J.; Noszál, B. *Eur. J. Pharm. Sci.* **2009**, *37*, 321-328.
46. Box, A. *J. Magn. Reson.* **1985**, *65*, 142-145.
47. Kemmer, G.; Keller, S. *Nat. Protoc.* **2010**, *5*, 267-281.
48. Epik, version 2.0, Schrödinger, LLC, New York, NY, 2009. Shelley, J. C.; Cholleti, A.; Frye, L. L.; Greenwood, J. R.; Timlin M. R.; Uchiyama, M. *J. Comput. Aided Mol. Des.* **2007**, *21*, 681-691.
49. Gottlieb, H. E.; Kotlyar, V.; Nudelman, A. *J. Org. Chem* **1997**, *62*, 7512-7515.
50. Altun, Y. *J. Solution Chem.* **2004**, *33*, 479-497.
51. Bruice, T. C.; Schmir, G. L. *J. Am. Chem. Soc.* **1958**, *80*, 148-156.
52. Brandt, W. W.; Gullstrom, D. K. *J. Am. Chem. Soc.* **1952**, *74*, 3532-3535.
53. Ramirez-Silva, M. T.; Gomez-Hernandez, M.; Pacheco-Hernandez, M. L.; Rojas-Hernandez, A.; Galicia, L. *Spectrochim. Acta A Mol. Biomol. Spectrosc.* **2004**, *60*, 781-789.
54. Yasuda, M.; Sone, K.; Yamasaki, K. *J. Phys. Chem.* **1956**, *60*, 1667-1668.
55. Sarmini, K.; Kenndler, E. *J. Biochem. Biophys. Methods* **1999**, *38*, 123-137.
56. Avdeef, A.; Box, K. J.; Comer, J. E. A.; Gilges, M.; Hadley, M.; Hibbert, C.; Patterson, W.; Tam, K. Y. *J. Pharm. Biomed. Anal.* **1999**, *20*, 631-641.

3.1 Pharmacokinetic properties of FimH antagonists with biphenyl-moiety

3 Results and discussion

The PADMET-platform was used to determine pharmacokinetic properties of compounds from various research projects. A choice of results and their implications is presented in this chapter.

3.1 Pharmacokinetic properties of FimH antagonists with biphenyl-moiety

The aim of the FimH project is to find highly active and orally available antibiotics to treat urinary tract infections. The PADMET platform was used to identify compounds with promising properties concerning their absorption from the gastrointestinal tract and a fast renal excretion.

Matthias Wittwer performed or supervised all experiments aimed at the determination of pharmacokinetic parameters and the interpretation of the results (except for the metabolic stability assay). Furthermore, he helped evaluating and interpreting the in vivo PK-experiments and wrote the experimental part (together with S. Kleeb) as well as the discussion part concerning the experiments mentioned above.

This work was published in the *Journal of Medicinal Chemistry*:

Klein, T.*; Abgottspon, D.*; Wittwer, M.*; Rabbani, S.*; Herold, J.*; Jiang, X.; Kleeb, S.; Lüthi, C.; Scharenberg, M.; Bezençon, J.; Gubler, E.; Pang, L.; Smiesko, M.; Cutting, B.; Schwardt, O.; Ernst, B. FimH Antagonists for the Oral Treatment of Urinary Tract Infections: From Design and Synthesis to in Vitro and in Vivo Evaluation *J. Med. Chem.* **2010**, *53*, 8627-8641.

* These authors contributed equally to the project.

Copyright © 2010, American Chemical Society

3.1 Pharmacokinetic properties of FimH antagonists with biphenyl-moiety

FimH Antagonists for the Oral Treatment of Urinary Tract Infections: From Design and Synthesis to in Vitro and in Vivo Evaluation

Tobias Klein,[†] Daniela Abgottspon,[†] Matthias Wittwer,[†] Said Rabbani,[†] Janno Herold,[†] Xiaohua Jiang, Simon Kleeb, Christine Lüthi, Meike Scharenberg, Jacqueline Bezençon, Erich Gubler, Lijuan Pang, Martin Smiesko, Brian Cutting, Oliver Schwardt, and Beat Ernst*

Institute of Molecular Pharmacy, Pharmacenter, University of Basel, Klingelbergstrasse 50, CH-4056 Basel, Switzerland.

[†]These authors contributed equally to the project

Received August 4, 2010

Urinary tract infection (UTI) by uropathogenic *Escherichia coli* (UPEC) is one of the most common infections, particularly affecting women. The interaction of FimH, a lectin located at the tip of bacterial pili, with high mannose structures is critical for the ability of UPEC to colonize and invade the bladder epithelium. We describe the synthesis and the in vitro/in vivo evaluation of α -D-mannosides with the ability to block the bacteria/host cell interaction. According to the pharmacokinetic properties, a prodrug approach for their evaluation in the UTI mouse model was explored. As a result, an orally available, low molecular weight FimH antagonist was identified with the potential to reduce the colony forming units (CFU) in the urine by 2 orders of magnitude and in the bladder by 4 orders of magnitude. With FimH antagonist **16b**, the great potential for the effective treatment of urinary tract infections with a new class of orally available antiinfectives could be demonstrated.

Introduction

Urinary tract infection (UTI⁶) is one of the most common infections, affecting millions of people each year. Particularly affected are women, who have a 40–50% risk to experience at least one symptomatic UTI episode at some time during their life. In addition, more than half of them experience a relapse of the infection within 6 months.^{1,2}

Although UTIs rarely cause severe diseases such as pyelonephritis or urosepsis, they are associated with high incidence rate and consume considerable healthcare resources.³ Uropathogenic *Escherichia coli* (UPEC) are the primary cause of UTIs, accounting for 70–95% of the reported cases. Symptomatic UTIs require antimicrobial treatment, often resulting in the emergence of resistant microbial flora. As a consequence, treatment of consecutive infections becomes increasingly difficult because the number of antibiotics is limited and the resistance of *E. coli* is increasing, especially in patients with diabetes, urinary tract anomaly, paraplegy, and those with permanent urinary catheter. Therefore, a new approach for the prevention and treatment of UTI with inexpensive, orally

applicable therapeutics with a low potential for resistance would have a great impact on patient care, public health care, and medical expenses.

UPEC strains express a number of well-studied virulence factors used for a successful colonization of their host.^{3–5} One important virulence factor is located on type 1 pili, allowing UPEC to adhere and invade host cells within the urinary tract. It enables UPEC to attach to oligomannosides, which are part of the glycoprotein uroplakin Ia on the urinary bladder mucosa. This initial step prevents the rapid clearance of *E. coli* from the urinary tract by the bulk flow of urine and at the same time enables the invasion of the host cells.^{3,6}

Type 1 pili are the most prevalent fimbriae encoded by UPEC, consisting of the four subunits FimA, FimF, FimG, and FimH, the latter located at the tip of the pili.⁷ As a part of the FimH subunit, a carbohydrate-recognizing domain (CRD) is responsible for bacterial interactions with the host cells within the urinary tract.⁶ The crystal structure of the FimH-CRD was solved⁸ and its complexes with *n*-butyl α -D-mannopyranoside⁹ and Man α (1–3)[Man α (1–6)]Man¹⁰ recently became available.

Previous studies showed that vaccination with FimH adhesin inhibits colonization and subsequent *E. coli* infection of the urothelium in humans.^{11,12} In addition, adherence and invasion of host cells by *E. coli* can also be prevented by α -D-mannopyranosides, which are potent antagonists of interactions mediated by type 1 pili.¹³ Whereas α -D-mannopyranosides efficiently prevent adhesion of *E. coli* to human urothelium, they are not exhibiting a selection pressure to induce antimicrobial resistance. Furthermore, environmental contamination is less problematic compared to antibiotics.¹⁴

More than two decades ago, Sharon and co-workers have investigated various mannosides and oligomannosides as

*To whom correspondence should be addressed. Phone: +41 61 267 1551. Fax: +41 61 267 1552. E-mail: beat.ernst@unibas.ch.

⁶ Abbreviations: AUC, area under the curve; Caco-2 cells, Caucasian colon adenocarcinoma cells; CFU, colony forming units; CRD, carbohydrate recognition domain; DC-SIGN, dendritic cell-specific intercellular adhesion molecule-3-grabbing nonintegrin; CES, carboxylesterase; IC₅₀, half maximal inhibitory concentration; iv, intravenous; D, distribution coefficient; GPE, guinea pig erythrocytes; LC-MS, liquid chromatography–mass spectrometry; MBP, mannose-binding protein; PAMPA, parallel artificial membrane permeation assay; *P*_{app}, apparent permeability; *P*_e, effective permeation; po, peroral; PPB, plasma protein binding; PSA, polar surface area; S, solubility; SAR, structure–activity relationship; sGF, simulated gastric fluid; sIF, simulated intestinal fluid; TEER, transepithelial resistance; UPEC, uropathogenic *E. coli*; UTI, urinary tract infection.

3 Results and discussion

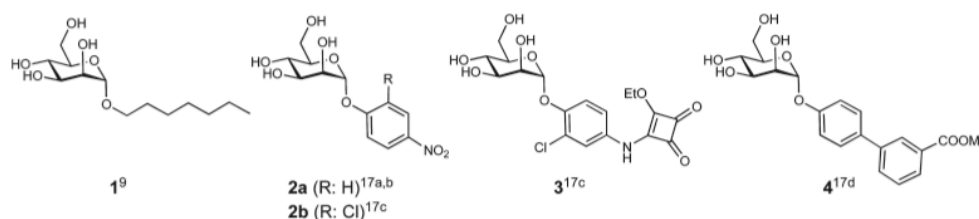
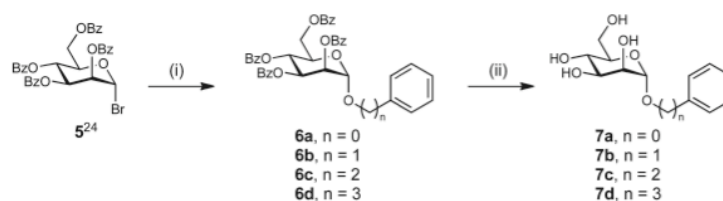


Figure 1. Known alkyl (1) and aryl (2–4) α -D-mannosides exhibiting nanomolar affinities.

Scheme 1. Phenyl α -D-mannosides **7a–7d** with Spacers of Different Lengths between the Carbohydrate Moiety and the Phenyl Substituent^a



^a(i) $\text{Ph}(\text{CH}_2)_n\text{OH}$, $\text{Hg}(\text{CN})_2$, HgBr_2 , DCM, 2 h to 7 d, rt, 57–99%; (ii) NaOMe , MeOH , 6–16 h, rt, 48–91%.

potential antagonists for type 1 fimbriae-mediated bacterial adhesion.¹⁵ However, for these mannosides, only weak interactions in the milli- to micromolar range were observed. In contrast, numerous reports on glycoconjugate dendrimers with nanomolar affinities have been published.¹⁶ However, on the basis of their large molecular weight and high polarity, they are predicted to exhibit only poor intestinal absorption and are therefore not amenable for oral dosing. Recently, some isolated reports on high affinity monovalent FimH antagonists were published¹⁷ and, in one case, a systematic structure–activity relationship (SAR) profile was established.^{17d} In summary,^{8,9,15–19} long chain alkyl and aryl mannosides (selected examples are presented in Figure 1) displayed the highest affinity, likely due to hydrophobic interactions with two tyrosines and one isoleucine forming the entrance to the binding site, the so-called “tyrosine gate”.¹⁸ Because binding affinities were obtained from diverse assay formats,^{9,17c,20} a direct comparison of the affinities is difficult. On the basis of various crystal structures of methyl-⁸ and *n*-butyl α -D-mannoside¹⁸ as well as oligomannose-3⁹ bound to FimH, Han et al. recently presented a rationale for the design of arylmannosides with increased affinities.^{17d}

To date, a few reports on the in vivo potential of methyl α -D-mannoside^{10,21,22} and *n*-heptyl α -D-mannoside (1)¹⁰ are available. In all cases, the FimH antagonists were directly instilled into the bladder concomitantly with uropathogenic *E. coli* (UPEC). In this communication, we present for the first time nanomolar FimH antagonists exhibiting appropriate pharmacokinetic properties for iv and oral treatment of urinary tract infections.

Results and Discussion

Identification of Lead Mannoside. In most of the reported FimH antagonists, aromatic aglycones have been applied.¹⁷ However, only limited information on the optimal spacer length between the mannose moiety and the aromatic substituent is available. Generally, the aromatic moiety is directly fused to the anomeric oxygen.^{17a–d} Extended spacers containing one^{17b,d} or two^{17c} methylene moieties were also reported,

however, the corresponding antagonists are not really comparable to each other because different assay formats were used for their evaluation. For the identification of the optimal spacer length, we therefore synthesized mannosides **7a–d** (Scheme 1). In a competitive binding assay,²³ mannoside **7a** showed a slightly higher affinity (Table 1, entry 2) compared with **7b–7d** (see Table 1, entries 3–5), confirming recent data for **7a** and **7b**.^{17d}

From the crystal structure of *n*-butyl α -D-mannoside bound to FimH,¹⁸ it becomes obvious that the hydrophobic rim formed by Tyr48, Tyr137, and Ile52 is not reached by an anomeric phenyl group. An extension by a second aromatic ring, i.e. a biphenyl α -D-mannoside, however, should be compatible for π – π stacking. Indeed, some recently published representatives of this compound class show excellent affinities.^{17d}

To achieve an optimal fit with the hydrophobic binding site of FimH, the conformation of the biphenyl aglycone in **1** was modified by different substitution patterns on ring A (Figure 2). Because electron poor aromatic rings substantially improve the binding affinities of FimH antagonists (a 10-fold improvement is reported for **2B** vs **2A**^{17c}), chloro substituents on ring A were used for the spatial exploration of the binding site. With substituents in *ortho*-position, only a minor change of the dihedral angle Φ_1 is observed (-3.3° to -0.7°). However, by an increased rotational barrier, the conformational flexibility is limited. The dihedral angle Φ_2 between the conjugated aromatic rings results from an interplay between π -conjugation and steric effects.^{24,25} By migrating the substituent to the *meta*-position, the torsion angle Φ_2 is substantially influenced. Whereas unsubstituted biphenyls show a global twisted minimum at a torsion angle Φ_2 of approximately 39° ,²⁶ substituents in the *meta*-position favor an increase of Φ_2 to 60° . Details of the conformational analyses are summarized in the Supporting Information.

Design Strategy for Intestinal Absorption and Renal Elimination. Besides high affinity, drug-like pharmacokinetic properties are a prerequisite for a successful in vivo application. In the present case, orally available FimH antagonists

3.1 Pharmacokinetic properties of FimH antagonists with biphenyl-moiety

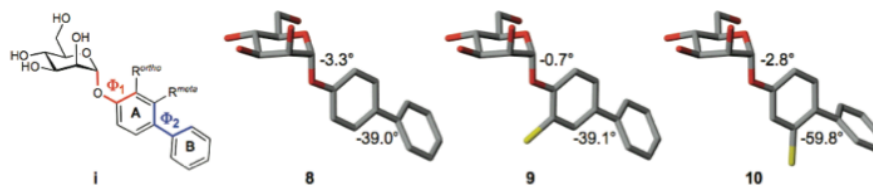


Figure 2. Conformational changes of the biphenyl aglycone by chloro substitutions in *ortho*- and *meta*-position of ring A.

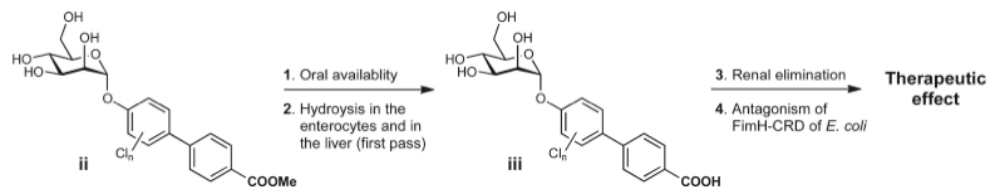


Figure 3. FimH antagonists with the pharmacodynamic and pharmacokinetic properties required for a therapeutic application. (1) For the prediction of oral availability, the PAMPA³⁰ and the Caco-2 cell assay³¹ are applied. (2) The hydrolysis of ester **ii** to carboxylate **iii** is evaluated by mouse liver microsomes. (3) Renal excretion is estimated based on a positive correlation with polar descriptors (polar surface area, H-bond donors, H-bond acceptors, rotatable bonds).³² (4) The potential of FimH antagonists is assessed with a target-based assay²³ and a function-based cellular assay.³³ For the evaluation of the therapeutic effect, a urinary tract infection mouse model (UTI mouse model in C3H/HeN mice) is applied.

that, once in circulation, are metabolically stable and undergo fast renal elimination, are required. This pharmacokinetic profile results from various serial and/or simultaneous processes that include dissolution, intestinal absorption, plasma protein binding, metabolic clearance, body distribution as well as renal and other clearance mechanisms. Because intestinal absorption and renal elimination are related to opposed properties, i.e. lipophilicity for intestinal absorption and hydrophilicity for renal elimination, a prodrug approach²⁷ was envisaged (Figure 3). Ester **ii** is expected to undergo intestinal absorption²⁸ and, later on, efficient hydrolysis to carboxylate **iii** by esterases²⁹ present in enterocytes lining the small intestine and in the liver.

For renal clearance, the net result of glomerular filtration, active tubular secretion, and reabsorption, carboxylate **iii** should exhibit low lipophilicity ($\log D_{7.4}$) and favorable polar descriptor values (polar surface area (PSA), H-bond capacity and rotatable bonds).³² By contrast, lipophilic compounds are efficiently reabsorbed (as the passive reabsorption process occurs throughout the length of the nephron, whereas the secretion predominantly occurs at the proximal tubule). The estimated negative $\log D_{7.4}$ for antagonists of type **iii** is expected to fulfill these specifications for an efficient renal elimination and a low reabsorption. Finally, once arrived at the site of action in the bladder, the antagonist binds to the carbohydrate recognition domain (CRD) located on the bacterial pili, thus interfering with the adhesion of *E. coli* to oligosaccharide structures on urothelial cells.³⁴ To identify antagonists with the pharmacokinetic properties required for oral absorption and fast renal elimination, it was planned to determine PK parameters such as $\log D_{7.4}$, pK_a , solubility, plasma protein binding, metabolic stability, and oral availability using the parallel artificial membrane permeation assay (PAMPA)³⁰ and the Caco-2 cell assay.³¹

Synthesis of FimH Antagonists. The aglycone in the α -1-position of D-mannose plays a ternary role, i.e. it mediates the lipophilic contact with the hydrophobic tyrosine gate, contains the elements required for intestinal absorption and, after metabolic cleavage of the prodrug, for a fast renal elimination.

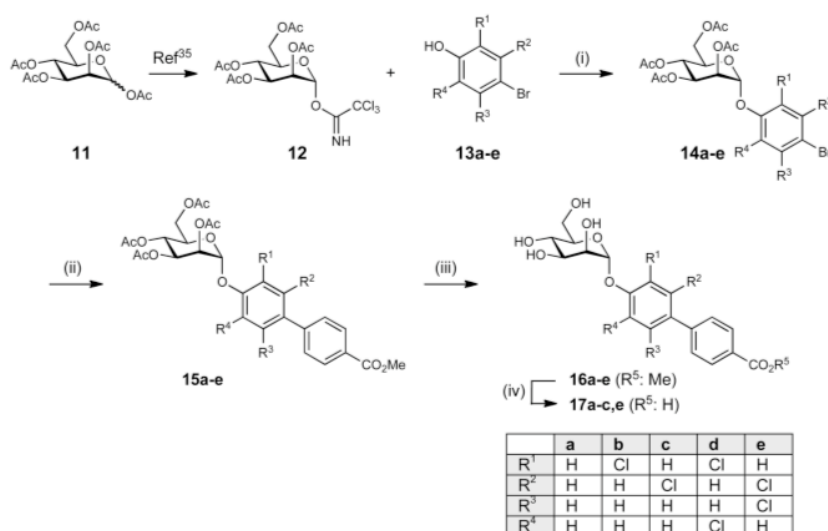
The syntheses of the *para*-substituted biphenyls **16a–e** and **17a–c,e** are outlined in Scheme 2. Lewis acid promoted glycosylation of the halogenated phenols **13a–e** with trichloroacetimidate **12**³⁵ yielded the phenyl α -D-mannosides **14a–e**. In a palladium-catalyzed Suzuki coupling with 4-methoxycarbonylphenylboronic acid, the biphenyls **15a–e** were obtained. For the deprotection of the mannose moiety, Zemplén conditions were applied (\rightarrow **16a–e**). Finally, the methyl esters were saponified, yielding the sodium salts **17a–c,e**.

In a similar approach, two *meta*-substituted biphenyls in their ester form (\rightarrow **21a,b**) and as free acids (\rightarrow **22a,b**) were obtained (see Scheme 3).

Binding Affinities and Activities. For the biological in vitro evaluation of the FimH antagonists, two assay formats have been developed. For an initial characterization, a cell-free competitive binding assay²³ and, later on, a cell-based aggregation assay,³³ were applied. Whereas in the cell-free competitive binding assay only the CRD of the pili was used, the complete pili are present in the cell-based assay format. Furthermore, both formats are competitive assays, i.e. the analyzed antagonists compete with mannosides for the binding site. In the cell-free competitive binding assay, the competitors are polymer-bound trimannosides, whereas in the aggregation assay, the antagonist competes with more potent oligo- and polysaccharide chains present on the surface of erythrocytes.³⁶ Therefore, lower IC_{50} values are expected for the cell-free competitive binding assay. In addition, switching from the cell-free target-based assay to the function-based assay generally leads to a reduction of potency by several orders of magnitude. The interaction is further complicated by the existence of a high- and a low-affinity state of the CRD of FimH. Aprikian et al. experimentally demonstrated that in full-length fimbriae the pilin domain stabilizes the CRD domain in the low-affinity state, whereas the CRD domain alone adopts the high-affinity state.³⁷ It was recently shown that the pilin domain allosterically causes a twist in the β -sandwich fold of the CRD domain, resulting in a loosening of the binding pocket.³⁸ On

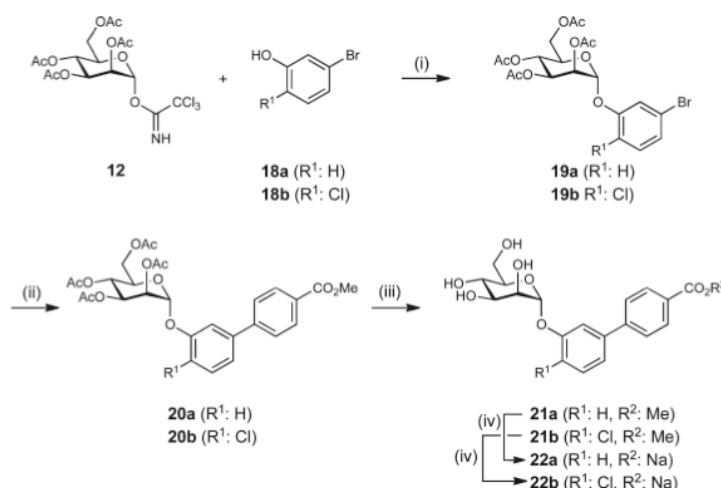
3 Results and discussion

Scheme 2^a



^a(i) TMSOTf, toluene, rt, 5 h (42–77%); (ii) 4-methoxycarbonylphenylboronic acid, Cs₂CO₃, Pd(PPh₃)₄, dioxane, 120°C, 8 h (28–85%); (iii) NaOMe, MeOH, rt, 4–24 h (22–86%); (iv) NaOMe, MeOH, rt, then NaOH/H₂O, rt, 16–24 h (63–94%).

Scheme 3^a



^a(i) TMSOTf, toluene, rt, 5 h (67–70%); (ii) 4-methoxycarbonylphenylboronic acid, Cs₂CO₃, Pd(PPh₃)₄, dioxane, 120°C, 8 h or Pd₂(dba)₃, S-Phos, dioxane, 80°C, overnight (46–56%); (iii) NaOMe, MeOH, rt, 24 h (52–67%); (iv) NaOMe, MeOH, rt, then NaOH/H₂O, rt, 24 h (75–95%).

the basis of these findings, we expect a loss of affinity of our antagonists toward full-length fimbriae, when compared to the CRD domain alone.

Cell-Free Competitive Binding Assay. The cell-free inhibition assay is based on the interaction of a biotinylated polyacrylamide glycopolymer with the FimH-CRD as previously reported.²³ A recombinant protein consisting of the carbohydrate recognition domain of FimH linked with a thrombin cleavage site to a 6His-tag (FimH-CRD-Th-6His) was expressed in *E. coli* strain HM125 and purified by affinity chromatography. The IC₅₀ values of the test compounds were determined in microtiter plates coated with

FimH-CRD-Th-6His. Complexation of the biotinylated glycopolymer with streptavidin coupled to horseradish peroxidase allowed the quantification of the binding properties of FimH antagonists (Figure 4a). To ensure comparability with different antagonists, the reference compound *n*-heptyl α-D-mannopyranoside (**1**)³³ was tested in parallel in each individual microtiter plate. The affinities are reported relative to *n*-heptyl α-D-mannopyranoside (**1**) as rIC₅₀ in Table 1.

The most active representatives from the ester group are **16a** (Table 1, entry 6) and **16b** (entry 8) with affinities in the low nanomolar range, which is an approximately 10-fold improvement compared to reference compound **1**. The

3.1 Pharmacokinetic properties of FimH antagonists with biphenyl-moiety

Table 1. Pharmacodynamic and Pharmacokinetic Parameters of FimH Antagonists^{a,b}

| |  | IC ₅₀ binding assay [nM] | rIC ₅₀ | IC ₅₀ Aggregometry assay [μM] | PAMPA log P _e [log(10 ⁻⁶ cm/s)/%Mm] | Caco-2 P _{app} [10 ⁻⁶ cm/s] | log D _{7.4} | pK _a | log S [μg/mL]/pH | PPB [%] |
|----|---|-------------------------------------|-------------------|--|---|---|----------------------|-----------------|------------------|---------|
| 1 |  | 73±7.9 | 1.0 | 77.14±8.7 | -4.89/21 | nd | 1.65 | - | >3000 | 81 |
| 2 |  | 150±11.5 | 1.9 | nd | nd/nd | nd | nd | - | >3000 | nd |
| 3 |  | 364±16.8 | 4.6 | nd | nd/nd | nd | nd | - | nd | nd |
| 4 |  | 210±11.2 | 2.6 | nd | nd/nd | nd | nd | - | nd | nd |
| 5 |  | 253±13.4 | 3.2 | nd | nd/nd | nd | nd | - | nd | nd |
| 6 |  | 10.4±1.2 | 0.14 | 42±7 | -4.7/-20% | 4.23 | 2.14 | - | 33.8/6.51 | 93 |
| 7 |  | 17.1±2.2 | 0.15 | 45±8 | np | nd | <-1.5 | 3.88 | >3000/6.61 | 73 |
| 8 |  | 4.8±1.2 | 0.06 | 9±2.7 | -4.6/41.00 | 2.05 | 2.32 | - | 11.9/6.53 | 94 |
| 9 |  | 6.7±2.1 | 0.09 | 10±2.3 | np/3.5 | nd | -0.77 | 3.98 | >3000/6.50 | 89 |
| 10 |  | 22.0±8.4 | 0.30 | 41 ¹¹ | -4.72/67.6 | nd | 2.42 | - | 11.5/6.50 | 95 |
| 11 |  | 27.6±3.9 | 0.38 | 17 ¹¹ | np | nd | -1.33 | 3.95 | >3000/6.50 | 83 |
| 12 |  | 16.0±0.8 | 0.22 | 14 ¹¹ | -4.29/54.3 | 3.32 | 2.31 | - | 4.6/6.53 | 98 |
| 13 |  | 15.3±0.4 | 0.07 | nd | -4.40/70.2 | 5.81 | 3.10 | - | 22.7/6.53 | 94 |
| 14 |  | 23.9±2.2 | 0.19 | nd | nd/nd | nd | nd | nd | nd | nd |
| 15 |  | 20.0±4.3 | 0.27 | 33 ¹¹ | -5.01/60.7 | 4.88 | 2.02 | - | 37.6/6.52 | 92 |
| 16 |  | 38.7±5.2 | 0.53 | 45 ¹¹ | np/9.7 | nd | <-1.5 | 3.60 | >3000/6.50 | 81 |
| 17 |  | 11.8±0.1 | 0.16 | 31 ¹¹ | -4.69/51.7 | 1.63 | 1.70 | - | 24.3/6.54 | 96 |
| 18 |  | 29.2±0.7 | 0.40 | nd | np/tr | 0.55 | <-1.5 | 3.41 | >3000/6.5 | 87 |

^aSingle determination; P_e, effective permeation; P_{app}, apparent permeability; np, no permeation; nr, no retention; nd, not determined. ^bThe IC₅₀s were determined with the cell-free competitive binding assay.²³ The rIC₅₀ of each substance was calculated by dividing the IC₅₀ of the compound of interest by the IC₅₀ of the reference compound **1** (entry 1). This leads to rIC₅₀ values below 1.00 for derivatives binding better than **1** and rIC₅₀ values above 1.00 for compounds with a lower affinity than **1**. The aggregation of *E. coli* and GPE were determined in the aggregometry assay.³⁷ Passive permeation through an artificial membrane and retention therein was determined by PAMPA (parallel artificial membrane permeation assay).³⁰ The permeation through cell monolayers was assessed by a Caco-2 assay.³¹ Distribution coefficients (log D values) were measured by a miniaturized shake flask procedure.³⁴ pK_a values were determined by NMR spectroscopy.⁴⁵ Plasma protein binding (PPB) was assessed by a miniaturized equilibrium dialysis protocol.⁴⁶ Thermodynamic solubility (S) was measured by an equilibrium shake flask approach.⁴⁷

3 Results and discussion

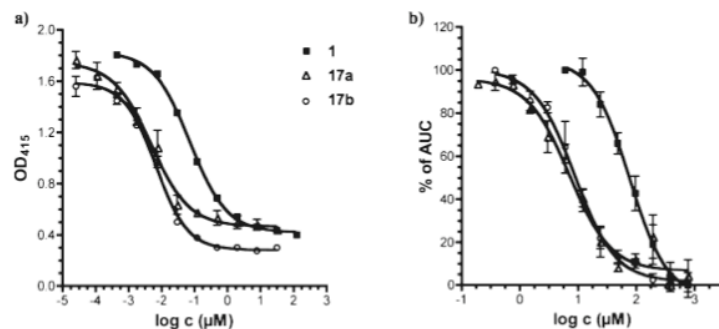


Figure 4. Affinities were determined in two different competitive assay formats. (a) a cell-free competitive binding assay²³ and (b) a cell-based aggregometry assay.³³ For antagonists **17a**, **17b**, and the reference compound **1**, IC₅₀ values in the nM and µM range, respectively, were obtained. The 1000-fold difference between the two assay formats is due to the different competitors used as well as the different affinity states present in FimH, i.e. the high-affinity state present in the CRD used in the cell-free competitive binding assay and the low-affinity state present in the pili of *E. coli* used in the aggregometry assay.

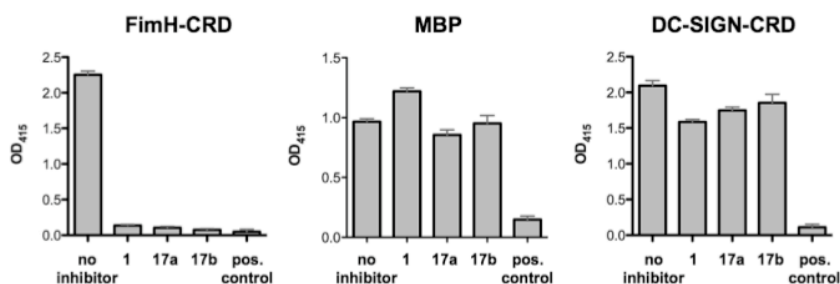


Figure 5. Competitive binding assay using FimH-CRD-Th-6His, DC-SIGN-CRD-IgG-Fc,⁴³ and MBP to evaluate the selectivity of compounds **1**, **17a**, and **17b**. Inhibitory capacities of the compounds were tested at a concentration of 1 mM. As positive control, D-mannose at a concentration of 50 mM was used.

corresponding carboxylic acids **17a** (entry 7) and **17b** (entry 9) exhibited a small reduction in affinity but are still 5-fold more active than reference compound **1**. All the remaining antagonists listed in Table 1 are slightly less active. For the in vivo examination, antagonists **17a** and **17b** were therefore foreseen for iv application and the prodrug **16b** for oral application.

Target selectivity is a further important issue. Mammalian mannose receptors are part of various biological processes, e.g. in cell–cell adhesion (DC-SIGN, dendritic cell-specific intercellular adhesion molecule-3-grabbing nonintegrin),³⁹ in the regulation of serum glycoprotein homeostasis (mannose receptor)⁴⁰ or in the innate and adaptive immune system by recognizing molecular patterns on pathogens (e.g., mannose-binding protein, mannose receptor, DC-SIGN).^{39,41,42} Non-specific interactions to the various mannose receptors by FimH inhibitors would have a profound impact on these processes. We therefore determined the affinity of reference compound **1** and the two antagonists **17a** and **17b** for two additional mannose binding proteins, DC-SIGN,^{39,43} and MBP (mannose-binding protein)⁴² (Figure 5). In both cases, affinities above 1 mM, i.e. a decrease of more than 5 orders of magnitude, was detected.

Aggregometry Assay. The potential of the biphenyl mannosides to disaggregate *E. coli* from guinea pig erythrocytes (GPE) was determined by a function-based aggregometry assay.³³ Antagonists were measured in triplicates, and the corresponding IC₅₀ values were calculated by plotting the

area under the curve (AUC) of disaggregation against the concentration of the antagonists. *n*-Heptyl α -D-mannopyranoside (**1**) was used again as reference compound and exhibits an IC₅₀ of $77.14 \pm 8.7 \mu\text{M}$. Antagonists **17a** and **17b** showed IC₅₀ values of $45 \pm 8 \mu\text{M}$ and $10 \pm 2.3 \mu\text{M}$, respectively (Figure 4b). In general, the activities obtained from the aggregometry assay are approximately 1000-fold lower than the affinities determined in the target-based competitive assay (discussion see above).

In Vitro Pharmacokinetic Characterization of FimH Antagonists. For an application in the UTI mouse model, iv or po available FimH antagonists are required that, once absorbed to circulation, are metabolically stable and undergo fast renal elimination. Sufficient bioavailability requires a combination of high solubility and permeability to maximize absorption and low hepatic clearance to minimize first pass extraction. Furthermore, for efficient renal elimination, active and/or passive membrane permeability and low reabsorption in the renal tubuli is required. From the series of FimH antagonists with nanomolar in vitro activities (see Table 1), representatives with appropriate pharmacokinetic properties were selected for in vivo experiments based on the parameters shown below.

Oral Absorption and Renal Excretion. For the evaluation of oral absorption and renal excretion of the esters **16** and **21** as well as the acids **17** and **22** physicochemical parameters such as pK_a values, lipophilicity (distribution coefficients, log *D*_{7,4}), solubility, and permeability were determined

3.1 Pharmacokinetic properties of FimH antagonists with biphenyl-moiety

Article

Journal of Medicinal Chemistry, 2010, Vol. 53, No. 24 8633

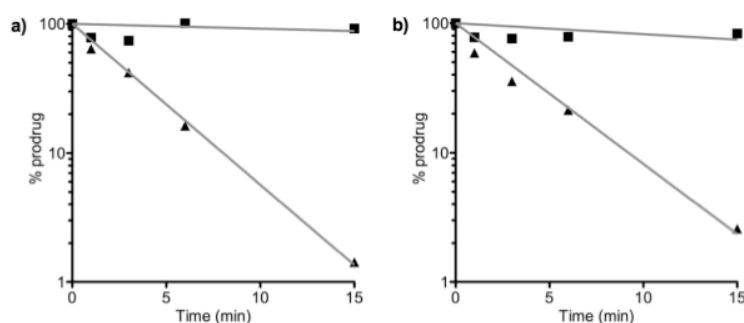


Figure 6. Incubation of (a) **16a** and (b) **16b** with pooled mouse liver microsomes (0.25 mg of protein/mL), in absence (\blacktriangle) and in presence (\blacksquare) of the specific carboxylesterase inhibitor bis(4-nitrophenyl) phosphate (BNPP).

(Table 1). Not surprisingly, the acids **17** and **22** showed $\log D_{7.4}$ values in the range of -1 to -2 and pK_a values of approximately 4. While these parameters are beneficial for renal excretion,³² oral absorption by passive diffusion seems unlikely. Indeed, when the permeation through an artificial membrane (PAMPA³⁰) was studied, neither significant permeation ($\log P_e$, P_e : effective permeation) nor membrane retention could be detected. Whereas for a successful oral absorption $\log P_e$ should be above -5.7 and/or the membrane retention above 80%,⁴⁸ the corresponding values for the carboxylic acids **17** and **22** are far from being in this range (see Table 1, e.g. entries 7 and 9). However, $\log D_{7.4}$ values and PAMPA results were markedly improved for the esters **16** and **21** (Table 1, e.g. entries 6 and 8), suggesting that these FimH antagonists are orally absorbed. This assumption was fully confirmed in a cell-based permeation assay with Caco-2 cells.³¹ For renal excretion, Varma et al.³¹ correlated low lipophilicity and the presence of a charged state at physiological pH positively with enhanced elimination. On the basis of $\log D_{7.4}$ and pK_a , summarized in Table 1, the carboxylates **17** and **22** fulfill these requirements. Overall, these results support the prodrug approach: (i) oral application of the esters **16** and **21** and (ii) renal elimination of the corresponding acids **17** and **22**.

Solubility. A major problem of the antagonists **16** and **21** is their insufficient solubility, ranging from 4.6 to 37.6 $\mu\text{g/mL}$. Even though the solubility issue can be addressed by appropriate formulations, further structural modifications to improve solubility are necessary. Opposite to the esters, the corresponding carboxylates **17** and **22** showed excellent solubility (>3 mg/mL). This enables their iv application in physiological solutions (PBS) in the UTI model without further needs to develop suitable formulations (see below).

Stability in Simulated Gastrointestinal Fluids. To exclude degradation in the gastrointestinal tract prior to absorption, the stability of **1**, **16b**, and **17b** in simulated gastric fluid (sGF) and simulated intestinal fluid (sIF) was determined. All three antagonists proved to be sufficiently stable with more than 80% of the initial concentrations found after two hours.

Metabolic Stability. Because the prodrug approach is only applicable when the esters **16a** and **16b** are rapidly metabolically cleaved into the corresponding acids, their propensity to enzymatic hydrolysis by carboxylesterase (CES) was studied. Mammalian CESs are localized in the endoplasmic reticulum of the liver and most other organs.²⁹ Because of the excellent affinity of the corresponding acids **17a** and

17b to FimH, we concentrated our metabolic studies on the ester prodrugs **16a** and **16b**, which were incubated with pooled male mouse liver microsomes to study the hydrolysis and the release of the metabolites. Preliminary experiments involving low substrate concentrations (2 μM) and a concentration of the microsomal protein of 0.25 mg/mL showed a fast degradation of the ester prodrugs (Figure 6). Addition of the specific CES inhibitor bis(4-nitrophenyl) phosphate (BNPP) prevented ester degradation, suggesting that the metabolic transformation can be attributed to CESs.⁴⁹

On the basis of these in vitro results, we also expect fast hydrolysis of the esters in vivo at the first liver passage. Current studies are focusing on the kinetic parameters of the enzymatic ester cleavage.

To reach the minimal therapeutic concentration in the bladder (approximately 1 $\mu\text{g/mL}$, as estimated from a cell-based infection assay⁵⁰), the FimH antagonists **17a** and **17b** should be efficiently renally eliminated and not further metabolically processed. Therefore, the metabolic fate of the free carboxylic acids **17a** and **17b** was examined. A common method to predict a compound's propensity to phase I metabolism is its incubation with liver microsomes in presence of NADPH.⁵¹ Under these conditions, in vitro incubations of the free carboxylic acids **17a** and **17b** with pooled male mouse liver microsomes (0.5 mg microsomal protein/mL) did not show significant compound depletion over a period of 30 min, suggesting a high stability against cytochrome P450 mediated metabolism in vivo. However, phase II metabolic pathways such as glucuronidation remain to be studied in details.

Plasma Protein Binding (PPB). Compared to the corresponding esters **16** and **21**, the antagonists **17** and **22** exhibit 5–20% lower plasma protein binding, typically in the range of 73–89%. This rather low PPB beneficially influences renal excretion because, in line with the free drug hypothesis,⁵² molecules bound to plasma proteins evade metabolism and excretion. However, for a concluding statement, the kinetics of PPB, i.e. association and dissociation rate constants, have to be determined because PPB alone is not necessarily predictive for distribution, metabolism, and clearance.^{53,54}

In Vivo Pharmacokinetics and Treatment Studies. The two mannose derivatives methyl α -D-mannoside and *n*-heptyl α -D-mannoside (**1**) were previously tested in the UTI mouse model.^{10,21,22} In all three studies, the FimH antagonists were first preincubated with the bacterial suspension, followed by transurethral inoculation. To efficiently reduce infection,

3 Results and discussion

| Antagonist | Compartment | C_{max} ($\mu\text{g/mL}$) | AUC_{0-24} ($\mu\text{g} \times \text{h/mL}$) | PPB |
|------------|-------------|--------------------------------|---|-----|
| 1 | plasma | 35 ± 14.1 | 34.3 ± 33.3 | 81% |
| | urine | 951.4 ± 249.6 | 2469.3 ± 636.4 | |
| 17a | plasma | 34.4 ± 11.8 | 19.3 ± 6.2 | 73% |
| | urine | 509.6 ± 427.5 | 139.9 ± 118.8 | |
| 17b | plasma | 39.4 ± 15.7 | 20.8 ± 7.3 | 89% |
| | urine | 588.4 ± 218.2 | 209.6 ± 72.3 | |

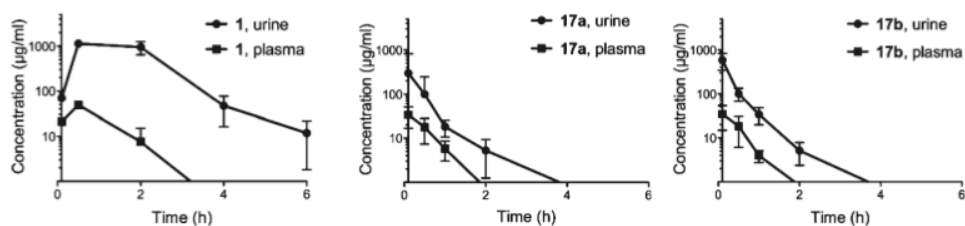


Figure 7. Determination of antagonist concentration in urine and plasma after a single iv application of 50 mg/kg. The data (table and graphs) show time-dependent urine and plasma concentrations of **1**, **17a**, and **17b**.

large amounts of methyl α -D-mannoside had to be applied (up to 1 M).²¹ For *n*-heptyl α -D-mannoside (**1**), an approximately one \log_{10} unit reduction of bacterial counts in the bladder was reached with lower, but still millimolar, concentration.¹⁰ In the previously presented studies, the FimH antagonists were exclusively instilled into the bladder, which is obviously not suitable for a therapeutic application. The aim of our project was therefore the identification of FimH antagonists suitable for iv or preferably po applications. Before infection studies in a mouse disease model could be performed, the in vivo pharmacokinetic parameters (C_{max} , AUC) had to be determined to ensure the antagonists availability in the target organ (bladder).

Pharmacokinetics of a Single iv Application in C3H/HeN Mice. Plasma and urine concentrations of the FimH antagonists **1**, **17a**, and **17b** after iv application were determined. With a single dose of 50 mg/kg, the control compound **1** exhibited availability in the bladder over a period of 6 h after administration ($n = 4$), whereas at similar doses, **17a** and **17b** showed lower urine concentrations over a reduced time period (max 2 h) ($n = 6$). In Figure 7, the pharmacokinetic parameters are summarized. Overall, for all three compounds, higher availability of the antagonists in the urine was observed compared to the plasma. Because plasma protein binding is of comparable scale for the three compounds (see Table 1 and Figure 7), it similarly influences urine concentrations.

Pharmacokinetics of a Single po Application in C3H/HeN Mice. Aiming for an orally available FimH antagonist, the prodrug **16b** and its metabolite **17b** were tested. Because of the in vitro pharmacokinetic properties of **17b** (Table 1, entry 9), its low oral bioavailability after the administration of a single po dose (50 mg/kg) was not surprising. For the determination of the availability of a similar dose of **16b** at the target organ (bladder), plasma and urine concentrations were determined over a period of 24 h ($n = 6$) (Figure 8). Because **16b** was designed as a prodrug expected to be rapidly

| Antagonist applied | Antagonist detected | Compartment | $AUC_{0-24 \text{ p.o.}}$ ($\mu\text{g} \times \text{h/mL}$) |
|--------------------|---------------------|-------------|--|
| 17b | 17b | Plasma | n.d. |
| | | Urine | 2.7 ± 3.2 |
| 16b | 16b | Plasma | 1.02 ± 0.32 |
| | | Urine | 1.89 ± 0.37 |
| | 17b | Plasma | 2.1 ± 0.61 |
| | | Urine | 21.69 ± 3.88 |

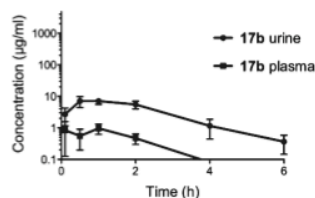


Figure 8. Determination of antagonist concentration in urine and plasma after a single po application of 50 mg/kg of antagonists **16b** and **17b**. The data (table and graph) show their time-dependent urine and plasma concentrations. When **17b** was orally applied, its plasma concentration was below the detection level, and only a small portion was present in the urine. However, after the application of the prodrug **16b**, metabolite **17b** was predominantly detected due to fast metabolic hydrolysis of **16b**. However, minor amounts of **16b** are still traceable in plasma as well as urine; nd, not detectable.

hydrolyzed, plasma and urine samples were analyzed not only for **16b** but also for its metabolite **17b**. **16b** was present only in minor concentrations in both plasma and urine. However, although the AUC of metabolite **17b** in urine is reduced by 90% compared to the iv application, its minimal therapeutic concentration can be maintained over a period of 2 to 3 h.

3.1 Pharmacokinetic properties of FimH antagonists with biphenyl-moiety

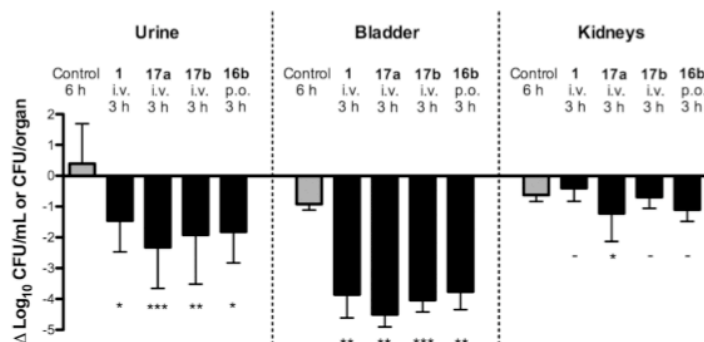


Figure 9. Treatment efficacy of the reference compound (**1**) and three FimH antagonists (**17a**, **17b**, **16b**) at a dosage of 50 mg/kg in the UTI mouse model after 3 h of infection, compared to a 6 h infection study ($n = 6$). **1**, **17a**, and **17b** were applied iv into the tail vein, whereas **16b** was applied orally. As baseline (reference), the mean counts of the 3 h infection were subtracted from the results of the tested antagonists and the 6 h control group. P values were calculated by comparing the treatment groups with the 3 h control group. (*) $P < 0.05$, (**) $P < 0.01$, (***) $P < 0.001$, (-) not significant (determined by Mann-Whitney test).

UTI Mouse Model: Treatment Study. Before treatment studies were started, the optimal infection profile was established. A 3 h infection exhibited the highest infection level in the C3H/HeN mouse strain. At longer infection times, e.g. 6 h, the control group showed indeed higher bacterial counts in the urine, however, the bladder and kidney counts already decreased due to self-clearance of the infection in the UTI mouse model.⁵⁵ For the in vivo UTI treatment studies (Figure 9), antagonists **1**, **17a**, **17b**, and **16b** were applied followed by infection with UPEC (UTI89). For each antagonist, a group of six animals was used. The animals were sacrificed 3 h after inoculation and urine and homogenized organs (bladder, kidneys) were examined for bacterial counts. The mean value in the untreated reference group ($n = 6$) showed 1.8×10^6 CFU/mL in the urine, 1.4×10^6 CFU in the bladder and 9.7×10^6 CFU in the kidneys. The bar diagram in Figure 9 summarizes the bacterial counts after iv (**1**, **17a**, and **17b**) and po (**16b**) treatment. The baseline represents the values obtained for the control group after 3 h and was used as reference for CFU reductions. **1** showed the lowest inhibition of growth in the urine with $1.5 \log_{10}$ CFU reduction and an approximately $4 \log_{10}$ reduction of bacterial counts in the bladder. After iv application of **17a**, a substantial decrease in the bacterial count was obtained ($> 2 \log_{10}$ CFU reduction in the urine and $4.5 \log_{10}$ reduction in the bladder). A slightly lower reduction was observed when **17b** was applied iv (a decrease of $2 \log_{10}$ CFU in the urine and $4 \log_{10}$ for bladder counts). Interestingly, almost the same reduction of the bacterial count was detected with orally applied **16b**.

In general, urine samples showed higher bacterial counts compared to the bladder. This could be due to the difficulties during urine sampling. We observed that infected C3H/HeN mice void considerably less urine (5–50 μ L) compared to healthy mice (50–100 μ L). As a consequence, the lower urine volume leads to a higher concentration of bacteria in the collected urine and therefore to higher bacterial counts compared to the bladder.

In all treated animals, bacterial counts were only marginally reduced in the kidneys. This lower response to the treatment with FimH antagonists is probably due to different bacterial adhesion mechanisms in bladder and kidney. Whereas in the bladder adhesion is mediated by type I pili (via the CRD of FimH), P pili-dependent interactions are crucial for the adhesion in the kidneys.⁶

Summary and Conclusions

With the objective to develop an oral treatment of urinary tract infections, we have synthesized a series of potent small molecular weight FimH antagonists. Starting from the known antagonist phenyl α -D-mannopyranoside (**7a**), two equally potent classes of biphenyl α -D-mannopyranoside, those with an ester function (**16** and **21**) and those with a carboxylate (**17** and **22**) on the terminal aromatic ring, were synthesized. According to their pharmacokinetic properties, the acids **17** and **22** were not expected to be orally absorbed, a prediction that was also confirmed by an in vivo PK study. Therefore, a prodrug approach was envisaged. On the basis of permeation assays (PAMPA and Caco-2), the esters **16** and **22** were expected to exhibit oral availability. Moreover, metabolic studies with mouse liver microsomes proposed fast in vivo hydrolysis of orally applied **16b** to the corresponding carboxylate **17b**. In vivo PK studies in mice finally confirmed the in vitro prediction of a fast renal elimination of **17b** to the target organ, the bladder. When orally applied **16b** was tested in the UTI mouse model, it reduced the colony forming units (CFU) in the urine by 2 orders of magnitude and in the bladder by 4 orders of magnitude. As a result, a low molecular weight FimH antagonist suitable for the oral treatment of urinary tract infections was identified.

However, a number of parameters remain to be improved. Because the solubilities of the esters **16** and **22** are in the low μ g/mL range, an iv application was impossible and the suspension in DMSO/1% Tween 80 used for oral dosing is not optimal. In addition, due to fast renal elimination, the minimal therapeutic concentration of **17b** in the bladder could only be maintained for 2–3 h. Because high plasma protein binding was observed, an unfavorable kinetic of dissociation of the active principle from plasma proteins followed by fast renal elimination might be the reason for these findings. An improvement of the corresponding pharmacokinetic parameters should positively influence the duration of action. Furthermore, a detailed analysis of the metabolic pathway of **16b** and its metabolite **17b** will elucidate their overall metabolic fate. Finally, a detailed PK/PD profile in the mouse model will elucidate the full potential of FimH antagonists for the therapy of urinary tract infections (UTI).

Experimental Section

General Methods. NMR spectra were recorded on a Bruker Avance DMX-500 (500 MHz) spectrometer. Assignment of ^1H

and ^{13}C NMR spectra was achieved using 2D methods (COSY, HSQC, TOCSY). Chemical shifts are expressed in ppm using residual CHCl_3 , CHD_2OD , and HDO as references. Optical rotations were measured using Perkin-Elmer polarimeter 341. Electron spray ionization mass spectra (ESI-MS) were obtained on a Waters micromass ZQ. HRMS analysis were carried out using a Bruker Daltonics micrOTOF spectrometer equipped with a TOF hexapole detector. Microanalyses were performed at the Department of Chemistry, University of Basel, Switzerland. Microwave-assisted reactions were carried out with a CEM Discover and Explorer. Reactions were monitored by TLC using glass plates coated with silica gel 60 F_{254} (Merck) and visualized by using UV light and/or by heating to 140 °C for 5 min with a molybdate solution (a 0.02 M solution of ammonium cerium sulfate dihydrate and ammonium molybdate tetrahydrate in aqueous 10% H_2SO_4). Column chromatography was performed on a CombiFlash Companion (Teledyne-ISCO, Inc.) using RediSep normal phase disposable flash columns (silica gel). Reversed phase chromatography was performed on LiChroprepRP-18 (Merck, 40–63 μm). Commercially available reagents were purchased from Fluka, Aldrich, Merck, AKSci, ASDI, or Alfa Aesar. Methanol (MeOH) was dried by refluxing with sodium methoxide and distilled immediately before use. Toluene was dried by filtration over Al_2O_3 (Fluka, type 5016 A basic). Dioxane was dried by distillation from sodium/benzophenone.

4-Bromophenyl 2,3,4,6-Tetra-O-acetyl- α -D-mannopyranoside (14a). To a stirred solution of **12** (1.17 g, 3.00 mmol) and 4-bromophenol (**13a**, 623 mg, 3.60 mmol) in toluene (12 mL), TMSOTf (65 μL , 0.36 mmol) was added dropwise under argon. The mixture was stirred at rt for 5 h and then diluted with toluene (15 mL) and washed with satd aq NaHCO_3 . The organic layer was separated, and the aqueous layer was extracted three times with toluene. The combined organic layers were dried over Na_2SO_4 and concentrated in vacuo. The residue was purified by flash chromatography on silica (petroleum ether/EtOAc, 19:1 to 1.5:1) to yield **14a** (1.17 g, 74%) as a white solid.

$[\alpha]_{\text{D}}^{20} +60.6$ (c 0.40, CHCl_3). ^1H NMR (500 MHz, CDCl_3): δ 2.06 (s, 9H, 3 COCH_3), 2.19 (s, 3H, COCH_3), 4.06 (m, 2H, H-5, H-6a), 4.27 (dd, $J = 5.6, 12.4$ Hz, 1H, H-6b), 5.36 (t, $J = 10.2$ Hz, 1H, H-4), 5.43 (dd, $J = 1.8, 3.5$ Hz, 1H, H-2), 5.48 (d, $J = 1.7$ Hz, 1H, H-1), 5.53 (dd, $J = 3.5, 10.1$ Hz, 1H, H-3), 6.98, 7.41 (AA', BB' of AA'BB', $J = 9.0$ Hz, 4H, C_6H_4). ^{13}C NMR (125 MHz, CDCl_3): δ 20.71, 20.73, 20.74, 20.9 (4 COCH_3), 62.1 (C-6), 65.9 (C-4), 68.8 (C-3), 69.2 (C-2), 69.3 (C-5), 95.9 (C-1), 115.6, 118.3, 132.6, 154.7 (6C, C_6H_4), 170.0 (4C, 4 CO).

4-Bromo-2-chlorophenyl 2,3,4,6-tetra-O-acetyl- α -D-mannopyranoside (14b). According to the procedure described for **14a**, compound **12** (2.38 g, 4.84 mmol) and 4-bromo-2-chlorophenol (**13b**, 1.20 g, 5.80 mmol) were treated with TMSOTf (107 mg, 0.484 mmol) to yield **14b** (1.54 g, 59%) as a white solid.

$[\alpha]_{\text{D}}^{20} +60.6$ (c 0.40, CHCl_3). ^1H NMR (500 MHz, CDCl_3): δ 2.02, 2.04, 2.18 (3s, 12H, 4 COCH_3), 4.05 (dd, $J = 2.3, 12.2$ Hz, 1H, H-6a), 4.10 (ddd, $J = 2.7, 5.3, 9.6$ Hz, 1H, H-5), 4.24 (dd, $J = 5.4, 12.2$ Hz, 1H, H-6b), 5.35 (t, $J = 10.1$ Hz, 1H, H-4), 5.48 (m, 2H, H-1, H-2), 5.56 (dd, $J = 3.2, 10.1$ Hz, 1H, H-3), 7.03 (d, $J = 8.8$ Hz, 1H, C_6H_3), 7.30 (dd, $J = 2.4, 8.8$ Hz, 1H, C_6H_3), 7.53 (d, $J = 2.4$ Hz, 1H, C_6H_3). ^{13}C NMR (125 MHz, CDCl_3): δ 20.9, 21.1 (4C, 4 COCH_3), 62.3 (C-6), 65.9 (C-4), 68.9 (C-3), 69.4 (C-2), 70.1 (C-5), 96.9 (C-1), 115.9, 118.4, 125.7, 130.8, 133.3, 150.6 (C_6H_3), 169.9, 170.0, 170.1, 170.7 (4 CO). ESI-MS calcd for $\text{C}_{20}\text{H}_{22}\text{BrClNaO}_{10} [\text{M} + \text{Na}]^+$ 559.0; found 559.0; Anal. Calcd for $\text{C}_{20}\text{H}_{22}\text{BrClO}_{10}$: C 44.67, H 4.12. Found: C 45.08, H 4.14.

Methyl 4'-(2,3,4,6-Tetra-O-acetyl- α -D-mannopyranosyloxy)-biphenyl-4-carboxylate (15a). A Schlenk tube was charged with **14a** (503 mg, 1.00 mmol), 4-methoxycarbonylphenylboronic acid (224 mg, 1.24 mmol), *S*-Phos (20.5 mg, 0.05 mmol), cesium carbonate (1.17 g, 3.6 mmol), $\text{Pd}_2(\text{dba})_3$ (10.4 mg, 0.01 mmol), and a stirring bar. The tube was closed with a rubber septum and was evacuated and flushed with argon. This procedure was

repeated once, and then freshly degassed dioxane (5 mL) was added under a stream of argon. The reaction tube was quickly sealed and the contents were stirred at 80 °C overnight. The reaction mixture was cooled to rt, diluted with EtOAc (10 mL), washed with satd aq NaHCO_3 (5 mL) and brine (5 mL), and dried over Na_2SO_4 . The solvents were removed in vacuo, and the residue was purified by flash chromatography on silica (petroleum ether/EtOAc, 3:1 to 3:2) to give **15a** (474 mg, 85%) as a white solid.

$[\alpha]_{\text{D}}^{20} +80.8$ (c 1.00, CHCl_3). ^1H NMR (500 MHz, CDCl_3): δ 2.02, 2.03, 2.04, 2.19 (4s, 12H, COCH_3), 3.91 (s, 3H, OCH_3), 4.08 (m, 2H, H-6a, H-5), 4.27 (dd, $J = 5.2, 12.2$ Hz, 1H, H-6b), 5.37 (t, $J = 10.1$ Hz, 1H, H-4), 5.45 (dd, $J = 1.8, 3.4$ Hz, 1H, H-2), 5.56 (m, 2H, H-1, H-3), 7.16 (AA' of AA'BB', $J = 8.7$ Hz, 2H, C_6H_4), 7.57 (m, 4H, C_6H_4), 8.07 (BB' of AA'BB', $J = 8.4$ Hz, 2H, C_6H_4). ^{13}C NMR (125 MHz, CDCl_3): δ 20.74, 20.75, 20.77, 21.0 (4 COCH_3), 52.2 (OCH_3), 62.1 (C-6), 65.9 (C-4), 68.9 (C-3), 69.3, 69.4 (C-2, C-5), 95.8 (C-1), 116.9, 126.7, 128.5, 128.7, 130.2, 134.8, 144.8, 155.7 (12C, 2 C_6H_4), 167.0, 169.8, 170.0, 170.1, 170.6 (5 CO). ESI-MS calcd for $\text{C}_{28}\text{H}_{30}\text{NaO}_{12} [\text{M} + \text{Na}]^+$ 581.2; found 581.0.

Methyl 4'-(2,3,4,6-Tetra-O-acetyl- α -D-mannopyranosyloxy)-3'-chlorobiphenyl-4-carboxylate (15b). A microwave tube was charged with bromide **14b** (720 mg, 1.34 mmol), 4-methoxycarbonylphenylboronic acid (289 mg, 1.61 mmol), cesium carbonate (1.31 g, 4.02 mmol), and $\text{Pd}(\text{PPh}_3)_4$ (77.4 mg, 0.067 mmol). The tube was sealed with a Teflon septum, evacuated through a needle, and flushed with argon. Degassed dioxane (1.5 mL) was added and the closed tube was degassed in an ultrasonic bath for 15 min, flushed again with argon for 20 min, and exposed to microwave irradiation at 120 °C for 500 min. The solvent was evaporated in vacuo. The residue was dissolved in DCM (10 mL), washed with brine (2 \times 10 mL), dried over Na_2SO_4 , and concentrated in vacuo. The residue was purified by flash chromatography on silica (petroleum ether/EtOAc, 5:1 to 0.5:1) to yield **15b** (333 mg, 42%) as a white foam.

$[\alpha]_{\text{D}}^{20} +66.3$ (c 1.06, CHCl_3). ^1H NMR (500 MHz, CDCl_3): δ 2.03, 2.06, 2.20 (3s, 12H, COCH_3), 3.92 (s, 3H, OCH_3), 4.08 (dd, $J = 2.4, 12.3$ Hz, 1H, H-6a), 4.17 (m, 1H, H-5), 4.28 (dd, $J = 5.4, 12.3$ Hz, 1H, H-6b), 5.39 (t, $J = 10.6$ Hz, 1H, H-4), 5.54 (dd, $J = 1.9, 3.4$ Hz, 1H, H-2), 5.59 (d, $J = 1.8$ Hz, 1H, H-1), 5.62 (dd, $J = 3.5, 10.1$ Hz, 1H, H-3), 7.24 (s, 1H, C_6H_3), 7.44 (dd, $J = 2.2, 8.5$ Hz, 1H, C_6H_3), 7.57 (AA' of AA'BB', $J = 8.5$ Hz, 2H, C_6H_4), 7.65 (d, $J = 2.2$ Hz, 1H, C_6H_3), 8.08 (BB' of AA'BB', $J = 8.5$ Hz, 2H, C_6H_4). ^{13}C NMR (125 MHz, CDCl_3): δ 20.9, 21.0, 21.1 (4C, 4 COCH_3), 52.5 (OCH_3), 62.3 (C-6), 66.0 (C-4), 69.0 (C-3), 69.5 (C-2), 70.0 (C-5), 96.8 (C-1), 117.4, 126.7, 126.9, 129.5, 130.5, 136.4, 143.6, 151.3 (12C, C_6H_3 , C_6H_4), 167.0, 169.9, 170.0, 170.2, 170.7 (5 CO). ESI-MS calcd for $\text{C}_{28}\text{H}_{29}\text{ClNaO}_{12} [\text{M} + \text{Na}]^+$ 615.1; found 615.2. Anal. Calcd for $\text{C}_{28}\text{H}_{29}\text{ClO}_{12}$: C 56.71, H 4.93. Found: C 56.79, H 4.92.

Methyl 4'-(α -D-Mannopyranosyloxy)-biphenyl-4-carboxylate (16a). To a solution of **15a** (170 mg, 0.304 mmol) in MeOH (3 mL) was added freshly prepared 1 M NaOMe in MeOH (100 μL) under argon. The mixture was stirred at rt until the reaction was complete (monitored by TLC), then neutralized with Amberlyst-15 (H^+) ion-exchange resin, filtered, and concentrated in vacuo. The residue was purified by reversed-phase chromatography (RP-18, $\text{H}_2\text{O}/\text{MeOH}$, 1:0–1:1) to give **16a** (90 mg, 76%) as white solid.

$[\alpha]_{\text{D}}^{20} +82.8$ (c 0.2, MeOH). ^1H NMR (500 MHz, CD_3OD): δ 3.62 (m, 1H, H-5), 3.72 (m, 3H, H-4, H-6a, H-6b), 3.92 (m, 4H, H-3, OCH_3), 4.03 (s, 1H, H-2), 5.55 (s, 1H, H-1), 7.24 (AA' of AA'BB', $J = 8.0$ Hz, 2H, C_6H_4), 7.64 (AA' of AA'BB', $J = 7.5$ Hz, 2H, C_6H_4), 7.71 (BB' of AA'BB', $J = 8.0$ Hz, 2H, C_6H_4), 8.07 (BB' of AA'BB', $J = 7.5$ Hz, 2H, C_6H_4). ^{13}C NMR (125 MHz, CD_3OD): δ 52.6 (OCH_3), 62.7 (C-6), 68.3 (C-4), 72.0 (C-2), 72.4 (C-3), 75.5 (C-5), 100.1 (C-1), 118.2, 127.7, 131.1, 135.1, 146.6, 158.2, 160.3 (12C, 2 C_6H_4), 166.1 (CO). HR-MS calcd for $\text{C}_{20}\text{H}_{22}\text{NaO}_8 [\text{M} + \text{Na}]^+$ 413.1212; found 413.1218.

3.1 Pharmacokinetic properties of FimH antagonists with biphenyl-moiety

Article

Journal of Medicinal Chemistry, 2010, Vol. 53, No. 24 8637

Methyl 3'-Chloro-4'-(α -D-mannopyranosyloxy)-biphenyl-4-carboxylate (16b). According to the procedure described for 16a, compound 16b was prepared from 15b (764 mg, 1.29 mmol). Yield: 69 mg, 12%.

$[\alpha]_D^{25} +97.4$ (c 1.01, MeOH). $^1\text{H NMR}$ (500 MHz, CD_3OD): δ 3.64 (m, 1H, H-5), 3.72 (m, 1H, H-6a), 3.78 (m, 2H, H-4, H-6b), 3.91 (s, 3H, OCH_3), 4.00 (dd, $J = 3.4, 9.5$ Hz, 1H, H-3), 4.11 (dd, $J = 1.8, 3.1$ Hz, 1H, H-2), 5.60 (d, $J = 1.1$ Hz, 1H, H-1), 7.46 (d, $J = 8.6$ Hz, 1H, C_6H_3), 7.58 (dd, $J = 2.2, 8.6$ Hz, 1H, C_6H_3), 7.69 (AA' of AA'BB', $J = 8.4$ Hz, 2H, C_6H_4), 7.72 (d, $J = 2.2$ Hz, 1H, C_6H_3), 8.08 (BB' of AA'BB', $J = 8.4$ Hz, 2H, C_6H_4). $^{13}\text{C NMR}$ (125 MHz, CD_3OD): δ 52.7 (OCH_3), 62.8 (C-6), 68.3 (C-4), 71.9 (C-2), 72.5 (C-3), 76.2 (C-5), 100.8 (C-1), 118.7, 125.58, 127.8, 127.9, 129.9, 130.3, 131.3, 136.4, 145.3, 153.5 (12C, C_6H_3 , C_6H_4), 168.4 (CO). HR-MS calcd for $\text{C}_{20}\text{H}_{21}\text{ClNaO}_8$ [$\text{M} + \text{Na}$] $^+$ 447.0823; found 447.082.

Sodium 4'-(α -D-mannopyranosyloxy)-biphenyl-4-carboxylate (17a). To a solution of 15a (228 mg, 0.408 mmol) in MeOH (6.0 mL) was added 1 M NaOMe in MeOH (60 μL) at rt. The reaction mixture was stirred at rt for 4 h, and then NaOH (82 mg) in water (6 mL) was added and stirring was continued at rt overnight. The reaction mixture was concentrated in vacuo, and the residue was purified by reversed-phase chromatography (RP-18, $\text{H}_2\text{O}/\text{MeOH}$, 1:0–1:1) to afford 17a (96 mg, 63%) as a white solid.

$[\alpha]_D^{25} +103$ (c 0.10, MeOH). $^1\text{H NMR}$ (500 MHz, CD_3OD): δ 3.60 (m, 1H, H-5), 3.72 (m, 3H, H-6a, H-6b, H-4), 3.89 (dd, $J = 3.4, 9.5$ Hz, 1H, H-3), 4.00 (dd, $J = 1.8, 3.3$ Hz, 1H, H-2), 5.51 (s, 1H, H-1), 7.19, 7.60 (AA', BB' of AA'BB', $J = 8.7$ Hz, 4H, C_6H_4), 8.01 (d, $J = 8.2$ Hz, 2H, C_6H_4), 8.46 (s, 2H, C_6H_4). $^{13}\text{C NMR}$ (125 MHz, CD_3OD): δ 63.2 (C-6), 68.9 (C-4), 72.6 (C-2), 73.0 (C-3), 76.1 (C-5), 100.7 (C-1), 118.7, 128.0, 129.9, 131.8 (12C, 2 C_6H_4). HR-MS calcd for $\text{C}_{19}\text{H}_{20}\text{NaO}_8$ [$\text{M} + \text{H}$] $^+$ 399.1056; found 399.1052.

Sodium 3'-Chloro-4'-(α -D-mannopyranosyloxy)-biphenyl-4-carboxylate (17b). To a solution of 15b (380 mg, 0.641 mmol) in MeOH (10 mL) was added 1 M NaOMe in MeOH (300 μL). After stirring at rt for 24 h, 0.5 M aq NaOH (18 mL) was added and stirring continued for another 24 h. The solution was concentrated in vacuo and the residue was purified by reversed-phase chromatography (RP-18, $\text{H}_2\text{O}/\text{MeOH}$, 1:0–1:1) to yield 17b (222 mg, 80%) as a white solid.

$[\alpha]_D^{25} +61.6$ (c 1.00, H_2O). $^1\text{H NMR}$ (500 MHz, D_2O): δ 3.66 (m, 1H, H-5), 3.73 (m, 2H, H-6a, H-6b), 3.79 (t, $J = 9.8$ Hz, 1H, H-4), 4.07 (dd, $J = 3.4, 9.8$ Hz, 1H, H-3), 4.14 (d, $J = 1.4$ Hz, 1H, H-2), 5.47 (bs, 1H, H-1), 7.04 (d, $J = 8.6$ Hz, 1H, C_6H_3), 7.24 (d, $J = 8.6$ Hz, 1H, C_6H_3), 7.37 (AA' of AA'BB', $J = 8.1$ Hz, 2H, C_6H_4), 7.41 (bs, 1H, C_6H_3), 7.86 (BB' of AA'BB', $J = 8.1$ Hz, 2H, C_6H_4). $^{13}\text{C NMR}$ (125 MHz, D_2O): δ 60.6 (C-6), 66.5 (C-4), 69.0 (C-2), 70.5 (C-3), 73.9 (C-5), 98.6 (C-1), 117.5, 123.9, 126.2, 126.4, 128.4, 129.6, 135.2, 135.3, 141.0, 150.4 (12C, C_6H_3 , C_6H_4), 175.0 (CO). HR-MS calcd for $\text{C}_{19}\text{H}_{18}\text{ClNaO}_8$ [$\text{M} + \text{H}$] $^+$ 433.0666; found 433.0670.

Competitive Binding Assay. A recombinant protein consisting of the CRD of FimH linked with a thrombin cleavage site to a 6His-tag (FimH-CRD-Th-6His) was expressed in *E. coli* strain HM125 and purified by affinity chromatography.²³ To determine the affinity of the various FimH antagonists, a competitive binding assay described previously²³ was applied. Microtiter plates (F96 MaxiSorp, Nunc) were coated with 100 μL /well of a 10 $\mu\text{g}/\text{mL}$ solution of FimH-CRD-Th-6His in 20 mM HEPES, 150 mM NaCl, and 1 mM CaCl_2 , pH 7.4 (assay buffer) overnight at 4 $^\circ\text{C}$. The coating solution was discarded and the wells were blocked with 150 μL /well of 3% BSA in assay buffer for 2 h at 4 $^\circ\text{C}$. After three washing steps with assay buffer (150 μL /well), a 4-fold serial dilution of the test compound (50 μL /well) in assay buffer containing 5% DMSO and streptavidin-peroxidase coupled Man- α (1-3)-[Man- α (1-6)]-Man- β (1-4)-GlcNAc- β (1-4)-GlcNAc β polyacrylamide (TM-PAA) polymer (50 μL /well of a 0.5 $\mu\text{g}/\text{mL}$ solution) were added. On each individual microtiter plate, *n*-heptyl α -D-mannopyranoside (1) was tested in parallel.

The plates were incubated for 3 h at 25 $^\circ\text{C}$ and 350 rpm and then carefully washed four times with 150 μL /well assay buffer. After the addition of 100 μL /well of 2,2'-azino-di-(3-ethylbenzthiazoline-6-sulfonic acid) (ABTS)-substrate, the colorimetric reaction was allowed to develop for 4 min and then stopped by the addition of 2% aqueous oxalic acid before the optical density (OD) was measured at 415 nm on a microplate-reader (Spectramax 190, Molecular Devices, California, USA). The IC_{50} values of the compounds tested in duplicates were calculated with prism software (GraphPad Software, Inc., La Jolla, California, USA). The IC_{50} defines the molar concentration of the test compound that reduces the maximal specific binding of TM-PAA polymer to FimH-CRD by 50%. The relative IC_{50} (rIC_{50}) is the ratio of the IC_{50} of the test compound to the IC_{50} of *n*-heptyl α -D-mannopyranoside (1).

Selectivity for FimH vs Mannose-Binding Protein and DC-SIGN. Recombinant FimH-CRD-Th-6His (10 $\mu\text{g}/\text{mL}$), DC-SIGN-CRD-Fc-IgG³⁹ (2.5 $\mu\text{g}/\text{mL}$), and mannose-binding protein⁴² (MBP, 10 $\mu\text{g}/\text{mL}$, R&D Systems, Minneapolis, MN) were each diluted in assay buffer (20 mM HEPES, pH 7.4, 150 mM NaCl, and 10 mM CaCl_2) and were coated on microtiter plates (F96 MaxiSorp, Nunc) with 100 μL /well overnight at 4 $^\circ\text{C}$. The further steps were performed as described above.

Aggregometry Assay. The aggregometry assay was carried out as previously described.³³ In short, the percentage of aggregation of *E. coli* UTI89 with guinea pig erythrocytes (GPE) was quantitatively determined by measuring the optical density at 740 nm and 37 $^\circ\text{C}$ under stirring at 1000 rpm using an APACT 4004 aggregometer (Endotell AG, Allschwil, Switzerland). Bacteria were cultivated as described below (see in vivo models). GPE were separated from guinea pig blood (Charles River Laboratories, Sulzfeld, Germany) using Histopaque (density of 1.077 g/mL at 24 $^\circ\text{C}$, Sigma-Aldrich, Buchs, Switzerland). Prior to the measurements, the cell densities of *E. coli* and GPE were adjusted to an OD_{600} of 4, corresponding to 1.9×10^8 CFU/mL and 2.2×10^6 cells/mL, respectively. For the calibration of the instrument, the aggregation of protein-poor plasma (PPP) using PBS alone was set as 100% and the aggregation of protein-rich plasma (PRP) using GPE as 0%. After calibration, measurements were performed with 250 μL of GPE and 50 μL of bacterial suspension and the aggregation monitored over 600 s. After the aggregation phase of 600 s, 25 μL of antagonist in PBS was added to each cuvette and disaggregation was monitored for 1400 s. UTI89 $\Delta\text{fimA-H}$ was used as negative control.

Determination of the Pharmacokinetic Parameters. Materials. Dimethyl sulfoxide (DMSO), 1-octanol, pepsin, pancreatin, reduced nicotinamide adenine dinucleotide phosphate (NADPH), Dulbecco's Modified Eagle's Medium (DMEM) high glucose, and bis(4-nitrophenyl) phosphate (BNPP) were purchased from Sigma-Aldrich (Sigma-Aldrich, St. Louis MO, USA). PAMPA System Solution, GIT-0 Lipid Solution, and Acceptor Sink Buffer were ordered from pIon (pIon, Woburn MA, USA). L-Glutamine-200 mM (100 \times) solution, MEM nonessential amino acid (MEM-NEAA) solution, fetal bovine serum (FBS), and DMEM without sodium pyruvate and phenol red were bought from Invitrogen (Invitrogen, Carlsbad CA, USA). Human plasma was bought from Biopredic (Biopredic, Rennes, France) and acetonitrile (MeCN) from Acros (Acros Organics, Geel, Belgium). Pooled male mouse liver microsomes were purchased from BD Bioscience (BD Bioscience, Woburn, MA, USA). Magnesium chloride was bought from Fluka (Fluka Chemie GmbH, Buchs, Switzerland). Tris(hydroxymethyl)-aminomethane (TRIS) was obtained from AppliChem (AppliChem, Darmstadt, Germany). The Caco-2 cells were kindly provided by Prof G. Imanidis, FHNW, Muttentz, and originated from the American Type Culture Collection (Rockville, MD, USA).

log $D_{7.4}$ Determination. The in silico prediction tool ALOGPS 2.1⁵⁶ was used to estimate the log P values of the compounds. Depending on these values, the compounds were classified into three categories: hydrophilic compounds (log P

3 Results and discussion

Table 2

| compound type | log <i>P</i> | ratios (1-octanol:buffer) |
|-----------------------|--------------|---------------------------|
| hydrophilic | < 0 | 30:140, 40:130 |
| moderately lipophilic | 0–1 | 70:110, 110:70 |
| lipophilic | > 1 | 3:180, 4:180 |

below zero), moderately lipophilic compounds (log *P* between zero and one) and lipophilic compounds (log *P* above one). For each category, two different ratios (volume of 1-octanol to volume of buffer) were defined as experimental parameters (Table 2):

Equal amounts of phosphate buffer (0.1 M, pH 7.4) and 1-octanol were mixed and shaken vigorously for 5 min to saturate the phases. The mixture was left until separation of the two phases occurred, and the buffer was retrieved. Stock solutions of the test compounds were diluted with buffer to a concentration of 1 μM. For each compound, six determinations, i.e., three determinations per 1-octanol:buffer ratio, were performed in different wells of a 96-well plate. The respective volumes of buffer containing analyte (1 μM) were pipetted to the wells and covered by saturated 1-octanol according to the chosen volume ratio. The plate was sealed with aluminum foil, shaken (1350 rpm, 25 °C, 2 h) on a Heidolph Titramax 1000 plate-shaker (Heidolph Instruments GmbH & Co. KG, Schwabach, Germany) and centrifuged (2000 rpm, 25 °C, 5 min, 5804 R Eppendorf centrifuge, Hamburg, Germany). The aqueous phase was transferred to a 96-well plate for analysis by liquid chromatography–mass spectrometry (LC-MS).

log *D*_{7.4} was calculated from the 1-octanol:buffer ratio (*o:b*), the initial concentration of the analyte in buffer (1 μM), and the concentration of the analyte in buffer (*c*_B) with equilibration:

$$\log D_{7.4} = \log \left(\frac{1 \mu\text{M} - c_B}{c_B} \times \frac{1}{o:b} \right)$$

The average of the three log *D*_{7.4} values per 1-octanol:buffer ratio was calculated. If the two mean values obtained for a compound did not differ by more than 0.1 unit, the results were accepted.

Parallel Artificial Membrane Permeation Assay (PAMPA). log *P*_c was determined in a 96-well format with the PAMPA³⁰ permeation assay. For each compound, measurements were performed at three pH values (5.0, 6.2, 7.4) in quadruplicates. For this purpose, 12 wells of a deep well plate, i.e., four wells per pH value, were filled with 650 μL of System Solution. Samples (150 μL) were withdrawn from each well to determine the blank spectra by UV-spectroscopy (SpectraMax 190, Molecular Devices, Silicon Valley CA, USA). Then, analyte dissolved in DMSO was added to the remaining System Solution to yield 50 μM solutions. To exclude precipitation, the optical density was measured at 650 nm, with 0.01 being the threshold value. Solutions exceeding this threshold were filtrated. Afterward, samples (150 μL) were withdrawn to determine the reference spectra. A further 200 μL were transferred to each well of the donor plate of the PAMPA sandwich (pIon, Woburn MA, USA, P/N 110 163). The filter membranes at the bottom of the acceptor plate were impregnated with 5 μL of GIT-0 Lipid Solution and 200 μL of Acceptor Sink Buffer were filled into each acceptor well. The sandwich was assembled, placed in the GutBox, and left undisturbed for 16 h. Then, it was disassembled and samples (150 μL) were transferred from each donor and acceptor well to UV-plates. Quantification was performed by both UV-spectroscopy and LC-MS. log *P*_c values were calculated with the aid of the PAMPA Explorer Software (pIon, version 3.5).

Colorectal Adenocarcinoma Cells (Caco-2 Cells) Permeation Assay. The cells were cultivated in tissue culture flasks (BD Biosciences, Franklin Lakes NJ, USA) with DMEM high glucose medium, containing 1% L-glutamine solution, 1% MEM-NEAA solution, and 10% FBS. The cells were kept at

37 °C in humidified air containing 8% CO₂, and the medium was changed every second to third day. When approximately 90% confluence was reached, the cells were split in a 1:10 ratio and distributed to new tissue culture flasks. At passage numbers between 60 and 65, they were seeded at a density of 5.33 × 10⁵ cells per well to Transwell 6-well plates (Corning Inc., Corning NY, USA) with 2.5 mL of culture medium in the basolateral compartment and 1.5 mL (days 1–10) or 1.8 mL (from day 10 on) in the basolateral compartment. The medium was renewed on alternate days. Experiments were performed between days 19 and 21 postseeding. DMEM without sodium pyruvate and phenol red was used as transport medium for experiments. Previous to the experiment, the integrity of the Caco-2 monolayers was evaluated by measuring the transepithelial resistance (TEER) in transport medium (37 °C) with an Endohm tissue resistance instrument (World Precision Instruments Inc., Sarasota, FL, USA). Only wells with TEER values higher than 300 Ωcm² were used. Experiments were performed in triplicates. Transport medium (10 μL) from the apical compartments of three wells were replaced by the same volume of compound stock solutions (10 mM). The Transwell plate was then shaken (250 rpm) in the incubator. Samples (100 μL) were withdrawn after 5, 15, 30, 60, and 120 min from the basolateral compartment and concentrations were analyzed by HPLC. Apparent permeability coefficients (*P*_{app}) were calculated according to the following equation

$$P_{\text{app}} = \frac{dQ}{dt} \times \frac{1}{A \times c_0}$$

where *dQ/dt* is the permeability rate, *A* the surface area of the monolayer, and *c*₀ the initial concentration in the donor compartment.³¹ After the experiment, TEER values were assessed again for every well and results from wells with values below 300 Ωcm² were discarded.

p*K*_a Values. The p*K*_a values were determined as described elsewhere.⁴⁵ Briefly, the pH of a sample solution was gradually changed and the chemical shift of protons adjacent to ionizable centers was monitored by ¹H nuclear magnetic resonance (NMR) spectroscopy. The shift was plotted against the pH of the respective sample, and the p*K*_a was read out from the inflection point of the resulting sigmoidal curve.

Plasma Protein Binding (PPB). The dialysis membranes (HTDialysis LCC, Gales Ferry, CT, USA; MWCO 12–14 K) were prepared according to company instructions. The human plasma was centrifuged (5800 rpm, 25 °C, 10 min), the pH of the centrifugate (without floating plasma lipids) was adjusted to 7.5, and analyte was added to yield 10 μM solutions. Equal volumes (150 μL) of phosphate buffer (0.1 M, pH 7.5) and analyte-containing plasma were transferred to the separated compartments of the assembled 96-well high throughput dialysis block (HTDialysis LCC, Gales Ferry, CT, USA). Measurements were performed in triplicates. The plate was covered with a sealing film and incubated (5 h, 37 °C). Buffer and plasma compartment were processed separately. From the buffer compartments, 90 μL were withdrawn and 10 μL of blank plasma were added. From the plasma compartments, 10 μL were withdrawn and 90 μL of blank buffer were added. After protein precipitation with 300 μL ice-cooled MeCN, the solutions were mixed, centrifuged (3600 rpm, 4 °C, 11 min), and 50 μL of the supernatant were retrieved. Analyte concentrations were determined by LC-MS. The fraction bound (*f*_b) was calculated as follows:

$$f_b = 1 - \frac{c_b}{c_p}$$

where *c*_b is the concentration in the buffer and *c*_p the concentration in the plasma compartment. Values were accepted if the recovery of analyte was between 80 and 120%.

Thermodynamic Solubility. Microanalysis tubes (Labo-Tech J. Stofer LTS AG, Muttenz, Switzerland) were charged with

3.1 Pharmacokinetic properties of FimH antagonists with biphenyl-moiety

Article

Journal of Medicinal Chemistry, 2010, Vol. 53, No. 24 8639

1 mg of solid substance and 250 μ L of phosphate buffer (50 mM, pH 6.5). The samples were briefly shaken by hand and then sonicated for 15 min and vigorously shaken (600 rpm, 25 °C, 2 h) on a Eppendorf Thermomixer Comfort. Afterward, the samples were left undisturbed for 24 h. After measuring the pH, the saturated solutions were filtered through a filtration plate (MultiScreen HTS, Millipore, Billerica MA, USA) by centrifugation (1500 rpm, 25 °C, 3 min). Prior to concentration determination by LC-MS, the filtrates were diluted (1:1, 1:10 and 1:100 or, if the results were outside of the calibration range, 1:1000 and 1:10000). The calibration was based on six values ranging from 0.1 to 10 μ g/mL.

Stability in Simulated Gastrointestinal Fluids. Simulated gastric fluid (sGF) and simulated intestinal fluid (sIF) were prepared according to the United States Pharmacopeia (USP 28). sGF contained sodium chloride (200 mg), pepsin (320 mg), and 37% aq HCl (0.7 mL) in bidistilled water (100 mL). sIF consisted of monopotassium phosphate (680 mg), 0.2 M NaOH (7.7 mL), and pancreatin (1 g) in bidistilled water (100 mL). sIF was adjusted to pH 6 by adding 0.2 M NaOH. sGF and sIF were preheated (37 °C), and the compounds were added to yield 10 μ M solutions. Incubations were performed on a Eppendorf Thermomixer Comfort (500 rpm, 37 °C). Before starting the experiment ($t = 0$ min) and after an incubation time of 15, 30, 60, and 120 min, samples (20 μ L) were withdrawn, precipitated with ice-cooled MeCN, and centrifuged (3600 rpm, 4 °C, 10 min). The concentrations of analyte in the supernatant were analyzed by LC-MS. Stability was expressed as percentage remaining compound relative to the initial concentration.

In Vitro Metabolism: Ester Hydrolysis. Incubations were performed in a 96-well format on a Eppendorf Thermomixer Comfort. Each compound was incubated with a reaction mixture (270 μ L) consisting of pooled male mouse liver microsomes in the presence of TRIS buffer (0.1 M, pH 7.4) and MgCl₂ (2 mM). After preheating (37 °C, 500 rpm, 10 min), the incubation was initiated by adding 30 μ L of compound solution (20 μ M) in TRIS buffer. The final concentration of the compounds was 2 μ M, and the microsomal concentration was 0.25 mg/mL. At the beginning of the experiment ($t = 0$ min) and after an incubation time of 1, 3, 6, and 15 min, samples (50 μ L) were transferred to 150 μ L of ice-cooled MeCN, centrifuged (3600 rpm, 4 °C, 10 min), and 80 μ L of supernatant were transferred to a 96-well plate for LC-MS analysis. Metabolic degradation was assessed as percentage remaining compound versus incubation time. Control experiments were performed in parallel by preincubating the microsomes with the specific carboxylesterase inhibitor BNPP (1 mM) for 5 min before addition of the antagonists.

In Vitro Metabolism: Cytochrome P450-Mediated Metabolism. Incubations consisted of pooled male mouse liver microsomes (0.5 mg microsomal protein/mL), compounds (2 μ M), MgCl₂ (2 mM), and NADPH (1 mM) in a total volume of 300 μ L TRIS buffer (0.1 M, pH 7.4) and were performed in a 96-well plate on a Thermomixer Comfort. Compounds and microsomes were preincubated (37 °C, 700 rpm, 10 min) before NADPH was added. Samples (50 μ L) at $t = 0$ min and after an incubation time of 5, 10, 20, and 30 min were quenched with 150 μ L of ice-cooled acetonitrile, centrifuged (3600 rpm, 4 °C, 10 min), and 80 μ L of each supernatant were transferred to a 96-well plate for LC-MS analysis. Control experiments without NADPH were performed in parallel.

LC-MS Measurements. Analyses were performed using a 1100/1200 series HPLC system coupled to a 6410 triple quadrupole mass detector (Agilent Technologies, Inc., Santa Clara, CA, USA) equipped with electrospray ionization. The system was controlled with the Agilent MassHunter Workstation Data Acquisition software (version B.01.04). The column used was an Atlantis T3 C18 column (2.1 mm \times 50 mm) with a 3 μ m particle size (Waters Corp., Milford, MA, USA). The mobile phase consisted of two eluents: solvent A (H₂O, containing 0.1%

formic acid, v/v) and solvent B (acetonitrile, containing 0.1% formic acid, v/v), both delivered at 0.6 mL/min. The gradient was ramped from 95% A/5% B to 5% A/95% B over 1 min, and then held at 5% A/95% B for 0.1 min. The system was then brought back to 95% A/5% B, resulting in a total duration of 4 min. MS parameters such as fragmentor voltage, collision energy, polarity were optimized individually for each drug, and the molecular ion was followed for each compound in the multiple reaction monitoring mode. The concentrations of the analytes were quantified by the Agilent Mass Hunter Quantitative Analysis software (version B.01.04).

In Vivo Pharmacokinetic and Disease Model. Bacteria. The clinical *E. coli* isolate UTI89⁵⁵ (UTI89wt) were kindly provided by the group of Prof. Urs Jenal, Biocenter, University of Basel. Microorganisms were stored at -70 °C and before experiment incubated for 24 h under static conditions at 37 °C in 10 mL of Luria-Bertani broth (Becton, Dickinson and Company, Le Pont de Claix, France) using 50 mL tubes. Prior to each experiment, the microorganisms were washed twice and resuspended in phosphate buffered saline (PBS, Hospital Pharmacy at the University Hospital Basel, Switzerland). Bacterial concentrations were determined by plating serial 1:10 dilutions on blood agar, followed by colony counting with 20–200 colonies after overnight incubation at 37 °C.

Animals. Female C3H/HeN mice weighting between 19 and 25 g were obtained from Charles River (Sulzfeld, Germany) and were housed four to a cage. Mice were kept under specific-pathogen-free conditions in the Animal House of the Department of Biomedicine, University Hospital Basel, and animal experimentation guidelines according to the regulations of Swiss veterinary law were followed. After seven days of acclimatization, 9- to 10-week old mice were used for the PK and infection studies. During the studies, animals were allowed free access to chow and water. Three days before infection studies and during infection, 5% D-(+)-glucose (AppliChem, Baden-Dättwil, Switzerland) was added to the drinking water to increase the number of bacterial counts in the urine and kidneys.⁵⁷

Pharmacokinetic Studies. Single-dose pharmacokinetic studies were performed by iv and po application of the FimH antagonists at a concentration of 50 mg/kg followed by urine and plasma sampling. For iv application, the antagonists (**1**, **17a**, **17b**) were diluted in 100 μ L of PBS and injected into the tail vein. For po application, antagonist **1** was diluted in 200 μ L of PBS and antagonists **17b** and **16b** were first dissolved in DMSO (20 \times) and then slowly diluted to the final concentration (1 \times) in 1% Tween-80/PBS to obtain a suspension. Antagonists were applied iv by injection into the tail vein and po using a gavage followed by blood and urine sampling (10 μ L) after 6 min, 30 min, 1 h, 2 h, 4 h, 6 h, 8 h, and 24 h. Before analysis, proteins in blood and urine samples were precipitated using methanol (Acros Organics, Basel, Switzerland) and centrifuged for 11 min at 13000 rpm. The supernatant was transferred into a 96-well plate (0.5 mL, polypropylene, Agilent Technologies, Basel, Switzerland) and analyzed by LC-MS as described above.

UTI Mouse Model. Mice were infected as previously described.⁵⁷ In brief, before infection, all remaining urine was depleted from the bladder by gentle pressure on the abdomen. Mice were anesthetized with 2.5 vol% isoflurane/oxygen mixture (Attane, Minrad Inc., Buffalo, NY, USA) and placed on their back. Anesthetized mice were inoculated transurethrally with the bacterial suspension by use of a 2 cm polyethylene catheter (Intramedic polyethylene tubing, inner diameter 0.28 mm, outer diameter 0.61 mm, Beckton Dickinson, Allschwil, Switzerland), which was placed on a syringe (Hamilton Gastight Syringe 50 μ L, removable 30G needle, BGB Analytik AG, Boeckten, Switzerland). The catheter was gently inserted through the urethra until it reached the top of the bladder, followed by slow injection of 50 μ L of bacterial suspension at a concentration of approximately 10⁹ to 10¹⁰ CFU/mL.

Antagonist Treatment Studies. FimH antagonists were applied iv in 100 μ L of PBS into the tail vein or po as a suspension by the help

of a gavage, 10 min (17a, 17b, 16b) or 1 h before infection (1). Three h after the onset of infection, urine was collected by gentle pressure on the abdomen and then the mouse was sacrificed with CO₂. Organs were removed aseptically and homogenized in 1 mL of PBS by using a tissue lyser (Retsch, Haan, Germany). Serial dilutions of urine, bladder, and kidneys were plated on Levine Eosin Methylene Blue Agar plates (Beckton Dickinson, Le Pont de Claix, France). CFU counts were determined after overnight incubation at 37 °C and expressed as CFU/mL for the urine and CFU/bladder and CFU/2 kidneys for the organs.

Acknowledgment. We thank Professor Rudi Glockshuber (ETH Zürich, Switzerland) for gratefully providing the plasmid pNT-FimH used for the cloning of the FimH CRD and *E. coli* strain HM 125. We thank Dr. Manfred Kansy and Dr. Christoph Funk, F. Hoffmann-La Roche AG, Basel, Switzerland, for supporting us with their expertise when we established the PADMET platform, and to Prof. Angelo Vedani, University of Basel, Switzerland, for fruitful discussions on conformational issues. We further appreciate the support by Prof. Dr. med. Radek Skoda, Department of Biomedicine, University Hospital Basel, Switzerland, for giving us access to the animal facility and Prof. Niels Frimodt-Møller, Statens Serum Institut, Copenhagen, Denmark for the introduction to the in vivo model. We thank Prof G. Imanidis, FHNW, Muttenz, Switzerland, for providing the Caco-2 cells, and Dr. M. Schneider, Department of Pharmaceutical Sciences, University of Basel, Switzerland, for his help during the assay build-up. We are grateful to Prof. Urs Jenal, Biocenter of the University of Basel, Switzerland, for the clinical *E. coli* isolate UTI89 and the FimH knock out strain UTI89Δ*fimA-H*. Finally, we thank the Swiss National Science Foundation (project K-32K1-120904) for their financial support.

Supporting Information Available: ¹H NMR spectra and HPLC traces for the target compounds 16a–e, 17a–c, 21a, b, and 22a, b and experimental and spectroscopic details for compounds 6a–d, 7a–d, 14c–e, 15c–e, 16c–e, 17c, e, 19a, b, 20a, b, and 21a, b. This material is available free of charge via the Internet at <http://pubs.acs.org>.

References

- Fihn, S. D. Clinical practice. Acute uncomplicated urinary tract infection in women. *N. Engl. J. Med.* **2003**, *349*, 259–266.
- Hooton, T. M. Recurrent urinary tract infection in women. *Int. J. Antimicrob. Agents* **2001**, *17*, 259–268.
- Wiles, T. J.; Kulesus, R. R.; Mulvey, M. A. Origins and virulence mechanisms of uropathogenic *Escherichia coli*. *Exp. Mol. Pathol.* **2008**, *85*, 11–19.
- Gouin, S. G.; Wellens, A.; Bouckaert, J.; Kovensky, J. Synthetic Multimeric Heptyl Mannosides as Potent Antiadhesives of Uropathogenic *Escherichia coli*. *ChemMedChem* **2009**, *4*, 749–755.
- Rosen, D. A.; Hung, C. S.; Kline, K. A.; Hultgren, S. J. Streptozocin-induced diabetic mouse model of urinary tract infection. *Infect. Immun.* **2008**, *76*, 4290–4298.
- Mulvey, M. A. Adhesion and entry of uropathogenic *Escherichia coli*. *Cell Microbiol.* **2002**, *4*, 257–271.
- Capitani, G.; Eidam, O.; Glockshuber, R.; Grutter, M. G. Structural and functional insights into the assembly of type 1 pili from *Escherichia coli*. *Microbes Infect.* **2006**, *8*, 2284–2290.
- Choudhury, D.; Thompson, A.; Stojanoff, V.; Langermann, S.; Pinkner, J.; Hultgren, S. J.; Knight, S. D. X-ray structure of the FimC–FimH chaperone–adhesin complex from uropathogenic *Escherichia coli*. *Science* **1999**, *285*, 1061–1066.
- Bouckaert, J.; Berglund, J.; Schembri, M.; Genst, E. D.; Cools, L.; Wuhler, M.; Hung, C. S.; Pinkner, J.; Slättergard, R.; Zavialov, A.; Choudhury, D.; Langermann, S.; Hultgren, S. J.; Wyns, L.; Klemm, P.; Oscarson, S.; Knight, S. D.; Greve, H. D. Receptor binding studies disclose a novel class of high-affinity inhibitors of the *Escherichia coli* FimH adhesin. *Mol. Microbiol.* **2005**, *55*, 441–455.
- Wellens, A.; Garofalo, C.; Nguyen, H.; Van Gerven, N.; Slättergard, R.; Hernalsteens, J.-P.; Wyns, L.; Oscarson, S.; De Greve, H.; Hultgren, S.; Bouckaert, J. Intervening with urinary tract infections using anti-adhesives based on the crystal structure of the FimH–oligomannose-3 complex. *PLoS ONE* **2008**, *3*, 4–13.
- Langermann, S.; Mollby, R.; Burlein, J. E.; Palaszynski, S. R.; Auguste, C. G.; DeFusco, A.; Strouse, R.; Schenerman, M. A.; Hultgren, S. J.; Pinkner, J. S.; Winberg, J.; Guldevall, L.; Soderhall, M.; Ishikawa, K.; Normark, S.; Koenig, S. Vaccination with FimH adhesin protects cynomolgus monkeys from colonization and infection by uropathogenic *Escherichia coli*. *J. Infect. Dis.* **2000**, *181*, 774–778.
- Langermann, S.; Palaszynski, S.; Barnhart, M.; Auguste, G.; Pinkner, J. S.; Burlein, J.; Barren, P.; Koenig, S.; Leath, S.; Jones, C. H.; Hultgren, S. J. Prevention of mucosal *Escherichia coli* infection by FimH-adhesin-based systemic vaccination. *Science* **1997**, *276*, 607–611.
- Bouckaert, J.; Mackenzie, J.; de Paz, J. L.; Chipwaza, B.; Choudhury, D.; Zavialov, A.; Mannerstedt, K.; Anderson, J.; Pierard, D.; Wyns, L.; Seeberger, P. H.; Oscarson, S.; De Greve, H.; Knight, S. D. The affinity of the FimH fimbrial adhesin is receptor-driven and quasi-independent of *Escherichia coli* pathotypes. *Mol. Microbiol.* **2006**, *61*, 1556–1568.
- Sharon, N. Carbohydrates as future anti-adhesion drugs for infectious diseases. *Biochim. Biophys. Acta* **2006**, *1760*, 527–537.
- (a) Firon, N.; Ofek, I.; Sharon, N. Interaction of mannose-containing oligosaccharides with the fimbrial lectin of *Escherichia coli*. *Biochem. Biophys. Res. Commun.* **1982**, *105*, 1426–1432. (b) Firon, N.; Ofek, I.; Sharon, N. Carbohydrate specificity of the surface lectins of *Escherichia coli*, *Klebsiella pneumoniae* and *Salmonella typhimurium*. *Carbohydr. Res.* **1983**, *120*, 235–249. (c) Sharon, N. Bacterial lectins, cell–cell recognition and infectious disease. *FEBS Lett.* **1987**, *217*, 145–157.
- (a) Neeser, J.-R.; Koellreutter, B.; Wuersch, P. Oligomannoside-type glycopeptides inhibiting adhesion of *Escherichia coli* strains mediated by type 1 pili: preparation of potent inhibitors from plant glycoproteins. *Infect. Immun.* **1986**, *52*, 428–436. (b) Lindhorst, T. K. Artificial multivalent sugar ligands to understand and manipulate carbohydrate–protein interactions. *Top. Curr. Chem.* **2002**, *218*, 201–235 (review); (c) Patel, A.; Lindhorst, T. K. A modular approach for the synthesis of oligosaccharide mimetics. *Carbohydr. Res.* **2006**, *341*, 1657–1668. (d) Nagahori, N.; Lee, R. T.; Nishimura, S.-L.; Pagé, S.; Roy, R.; Lee, Y. C. Inhibition of adhesion of type 1 fimbriated *Escherichia coli* to highly mannosylated ligands. *ChemBioChem* **2002**, *3*, 836–844. (e) Appeldoorn, C. C. M.; Joosten, J. A. F.; Maate, F. A.; Dobrindt, U.; Hacker, J.; Liskamp, R. M. J.; Khan, A. S.; Pieters, R. J. Novel multivalent mannose compounds and their inhibition of the adhesion of type 1 fimbriated uropathogenic *E. coli*. *Tetrahedron Asymmetry* **2005**, *16*, 361–372. (f) Touaibia, M.; Wellens, A.; Shiao, T. C.; Wang, Q.; Sirois, S.; Bouckaert, J.; Roy, R. Mannosylated G(0) dendrimers with nanomolar affinities to *Escherichia coli* FimH. *ChemMedChem* **2007**, *2*, 1190–1201.
- (a) Firon, N.; Ashkenazi, S.; Mirelman, D.; Ofek, I.; Sharon, N. Aromatic alpha-glycosides of mannose are powerful inhibitors of the adherence of type 1 fimbriated *Escherichia coli* to yeast and intestinal epithelial cells. *Infect. Immun.* **1987**, *55*, 472–476. (b) Lindhorst, T. K.; Köter, S.; Kubisch, J.; Krallmann-Wenzel, U.; Ehlers, S.; Kren, V. Effect of p-substitution of aryl α-D-mannosides on inhibiting mannose-sensitive adhesion of *Escherichia coli*—synthesis and testing. *Eur. J. Org. Chem.* **1998**, 1669–1674. (c) Sperling, O.; Fuchs, A.; Lindhorst, T. K. Evaluation of the carbohydrate recognition domain of the bacterial adhesin FimH: design, synthesis and binding properties of mannoside ligands. *Org. Biomol. Chem.* **2006**, *4*, 3913–3922. (d) Han, Z.; Pinker, J. S.; Ford, B.; Obermann, R.; Nolan, W.; Wildman, S. A.; Hobbs, D.; Ellenberger, T.; Cusumano, C. K.; Hultgren, S. J.; Janetka, J. W. Structure-Based Drug Design and Optimization of Mannoside Bacterial FimH Antagonists. *J. Med. Chem.* **2010**, *53*, 4779–4792. (e) Berglund, J.; Bouckaert, J.; De Greve, H.; Knight, S. Anti-adhesive compounds to prevent and treat bacterial infections. International Patent Application PCT/US 2005/089733, 2005.
- Hung, C. S.; Bouckaert, J.; Hung, D.; Pinkner, J.; Widberg, C.; Defusco, A.; Auguste, C. G.; Strouse, R.; Langermann, S.; Waksman, G.; Hultgren, S. J. Structural basis of tropism of *Escherichia coli* to the bladder during urinary tract infection. *Mol. Microbiol.* **2002**, *44*, 903–918.
- Ernst, B.; Magnani, J. L. From carbohydrate leads to glycomimetic drugs. *Nature Rev. Drug Discovery* **2009**, *8*, 661–677.
- (a) Lindhorst, T. K.; Kieburg, C.; Krallmann-Wenzel, U. Inhibition of the type 1 fimbriae-mediated adhesion of *Escherichia coli* to erythrocytes by multiantennary α-mannosyl clusters: the effect of multivalency. *Glycoconjugate J.* **1998**, *15*, 605–613. (b) Dubber, M.; Sperling, O.; Lindhorst, T. K. Oligomannoside mimetics by glycosylation of 'octopus glycosides' and their investigation as inhibitors of type 1

3.1 Pharmacokinetic properties of FimH antagonists with biphenyl-moiety

Article

Journal of Medicinal Chemistry, 2010, Vol. 53, No. 24 8641

- fimbriae-mediated adhesion of *Escherichia coli*. *Org. Biomol. Chem.* **2006**, *4*, 3901–3912. (c) Touaibia, M.; Wellens, A.; Shiao, T. C.; Wang, Q.; Sirois, S.; Bouckaert, J.; Roy, R. Mannosylated G0 dendrimers with nanomolar affinities to *Escherichia coli* FimH. *ChemMedChem* **2007**, *2*, 1190–1201.
- (21) Aronson, M.; Medalia, O.; Schori, L.; Mirelman, D.; Sharon, N.; Ofek, I. Prevention of colonization of the urinary tract of mice with *Escherichia coli* by blocking of bacterial adherence with methyl α -D-mannopyranoside. *J. Infect. Dis.* **1979**, *139*, 329–332.
- (22) Svanborg Eden, C.; Freter, R.; Hagberg, L.; Hull, R.; Leffer, H.; Schoolnik, G. Inhibition of experimental ascending urinary tract infection by an epithelial cell-surface receptor analog. *Nature* **1982**, *298*, 560–562.
- (23) Rabbani, S.; Jiang, X.; Schwardt, O.; Ernst, B. Expression of the carbohydrate recognition domain of FimH and development of a competitive binding assay. *Anal. Biochem.* **2010**, *407*, 188–195.
- (24) Ness, R. K.; Fletcher, H. G.; Hudson, C. S. Reaction of 2,3,4,6-tetrabenzoyl- α -D-glucopyranosyl bromide and 2,3,4,6-tetrabenzoyl- α -D-mannopyranosyl bromide with methanol. Certain benzoylated derivatives of D-glucose and D-mannose. *J. Am. Chem. Soc.* **1950**, *72*, 2200–2205.
- (25) Sancho-Garcia, J. C.; Cornil, J. Anchoring the Torsional Potential of Biphenyl at the ab Initio Level: The Role of Basis Set versus Correlation Effects. *J. Chem. Theory Comput.* **2005**, *1*, 581–589.
- (26) Eaton, V. J.; Steele, D. Dihedral angle of biphenyl in solution and the molecular force field. *J. Chem. Soc., Faraday Trans. 2* **1973**, 1601–1608.
- (27) Albert, A. Chemical aspects of selective toxicity. *Nature* **1958**, *182*, 421–422.
- (28) Winiwarter, S.; Bonham, N. M.; Ax, F.; Hallberg, A.; Lennernäs, H.; Karlén, A. Correlation of Human Jejunal Permeability (in Vivo) of Drugs with Experimentally and Theoretically Derived Parameters. A Multivariate Data Analysis Approach. *J. Med. Chem.* **1998**, *41*, 4939–4949.
- (29) Taketani, M.; Shii, M.; Ohura, K.; Ninomiya, S.; Imai, T. Carboxylesterase in the liver and small intestine of experimental animals and human. *Life Sci.* **2007**, *81*, 924–932.
- (30) Kansy, M.; Senner, F.; Gubernator, K. Physicochemical High Throughput Screening: Parallel Artificial Membrane Permeation Assay in the Description of Passive Absorption Processes. *J. Med. Chem.* **1998**, *41*, 1007–1010.
- (31) Artursson, P.; Karlsson, J. Correlation between oral drug absorption in humans and apparent drug permeability coefficients in human intestinal epithelial (Caco-2) cells. *Biochem. Biophys. Res. Com.* **1991**, *175*, 880–885.
- (32) Varma, M. V. S.; Feng, B.; Obach, R. S.; Troutman, M. D.; Chupka, J.; Miller, H. R.; El-Kattan, A. Physicochemical Determinants of Human Renal Clearance. *J. Med. Chem.* **2009**, *52*, 4844–4852.
- (33) Abgottspon, D.; Rölli, G.; Hosch, L.; Steinhuber, A.; Jiang, X.; Schwardt, O.; Cutting, B.; Smiesko, M.; Jenal, U.; Ernst, B.; Trampuz, A. Development of an Aggregation Assay to Screen FimH Antagonists. *J. Microbiol. Methods* **2010**, *82*, 249–255.
- (34) Zhou, G.; Mo, W.-J.; Sebbel, P.; Min, G.; Neubert, T. A.; Glockshuber, R.; Wu, X.-R.; Sun, T.-T.; Kong, X.-P. Uroplakin Ia is the urothelial receptor for uropathogenic *Escherichia coli*: evidence from in vitro FimH binding. *J. Cell Sci.* **2001**, *114*, 4095–4103.
- (35) (a) Kartha, K. P. R.; Field, R. A. Iodine: a versatile reagent in carbohydrate chemistry. IV. Per-O-acetylation, regioselective acylation and acetyolysis. *Tetrahedron* **1997**, *53*, 11753–11766. (b) Chittaboina, S.; Hodges, B.; Wang, Q. A facile route for the regioselective deacetylation of peracetylated carbohydrates at anomeric position. *Lett. Org. Chem.* **2006**, *3*, 35–38. (c) Mori, M.; Ito, Y.; Ogawa, T. Total synthesis of the mollu-series glycosyl ceramides α -D-Manp-(1 \rightarrow 3)- β -D-Manp-(1 \rightarrow 4)- β -D-Glcp-(1 \rightarrow 1)-Cer and α -D-Manp-(1 \rightarrow 3)- $[\beta$ -D-Xylp-(1 \rightarrow 2)]- β -D-Manp-(1 \rightarrow 4)- β -D-Glcp-(1 \rightarrow 1)-Cer. *Carbohydr. Res.* **1990**, *195*, 199–224. (d) Egusa, K.; Kusumoto, S.; Fukase, K. Solid-phase synthesis of a phytoalexin elicitor pentasaccharide using a 4-azido-3-chlorobenzyl group as the key for temporary protection and catch-and-release purification. *Eur. J. Org. Chem.* **2003**, 3435–3445.
- (36) Giampapa, C. S.; Abraham, S. N.; Chiang, T. M.; Beachey, E. H. Isolation and characterization of a receptor for type 1 fimbriae of *Escherichia coli* from guinea pig erythrocytes. *J. Biol. Chem.* **1988**, *263*, 5362–5367.
- (37) Aprikian, P.; Tchesnokova, V.; Kidd, B.; Yakovenko, O.; Yarov-Yarovoy, V.; Trinchina, E.; Vogel, V.; Thomas, W.; Sokurenko, E. Interdomain interaction in the FimH adhesin of *Escherichia coli* regulates the affinity to mannose. *J. Biol. Chem.* **2007**, *282*, 23437–23446.
- (38) Trong, I. L.; Aprikian, P.; Kidd, B. A.; Forero-Shelton, M.; Tchesnokova, V.; Rajagopal, P.; Rodriguez, V.; Interlandi, G.; Klevit, R.; Vogel, V.; Stenkamp, R. E.; Sokurenko, E. V.; Thomas, W. E. Structural basis for mechanical force regulation of the adhesin FimH via finger trap-like beta sheet twisting. *Cell* **2010**, *141*, 645–655.
- (39) Khoo, U. S.; Chan, K. Y. K.; Chan, V. S. F.; Lin, C. L. S. DC-SIGN and L-SIGN: the SIGNs for infection. *J. Mol. Med.* **2008**, *86*, 861–874.
- (40) Lee, S. J.; Evers, S.; Roeder, D.; Parlow, A. F.; Risteli, J.; Risteli, L.; Lee, Y. C.; Feizi, T.; Langen, H.; Nussenzweig, M. C. Mannose receptor-mediated regulation of serum glycoprotein homeostasis. *Science* **2002**, *295*, 1898–1901.
- (41) East, L.; Isacke, C. M. The mannose receptor family. *Biochim. Biophys. Acta* **2002**, *1572*, 364–386.
- (42) Dommett, R. M.; Klein, N.; Turner, M. W. Mannose-binding lectin in innate immunity: past, present and future. *Tissue Antigens* **2006**, *68*, 193–209.
- (43) Scharenberg, M. Expression and purification of DC-SIGN-CRD-Fc-IgG. Unpublished results.
- (44) Dearden, J. C.; Bresnen, J. G. M. The measurement of partition coefficients. *QSAR Comb. Sci.* **1988**, *7*, 133–144.
- (45) Wittwer, M.; Bezençon, J.; Cutting, B.; Wagner, B.; Kansy, M.; Ernst, B. pK_a determination by ¹H-NMR spectroscopy—an old methodology revisited. Unpublished results.
- (46) Banker, M. J.; Clark, T. H.; Williams, J. A. Development and validation of a 96-well equilibrium dialysis apparatus for measuring plasma protein binding. *J. Pharm. Sci.* **2003**, *92*, 967–974.
- (47) Kerns, E. H. High throughput physicochemical profiling for drug discovery. *J. Pharm. Sci.* **2001**, *90*, 1838–1858.
- (48) Avdeef, A.; Bendels, S.; Di, L.; Faller, B.; Kansy, M.; Sugano, K.; Yamauchi, Y. Parallel artificial membrane permeability assay (PAMPA)-critical factors for better predictions of absorption. *J. Pharm. Sci.* **2007**, *96*, 2893–2909.
- (49) Brandt, E.; Heymann, E.; Mentlein, R. Selective inhibition of rat liver carboxylesterases by various organophosphorus diesters in vivo and in vitro. *Biochem. Pharmacol.* **1980**, *29*, 1927–1931.
- (50) Scharenberg, M.; Abgottspon, D. Personal communication.
- (51) Obach, R. S. Prediction of human clearance of twenty-nine drugs from hepatic microsomal intrinsic clearance data: an examination of in vitro half-life approach and nonspecific binding to microsomes. *Drug Metab. Dispos.* **1999**, *27*, 1350–1359.
- (52) Trainor, G. L. The importance of plasma protein binding in drug discovery. *Expert Opin. Drug Discovery* **2007**, *2*, 51–64.
- (53) Weisiger, R. A. Dissociation from albumin: a potentially rate-limiting step in the clearance of substances by the liver. *Proc. Natl. Acad. Sci. U.S.A.* **1985**, *82*, 1563–1567.
- (54) Urien, S.; Tillement, J.-P.; Barre, J. The significance of plasma protein binding in drug research. In *Pharmacokinetic Optimization in Drug Research: Biological, Physicochemical, and Computational Strategies*; Wiley-VCH: Weinheim, Germany, 2001; pp 189–197.
- (55) Mulvey, M. A.; Schilling, J. D.; Hultgren, S. J. Establishment of a persistent *Escherichia coli* reservoir during the acute phase of a bladder infection. *Infect. Immun.* **2001**, *69*, 4572–4579.
- (56) (a) VCCLAB, *Virtual Computational Chemistry Laboratory*; <http://www.vcclab.org>, 2005; (b) Tetko, I. V.; Gastegger, J.; Todeschini, R.; Mauri, A.; Livingstone, D.; Ertl, P.; Palyulin, V. A.; Radchenko, E. V.; Zefirov, N. S.; Makarenko, A. S.; Tanchuk, V. Y.; Prokopenko, V. V. Virtual computational chemistry laboratory—design and description. *J. Comput.-Aided Mol. Des.* **2005**, *19*, 453–463.
- (57) Kern, M. B.; Frimodt-Møller, N.; Espersen, F. Effects of Sulfamethizole and Aminocillin against *Escherichia coli* Strains (with Various Susceptibilities) in an Ascending Urinary Tract Infection Model. *Antimicrob. Agents Chemother.* **2003**, *47*, 1002–1009.

3 Results and discussion

3.2 Factors influencing the permeation properties of carbohydrate mimetics

Carbohydrate mimetics are generally not expected to permeate through membranes by passive diffusion. Nevertheless, for several FimH antagonists promising PAMPA results were achieved and confirmed by in vivo PK-experiments, as described before. As a consequence, the parameters influencing the penetration of carbohydrate mimetics through a lipid bilayer by passive diffusion were explored. Various in silico descriptors and experimental $\log D_{7.4}$ values were thus tested regarding their capability of explaining PAMPA results.

Matthias Wittwer performed or supervised all PAMPA and $\log D_{7.4}$ determinations and interpreted the results. The work on the manuscript was shared between the two equally contributing authors of this publication.

This manuscript is in preparation for the *Journal of Medicinal Chemistry*.

3.2 Factors influencing the permeation properties of carbohydrate mimetics

Sweet previsions: Modeling the permeation of carbohydrate mimetics

Matthias Wittwer⁺, Martin Smiesko⁺, Beat Ernst*

Institute of Molecular Pharmacy, Pharmacenter, University of Basel,
Klingelbergstrasse 50, CH-4056 Basel, Switzerland

⁺ These authors contributed equally to this publication.

* *Correspondence:* Prof. Dr. Beat Ernst

Institute of Molecular Pharmacy

University of Basel

Klingelbergstrasse 50

CH-4056 Basel

Tel.: +41 61 267 1551,

Fax: +41 61 267 1552

Keywords: Membrane permeation, transcellular diffusion, PAMPA, modeling, in silico descriptors.

Abbreviations: HB, hydrogen bond; PAMPA, parallel artificial membrane permeation assay; PSA, polar surface area; QSAR, qualitative structure-activity relationships; SASA, solvent accessible surface area; VCCLAB, virtual computational chemistry laboratory.

3 Results and discussion

Abstract

Since the oral application of drugs is the most convenient way of therapy it is the aim of most drug discovery projects to identify orally available compounds. Besides metabolism and solubility problems, the crossing of the intestinal mucosa represents a major obstacle and properties related to good permeation are thus beneficial. Various assays have been developed to predict the uptake from the gastrointestinal tract, amongst them the parallel artificial membrane permeation assay (PAMPA). The special characteristics of this assay enable the determination of passive permeation without the influence of active transport processes. Even though the latter are important for distribution and uptake in various tissues and organs, they are suspected to play a small role for gastrointestinal absorption.

Although the *in silico* prediction of oral bioavailability remains difficult, considerable success has been achieved regarding the prediction of passive membrane permeation. The descriptors involved in this process are generally well understood and readily accessible. Single or combined descriptor models (typically including molecular weight, calculated logP, number of hydrogen bond donors and acceptors or surface area descriptors) have been developed.

While these concepts have been extensively utilized for peptides and marketed drugs, no studies examining the permeation behavior of carbohydrate mimetics have been released up to date. This work therefore focuses on the elucidation of factors influencing the passive permeation of such compounds. For this purpose, PAMPA as well as logD_{7.4} values were determined and *in silico* descriptors were calculated for a homologous set of 62 carbohydrate mimetics containing mannose. Calculated logP values as single descriptor proved to correlate best to PAMPA results of this data set. A combination of descriptors did not yield a better correlation. Interestingly, surface area descriptors that are commonly used for the prediction of permeation were much less correlated to PAMPA results than calculated logP values. Furthermore, calculated logP values were superior to experimental logD_{7.4} values. In conclusion, the results presented here suggest that the permeation behavior of carbohydrates is influenced primarily by lipophilicity and that other descriptors are less relevant. This is in contrast to previous findings for other compound classes.

3.2 Factors influencing the permeation properties of carbohydrate mimetics

1. Introduction

The oral application of a drug is the most convenient way of therapy for patients. Therefore, whenever possible it is the aim of drug discovery projects to find orally available molecules for the treatment of diseases. Amongst other barriers such as metabolism and solubility problems, the crossing of the intestinal mucosa represents a major obstacle on the way of a drug to its target.¹ Properties related to good permeation or factors enabling active transportation are thus essential and numerous assays have been developed to assess these parameters. For the determination of a compound's ability to cross a membrane by passive diffusion, PAMPA (parallel artificial membrane permeation assay) has been introduced.² The study of active transport processes and to a limited extent also metabolism is performed with cell-based assays using Caco-2³ and MDCK⁴ cells. There is an ongoing debate on whether active transport processes play a role for oral absorption or if concentrations in the gastrointestinal tract after oral dosing are too high and thus transporters would be saturated.^{5,6} The in-silico prediction of oral bioavailability as a whole remains a difficult task within pharmacokinetic modeling.^{7,8} Considerable success has been reached, though, concerning the prediction of transcellular permeation by passive diffusion.⁹ Different approaches have been used to identify descriptors that significantly correlate with good permeation.¹⁰ The simplest method for permeation prediction is the use of rules of thumb such as Lipinski's Rule of Five¹¹ or the Veber rules.¹² Concerning prediction of passive permeation with artificial membranes, models based on a single descriptor such as H-bonding have been published.¹³ Most publications, however, focus on models with combined descriptors that are either partially of experimental origin¹⁴ or purely computational (e.g. PSA and logP).^{15, 16} Furthermore, QSAR models for the prediction of permeation have been developed,¹⁷⁻²¹ in one case even a bilinear QSAR model.²² Similar models were also described for permeation results based on Caco 2-assays²³⁻²⁷ or on intestinal permeability determinations in animals and humans.²⁸⁻³³ These models are usually similar to the ones derived from PAMPA results regarding the utilized descriptors, typically including molecular weight, calculated logP values, number of hydrogen-bond donors and acceptors, pK_a values, number of rotatable bonds, or surface area descriptors.

To our knowledge, no studies examining the permeation by passive diffusion of carbohydrate mimetics have been released up to date. A possible reason might be that carbohydrates and mimetics thereof are generally considered to be drug-unlike³⁴ and that permeation is generally not expected for this class unless active transport processes can be exploited like in the

3 Results and discussion

example of Valacyclovir.³⁵ This does not hold true, as exemplified by compounds presented in a recently published paper and by compounds not yet published.³⁶⁻³⁸ In this study, we focus on the elucidation of important factors contributing to PAMPA permeation of carbohydrate mimetics by quantifying the predictive power of several molecular descriptors. Thereby, requirements for orally available carbohydrate mimetic drugs were identified.

2. Materials and methods

logD_{7.4} determination. The online *in silico* prediction tool Virtual Computational Chemistry Laboratory (VCCLAB)^{39, 40} was used to estimate the logP values of the compounds. Depending on these values, the compounds were classified into three categories: hydrophilic compounds (logP below zero), moderately lipophilic compounds (logP between zero and one) and lipophilic compounds (logP above one). For each category, two different ratios (volume of 1-octanol to volume of buffer) were defined as experimental parameters:

| Compound type | logP | Ratios (1-octanol: buffer) |
|-----------------------|-------|----------------------------|
| hydrophilic | < 0 | 30:140, 40:130 |
| moderately lipophilic | 0 - 1 | 70:110, 110:70 |
| lipophilic | > 1 | 3:180, 4:180 |

Equal amounts of phosphate buffer (0.1 M, pH 7.4) and 1-octanol (Sigma-Aldrich, St. Louis MI, USA) were mixed and shaken vigorously for 5 min to saturate the phases. The mixture was left until separation of the two phases occurred, and the buffer was retrieved. Stock solutions of the test compounds were diluted with buffer to a concentration of 1 μ M. For each compound, six determinations, i.e., three determinations per 1-octanol:buffer ratio, were performed in different wells of a 96-well plate. The respective volumes of buffer containing analyte (1 μ M) were pipetted to the wells and covered by saturated 1-octanol according to the chosen volume ratio. The plate was sealed with aluminium foil, shaken (1350 rpm, 25 °C, 2 h) on a Heidoph Titramax 1000 plate-shaker (Heidolph Instruments GmbH & Co. KG, Schwabach, Germany) and centrifuged (2000 rpm, 25 °C, 5 min, 5804 R Eppendorf centrifuge, Hamburg, Germany). The aqueous phase was transferred to a 96-well plate for analysis by liquid chromatography-mass spectrometry (LC-MS).

3.2 Factors influencing the permeation properties of carbohydrate mimetics

$\log D_{7.4}$ was calculated from the 1-octanol:buffer ratio (o:b), the initial concentration of the analyte in buffer (1 μM), and the concentration of the analyte in buffer (c_B) with equilibration:

$$\log D_{7.4} = \frac{1\mu\text{M} - c_B}{c_B} \times \frac{1}{o:b}$$

The average of the three $\log D_{7.4}$ values per 1-octanol:buffer ratio was calculated. If the two mean values obtained for a compound did not differ by more than 0.1 unit, the results were accepted.

PAMPA: The conditions for $\log P_e$ determination with the PAMPA permeation assay were chosen according to the manufacturer's recommendations due to the fact that calculated $\log P$ values were lower than two.⁴¹ For each compound, measurements were performed at three pH values (5.0, 6.2, 7.4) in quadruplicates. For this purpose, 12 wells of a deep well plate, i.e., four wells per pH-value, were filled with 650 μL System Solution (pIon, Woburn MA, USA, P/N 110151). Samples (150 μL) were withdrawn from each well to determine the blank spectra by UV-spectroscopy (SpectraMax 190, Molecular Devices, Silicon Valley Ca, USA). Then, analyte dissolved in DMSO was added to the remaining System Solution to yield 50 μM solutions. To exclude precipitation, the optical density was measured at 650 nm, with 0.01 being the threshold value. Solutions exceeding this threshold were filtrated. Afterwards, samples (150 μL) were withdrawn to determine the reference spectra. Further 200 μL were transferred to each well of the donor plate of the PAMPA sandwich (pIon, P/N 110 163). The filter membranes at the bottom of the acceptor plate were impregnated with 5 μL of GIT-0 Lipid Solution (pIon, P/N 110669) and 200 μL of Acceptor Sink Buffer (pIon, P/N 110139) were filled into each acceptor well. The sandwich was assembled, placed in the GutBoxTM, and left undisturbed for 16 h. Then, it was disassembled and samples (150 μL) were transferred from each donor and acceptor well to UV-plates. Quantification was performed by both UV-spectroscopy and LC-MS. $\log P_e$ -values were calculated based on LC-MS results with the aid of the PAMPA Explorer Software (pIon, version 3.5). For LC-MS determinations, the acceptor medium was diluted with acetonitrile at a 1:1 ratio (to break up the micelles) and each reference well was measured directly after the according donor well (leading to less variability). Furthermore, both donor and reference samples were diluted in order not to exceed the linear concentration range of triple quadrupole-MS instruments.

3 Results and discussion

LC-MS measurements. Analyses were performed using a 1100/1200 Series HPLC System coupled to a 6410 Triple Quadrupole mass detector (Agilent Technologies, Inc., Santa Clara CA, USA) equipped with electrospray ionization. The system was controlled with the Agilent MassHunter Workstation Data Acquisition software (version B.01.04). The column used was an Atlantis[®] T3 C18 column (2.1 x 50 m) with a 3- μ m particle size (Waters Corp., Milford MA, USA). The mobile phase consisted of two eluents: solvent A (H₂O, containing 0.1% formic acid, v/v) and solvent B (acetonitrile, containing 0.1% formic acid, v/v), both delivered at 0.6 mL/min. The gradient was ramped from 95% A/5% B to 5% A/95% B over 1 min, and then hold at 5% A/95% B for 0.1 min. The system was then brought back to 95% A/5% B, resulting in a total duration of 4 min. MS parameters such as fragmentor voltage, collision energy, polarity were optimized individually for each drug, and the molecular ion was followed for each compound in the multiple reaction monitoring mode. The concentrations of the analytes were quantified by the Agilent Mass Hunter Quantitative Analysis software (version B.01.04).

Molecular modeling: The main goal was to identify descriptors with the highest information content regarding the quantitative description of structure-property (permeation) relationship for a set of carbohydrate mimetics. Such descriptors could be used in the later development phases to rapidly identify drug candidates with decreased permeation.

Each molecule was subjected to a thorough conformational analysis using the mixed torsional/low-mode sampling algorithm as implemented in the MacroModel software.⁴² The search for energetically accessible conformations was done using water and 1-octanol implicit solvation models in order to properly account for conformational differences in polar and organic solvent. In total, 2000 starting geometries were generated for each compound and minimized using a TNCG gradient method and an OPLS2005 force-field. Resulting conformations within an energy window of 2 kcal/mol were saved. On average, for a single compound this approach yielded ~70 conformers in water and ~60 in octanol.

A large pool of various descriptors was calculated using the QikProp program by Schrodinger, LCC⁴³ and the online version of the Dragon software (E-DRAGON) available within the VCCLAB.³⁹ These descriptors were calculated taking only a single conformation into account – the global minimum in the case of the QikProp program and a pseudo-random geometry generated by the CORINA molecular builder as implemented in the VCCLAB in the case of the E-DRAGON software.

3.2 Factors influencing the permeation properties of carbohydrate mimetics

Special attention was paid to the evaluation of the descriptors which depend on the 3D structure of the molecule and are well known to significantly correlate with permeation, namely (polar) surface area and lipophilicity. Thus, besides the global minimum conformation (descriptor values denoted by the subscript index “global minimum”) as calculation basis, the values of these descriptors were calculated also based on several conformations within an energy window of 2 kcal/mol from the global minimum. The final values were adjusted by either the Boltzmann weighting algorithm (values denoted by the subscript index “Boltzmann”) or by simple averaging (denoted by “averaged”). In order to calculate the Boltzmann weighting factors, relative energies from molecular mechanics or quantum mechanics calculations were used.

The lipophilicity coefficient $\log P_{\text{Octanol/Water}}$ was calculated based on the solvation energies in the respective solvents using the following equation:

$$\log P_{\text{Octanol/Water}} = (DG_{\text{s Water}} - DG_{\text{s Octanol}}) / 2.303 RT$$

For each single conformer the solvation energies $DG_{\text{s Water}}$ and $DG_{\text{s Octanol}}$ were obtained from single point calculations using a SM5.42 solvation model,⁴⁴ PM3 Hamiltonian and CM3 charge model (ICMD=312, ICDS=12) as implemented in the GAMESS-Plus software.⁴⁵ For comparison, the lipophilicity coefficients were additionally calculated using the ALOGPs 2.1 program of the VCCLAB.³⁹

Surface area descriptors were calculated using an in-house program. First, the solvent accessible surface area (SASA) was calculated using the rolling sphere approach. Next, the solvent accessible surface was atom-mapped and the sum of areas assigned to oxygen and nitrogen atoms was calculated (polar surface area, PSA).

3. Results and discussion

The main interest of this study was to elucidate which factors influence the permeation properties of carbohydrate mimetics. Similar studies have been performed for other compound classes and various descriptors influencing passive permeation have been identified, most prominently for lipophilicity, molecular weight, surface area, and hydrogen bonding. PAMPA was used as reference assay since passive diffusion can be studied without disturbing influences of active transport processes.

3 Results and discussion

All $\log P_e$ and $\log D_{7.4}$ values presented here were determined in the same laboratory under the same conditions and thus represent a homogeneous data set. Three compounds were excluded due to their low solubility (thermodynamic solubility at pH 6.5 less than 1 μmol [33-35]), which could possibly interfere with assay results. This represents just a measure of precaution since normally precipitation is detected by UV-spectroscopy and the samples are filtered prior to PAMPA execution. Since no ionized compound (at assay pH values) showed any permeation ($\log P_e = -10$), there was no need to calculate and consider pK_a values.

Furthermore, it is obviously of critical importance for the validity of the approach to correctly interpret the role that active transport processes might play for *in vivo* availability. For the biphenyl-compounds a comparison of PAMPA with Caco-2 results suggests a weak influence of active transportation for compounds with the carboxy-moiety while no such effect is seen for the respective esters that are permeating well in both assays.³⁶ In a mouse *in vivo* model in the same publication no detectable appearance of the carboxy-compounds in plasma but low concentrations in the urine were observed. Contrastingly, a bioavailability of 10% was determined for the esterified compounds. Furthermore, the esterified compound showed a similar treatment efficacy in an infection study after p.o. application as the according carboxy-compound after i.v. injection. These results, though only punctiform, suggest that PAMPA results of the carbohydrate mimetics presented in this study are relevant with respect to *in vivo* application, especially when combined with Caco-2 measurements. An *in silico* prediction approach thus bears the advantage of yielding relevant information at lower time consumption. Moreover, better understanding of the factors influencing permeation can be used for rational design approaches.

3.2 Factors influencing the permeation properties of carbohydrate mimetics

Table 1. Correlation of selected experimental and calculated descriptors with PAMPA permeation ($\log P_e$). Remark: nonPSA was calculated as SASA – PSA; fractionPSA was calculated as PSA/SASA.

| Descriptor | <i>r</i> | <i>r</i> ² | Descriptor | <i>r</i> | <i>r</i> ² |
|-----------------------------------|----------|-----------------------|---------------------------------------|----------|-----------------------|
| 0D - 2D | | | 3D continued | | |
| $\log P_{o/w}$ QikProp | 0.790 | 0.624 | PSA _{global minimum} | -0.541 | 0.293 |
| # of HB acceptors QikProp | -0.694 | 0.482 | PSA _{averaged} | -0.525 | 0.276 |
| SASA _{QikProp} | 0.647 | 0.418 | PSA _{Boltzmann} | -0.536 | 0.287 |
| Polarizability _{QikProp} | 0.614 | 0.377 | SASA _{global minimum} | 0.563 | 0.317 |
| Volume _{QikProp} | 0.608 | 0.369 | SASA _{averaged} | 0.539 | 0.291 |
| Globularity _{QikProp} | -0.592 | 0.350 | SASA _{Boltzmann} | 0.542 | 0.293 |
| Molecular weight | 0.485 | 0.235 | Volume _{global minimum} | 0.429 | 0.184 |
| PSA _{QikProp} | -0.412 | 0.170 | Volume _{averaged} | 0.467 | 0.218 |
| AC $\log P$ _{VCC Lab} | 0.894 | 0.800 | Volume _{Boltzmann} | 0.461 | 0.213 |
| XLOGP3 _{VCC Lab} | 0.879 | 0.773 | Globularity _{global minimum} | -0.558 | 0.312 |
| miLogP _{VCC Lab} | 0.877 | 0.769 | Globularity _{averaged} | -0.583 | 0.340 |
| XLOGP2 _{VCC Lab} | 0.851 | 0.724 | Globularity _{Boltzmann} | -0.573 | 0.329 |
| KOWWIN _{VCC Lab} | 0.848 | 0.719 | nonPSA _{global minimum} | 0.768 | 0.590 |
| ALOGP _{VCC Lab} | 0.830 | 0.689 | nonPSA _{averaged} | 0.757 | 0.573 |
| ALOGPs _{VCC Lab} | 0.791 | 0.626 | nonPSA _{Boltzmann} | 0.760 | 0.578 |
| MLOGP _{VCC Lab} | 0.764 | 0.583 | fractionPSA _{global minimum} | -0.776 | 0.603 |
| 3D | | | fractionPSA _{averaged} | -0.768 | 0.590 |
| $\log P_{calc.}$ global minimum | 0.849 | 0.721 | fractionPSA _{Boltzmann} | -0.772 | 0.596 |
| $\log P_{calc.}$ averaged | 0.887 | 0.787 | experimental | | |
| $\log P_{calc.}$ Boltzmann MM | 0.895 | 0.800 | $\log D_{7.4}$ | 0.802 | 0.642 |
| $\log P_{calc.}$ Boltzmann QM | 0.921 | 0.848 | | | |

An overview of selected calculated descriptors and their correlation with the PAMPA permeation coefficient $\log P_e$ is summarized in Table 1. The strongest predictors for good permeation were clearly lipophilicity descriptors. Interestingly, several calculated partitioning coefficients were better correlated with permeation behavior than experimentally measured distribution coefficients as reflected by their respective r^2 values (e.g. $\log P_{calculated}$ Boltzmann QM 0.848 vs. $\log D_{7.4}$ 0.642; Figure 1). This finding might be explained by the fact that the determination method for $\log D$ values used here is limited to a range between -1.5 to 4 thus

3 Results and discussion

lacking an exact attribution for highly hydrophilic compounds. Indeed, the calculated results span over 6.25 units whereas the measured values cover only 4.5 units, so the extreme data points (positively) influencing the correlation are missing. Calculated logP values are well correlated with experimental logD_{7.4} values ($r^2 = 0.753$), although the calculated values are shifted towards the lower range and have a slightly steeper slope. This can be explained by the worse absolute accuracy of the solvation energies produced by the universal SM5.42 solvation model in case of the octanol. However, the description of the relative trends in solvation among the structures in the dataset remains very good.

The quality of the calculated logP descriptors based on the 3D structures (and their respective solvation energies) largely depends on the final evaluation algorithm. If only the global minimum is taken into account, the approach produces values with a quality similar to pure fragment-based algorithms ($\log P_{\text{calc. global minimum}}$ $r^2 = 0.721$, average of all the correlation coefficients for logPs from the VCCLAB is 0.710). Simple averaging of the contributions from the low-energy conformers improves the correlation to $r^2 = 0.787$ of $\log P_{\text{calc. averaged}}$, while applying Boltzmann weighting leads to an even better correlation of $r^2 = 0.800$, which is just equal to the best fragment based method AC logP. When the Boltzmann weights are calculated based on the quantum-mechanical single point energies instead of molecular mechanics, the resulting correlation r^2 reaches 0.848, which is the highest value of all descriptors. This confirms that a 3D-based approach might provide added value in terms of accuracy, if the contained information is extracted in a proper way.

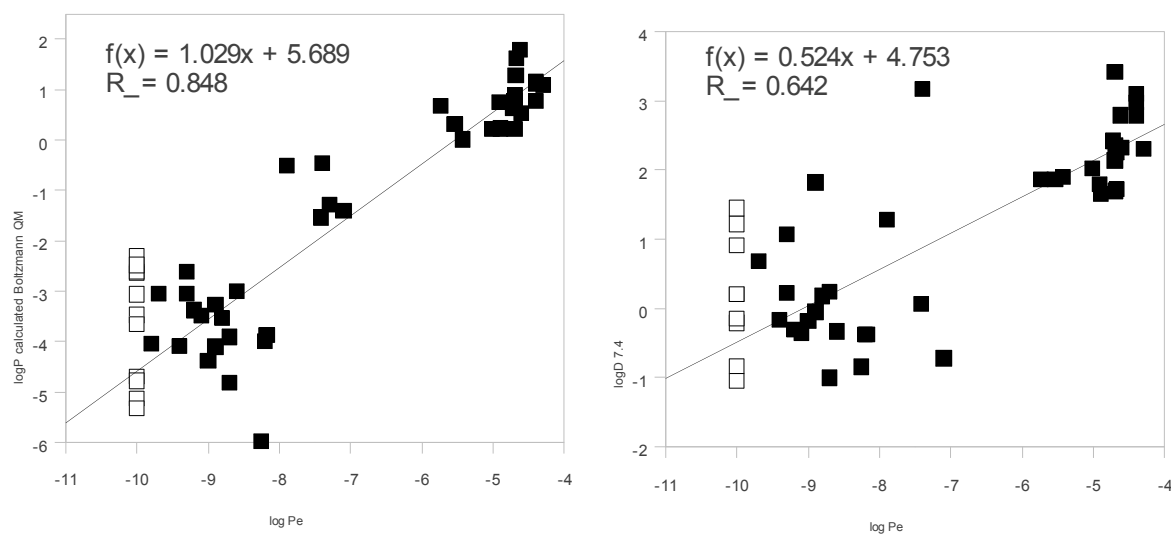


Figure 1. $\log P_{\text{calculated Boltzmann QM}}$ (left) and $\log D_{7.4}$ (right) plotted vs. $\log P_{\text{e}}$ with the respective r^2 values. Empty squares represent the control group (see text).

3.2 Factors influencing the permeation properties of carbohydrate mimetics

Three groups can be distinguished when looking at the $\log P_e$ vs. calculated $\log P$ correlation (Figure 1, left). The first group is composed of compounds that unambiguously permeate through membranes by passive diffusion ($\log P_e > -6$, top right-hand corner), the second is represented by compounds with insufficient permeation properties ($\log P_e < -7.5$, bottom left-hand corner), and the third group is situated in between. All three groups can be separated into clogP bins (> 0 for the first and < -2 for the second group) which emphasizes again the importance of this descriptor for passive permeation of the carbohydrate mimetics used in this study.

The plots in Figure 1 represent just the best fit of a single descriptor to permeation values, i.e. no measure of reliability (such as a cross-validated r^2) is explicitly given. Instead, compounds with no permeation (i.e. no measurable concentration is reached in the acceptor compartment after 16 hours) were used as control. When these compounds are plotted at the PAMPA threshold value ($\log P_e = -10$) against $\log P_{\text{calculated Boltzmann QM}}$ no false positive is observed (Figure 1, empty squares).

In contrast to previously published studies, neither polar surface area (PSA) nor molecular weight, polarizability or descriptors of hydrogen bonding correlate strongly with permeation results. The rather low r^2 values of PSA and the number of hydrogen bond acceptors as descriptors compared to calculated $\log P$ could be explained by the special chemical structure of the carbohydrate mimetics used in this study. The mannose moiety already contains 4 hydrogen bond donors and 6 hydrogen bond acceptors and significantly contributes to a high PSA compared to other compound classes (PSA values observed in the current data set are between 100 \AA^2 and 177.5 \AA^2 , the average is 131.5 \AA^2). As a comparison, the data set used by Veber containing 1117 compounds had an average PSA of 102.2 \AA^2 .¹² Therefore, for carbohydrate mimetics these descriptors might be less useful for the explanation of passive diffusion since they are less distinctive than for other classes. In the case of PSA, values calculated based on 3D structures showed a slightly increased correlation to permeation compared to those obtained from fragment-based summing. Nevertheless, they remain far from the predictive range (r^2 values above 0.7). In contrast to this finding, the other descriptors (such as molecular volume, globularity or total solvent accessible surface area) showed even slightly lower correlations to permeation when calculated based on the 3D structures compared to their fragment-based analogs. Therefore, in these cases the increased computational costs would not be justified.

Interestingly, the descriptors derived from PSA and SASA (solvent accessible surface area), namely the non-polar surface area (nonPSA) and the fraction of polar surface area

3 Results and discussion

(fractionPSA, negative slope) showed some moderate correlation with permeation (r^2 around 0.590), indicating that the presence of lipophilic fragments compensating the rather high PSA of the mannose unit is indeed important for a successful transfer through the membrane layer. The lacking correlation between permeation and molecular weight might be explained by the homologous data set used in this study and consequently by the limited variability of this parameter (278.3 to 498.9, covering 220.6 units with a standard deviation of only 46.24). In the present dataset, there is no compound that would disqualify itself for passive permeation just based on the molecular weight when applying Lipinski's Rule of Five.¹¹

None of the 1664 descriptors calculated with the software Dragon showed better correlation than the lipophilicity factors, which confirms the unique value of this descriptor for prediction of the passive permeation of the carbohydrate mimetics. Furthermore, it has the advantage to be easily comprehensible, intuitive, and facilely computable

4. Conclusions

In summary, clogP is the best descriptor for passive permeation of carbohydrate mimetics. A combination with other descriptors does not lead to a better correlation with PAMPA results thus emphasizing the importance of this single parameter for passive permeation of carbohydrate mimetics. This finding is remarkable since it differs from results of previously published studies with other compound classes. The results therefore suggest that the permeation behavior of carbohydrate mimetics is primarily influenced by lipophilicity and that other descriptors are less relevant. A possible explanation for this might be the high hydrophilicity of the mannose moiety that needs to be compensated in order to enable membrane permeation.

Furthermore, the results can be used for the estimation of permeation within the restricted compound family of mannose derivatives similar to the ones used in this study. Compounds with logP values above 0, calculated according to the best methodology, are probably to exhibit high membrane permeation. On the other hand, compounds with values between -2 and 0 might permeate to a limited extent and compounds with values below -2 cannot be expected to cross membranes.

3.2 Factors influencing the permeation properties of carbohydrate mimetics

References

1. Dressman, J. B.; Thelen, K.; Jantravid, E. Towards quantitative prediction of oral drug absorption. *Clinical Pharmacokinetics* **2008**, 47, 655-667.
2. Kansy, M.; Senner, F.; Gubernator, K. Physicochemical high throughput screening: Parallel artificial membrane permeation assay in the description of passive absorption processes. *J. Med. Chem.* **1998**, 41, 1007-1010.
3. Artursson, P.; Karlsson, J. Correlation between Oral Drug Absorption in Humans and Apparent Drug Permeability Coefficients in Human Intestinal Epithelial (Caco-2) Cells. *Biochem. Biophys. Res. Commun.* **1991**, 175, 880-885.
4. Irvine, J. D.; Takahashi, L.; Lockhart, K.; Cheong, J.; Tolan, J. W.; Selick, H. E.; Grove, J. R. MDCK (Madin-Darby canine kidney) cells: A tool for membrane permeability screening. *Journal of Pharmaceutical Sciences* **1999**, 88, 28-33.
5. Kansy, M.; Avdeef, A.; Fischer, H. Advances in screening for membrane permeability: high-resolution PAMPA for medicinal chemists. *Drug. Discov. Today.* **2004**, 1, 349-355.
6. Sugano, K.; Kansy, M.; Artursson, P.; Avdeef, A.; Bendels, S.; Di, L.; Ecker, G.; Faller, B.; Fischer, H.; Gerebtzoff, G.; Lennernaes, H.; Senner, F. Coexistence of passive and carrier-mediated processes in drug transport. *Nat Rev Drug Discov* **2010**, 9, 597-614.
7. Burton, P.; Goodwin, J.; Vidmar, T.; Amore, B. Predicting drug absorption: how nature made it a difficult problem. *J Pharmacol Exp Ther* **2002**, 303, 889-95.
8. Metcalfe, P.; Thomas, S. Challenges in the prediction and modeling of oral absorption and bioavailability. *Curr Opin Drug Discov Devel* **2010**, 13, 104-10.
9. Linnankoski, J.; Ranta, V.; Yliperttula, M.; Urtti, A. Passive oral drug absorption can be predicted more reliably by experimental than computational models--fact or myth. *Eur J Pharm Sci* **2008**, 34, 129-39.
10. Egan, W. J.; Lauri, G. Prediction of intestinal permeability. *Advanced Drug Delivery Reviews* **2002**, 54, 273-289.
11. Lipinski, C. A.; Lombardo, F.; Dominy, B. W.; Feeney, P. J. Experimental and computational approaches to estimate solubility and permeability in drug discovery and development settings. *Advanced Drug Delivery Reviews* **1997**, 23, 3-25.
12. Veber, D. F.; Johnson, S. R.; Cheng, H. Y.; Smith, B. R.; Ward, K. W.; Kopple, K. D. Molecular properties that influence the oral bioavailability of drug candidates. *J. Med. Chem.* **2002**, 45, 2615-2623.

3 Results and discussion

13. Du Plessis, J.; Pugh, W. J.; Judefeind, A.; Hadgraft, J. The effect of hydrogen bonding on diffusion across model membranes: consideration of the number of H-bonding groups. *European Journal of Pharmaceutical Sciences* **2001**, 13, 135-141.
14. Egan, W. J.; Merz, K. M.; Baldwin, J. J. Prediction of drug absorption using multivariate statistics. *Journal of Medicinal Chemistry* **2000**, 43, 3867-3877.
15. Acharya, C.; Seo, P. R.; Polli, J. E.; MacKerell, A. D. Computational model for predicting chemical substituent effects on passive drug permeability across parallel artificial membranes. *Molecular Pharmaceutics* **2008**, 5, 818-828.
16. Kalyanaraman, C.; Jacobson, M. P. An atomistic model of passive membrane permeability: application to a series of FDA approved drugs. *Journal of Computer-Aided Molecular Design* **2007**, 21, 675-679.
17. Akamatsu, M.; Fujikawa, M.; Nakao, K.; Shimizu, R. In silico prediction of human oral absorption based on QSAR analyses of PAMPA permeability. *Chem Biodivers* **2009**, 6, 1845-66.
18. Fujikawa, M.; Ano, R.; Nakao, K.; Shimizu, R.; Akamatsu, M. Relationships between structure and high-throughput screening permeability of diverse drugs with artificial membranes: Application to prediction of Caco-2 cell permeability. *Bioorganic & Medicinal Chemistry* **2005**, 13, 4721-4732.
19. Nakao, K.; Fujikawa, M.; Shimizu, R.; Akamatsu, M. QSAR application for the prediction of compound permeability with in silico descriptors in practical use. *J Comput Aided Mol Des* **2009**, 23, 309-19.
20. Verma, R.; Hansch, C.; Selassie, C. Comparative QSAR studies on PAMPA/modified PAMPA for high throughput profiling of drug absorption potential with respect to Caco-2 cells and human intestinal absorption. *J Comput Aided Mol Des* **2007**, 21, 3-22.
21. Tulp, I.; Sild, S.; Maran, U. Relationship Between Structure and Permeability in Artificial Membranes: Theoretical Whole Molecule Descriptors in Development of QSAR Models. *Qsar & Combinatorial Science* **2009**, 28, 811-814.
22. Fujikawa, M.; Nakao, K.; Shimizu, R.; Akamatsu, M. QSAR study on permeability of hydrophobic compounds with artificial membranes. *Bioorganic & Medicinal Chemistry* **2007**, 15, 3756-3767.
23. Ano, R.; Kimura, Y.; Urakami, M.; Shima, M.; Matsuno, R.; Ueno, T.; Akamatsu, M. Relationship between structure and permeability of dipeptide derivatives containing tryptophan and related compounds across human intestinal epithelial (Caco-2) cells. *Bioorganic & Medicinal Chemistry* **2004**, 12, 249-255.

3.2 Factors influencing the permeation properties of carbohydrate mimetics

24. Ano, R.; Kimura, Y.; Shima, M.; Matsuno, R.; Ueno, T.; Akamatsu, M. Relationships between structure and high-throughput screening permeability of peptide derivatives and related compounds with artificial membranes: application to prediction of Caco-2 cell permeability. *Bioorganic & Medicinal Chemistry* **2004**, *12*, 257-264.
25. Stenberg, P.; Luthman, K.; Artursson, P. Prediction of membrane permeability to peptides from calculated dynamic molecular surface properties. *Pharmaceutical Research* **1999**, *16*, 205-212.
26. Stenberg, P.; Norinder, U.; Luthman, K.; Artursson, P. Experimental and computational screening models for the prediction of intestinal drug absorption. *Journal of Medicinal Chemistry* **2001**, *44*, 1927-1937.
27. Degim, Z. Prediction of permeability coefficients of compounds through Caco-2 cell monolayer using artificial neural network analysis. *Drug Development and Industrial Pharmacy* **2005**, *31*, 935-942.
28. Palm, K.; Stenberg, P.; Luthman, K.; Artursson, P. Polar molecular surface properties predict the intestinal absorption of drugs in humans. *Pharmaceutical Research* **1997**, *14*, 568-571.
29. Kelder, J.; Grootenhuis, P. D. J.; Bayada, D. M.; Delbressine, L. P. C.; Ploemen, J. P. Polar molecular surface as a dominating determinant for oral absorption and brain penetration of drugs. *Pharmaceutical Research* **1999**, *16*, 1514-1519.
30. Martin, Y. C. A bioavailability score. *Journal of Medicinal Chemistry* **2005**, *48*, 3164-3170.
31. Winiwarter, S.; Bonham, N. M.; Ax, F.; Hallberg, A.; Lennernas, H.; Karlen, A. Correlation of human jejunal permeability (in vivo) of drugs with experimentally and theoretically derived parameters. A multivariate data analysis approach. *Journal of Medicinal Chemistry* **1998**, *41*, 4939-4949.
32. Winiwarter, S.; Ax, F.; Lennernas, H.; Hallberg, A.; Pettersson, C.; Karlen, A. Hydrogen bonding descriptors in the prediction of human in vivo intestinal permeability. *Journal of Molecular Graphics & Modelling* **2003**, *21*, 273-287.
33. Ertl, P.; Rohde, B.; Selzer, P. Fast calculation of molecular polar surface area as a sum of fragment-based contributions and its application to the prediction of drug transport properties. *Journal of Medicinal Chemistry* **2000**, *43*, 3714-3717.
34. Ernst, B.; Magnani, J. L. From carbohydrate leads to glycomimetic drugs. *Nature Reviews Drug Discovery* **2009**, *8*, 661-677.

3 Results and discussion

35. Inui, K.; Terada, T.; Masuda, S.; Saito, H. Physiological and pharmacological implications of peptide transporters, PEPT1 and PEPT2. *Nephrology Dialysis Transplantation* **2000**, 15, 11-13.
36. Klein, T.; Abgottspon, D.; Wittwer, M.; Rabbani, S.; Herold, J.; Jiang, X.; Kleeb, S.; Lüthi, C.; Scharenberg, M.; Bezencon, J.; Gubler, E.; Pang, L.; Smiesko, M.; Cutting, B.; Schwardt, O.; Ernst, B. FimH Antagonists for the Oral Treatment of Urinary Tract Infections: From Design and Synthesis to *In Vitro* and *In Vivo* Evaluation. Submitted to *J. Med. Chem.*
37. Hartmann, M.; Schwardt, O.; Abgottspon, D.; Wittwer, M.; Rabbani, S.; Scharenberg, M.; Bezencon, J.; Cutting, B.; Ernst, B. *unpublished results*
38. Jiang, X.; Haug, M.; Abgottspon, D.; Wittwer, M.; Kleeb, S.; Gubler, E.; Scharenberg, M.; Schwardt, O.; Rabbani, S.; Cutting, B.; Ernst, B. *unpublished results*.
39. Tetko, I. V.; Gasteiger, J.; Todeschini, R.; Mauri, A.; Livingstone, D.; Ertl, P.; Palyulin, V.; Radchenko, E.; Zefirov, N. S.; Makarenko, A. S.; Tanchuk, V. Y.; Prokopenko, V. V. Virtual computational chemistry laboratory - design and description. *Journal of Computer-Aided Molecular Design* **2005**, 19, 453-463.
40. VCCLAB, Virtual Computational Chemistry Laboratory. <http://www.vcclab.org>
41. pION's Guide to Improved Double-Sink(TM) PAMPA. In Revision 1.2 ed.; pION, 5 Constitution Way, Woburn, MA 01801, USA: 2005.
42. *MacroModel*, 9.6; Schrodinger, LCC: New York, NY, 2005.
43. *QuiProp*, 3.1; Schrödinger, LCC: New York, NY, 2008.
44. Hawkins, G. D.; Zhu, T.; Li, J.; Chambers, C. C.; J., G. D.; Liotard, D. A.; Cramer, C. J.; Truhlar, D. G. Universal Solvation Models. In *Combined Quantum Mechanical and Molecular Mechanics Methods*, Gao, J.; Thompson, M. A., Eds. American Chemical Society: Washington D. C., 1993; pp 201-219.
45. Higashi, M.; Marenich, A. V.; Olson, R. M.; Chamberlin, A. C.; Pu, J.; Kelly, C. P.; Thompson, J. D.; Xidos, J. D.; Li, J.; Zhu, T.; Hawkins, G. D.; Chuang, Y.-Y.; Fast, P. L.; Lynch, B. J.; Liotard, D. A.; Rinaldi, D.; Gao, J.; Cramer, C. J.; Truhlar, D. G. *GAMESSPLUS*, 2008-2; University of Minnesota, Minneapolis: 2008.

3.3 Pharmacokinetic behavior of MAG antagonists

3.3 Pharmacokinetic behavior of MAG antagonists

MAG antagonists are used to treat central nervous lesions and are generally applied directly at the site of action, i.e., they are injected intrathecally. A compound's stability in cerebrospinal fluid and the maintenance of a sufficiently high concentration in this compartment are critical parameters that were addressed by the means of the PADMET platform.

The author determined the stability in artificial cerebrospinal fluid, the $\log D_{7.3}$ values, and the permeation through an artificial blood-brain barrier of all compounds and interpreted the results.

This work was published in the *Journal of Medicinal Chemistry*:

Mesch, S.; Moser, D.; Strasser, D. S.; Kelm, A.; Cutting, B.; Rossato, G.; Vedani, A.; Koliwer-Brandl, H.; Wittwer, M.; Rabbani, S.; Schwardt, O.; Kelm, S.; Ernst, B. Low Molecular Weight Antagonists of the Myelin-Associated Glycoprotein: Synthesis, Docking, and Biological Evaluation *J. Med. Chem.* **2010**, *53*, 1597-1615.

Copyright © 2010, American Chemical Society

Low Molecular Weight Antagonists of the Myelin-Associated Glycoprotein: Synthesis, Docking, and Biological Evaluation

Stefanie Mesch,[†] Delia Moser,[†] Daniel S. Strasser,[†] Antje Kelm,[‡] Brian Cutting,[†] Gianluca Rossato,[†] Angelo Vedani,[†] Hendrik Koliwer-Brandl,[‡] Matthias Wittwer,[†] Said Rabbani,[†] Oliver Schwarzt,[†] Soerge Kelm,[‡] and Beat Ernst^{*†}[†]Institute of Molecular Pharmacy, Pharmazentrum, University of Basel, Klingelbergstrasse 50, CH-4056 Basel, Switzerland and [‡]Department of Physiological Biochemistry, University of Bremen, D-28334 Bremen, Germany

Received August 10, 2009

The injured adult mammalian central nervous system is an inhibitory environment for axon regeneration due to specific inhibitors, among them the myelin-associated glycoprotein (MAG), a member of the Siglec family (sialic-acid binding immunoglobulin-like lectin). In earlier studies, we identified the lead structure **5**, which shows a 250-fold improved in vitro affinity for MAG compared to the tetrasaccharide binding epitope of GQ1b α (**1**), the best physiological MAG ligand described so far. By modifying the 2- and 5-position, the affinity of **5** could be further improved to the nanomolar range (\rightarrow **19a**). Docking studies to a homology model of MAG allowed the rationalization of the experimental binding properties. Finally, pharmacokinetic parameters (stability in the cerebrospinal fluid, logD and permeation through the BBB) indicate the drug-like properties of the high-affinity antagonist **19a**.

Introduction

The injured adult mammalian central nervous system (CNS) lacks the ability for axon regeneration,^{1,2} predominantly due to specific inhibitors expressed on residual myelin and on astrocytes recruited to the site of injury.^{3–7} Several inhibitor proteins have been identified, one of them being the myelin-associated glycoprotein (MAG).⁸ MAG is a transmembrane glycoprotein⁹ belonging to the family of the sialic acid-binding immunoglobulin like lectins, the so-called Siglecs.^{10,11} On the surface of neurons, MAG interacts with two classes of targets: proteins of the family of Nogo receptors (NgR)^{12,13} and the gangliosides GD1a and GT1b.^{11,14–16} Although the relative roles of gangliosides and NgRs as MAG ligands have yet to be resolved,^{8,17} in some systems, MAG inhibition is completely reversed by sialidase treatment, suggesting that MAG uses sialylated glycans as its major axonal ligands.¹⁸ Therefore, blocking MAG with potent antagonists may be a valuable therapeutic approach to enhance axon regeneration.

So far, the native carbohydrate ligand with the highest affinity to MAG is the ganglioside GQ1b α (Figure 1).¹⁹ Recently, MAG affinity of a partial structure of GQ1b α , the tetrasaccharide **1**, could clearly be correlated with its ability to reverse MAG-mediated inhibition of axonal outgrowth.²⁰

To reduce the structural complexity of tetrasaccharide **1** and, at the same time, improve its pharmacodynamic and pharmacokinetic properties, numerous MAG antagonists have been prepared. Because the affinity of a series of gangliosides indicated that not only the terminal Neu5Ac α (2–3)Gal structure is essential for MAG binding but also the internal sialic acids, the corresponding sialylated and sulfated analogues were synthesized.^{21,22} Furthermore, structural information obtained by trNOE NMR²³ and STD NMR²⁴ suggested that the Gal β (1–3)GalNAc core contributes to binding mainly by hydrophobic contacts. This was confirmed by the successful replacement of this disaccharide substructure by noncarbohydrate linkers.²⁵ In addition, the α (2–6)-linked sialic acid could also be replaced by lipophilic substituents.²² Finally, a pivotal simplification was reported by Kelm and Brossmer when they found that sialic acid derivatives modified in the 2- (e.g., **2**),^{26,27} 5- (e.g., **3**),^{26,27} or 9-position^{26,28} (e.g., **4**) exhibited enhanced antagonistic activity.²⁶ Combining the best modifications found for the 2nd- and 9th-position³⁰ in one molecule led to antagonists, e.g., **5**, with affinities in the low micromolar range.³⁰

In this communication, we report a small library of MAG antagonists based on lead compound **5**. The binding properties, evaluated by a hapten binding assay, surface plasmon resonance (SPR), and competitive NMR experiments were rationalized by docking studies to a homology model of MAG. Finally, according to pharmacokinetic parameters, e.g., stability in the cerebrospinal fluid, the drug-likeness of the identified high-affinity antagonists could be demonstrated.

Results and Discussion

The sialic acid derivatives reported by Kelm and Brossmer²⁶ and our group^{29,30} exhibit MAG affinities in the low μ M range. An example is the neuraminic acid (Neu5Ac) derivative

*To whom correspondence should be addressed. Phone: 0041 267 15 51. Fax: 0041 267 15 52. E-mail: beat.ernst@unibas.ch.

[†]BBB, blood–brain barrier; CHO, Chinese hamster ovary; ClAc, 2-chloroacetyl; DCE, 1,2-dichloroethane; DCM, dichloromethane; DMAP, 4-dimethylamino-pyridine; DMF, *N,N*-dimethylformamide; FAc, 2-fluoroacetyl; Gal, galactose; GalNAc, *N*-acetylgalactosamine; IgG, immunoglobulin G; K_D , dissociation constant; MS, molecular sieve; Neu5Ac, *N*-acetylneuraminic acid; NgR, Nogo receptor; NIS, *N*-iodosuccinimide; NMR, nuclear magnetic resonance; nosyl, 2-nitrobenzylsulfonyl; PAMPA, parallel artificial membrane permeation assay; PDB, Protein Data Bank; *i*PrOH, 2-propanol; RP, reversed phase; STD NMR, saturation transfer difference NMR; TfOH, trifluoroacetic acid; THF, tetrahydrofuran; TMS, trimethylsilyl; trNOE, transfer nuclear Overhauser enhancement; *p*-Ts, *p*-tolylsulfonyl.

3.3 Pharmacokinetic behavior of MAG antagonists

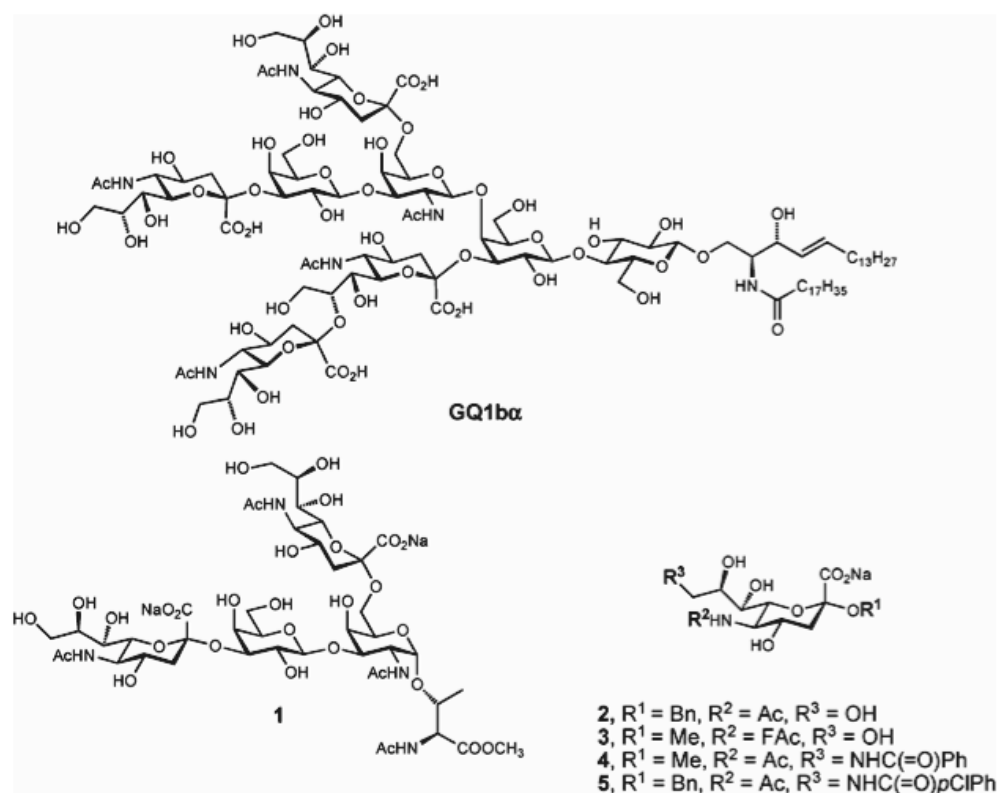


Figure 1. MAG antagonists; GQ1b α , the partial structure **1**,^{19,20} and sialic acid derivatives **2–5**.^{26,30}

5³⁰ with a K_D of 17 μ M. Because a broad optimization effort for the 9-position had led to the identification of *p*-chlorobenzamide as the best substituent,³⁰ this position was not further investigated. The changeover from a methyl substituent in the 2-position to a benzyl group was rewarded by a 10-fold gain in affinity.²⁶ This effect can be rationalized by the results of STD-NMR investigations,²³ indicating a hydrophobic interaction of the α -face of D-galactose (see **1** in Figure 1) with MAG. When the hydrophobic contact was further extended by replacing the benzyl group with phenoxybenzyl or biphenyl substituents, only marginally improved affinities were detected.²⁹ Because the sheer enlargement of the hydrophobic group did not exhibit improved affinities, the electron density of the aglycone was altered in a next step. Finally, with the substituents in the 2- and 9-position set, a further optimization of the acyl group in the 5-position was conducted.^{26,27}

Synthesis of Sialosides 13a–f. Starting from Neu5Ac, thioglycoside **6** was synthesized according to a reported procedure.³¹ After deprotection by Zemplén conditions (\rightarrow **7**), the hydroxy group in the 9-position was selectively tosylated (\rightarrow **8**).³² Substitution of the tosylate using sodium azide and 15-crown-5 in DMF (\rightarrow **9**)³³ followed by acetylation yielded the sialyl donor **10**. For the introduction of the aglycone, **10** was then reacted with various benzyl alcohols (see Table 1, entries 2–9) in the presence of the promoters NIS/TfOH.³⁴ The sialosides **11a–f** were obtained as separable anomeric mixtures ($\alpha/\beta = 7/1$ to 9/1). Amidation with *p*-chlorobenzoylchloride under modified Staudinger conditions³⁵ (\rightarrow **12a–f**) and final deprotection gave the amides **13a–f** in good yields (Scheme 1, Table 1).

Synthesis of Sialosides 19a–g. As reported earlier, halogenation of the *N*-acetyl group at the 5-position increases the binding affinity toward MAG by a factor of 10–20.²⁶ Therefore, both the *N*-fluoroacetyl and *N*-chloroacetyl derivatives **19a** and **19b** were prepared. As sulfonamides adapt a different geometry³⁶ compared to the corresponding amides, **19c** and **19d** allow a further exploration of the binding site. Finally, the cyclopropyl and cyclobutyl derivatives **19f** and **19g** were synthesized in order to explore the possibility for extended hydrophobic contacts.

For the cleavage of the *N*-acetate group, **10** was treated with hydrazine in the presence of (Boc)₂O^{37,38} and subsequently reacylated (\rightarrow **14**). Deprotection with TMSCl and PhOH³⁹ (\rightarrow **15**), followed by acylation with carboxylic or sulfonic acid derivatives, yielded **16a–d**. Glycosylation using 2,3-difluorobenzyl alcohol (\rightarrow **17a–d**), amidation using modified Staudinger conditions³⁵ (\rightarrow **18a–d**) and final deprotection gave the test compounds **19a–d**. When methanolic NaOH was used in the final deprotection step of **18b**, a nucleophilic substitution occurred, leading to a 1:1 mixture of the desired **19b** and the methoxyacetamide derivative **19e** (Scheme 2).

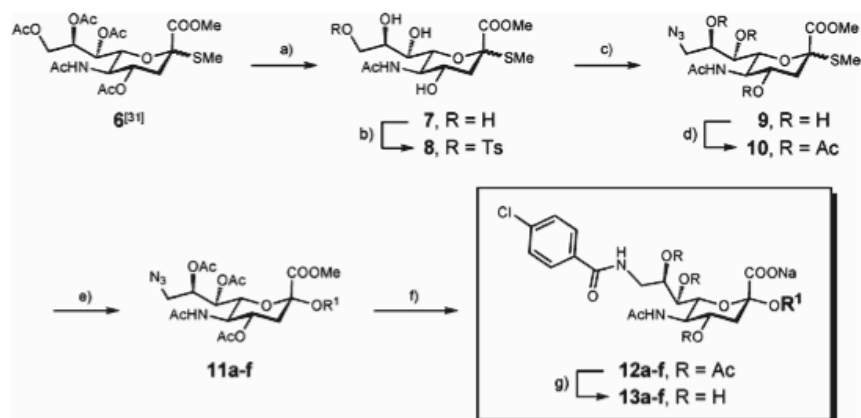
For the synthesis of the two remaining test compounds **19f** and **19g**, an analogue approach starting from the thiosialoside **10** was accomplished. However, in contrast to the synthesis of **19a–e**, a different sequence of the modifications conducted at the 2-, 5-, and 9-position was performed (Scheme 3). Cleavage of the *N*-acetate (\rightarrow **14**) and amidation under modified Staudinger conditions yielded compound **20**. Next, *N*-deprotection followed by *N*-acylation (\rightarrow **22f** and **22g**) and benzylation (\rightarrow **23f** and **23g**) yielded, after final

3 Results and discussion

Article

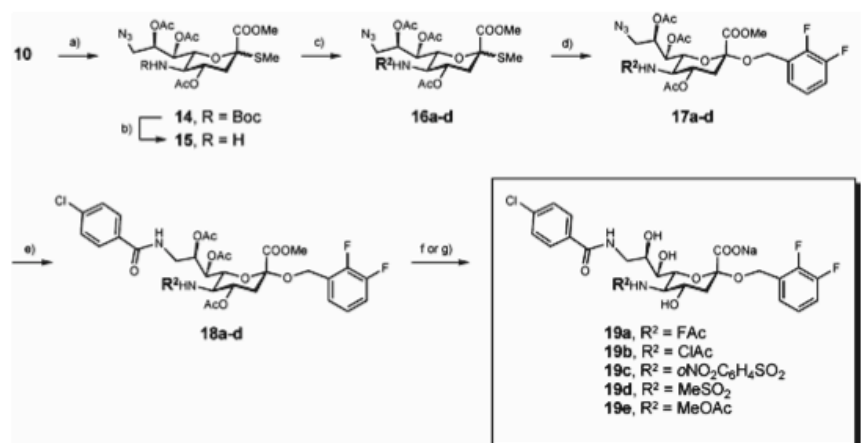
Journal of Medicinal Chemistry, 2010, Vol. 53, No. 4 1599

Scheme 1^a



^a (a) NaOMe, MeOH (61%); (b) *p*-TsCl, pyridine (66%); (c) NaN₃, 15-crown-5, DMF (78%); (d) Ac₂O, DMAP, pyridine (73%); (e) R¹OH, NIS, TfOH, MeCN (**11a-f**, α-isomers: 54–76%; β-isomers: 8–11%); (f) PPh₃, *p*-chlorobenzoylchloride, DCE, rt (**12a-f**, 45–60%); (g) 10% aq NaOH; Dowex 50 × 8, Na⁺ form (**13a-f**, 39–70%).

Scheme 2^a



^a (a) (i) Boc₂O, DMAP, THF, 60 °C, 4 h, (ii) N₂H₄·H₂O, MeOH, rt, 24 h, (iii) Ac₂O, pyridine (76%); (b) 4 M PhOH, 4 M TMSCl in abs DCM (70%);³⁹ (c) acylation agent, NEt₃, DMAP, abs DCM, rt, 4 h or [ClCH₂C(=O)]₂O, NEt₃, dioxane/H₂O, rt (**16a-d**, 66–85%); (d) 2,3-difluorobenzyl alcohol, NIS, TfOH, MeCN (**17a-d**, α-isomers: 56–68%; β-isomers: 8–11%); (e) PPh₃, *p*-chlorobenzoylchloride, DCE, rt (**18a-d**, 48–58%); (f) 10% aq LiOH, THF/H₂O; Dowex 50 × 8, Na⁺ form (**19a-d**, 30–60%); (g) **18b**, 10% aq NaOH; Dowex 50 × 8, Na⁺ form (**19b**, 21%, **19e**, 19%).

deprotection, the desired cycloalkylacetic acid derivatives **19f** and **19g** in excellent overall yields.

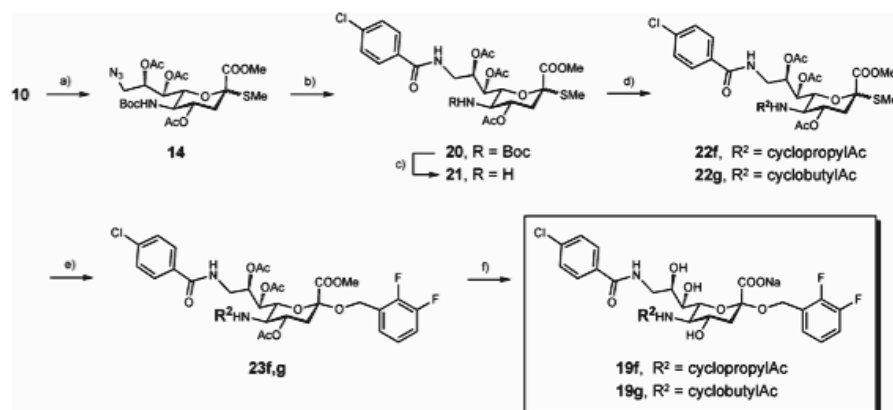
Biological Evaluation. For the evaluation of the binding properties of the sialosides **13a–f** and **19a–g**, two previously reported assay formats were applied: a fluorescent hapten binding assay⁴⁰ and a SPR based biosensor (Biacore) experiment²² (Table 1). For the hapten inhibition assay, a recombinant protein consisting of the three *N*-terminal domains of MAG and the Fc part of human IgG (MAG_{d1–3}-Fc) was produced by expression in CHO cells and affinity purification on protein A-agarose.⁴⁰ The relative inhibitory concentrations (rIC₅₀) of the test compounds as competitive ligands were determined in microtiter plates coated with fetuin as the binding target for MAG_{d1–3}-Fc. By complexing the Fc-part with alkaline phosphatase-labeled anti-Fc antibodies and measuring the initial velocity of fluorescein release from fluorescein diphosphate, the amount of bound MAG_{d1–3}-Fc could be determined. At least three independent titrations

were performed for each compound tested with seven or eight concentrations in triplicates. The affinities were measured relative to the reference compound **5** (rIC₅₀ of 1, Table 1, entry 2). For the *K_D* determination in the Biacore assay, MAG_{d1–3}-Fc was immobilized on a dextran chip containing a surface of covalently bound protein A. A reference cell providing only protein A was used to compensate unspecific binding to the matrix.

By analyzing the affinities of **13a–f**, a substantial increase in affinity was achieved when the aromatic aglycone was halogenated in *ortho*- and *meta*-positions (entries 8 and 9). Less effective were halogens in the *para*-position (entries 4 and 5). In addition, with fluorine instead of chlorine, consistently slightly higher affinities (entries 4 and 8 vs entries 5 and 9) were obtained. With the symmetric pentafluoro benzyl group in **13c** (entry 6), an increase in affinity was expected, caused by an improved preorganization of the aglycone in the bioactive conformation. The observed

3.3 Pharmacokinetic behavior of MAG antagonists

Scheme 3^a



^a (a) (i) Boc_2O , DMAP, THF, 60 °C, 4 h, (ii) $\text{N}_2\text{H}_4 \cdot \text{H}_2\text{O}$, MeOH, rt, 24 h, (iii) Ac_2O , pyridine (76%); (b) PPh_3 , *p*-chlorobenzoylchloride, DCE, rt (48%); (c) 4 M PhOH, 4 M TMSCl in abs DCM (63%);³⁹ (d) R^2COCl , NEt_3 , DMAP, abs DCM, rt, 4 h (**22f**, 75%, **22g**, 39%); (e) 2,3-difluorobenzyl alcohol, NIS, TIOH, MeCN (**23f**, α : 73%, β : 8%; **23g**, α : 72%, β : 8%); (f) 10% aq LiOH, THF/ H_2O ; Dowex 50 \times 8, Na^+ form (**19f**, 44%; **19g**, 50%).

diminished affinity, i.e., a loss of a factor 3 compared to **13f**, may be the result of steric hindrance. Finally, when a 2-naphthylmethyl substituent was introduced (**13d**), a slight improvement of affinity compared to the benzyl substituent as present in **5** was obtained, presumably due to a favorable π - π interaction of the extended aromatic system. In a next step, substituent R^2 was optimized based on the so far most active antagonist **13f**. Kelm and Brossmer have demonstrated that halogenated acetamides in the 5-position of sialic acid derivatives strongly improve binding of MAG antagonists.²⁶ When this observation was applied to our series, the nanomolar fluoroacetamide **19a** (entry 10) was obtained. For chloroacetamide derivative **19b** (entry 11), the effect was less pronounced. Interestingly, an equally potent antagonist was achieved with the phenylsulfone substituent (**19c**, entry 12), while sulfone **19d** (entry 13) suffers from a drastic loss in activity. This is quite unexpected because an increase in the size of the acyl substituent was reported to lead to a reduction in affinity,²⁷ an observation that was confirmed by compounds **19e–g** (entries 14–16).

Stability in Cerebrospinal Fluid. For nerve regeneration, MAG antagonists will most likely be applied to the CNS by a local infusion. We therefore tested the stability of the fluoroacetate **19a** and the corresponding acetate **13f** in artificial cerebrospinal fluid (aCSF)⁴¹ and, as a control, in buffer solution for 19 h at 37 °C. According to LC-MS analysis, more than 95% of the initial concentrations of both antagonists were recovered from both media, predicting a high stability in the CNS, the target compartment of an in vivo application. Furthermore, $\log D_{\text{octanol/water}}$ values from -0.27 to 0.87 (see Table 1) might be beneficial for an intrathecal application because these distribution coefficients suggest a loss from the CNS compartment by a passive transport mechanism to be unlikely. This hypothesis is further supported by the results of the BBB-PAMPA assay showing $\log P_c$ values for **13f** and **19a** in the range of -10 . For values below -5.7 ,⁴² no passive permeation through the BBB is expected.

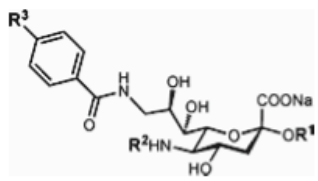
Surface Plasmon Resonance (SPR). The interaction between MAG and MAG antagonists was analyzed by SPR experiments.^{43–45} For this purpose, $\text{MAG}_{\text{d}1-3}\text{-Fc}$ was

immobilized on protein A, which on its part was covalently linked to a carboxymethyl dextrane surface of the chip. Whereas earlier Biacore investigations with MAG antagonists produced traditional sensorgrams,²² consistently negative sensorgrams, i.e., a net decrease in resonance units, were obtained with the compound series reported in Table 1. As an example, the sensorgram of **13f** is shown in Figure 2a. When fitted to a binding isotherm, these negative sensorgrams appear to clearly result from specific receptor–ligand interactions. To elucidate the origin of this unusual result, numerous factors such as the buffer capacity, the ion strength of the buffer, type, and matrix of the sensor chip as well as the applied type of immobilization of $\text{MAG}_{\text{d}1-3}\text{-Fc}$ were analyzed.

As a result of ionizable functional groups of the analytes, pH variabilities could occur, a phenomenon previously reported by Mannen et al.⁴⁶ To avoid this effect, a sufficient buffer capacity, 50 mM instead of 10 mM HEPES, was applied. Furthermore, to exclude ionic repulsion effects, measurements were carried out at increased salt concentrations (150–500 mM NaCl). In addition, the effect of potential nonspecific binding to the dextran matrix or to protein A was analyzed by adding either dextran (1 mg/mL) to the buffer system or by conducting the experiment on a regenerated protein A surface. Because all these modifications of assay parameters did not provide an indication for the cause of the negative sensorgrams, different dextran biosensor chips, varying in carboxylate density (CM5 vs CM4), were analyzed as well. Although the reduction in signal intensity correlated well with the degree of functionalization of the chip surface, no influence on the sign of the sensorgrams could be detected (see Table S1 in Supporting Information). A further explanation for the negative sensorgrams could be a ligand-induced conformational change of the immobilized receptor leading to a decrease of its hydrodynamic radius and, as a consequence, yielding a negative refraction index.^{47,48} Because the negative refraction index correlates with the analyte concentration, we mirrored the negative sensorgrams, for an example see the sensorgram of **13f** in Figure 2b, to obtain SPR-determined equilibrium dissociation constants (K_{DPS} , see Table 1).

3 Results and discussion

Table 1. Relative Inhibitory Concentrations (rIC_{50}) Relative to Reference Compound **5**, K_D Values, and $\log D_{7.3}$ of Sialosides **13a–f** and **19a–g**



| Entry | Compound | R ¹ | R ² | R ³ | rIC_{50} ^{a)} | K_D [μ M] | $\log D$ (pH 7.3) |
|-------|---------------------------|---|---|----------------|--------------------------|-------------------|--------------------|
| 1 | 4 ²⁶⁻²⁸ | -CH ₃ | Ac | H | 18.00 | 137 ^{b)} | n.d. ^{c)} |
| 2 | 5 ³⁰ |  | Ac | Cl | 1.00 | 17 | n.d. ^{c)} |
| 3 | 24 ³⁰ |  | Ac | H | 1.50 | 26 | n.d. ^{c)} |
| 4 | 13a |  | Ac | Cl | 1.30 | 15 | 0.36 |
| 5 | 13b |  | Ac | Cl | 1.20 | 13 | -0.11 |
| 6 | 13c |  | Ac | Cl | 0.26 | 6.1 | -0.11 |
| 7 | 13d |  | Ac | Cl | 0.74 | 11.6 | 0.58 |
| 8 | 13e |  | Ac | Cl | 0.50 | 4.3 | 0.53 |
| 9 | 13f |  | Ac | Cl | 0.30 | 2.4 | -0.27 |
| 10 | 19a |  |  | Cl | 0.02 | 0.5 | -0.26 |
| 11 | 19b |  |  | Cl | 0.07 | 2.1 | 0.35 |
| 12 | 19c |  |  | Cl | 0.05 | 1.4 | 0.87 |
| 13 | 19d |  |  | Cl | 0.60 | 17 | -0.17 |
| 14 | 19e |  |  | Cl | 0.14 | 2.3 | 0.06 |
| 15 | 19f |  |  | Cl | 0.10 | 4.1 | 0.31 |
| 16 | 19g |  |  | Cl | 0.14 | 5.8 | 0.75 |

^a rIC_{50} is the concentration when 50% of the protein are inhibited, measured relative to reference compound **5**. ^b The affinity of compound **4** was measured using different protein batches, resulting in K_D s of 137 μ M and 105 μ M (Table 2). All affinity data given in Table 1 were obtained with the protein batch showing a K_D of 137 μ M for compound **4**; ^c n.d. not determined

To justify this procedure, we analyzed whether K_D s obtained by mirroring the negative sensorgrams can be correlated with rIC_{50} values determined by the fluorescent hapten

binding assay⁴⁰ (Figure 3). K_D s from previously reported compounds^{25,30} (see Table S2, Supporting Information), which exhibit much higher molecular weights and therefore

3.3 Pharmacokinetic behavior of MAG antagonists

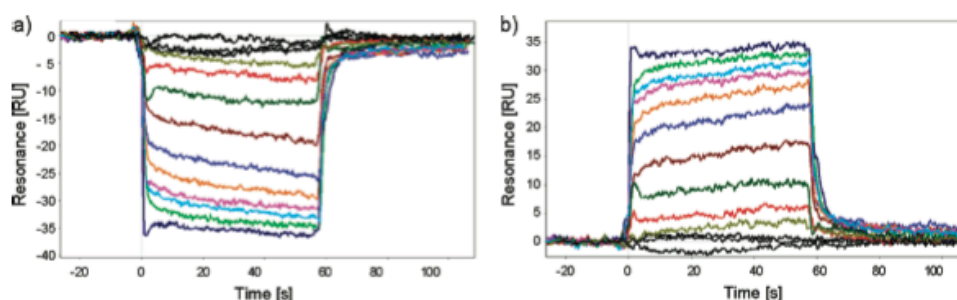


Figure 2. (a) Biacore sensorgrams for **13f** after subtraction of the reference; (b) mirrored sensorgrams of **13f**.

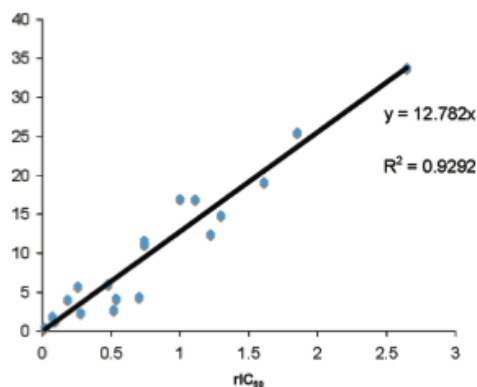


Figure 3. Correlation of K_D values obtained by SPR measurements with rIC_{50} values determined in the competitive inhibition assay.⁴⁰ Compounds **5**, **13a–f**, **19a–g**, and the compounds **25–29** from Table S2 (Supporting Information) were included.

generate positive sensorgrams, were also included in this correlation. The obtained correlation factor R^2 of 0.93 clearly suggests that the mirroring procedure does not falsify the binding information.

Determination of Relative Affinities by NMR. A further argument for the acceptance of the above-described mirroring of the sensorgrams was accomplished by competitive NMR experiments.⁴⁹ The approach is based on the molecular weight dependence of selective inversion recovery experiments (sT1). In the absence of binding, a selectively inverted NMR signal of a ligand requires a relatively long time to recover back to equilibrium. By contrast, if the ligand binds to a receptor, the time required to recover back to equilibrium is reduced. As a result, the binding of a ligand to a receptor is detectable through sT1 experiments. Furthermore, these sT1 experiments can be used for the ranking of the affinities of ligands relative to a reference compound.

For our purpose, the binding of antagonist **4** to MAG_{d1-3} -Fc was used as reference (K_D determined by Biacore is $137 \mu M$), whereas compounds **13f** and **25**²² (for the structure, see Supporting Information) were chosen as competitors because they fulfill two criteria. First, SPR experiments with both **13f** and **25** gave comparable K_D values, 2.4 and $2.8 \mu M$, respectively, and therefore require comparable concentrations for the observation of competitive binding. Second, the observed sensorgrams of compounds **13f** and **25** are of opposite sign, negative and positive, respectively.

In a first NMR experiment, it was demonstrated that **4** binds to MAG_{d1-3} -Fc according to the large differences

between selective inversion recovery of the *para*-hydrogen of the benzamide substituent in the presence or absence of MAG_{d1-3} -Fc (Figure 4a). For a quantitative evaluation of the relative affinities of **13f** and **25**, a titration curve describing the concentration dependence of the selective inversion recovery time of **4** was required (Figure 4b). The selective inversion time constants (sT1) were fit to a one-site binding model.

On the basis of the titration curve shown in Figure 4b, the determination of the relative affinities of **13f** and **25** became possible. With a NMR sample consisting of MAG_{d1-3} -Fc and compound **4** ($500 \mu M$), sT1 for the initial point of the titration curve was remeasured. The obtained sT1 of 1.03 ± 0.08 s compared to 1.05 ± 0.06 s for the first sample indicated a high degree of reproducibility. In a second step, $25 \mu M$ of either compound **13f** or **25** were added. Then, the sT1s were measured and the apparent concentration of compound **4** determined. When $25 \mu M$ of compound **13f** were added, the sT1 increased to 1.84 ± 0.06 s, indicating an apparent concentration of compound **4** of 1.36 mM. Subtracting the actual concentration of compound **4** from its apparent concentration and dividing the result by the concentration of the inhibitor yields a relative affinity of 34.4 ± 2.1 for compound **13f** with respect to the reference compound **4** with the relative affinity of 1. With the identical procedure, a relative affinity of 17.6 ± 1.0 for compound **25** with respect to compound **4** was found (Figure 5).

The competitive NMR assay demonstrates that compounds **13f** and **25** both bind to MAG_{d1-3} -Fc with an affinity more than 1 order of magnitude greater than reference compound **4**. The relative affinities displayed in Figure 5 are in good agreement with the corresponding values determined by Biacore and the hapten inhibition assay.⁴⁰ Allowing a factor of 2 in the estimation of a compound's affinity with a single technology implies that the comparison of affinities between two assay formats may differ by as much as a factor of 4. Because for any of the three assays employed the affinities of **13f** and **25** to MAG_{d1-3} -Fc are within this range, the mirroring of the negative sensorgrams for the determination of K_D values is further justified.

Determination of Enthalpic and Entropic Contributions to Binding. For the elucidation of the thermodynamic parameters of the MAG/antagonist interaction, K_D s were measured in the Biacore assay at different temperatures. The analysis of a library of ligands containing structural modifications at the 2-, 5-, and 9-position of the neuraminic acid scaffold should allow the assignment of the enthalpic and entropic contributions to the various structural elements. The K_D values were determined at six different temperatures, starting at $5^\circ C$ and elevating the temperature by $5^\circ C$

3 Results and discussion

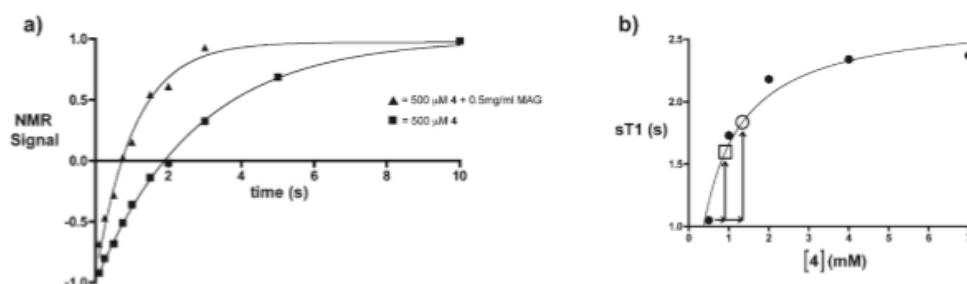


Figure 4. (a) Selective inversion recovery (sT1) of the *para*-hydrogen of the benzamide in compound **4**, either in the presence of MAG_{d1-3}-Fc (filled triangles) or in the absence of MAG_{d1-3}-Fc (filled squares). The normalized NMR signal represents the intensity of the *para*-hydrogen at a particular time divided by its intensity after 60 s of relaxation. (b) Titration of MAG_{d1-3}-Fc with compound **4**, and the observed sT1 (filled circles), observed sT1 when 500 μM of **4** were mixed with 25 μM **13f** (hollow circle), and observed sT1 when 500 μM of **4** were mixed with 25 μM **25** (hollow square). Vertical and horizontal arrows indicate the extent of attenuated relaxation of **4** when mixed with 25 μM or competitor **13f** or **25** and the apparent concentration of **4**, respectively.

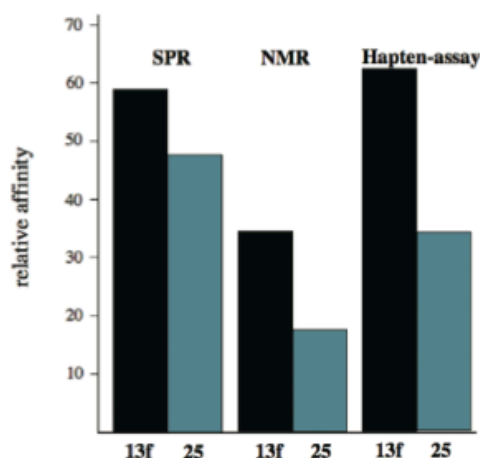


Figure 5. Affinity of compounds **13f** (black) and **25** (gray), relative to the affinity of compound **4** (= relative affinity of 1). The relative affinities are determined by NMR, Biacore, and the fluorescent hapten assay.⁴⁰

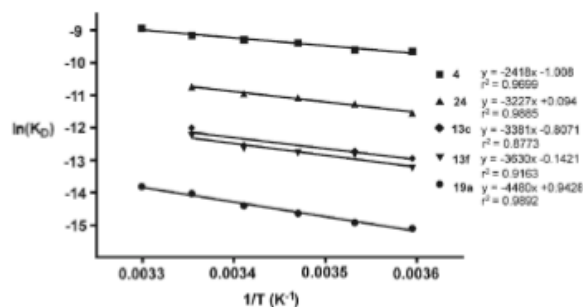


Figure 6. Van't Hoff plot. Measured data (dots) and corresponding linear fits according to eq 1.

$$\ln K_D = \frac{\Delta H}{RT} - \frac{\Delta S}{R} \quad (1)$$

steps up to 30 °C. The values were fitted according to eq 1 (Figure 6) leading to ΔH and ΔS ⁵⁰ (Table 2).

The analysis (Table 2) revealed that the improvement of the binding energies ΔG resulted mainly from enhanced binding enthalpies ΔH . The substitution of the methoxy group at

Table 2. Weighting of ΔH and ΔS with Respect to ΔG

| entry | compd | ΔH [kJ/mol] | $-T^a\Delta S^*$ [kJ/mol] | ΔG [kJ/mol] | K_D [μM] |
|-------|-------------------------|---------------------|---------------------------|---------------------|------------------|
| 17 | 4 ³⁰ | -20.09 | -2.52 | -22.61 | 106 ^b |
| 18 | 24 ³⁰ | -26.85 | 0.25 | -26.60 | 22 |
| 19 | 13c | -28.13 | -1.98 | -30.1 | 6.1 |
| 20 | 13f | -30.31 | -0.20 | -30.52 | 2.4 |
| 21 | 19a | -37.33 | 2.42 | -34.91 | 0.5 |

^a $T = 298.13$ K. ^b The affinity of compound **4** was measured using different protein batches, resulting in K_D s of 137 μM and 106 μM. For the data given in Table 2, the protein batch showing a K_D of 106 μM for compound **4** was used.

position 2 in **4** by a benzyloxy group (**24**, entry 18)³⁰ increased binding enthalpy by more than 6 kJ/mol and at the same time caused substantial entropy costs upon binding. With the pentafluorobenzyloxy substituent (**13c**, entry 19), both ΔH and ΔS were improved. Apparently, the interaction of the reducing end substituent can be optimized with an electron-poor aromatic ring. When the 2,3-difluorinated benzyloxy substituent (**13f**, entry 20) was introduced, ΔG could be further improved, mainly by a favorable enthalpy change. On the other hand, entropy costs increased as a result of the asymmetric substitution. The binding energy of the most active compound **19a** (entry 21, *N*-acetate replaced by *N*-fluoroacetate) is mainly based on a further enthalpic improvement. Unfortunately, in this case entropy costs of more than 2 kJ/mol have to be compensated, probably due to a specific conformational orientation requested for an optimal interaction of the FAc group.

Structure–Affinity Relationships. To interpret the binding affinities at the molecular level, we performed molecular docking studies. In the absence of a crystal structure, we used a homology model of the ligand-binding domain of MAG, which was recently applied successfully to a series of MAG antagonists (Figure 7).²² The compounds were manually docked using the salt bridge between the carboxylate of the sialosides with Arg118 and the hydrogen bond of C(9)-NH to the backbone nitrogen of Thr128 as anchor points. Finally, the protein–ligand complexes were fully minimized in aqueous solution.

For validation purposes, 12 compounds were docked and their binding strength quantified. Because these compounds bind at the protein surface, the contribution of solvation and entropy are difficult to estimate from thermodynamic docking studies. We therefore performed a series of molecular-dynamical simulations (4.0×10^{-9} s at 300 K) to elucidate the

3.3 Pharmacokinetic behavior of MAG antagonists

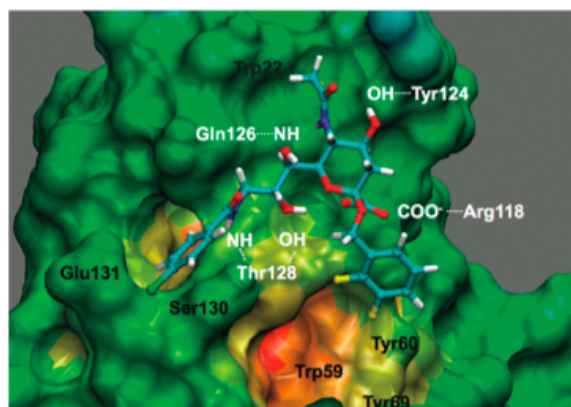


Figure 7. Homology model of MAG²² complexed with **19a** (most active compound of the series). Amino acids in white are forming hydrogen bonds and amino acids in black contribute to hydrophobic pockets. The salt bridge formed by the carboxylate group of **19a** with Arg118 and a hydrogen bond by C(9)-NH and the backbone nitrogen of Thr128 were used as anchor points for the docking. Hydrophobic interactions are established by the fluoroacetamido group and the side chains of Trp22 and Tyr124, the *p*-chlorobenzamide, and the side chains of Ser130 and Glu131, and the reducing end substituent, the 2,3-difluorobenzyl and the side chains of Trp59, Tyr60, and Tyr69, lining the main hydrophobic pocket. The image has been generated using VMD.⁵¹

kinetic aspects of binding and to quantify the contribution of hydrogen bonding over time. Details are given in the Supporting Information.

Upon analyzing the docking studies, the binding affinity could be associated to hydrophilic as well as hydrophobic interactions. The most important contribution is the salt bridge between the carboxylic acid and Arg118.^{26,52,53} Additionally, hydrogen-bond formations between 5-NH and the backbone carbonyl of Gln126, the carboxylate and the OH of Thr128, 8-OH and the backbone NH of Thr128 and 9-NH and the backbone carbonyl of Thr128 are observed. This latter finding is in good agreement with previous studies, where the abolishment of a hydrogen bond donor at position 9 resulted in a reduced binding affinity.²⁶ A considerable contribution to the binding affinity results from hydrophobic interactions. Thus, the *p*-chlorobenzamide is shown to point into a hydrophobic pocket, built by Ser130 and Glu131. A second hydrophobic pocket, which hosts the aglycone substituents, is defined by the side chains of Trp59, Tyr60, and Tyr69. With respect to different substitution patterns, the dichloro compound **13e** (Table 1, entry 8) shows a 4-fold and the difluoro compound **13f** (see Table 1, entry 9), a 7-fold enhancement in affinity compared to reference compound **5**, indicating a charge transfer complex with the electron rich aromatic ring of Tyr60. The only moderate improvement in binding affinity for the halogenated compounds **13a** and **13b** could be due to a steric clash of the *p*-substituent with the protein. Compound **13c** was synthesized as a symmetric analogon of compound **13f** in order to compensate entropy loss due to the orientation of the 2,3-difluorobenzyl ring. Again, that there is no improvement of the binding affinity in comparison to compound **13f** may be the consequence of a steric clash based on the *p*-substituent. Finally, the improved binding of **13d** might result from favorable π - π interactions of the naphthalene with Tyr69.

Some of the compounds modified at the 5-position seem to undergo a favorable σ - π interaction with Trp22. In case of **19a** and **19b**, we assume that the positively polarized hydrogens of the FAc or ClAc, respectively, stick favorably into the aromatic ring.⁵⁴ As fluorine is more electronegative, the polarization of the hydrogens is stronger and therefore the interaction is more favorable. For compounds **19f** and **19g**, additional hydrophobic interactions are possible, but the binding site seems to be spatially limited.²⁷ The reduced affinity of **19d** could be a consequence of the different bond angle for the sulfonamide substituent compared to an acetate in the same position (**13f**, entry 9), leading to different spatial requirements. Whereas methylsulfonamide **19d** shows a decrease in binding affinity, the nosyl substituent (**19c**) shows an opposite behavior. This might be due to the formation of a charge transfer complex with Trp22. To summarize, modifications at the reducing end improved binding affinity by a factor of 7 (**5**→**13f**). Combined with the best modification at the 5-position, the high affinity ligand **19a** was obtained.

Conclusion

In conclusion, the nanomolar affinity of the sialic acid derivative **19a** containing a difluorobenzyl substituent at the 2-, a fluoroacetate at the 5-, and *p*-chlorobenzamide at the 9-position clearly indicates the additivity of the beneficial effect of the various modifications. In addition, the thermodynamic analysis reveals that the improved affinity of **19a** predominantly results from an increased binding enthalpy and not from an entropy gain. The beneficial pharmacokinetic properties, e.g., a high stability in the cerebrospinal fluid, also support the drug-like properties of the newly identified MAG antagonist. However, due to the shallow binding site generally responsible for short half-lives of carbohydrate-protein complexes,^{22,55-58} it remains to be shown whether the complex formed by **19a** and MAG exhibits sufficient kinetic stability for in vivo applications.

Experimental Section

Chemistry. NMR spectra were recorded on a Bruker Avance DMX-500 (500 MHz) spectrometer. Assignment of ¹H and ¹³C NMR spectra was achieved using 2D methods (COSY, HSQC, TOCSY). Chemical shifts are expressed in ppm using residual CHCl₃, CHD₂OD, and HDO as references. Optical rotations were measured using Perkin-Elmer polarimeters 241 and 341. MS analyses were carried out using a Waters Micromass ZQ Detector system. The spectra were recorded in positive or negative ESI mode. The HPLC/HRMS analyses were carried out using an Agilent 1100 equipped with a photodiode array detector and a Micromass QTOF I equipped with a 4 GHz digital-time converter. All target compounds exhibit a purity of $\geq 95\%$. Reactions were monitored by TLC using glass plates coated with silica gel 60 F₂₅₄ (Merck) and visualized by using UV light and/or by charring with a molybdate solution (a 0.02 M solution of ammonium cerium sulfate dihydrate and ammonium molybdate tetrahydrate in aqueous 10% H₂SO₄). Column chromatography was performed on silica gel (Uetikon, 40-60 mesh). Methanol was dried by refluxing with sodium methoxide and distilled immediately before use. Pyridine was freshly distilled under argon over CaH₂. Dichloromethane (DCM), dichloroethane (DCE), acetonitrile (MeCN), toluene, and benzene were dried by filtration over Al₂O₃ (Fluka, type 5016 A basic). Molecular sieves (3 Å) were activated under vacuum at 500 °C for 2 h immediately before use. Compound **6** was prepared according to a published procedure.³¹ HPLC chromatograms and ¹H NMR spectra of the target compounds can be found in the Supporting Information.

Methyl (Methyl 5-Acetamido-3,5-dideoxy-2-thio-D-glycero- α -D-galacto-2-nonulopyranosid)onate (7). Compound **6** (217 mg, 42.0 mmol) was dissolved in dry MeOH (8.0 mL) and treated with NaOMe (1 M, 1.0 mL) for 2 h. The reaction mixture was neutralized with Amberlyst 15, filtered over a pad of celite, and the celite washed thoroughly with MeOH. The solvent was evaporated under reduced pressure, and the crude product was purified by chromatography on silica gel (1% gradient MeOH in DCM) to yield **7** as a white foam (90.0 mg, 61%). ^1H NMR (500 MHz, CD_3OD) δ 1.97 (dd, $J = 11.5, 13.9$ Hz, 1H, H-3a), 2.03 (s, 3H, SMe), 2.09 (s, 3H, NHAc), 2.47 (dd, $J = 4.9, 13.9$ Hz, 1H, H-3b), 3.54 (d, $J = 9.4$ Hz, 1H, H-7), 3.67 (dd, $J = 5.6, 11.6$ Hz, 1H, H-9a), 3.81–3.86 (m, 6H, H-5, H-8, H-9b, OMe), 4.11 (m, 2H, H-4, H-6). ^{13}C NMR (CD_3OD) δ 11.2 (SMe), 22.7 (NHAc), 41.2 (C-3), 53.1 (OMe), 54.1 (C-5), 65.2 (C-9), 68.3 (C-4), 70.2 (C-7), 71.2 (C-8), 72.6 (C-6), 84.6 (C-2), 170.8, 175.0 (2 CO). ESI-MS calcd for $\text{C}_{13}\text{H}_{23}\text{NO}_8\text{S} [\text{M} + \text{Na}]^+$ 376.10; found m/z 376.10.

Methyl (Methyl 5-Acetamido-3,5-dideoxy-2-thio-9-tosyl-D-glycero- α -D-galacto-2-nonulopyranosid)onate (8). To a solution of **7** (3.20 g, 9.07 mmol) in freshly distilled pyridine (80 mL) *p*-toluenesulfonyl chloride (1.90 g, 10.0 mmol) was added at 0 °C and the mixture was stirred for 2 h at 0 °C. Afterward tosyl chloride (0.70 g, 3.68 mmol) was added and the solution stirred continuously for 16 h at 5 °C. The reaction mixture was warmed to rt, methanol (20 mL) was added and stirring continued for 30 min. After evaporation of the solvents, the crude product was purified by chromatography on silica gel (DCM:MeOH, 19:1) to give **8** as a foam (3.00 g, 66%). ^1H NMR (500 MHz, CDCl_3) δ 1.79 (dd, $J = 11.2, 13.4$ Hz, 1H, H-3a), 1.96 (s, 3H, SMe), 1.99 (s, 3H, NHAc), 2.37 (s, 3H, CH_3), 2.74 (dd, $J = 3.7, 13.2$ Hz, 1H, H-3b), 3.25 (d, $J = 9.5$ Hz, 1H, H-6), 3.41 (d, $J = 9.7$ Hz, 1H, H-7), 3.66 (s, 3H, OMe), 3.98 (m, 1H, H-8), 4.10 (m, 1H, H-9a), 4.24 (m, 1H, H-9b), 6.94 (d, $J = 7.2$ Hz, 1H, NHAc), 7.28, 7.72 (AA', BB' of AA'BB', $J = 8.2$ Hz, 4H, CH_{ar}). ^{13}C NMR (CDCl_3) δ 11.9 (SMe), 21.7 (CH_3), 23.0 (NHAc), 40.4 (C-3), 52.7 (C-5), 53.7 (OMe), 67.8, 68.6, 69.1 (C-4, C-7, C-8), 72.0 (C-6), 82.4 (C-2),

Methyl (Methyl 5-Acetamido-9-azido-3,5,9-trideoxy-2-thio-D-glycero- α -D-galacto-2-nonulopyranosid)onate (9). Compound **8** (160 mg, 0.32 mmol) was dissolved in dry DMF (5 mL). NaN_3 (103 mg, 1.58 mmol) and 15-crown-5 (28.6 mg, 0.13 mmol) were added successively and the reaction mixture was stirred at 60 °C for 24 h. After filtration through a pad of celite, the solvent was evaporated and the residue was purified by chromatography on silica gel (gradient 1% MeOH in DCM) to yield **9** (96.0 mg, 78%). ^1H NMR (500 MHz, CD_3OD) δ 1.79 (m, 1H, H-3a), 2.03 (s, 3H, SMe), 2.17 (s, 3H, NHAc), 2.77 (dd, $J = 4.5, 12.8$ Hz, 1H, H-3b), 3.39 (dd, $J = 6.2, 12.7$ Hz, 1H, H-9a), 3.48 (m, 2H, H-6, H-7), 3.57 (dd, $J = 2.3, 12.7$ Hz, 1H, H-9b), 3.69 (m, 1H, H-4), 3.79 (m, 1H, H-5), 3.86 (s, 3H, OMe), 3.93 (ddd, $J = 2.6, 5.7, 8.5$ Hz, 1H, H-8), 4.01 (m, 1H, H-6). ^{13}C NMR (CD_3OD) δ 12.0 (SMe), 22.7 (NHAc), 41.8 (C-3), 53.6 (C-5), 53.8 (OMe), 55.2 (C-9), 69.0 (C-4), 71.0 (C-7), 71.7 (C-8), 76.8 (C-6), 171.7, 175.2 (2 CO). ESI-MS calcd for $\text{C}_{13}\text{H}_{22}\text{N}_4\text{O}_7\text{S} [\text{M} + \text{Na}]^+$ 401.11; found m/z 401.15.

Methyl (Methyl 5-Acetamido-4,7,8-tri-O-acetyl-9-azido-3,5,9-trideoxy-2-thio-D-glycero- α -D-galacto-2-nonulopyranosid)onate (10). Compound **9** (87.0 mg, 0.23 mmol) was dissolved in dry pyridine (1.0 mL) and cooled to 0 °C. After 15 min, DMAP (4.47 mg, 0.04 mmol) and Ac_2O (0.5 mL) were added successively. The reaction mixture was warmed to rt and stirred for 14 h. The solvent was evaporated and the residue purified by chromatography on silica gel (toluene/ethylacetate, 1:3) to afford **10** (85.0 mg, 73%). ^1H NMR (500 MHz, CDCl_3) δ 1.81 (s, 3H, NHAc), 1.91 (m, 1H, H-3a), 1.97, 2.05, 2.10 (3 s, 9H, 3 OAc), 2.13 (s, 3H, SMe), 2.67 (dd, $J = 4.4, 12.5$ Hz, 1H, H-3b), 3.19 (dd, $J = 5.7, 13.4$ Hz, 1H, H-9a), 3.59 (m, 1H, H-9b), 3.76 (m, 4H, H-6, OMe), 4.01 (m, 1H, H-5), 4.81 (m, 1H, H-4), 4.91 (d, $J = 7.7$ Hz,

1H, NHAc), 5.24 (m, 2H, H-7, H-8). ^{13}C NMR (CDCl_3) δ 12.1 (SMe), 20.9, 21.1 (3C, 3 OAc), 23.2 (NHAc), 37.8 (C-3), 49.4 (C-5), 50.6 (C-9), 53.0 (OMe), 68.1 (C-4), 69.7 (C-7), 72.3 (C-6), 74.6 (C-8), 88.4 (C-2), 170.2, 170.3, 171.0 (5C, CO). ESI-MS calcd for $\text{C}_{19}\text{H}_{28}\text{N}_4\text{O}_{10}\text{S} [\text{M} + \text{Na}]^+$ 527.40; found m/z 527.21.

General Procedure for the Synthesis of Compounds 11a–f, 17a–d, 18f,g. Compound **10** (0.12 mmol) was dissolved in dry acetonitrile (2.0 mL) under argon. The alcohol (0.26 mmol) and powdered MS 3 Å (80.0 mg) were added. The mixture was stirred at rt for 1.5 h. Then the suspension was cooled to –40 °C and subsequently treated with *N*-iodosuccinimide (0.60 mmol) and triflic acid (0.06 mmol in 0.2 mL MeCN). After 30 min, the reaction mixture was warmed to –30 °C and stirring continued for 16 h. The mixture was then warmed to rt, stirred for another 2 h, and filtered through a pad of celite. The celite was washed with DCM (10 mL), and the filtrate was subsequently washed with 20% aqueous $\text{Na}_2\text{S}_2\text{O}_3$ (1 mL) and saturated aqueous NaHCO_3 (3 \times 5 mL). The organic phase was dried over Na_2SO_4 , filtered, and concentrated under reduced pressure. The crude product was purified by chromatography on silica gel.

General Procedure for the Synthesis of Compounds 12a–f, 20, 18a–d. Compounds **11a–f** (**14** or **17a–d**) (0.09 mmol) and *p*-chlorobenzoyl chloride (0.36 mmol) were dissolved in dry DCE (3.0 mL) under argon. Triphenylphosphine (0.18 mmol) in dry DCE (1.5 mL) was added after 5 min, and the solution was stirred at rt for 24 h. The reaction mixture was diluted with DCM (10 mL) and washed with saturated aqueous NaHCO_3 (3 \times 10 mL). The organic phase was dried over Na_2SO_4 , filtered, and concentrated under reduced pressure. The residue was purified by chromatography on silica gel.

General Procedure for the Deprotection of 12a–f, 18b. Compound **12a–f** (**18b**) (0.06 mmol) was dissolved in MeOH (1.5 mL) and treated with 10% aqueous NaOH (0.3 mL). The reaction mixture was stirred at rt for 3 h. Then the reaction mixture was neutralized with 7% aqueous HCl (0.2 mL). The solvent was evaporated, and the crude product was purified by chromatography on RP-18.

(2 mL/0.5 mL) and was reacted with LiOH (0.28 mmol). The crude product was purified on RP-18 (10% gradient MeOH in water) followed by ion exchange chromatography (Dowex-50) and P2 size exclusion chromatography to yield **19**.

Methyl (4-Chlorobenzyl 5-Acetamido-4,7,8-tri-O-acetyl-9-azido-3,5,9-trideoxy-D-glycero- α -D-galacto-2-nonulopyranosid)onate (11a). Compound **10** (61.0 mg, 0.12 mmol) was reacted with 4-chlorobenzyl alcohol (38.0 mg, 0.26 mmol), *N*-iodosuccinimide (134 mg, 0.601 mmol), and triflic acid (6.00 μL , 9.00 mg, 0.06 mmol). The crude product was purified by chromatography on silica gel (0.5% gradient *i*PrOH in petrol ether/DCM 8:4) to yield **11a** (55.0 mg, 76%) as a colorless oil. $[\alpha]_{\text{D}}^{20} -0.02$ (*c* 0.28, CH_2Cl_2). ^1H NMR (500 MHz, CDCl_3) δ 1.90 (s, 3H, NHAc), 2.03 (m, 4H, OAc, H-3a), 2.17, 2.20 (2 s, 6H, 2 OAc), 2.65 (dd, $J = 4.6, 12.9$ Hz, 1H, H-3b), 3.26 (dd, $J = 5.7, 13.4$ Hz, 1H, H-9a), 3.55 (dd, $J = 2.8, 13.4$ Hz, 1H, H-9b), 3.71 (s, 3H, OMe), 4.12 (m, 2H, H-5, H-6), 4.41, 4.76 (A, B of AB, $J = 12.3$ Hz, 2H, CH_2Ar), 4.87 (m, 1H, H-4), 5.15 (d, $J = 9.8$ Hz, 1H, NH), 5.35 (m, 2H, H-7, H-8) 7.30 (m, 4H, CH_{ar}). ^{13}C NMR (CDCl_3) δ 20.8, 20.9, 21.1 (3 OAc), 23.3 (NHAc), 38.0 (C-3), 49.4 (C-5), 51.0 (C-9), 52.8 (OMe), 66.1 (CH_2Ar), 67.9 (C-7), 68.9 (C-4), 69.4 (C-8), 72.8 (C-6), 98.6 (C-2), 128.4, 129.1, 133.5, 135.7 (6 C–Ar), 168.3, 170.3, 170.3, 171.0 (5C, 5 CO). ESI-MS calcd for $\text{C}_{25}\text{H}_{31}\text{ClN}_4\text{O}_{11} [\text{M} + \text{Na}]^+$ 621.17; found m/z 621.24.

Methyl (4-Fluorobenzyl 5-Acetamido-4,7,8-tri-O-acetyl-9-azido-3,5,9-trideoxy-D-glycero- α -D-galacto-2-nonulopyranosid)onate (11b). Compound **10** (62.0 mg, 0.12 mmol) was reacted with 4-fluorobenzyl alcohol (38.0 mg, 0.26 mmol), *N*-iodosuccinimide (134 mg, 0.601 mmol), and triflic acid (6.00 μL , 9.00 mg, 0.06 mmol). The crude product was purified by chromatography on silica gel (0.5% gradient *i*PrOH in petrol ether/DCM 8:4) to yield **11b** (53.0 mg, 76%) as a colorless oil. $[\alpha]_{\text{D}}^{20}$

3.3 Pharmacokinetic behavior of MAG antagonists

-0.01, (c 2.6, CH₂Cl₂). ¹H NMR (500 MHz, CDCl₃) δ 1.89 (s, 3H, NHAc), 2.02 (m, 1H, H-3a), 2.03, 2.17, 2.20 (3 s, 9H, 3 OAc), 2.65 (dd, *J* = 4.5, 12.8 Hz, 1H, H-3b), 3.29 (dd, *J* = 5.4, 13.3 Hz, 1H, H-9a), 3.58 (dd, *J* = 2.0, 13.1 Hz, 1H, H-9b), 3.71 (s, 3H, OMe), 4.13 (m, 2H, H-5, H-6), 4.41, 4.76 (A, B of AB, *J* = 11.9 Hz, 2H, CH₂Ar), 4.85 (m, 1H, H-4), 5.35 (m, 2H, H-8, H-7), 7.02 (t, *J* = 8.6 Hz, 2H, CH_{ar}), 7.31 (dd, *J* = 5.6, 8.2 Hz, 2H, CH_{ar}). ¹³C NMR (CDCl₃) δ 20.8, 20.9, 21.1 (3 OAc), 23.2 (NHAc), 49.3 (C-3), 51.0 (C-5), 52.8 (C-9), 53.5 (OMe), 66.1 (CH₂Ar), 68.0 (C-7), 68.9 (C-4), 69.7 (C-8), 72.8 (C-6), 98.5 (C-2), 115.2 (*J* = 21.7 Hz), 129.6 (*J* = 8.4 Hz), 132.9 (*J* = 2.9 Hz), 162.4 (*J* = 246.0 Hz) (6 C-Ar), 168.4, 170.2, 170.3, 170.4, 171.0 (6C, 6 CO). ESI-MS calcd for C₂₅H₃₁FN₄O₁₁ [M + Na]⁺ 605.20; found *m/z* 605.22.

Methyl (Pentafluorobenzyl 5-Acetamido-4,7,8-tri-*O*-acetyl-9-azido-3,5,9-trideoxy-*D*-glycero- α -*D*-galacto-2-nonulopyranosid)onate (11c). Compound 10 (60.0 mg, 0.12 mmol) was reacted with pentafluorobenzyl alcohol (60.0 mg, 0.30 mmol), *N*-iodosuccinimide (32.0 mg, 0.14 mmol), and triflic acid (4.00 μ L, 7.00 mg, 0.04 mmol). The crude product was purified by chromatography on silica gel (0.5% gradient *i*PrOH in petrol ether/DCM 8:4) to yield 11c (47.0 mg, 66%) as a colorless oil. [α]_D²⁰ -0.03 (c 0.5, CH₂Cl₂). ¹H NMR (500 MHz, CDCl₃) δ 1.90 (s, 3H, NHAc), 1.94 (dd, *J* = 10.4, 12.6 Hz, 1H, H-3a), 2.03, 2.19, 2.21 (3 s, 9H, 3 OAc), 2.59 (dd, *J* = 4.6, 12.8 Hz, 1H, H-3b), 3.30 (dd, *J* = 5.6, 13.5 Hz, 1H, H-9a), 3.59 (dd, *J* = 2.9, 13.5 Hz, 1H, H-9b), 3.86 (s, 3H, OMe), 4.12 (m, 2H, H-5, H-6), 4.43 (A of AB, *J* = 11.0 Hz, 1H, CH₂Ar), 4.87 (m, 1H, H-4), 4.90 (B of AB, *J* = 10.7 Hz, 1H, CH₂Ar), 5.19 (d, *J* = 9.3 Hz, 1H, NH), 5.39 (m, 2H, H-7, H-8). ¹³C NMR (CDCl₃) δ 20.8, 20.9, 21.1 (3 OAc), 23.2 (NHAc), 37.7 (C-3), 49.4 (C-5), 51.0 (C-9), 53.0 (OMe), 54.0 (CH₂Ar), 67.8, 68.8, 69.3 (C-4, C-7, C-8), 72.9 (C-6), 98.7 (C-2), 167.8, 170.3 (5C, 5 CO). ESI-MS calcd for C₂₅H₂₇F₅N₄O₁₁ [M + Na]⁺ 677.16; found *m/z* 677.32.

Methyl (2-Naphthyl 5-Acetamido-4,7,8-tri-*O*-acetyl-9-azido-3,5,9-trideoxy-*D*-glycero- α -*D*-galacto-2-nonulopyranosid)onate (11d). Compound 10 (50.0 mg, 0.10 mmol) was reacted with 2-naphthalenemethanol (24.0 mg, 0.15 mmol), *N*-iodosuccinimide (27.0 mg, 0.12 mmol), and triflic acid (4.00 μ L, 7.00 mg, 0.04 mmol). The crude product was purified by chromatography on silica gel (0.5% gradient *i*PrOH in petrol ether/DCM 8:4) to yield 11d (37.0 mg, 61%) as a colorless oil. ¹H NMR (500 MHz, CDCl₃) δ 1.85 (s, 3H, NHAc), 2.09 (m, 1H, H-3a), 2.03, 2.15, 2.21 (3 s, 9H, 3 OAc), 2.26 (dd, *J* = 6.0, 13.5 Hz, 1H, H-9a), 3.59 (dd, *J* = 2.9, 13.5 Hz, 1H, H-9b), 3.67 (s, 3H, OMe), 4.14 (m, 2H, H-5, H-6), 4.63 (A of AB, *J* = 12.2 Hz, 1H, CH₂Ar), 4.89 (m, 1H, H-4), 4.96 (B of AB, *J* = 12.2 Hz, 1H, CH₂Ar), 5.34 (m, 2H, H-7, H-8), 5.38 (m, 1H, H-8), 7.45-7.48 (m, 3H, CH_{ar}), 7.79-7.83 (m, 4H, CH_{ar}). ¹³C NMR (CDCl₃) δ 21.3, 21.5 (3C, 3 OAc), 23.6 (NHAc), 38.5 (C-3), 49.9 (C-5), 51.3 (C-9), 53.1 (OMe), 67.4 (CH₂Ar), 68.4 (C-7), 69.4 (C-4), 70.2 (C-8), 73.3 (C-6), 126.1, 126.4, 126.5, 126.9, 128.1, 128.3, 128.4 (10 C-Ar), 170.7 (6C, 6 CO). ESI-MS calcd for C₂₉H₃₄N₄O₁₁ [M + Na]⁺ 637.33; found *m/z* 637.20.

Methyl (2,3-Dichlorobenzyl 5-Acetamido-4,7,8-tri-*O*-acetyl-9-azido-3,5,9-trideoxy-*D*-glycero- α -*D*-galacto-2-nonulopyranosid)onate (11e). Compound 10 (45.0 mg, 0.09 mmol) was reacted with 2,3-dichlorobenzyl alcohol (24.0 mg, 0.13 mmol), *N*-iodosuccinimide (24.0 mg, 0.12 mmol), and triflic acid (3.00 μ L, 6.00 mg, 0.04 mmol). The crude product was purified by chromatography on silica gel (0.5% gradient *i*PrOH in petrol ether/DCM 8:4) to yield 11e (30.0 mg, 54%) as a yellow oil. ¹H NMR (500 MHz, CDCl₃) δ 1.83 (s, 3H, NHAc), 2.01 (t, *J* = 12.9 Hz, 1H, H-3a), 1.97, 2.08, 2.11 (3 s, 9H, 3 OAc), 2.63 (dd, *J* = 4.7, 12.9 Hz, 1H, H-3b), 3.19 (dd, *J* = 6.0, 13.6 Hz, 1H, H-9a), 3.50 (dd, *J* = 3.0, 13.6 Hz, 1H, H-9b), 3.72 (s, 3H, OMe), 4.05 (m, 2H, H-5, H-6), 4.50, 4.82 (A, B of AB, *J* = 13.0 Hz, 2H, CH₂Ar), 4.85 (m, 1H, H-4), 5.13 (d, *J* = 8.0 Hz, 1H, NHAc), 5.24 (m, 2H, H-7, H-8), 7.14 (t, *J* = 8.0 Hz, 1H, CH_{ar}), 7.34 (d, *J* = 8.1 Hz, 2H, CH_{ar}). ¹³C NMR (CDCl₃) δ 21.3, 21.5 (3C, 3 OAc), 23.6 (NHAc), 38.2 (C-3), 49.9 (C-5), 51.2 (C-9), 53.4 (OMe), 64.7 (CH₂Ar), 68.4

(C-8), 69.3 (C-4), 70.5 (C-7), 73.5 (C-6), 109.6 (C-2), 127.6, 127.7, 130.0 (6C, 6 C-Ar), 168.5, 170.5, 170.6, 170.7, 171.4 (5 CO). ESI-MS calcd for C₂₅H₃₀Cl₂N₄O₁₁ [M + Na]⁺ 655.13; found *m/z* 655.07.

Methyl (2,3-Difluorobenzyl 5-Acetamido-4,7,8-tri-*O*-acetyl-9-azido-3,5,9-trideoxy-*D*-glycero- α -*D*-galacto-2-nonulopyranosid)onate (11f). Compound 10 (86.0 mg, 0.17 mmol) was reacted with 2,3-difluorobenzyl alcohol (29.0 μ L, 37.0 mg, 0.26 mmol), *N*-iodosuccinimide (46.0 mg, 0.21 mmol), and triflic acid (6.00 μ L, 10.0 mg, 0.07 mmol). The crude product was purified by chromatography on silica gel (0.5% gradient *i*PrOH in petrol ether/DCM 8:4) to yield 11f (67.0 mg, 66%) as a yellow oil. ¹H NMR (500 MHz, CDCl₃) δ 1.82 (s, 3H, NHAc), 1.95 (m, 1H, H-3a), 1.96, 2.10, 2.13 (3 s, 9H, 3 OAc), 2.58 (m, 1H, H-3b), 3.20 (m, 1H, H-9a), 3.50 (m, 1H, H-9b), 3.72 (s, 3H, OMe), 4.06 (m, 2H, H-5, H-6), 4.46, 4.75 (A, B of AB, *J* = 12.0 Hz, 2H, CH₂Ar), 4.82 (m, 1H, H-4), 5.29 (m, 2H, H-8, H-7), 7.05 (m, 3H, CH_{ar}). ¹³C NMR (CDCl₃) δ 21.3, 21.6 (3C, 3 OAc), 23.6 (NHAc), 38.2 (C-3), 49.8 (C-5), 51.3 (C-9), 53.3 (OMe), 60.8 (CH₂Ar), 68.4 (C-7), 69.3 (C-8), 70.3 (C-4), 73.4 (C-6), 99.1 (C-2), 117.4, 119.1 (*J* = 17.0 Hz), 124.3, 125.5 (6 C-Ar), 168.5, 170.5, 170.6, 170.8, 171.4 (5 CO). ESI-MS calcd for C₂₅H₃₀F₂N₄O₁₁ [M + 2Na]⁺ 645.99; found *m/z* 645.26.

Methyl (4-Chlorobenzyl 5-Acetamido-4,7,8-tri-*O*-acetyl-9-(4-chlorobenzamido)-3,5,9-trideoxy-*D*-glycero- α -*D*-galacto-2-nonulopyranosid)onate (12a). Compound 11a (55.0 mg, 0.09 mmol) was reacted with *p*-chlorobenzoyl chloride (46.0 μ L, 63.0 mg, 0.36 mmol) and triphenylphosphine (47.0 mg, 0.18 mmol). The crude product was purified by chromatography on silica gel (0.5% gradient of MeOH in DCM) to yield 12a (35.0 mg, 59%) as a yellow solid. [α]_D²⁰ -0.01 (c 2.9, CH₂Cl₂). ¹H NMR (500 MHz, CDCl₃) δ 1.89 (s, 3H, NHAc), 2.05 (m, 4H, H-3a, OAc), 2.14, 2.27 (2 s, 6H, 2 OAc), 2.67 (dd, *J* = 4.6, 12.8 Hz, 1H, H-3b), 2.92 (dt, *J* = 3.3, 14.9 Hz, 1H, H-9a), 3.65 (s, 3H, OMe), 4.05 (dd, *J* = 2.0, 10.7 Hz, 1H, H-6), 4.21 (q, *J* = 10.4 Hz, 1H, H-5), 4.36 (ddd, *J* = 3.0, 8.7, 15.1 Hz, 1H, H-9b), 4.41, 4.78 (A, B of AB, *J* = 12.3 Hz, 2H, CH₂Ar), 4.84 (m, 1H, H-4), 5.15 (dd, *J* = 2.0, 10.0 Hz, 1H, H-7), 5.31 (m, 2H, NHAc, H-8), 7.10 (dd, *J* = 4.0, 8.5 Hz, 1H, NH), 7.29 (m, 4H, CH_{ar}), 7.41, 7.77 (AA', BB' of AA'/BB', *J* = 8.5 Hz, 4H, CH_{ar}). ¹³C NMR (CDCl₃) δ 20.9, 21.2, 21.3 (3 OAc), 23.2 (NHAc), 38.1 (C-3), 38.4 (C-9), 49.5 (C-5), 52.7 (OMe), 66.1 (CH₂Ar), 67.9 (C-7), 68.2 (C-8), 69.0 (C-4), 72.2 (C-6), 98.4 (C-2), 128.4, 128.5, 128.8, 129.2, 132.0, 132.6, 133.5, 135.7, 137.7 (12 C-Ar), 168.1, 170.4, 171.2, 172.6 (6C, 6 CO). ESI-MS calcd for C₃₂H₃₆Cl₂N₂O₁₂ [M + Na]⁺ 733.16; found *m/z* 733.25.

Methyl (4-Fluorobenzyl 5-Acetamido-4,7,8-tri-*O*-acetyl-9-(4-chlorobenzamido)-3,5,9-trideoxy-*D*-glycero- α -*D*-galacto-2-nonulopyranosid)onate (12b). Compound 11b (52.0 mg, 0.09 mmol) was reacted with *p*-chlorobenzoyl chloride (46.0 μ L, 63.0 mg, 0.36 mmol) and triphenylphosphine (52.0 mg, 0.19 mmol). The crude product was purified by chromatography on silica gel (0.5% gradient of MeOH in DCM) to yield 12b (37.0 mg, 60%) as a yellow solid. ¹H NMR (500 MHz, CDCl₃) δ 1.85 (s, 3H, NHAc), 2.00 (m, 1H, H-3a), 2.03, 2.11, 2.26 (3 s, 9H, 3 OAc), 2.68 (dd, *J* = 4.5, 12.7 Hz, 1H, H-3b), 2.96 (dt, *J* = 3.5, 15.0 Hz, 1H, H-9a), 3.61 (s, 3H, OMe), 4.12 (d, *J* = 10.7 Hz, 1H, H-6), 4.23 (q, *J* = 10.2 Hz, 1H, H-5), 4.36 (ddd, *J* = 3.0, 8.7, 15.3 Hz, 1H, H-9b), 4.40, 4.78 (A, B of AB, *J* = 11.9 Hz, 2H, CH₂Ar), 4.87 (m, 1H, H-4), 5.20 (dd, *J* = 1.1, 9.9 Hz, 1H, H-7), 5.35 (dt, *J* = 2.9, 9.9 Hz, 1H, H-8), 5.99 (m, 1H, NHAc), 7.00 (t, *J* = 8.7 Hz, 2H, CH_{ar}), 7.17 (dd, *J* = 3.8 Hz, 8.1 Hz, 1H, NH), 7.49 (dd, *J* = 5.4 Hz, 8.5 Hz, 1H, CH_{ar}), 7.38, 7.76 (AA', BB' of AA'/BB', *J* = 8.4 Hz, 4H, CH_{ar}). ¹³C NMR (CDCl₃) δ 21.2, 21.3 (3 OAc), 23.1 (NHAc), 38.3 (C-3), 38.5 (C-9), 49.4 (C-5), 52.6 (OMe), 66.1 (CH₂Ar), 68.0 (C-7), 68.2 (C-8), 69.2 (C-4), 72.2 (C-6), 98.4 (C-2), 115.0, 115.2 (*J* = 21.3 Hz), 128.6, 129.6, 129.7 (*J* = 7.5 Hz), 132.0, 132.8, 132.9, 137.7, 161.3, 163.5 (*J* = 275.1 Hz), 168.1, 166.3 (*J* = 237.5 Hz) (12 C-Ar), 170.39, 170.4, 171.0, 172.5 (6C, 6 CO). ESI-MS calcd for C₃₂H₃₆FClN₂O₁₂ [M + Na]⁺ 717.19; found *m/z* 717.34.

Methyl (Pentafluorobenzyl 5-Acetamido-4,7,8-tri-*O*-acetyl-9-(4-chlorobenzamido)-3,5,9-trideoxy- β -glycero- α -*D*-galacto-2-nonulopyranosid)onate (12c). Compound **11c** (47.0 mg, 0.07 mmol) was reacted with *p*-chlorobenzoyl chloride (36.0 μ L, 49.0 mg, 0.28 mmol) and triphenylphosphine (41.0 mg, 0.16 mmol). The crude product was purified by chromatography on silica gel (0.5% gradient of MeOH in DCM) to yield **12c** (25.0 mg, 45%). ¹H NMR (500 MHz, CDCl₃) δ 1.86 (s, 3H, NHAc), 1.94 (m, 1H, H-3a), 2.02, 2.16, 2.19 (3 s, 9H, 3 OAc), 2.60 (dd, *J* = 4.5, 12.8 Hz, 1H, H-3b), 3.55 (dd, *J* = 6.3, 12.3 Hz, 1H, H-9a), 3.81 (m, 4H, OMe, H-9b), 4.07 (d, *J* = 10.3 Hz, 1H, H-6), 4.20 (dd, *J* = 2.0, 10.8 Hz, 1H, H-5), 4.45, 4.93 (A, B of AB, *J* = 11.3 Hz, 2H, CH₂Ar), 5.37 (dd, *J* = 2.1, 8.1 Hz, 1H, H-7), 5.46 (m, 1H, H-8), 5.68 (d, *J* = 9.6 Hz, 1H, NHAc), 7.38, 8.00 (AA', BB' of AA'BB', *J* = 8.4 Hz, 4H, CH_{ar}). ¹³C NMR (CDCl₃) δ 21.0, 21.2, 21.3 (3 OAc), 23.3 (NHAc), 37.8 (C-3), 43.7 (C-9), 49.5 (C-5), 53.1 (OMe), 54.1 (CH₂Ar), 68.3, 69.0 (C-4, C-7), 70.0 (C-8), 72.9 (C-6), 98.8 (C-2), 128.8, 128.9, 129.1, 131.5, 132.9, 133.2, 133.3 (12 C-Ar), 167.6, 167.9, 168.7, 170.3, 170.4, 170.6 (6 CO). ESI-MS calcd for C₃₂H₃₂ClF₅N₂O₁₂ [M + Cl]⁻ 801.45; found *m/z* 801.36.

Methyl (2-Naphthyl 5-Acetamido-4,7,8-tri-*O*-acetyl-9-(4-chlorobenzamido)-3,5,9-trideoxy- β -glycero- α -*D*-galacto-2-nonulopyranosid)onate (12d). Compound **11d** (50.0 mg, 0.08 mmol) was reacted with *p*-chlorobenzoyl chloride (42.0 μ L, 57.0 mg, 0.32 mmol) and triphenylphosphine (47.0 mg, 0.18 mmol). The crude product was purified by chromatography on silica gel (0.5% gradient of MeOH in DCM) to yield **12d** (25.0 mg, 47%). ¹H NMR (500 MHz, CDCl₃) δ 1.87 (s, 3H, NHAc), 2.04 (s, 3H, OAc), 2.10 (t, *J* = 12.4 Hz, 1H, H-3a), 2.14, 2.24 (2 s, 6H, 2 OAc), 2.72 (dd, *J* = 4.5, 12.8 Hz, 1H, H-3b), 2.92 (m, 1H, H-9a), 3.59 (s, 3H, OMe), 4.11 (m, 1H, H-6), 4.23 (q, *J* = 10.3 Hz, 1H, H-5), 4.34 (ddd, *J* = 3.0, 8.5, 15.2 Hz, 1H, H-9b), 4.63 (A of AB, *J* = 12.3 Hz, 1H, CH₂Ar), 4.87 (dt, *J* = 4.6, 12.3 Hz, 1H, H-4), 4.98 (B of AB, *J* = 12.3 Hz, 1H, CH₂Ar), 5.17 (d, *J* = 9.8 Hz, 1H, H-7), 5.34 (d, *J* = 9.9 Hz, 1H, H-8), 5.50 (m, 1H, NHAc), 7.11 (m, 1H, NH), 7.39 (AA' of AA'BB', *J* = 8.5 Hz, 2H, CH_{ar}), 7.44–7.47 (m, 3H, CH_{ar}), 7.76 (BB' of AA'BB', *J* = 8.5 Hz, 2H, CH_{ar}), 7.75–7.83 (m, 4H, CH_{ar}). ¹³C NMR (CDCl₃) δ 21.3, 21.5, 21.6 (3 OAc), 23.5 (NHAc), 38.6 (C-3), 38.9 (C-9), 49.9 (C-5), 53.0 (OMe), 67.4 (CH₂Ar), 68.4 (C-7), 68.7 (C-8), 69.5 (C-4), 72.6 (C-6), 98.9 (C-2), 126.2, 126.3, 126.5, 127.0, 128.0, 128.3, 128.9, 129.0, 129.2, 132.4, 133.1, 133.3, 133.5, 135.1 (14 C-Ar), 166.6, 168.7, 170.8, 171.5, 172.9 (6C, 6 CO). ESI-MS calcd for C₃₆H₃₉ClN₂O₁₂ [M + Na]⁺ 749.22; found *m/z* 749.25.

Methyl (2,3-Dichlorobenzyl 5-Acetamido-4,7,8-tri-*O*-acetyl-9-(4-chlorobenzamido)-3,5,9-trideoxy- β -glycero- α -*D*-galacto-2-nonulopyranosid)onate (12e). Compound **11e** (47.0 mg, 0.07 mmol) was reacted with *p*-chlorobenzoyl chloride (38.0 μ L, 52.0 mg, 0.30 mmol) and triphenylphosphine (43.0 mg, 0.16 mmol). The crude product was purified by chromatography on silica gel (0.5% gradient of MeOH in DCM) to yield **12e** (25.0 mg, 47%) as a yellow solid. ¹H NMR (500 MHz, CDCl₃) δ 1.78 (t, *J* = 12.4 Hz, 1H, H-3a), 1.80 (s, 3H, NHAc), 1.97, 2.04, 2.17 (3 s, 9H, 3 OAc), 2.63 (dd, *J* = 4.8, 12.8 Hz, 1H, H-3b), 2.90 (ddd, *J* = 3.3, 3.7, 15.1 Hz, 1H, H-9a), 3.64 (s, 3H, OMe), 4.01 (d, *J* = 10.8 Hz, 1H, H-6), 4.15 (q, *J* = 10.4 Hz, 1H, H-5), 4.23 (m, 1H, H-9b), 4.49 (A of AB, *J* = 13.0 Hz, 1H, CH₂Ar), 4.30 (m, 2H, H-4, CH₂Ar), 5.11 (d, *J* = 1.6 Hz, 1H, H-7), 5.20 (m, 1H, H-8), 5.55 (d, *J* = 8.8 Hz, 1H, NHAc), 7.03 (dd, *J* = 3.8 Hz, 1H, NH), 7.13 (t, *J* = 7.8 Hz, 1H, CH_{ar}), 7.39 (m, 2H, CH_{ar}), 7.68, 7.93 (AA', BB' of AA'BB', *J* = 8.5 Hz, 4H, CH_{ar}). ¹³C NMR (CDCl₃) δ 21.3, 21.5, 21.6 (3 OAc), 23.5 (NHAc), 38.2 (C-3), 39.0 (C-9), 49.9 (C-5), 53.2 (OMe), 64.8 (CH₂Ar), 68.4 (C-8), 68.8 (C-7), 69.5 (C-4), 72.7 (C-6), 110.0 (C-2), 127.6, 128.1, 130.0, 131.8, 133.0, 136.0, 138.1 (12 C-Ar), 160.0, 168.0, 170.6, 170.9, 171.5, 172.8 (6 CO). ESI-MS calcd for C₃₂H₃₅Cl₃N₂O₁₂ [M + Na]⁺ 767.13; found *m/z*: 767.12.

Methyl (2,3-Difluorobenzyl 5-Acetamido-4,7,8-tri-*O*-acetyl-9-(4-chlorobenzamido)-3,5,9-trideoxy- β -glycero- α -*D*-galacto-2-nonulopyranosid)onate (12f). Compound **11f** (67.0 mg, 0.11 mmol)

was reacted with *p*-chlorobenzoyl chloride (57.0 μ L, 78.0 mg, 0.45 mmol) and triphenylphosphine (65.0 mg, 0.25 mmol). The crude product was purified by chromatography on silica gel (0.5% gradient of MeOH in DCM) to yield **12f** (44.0 mg, 55%) as a yellow solid. ¹H NMR (500 MHz, CDCl₃) δ 1.80 (s, 3H, NHAc), 2.04 (m, 4H, H-3a, OAc), 2.14, 2.27 (2 s, 6H, 2 OAc), 2.65 (dd, *J* = 4.6, 12.8 Hz, 1H, H-3b), 2.97 (dt, *J* = 3.5, 15.0 Hz, 1H, H-9a), 3.74 (s, 3H, OMe), 4.08 (m, 1H, H-6), 4.23 (q, *J* = 10.4 Hz, 1H, H-5), 4.33 (m, 1H, H-9b), 4.52, 4.84 (A, B of AB, *J* = 12.0 Hz, 2H, CH₂Ar), 5.17 (dd, *J* = 1.9, 9.8 Hz, 1H, H-7), 5.31 (m, 1H, H-8), 5.43 (m, 1H, NHAc), 7.75 (m, 4H, NH, CH_{ar}), 7.39, 7.77 (AA', BB' of AA'BB', *J* = 8.5 Hz, 4H, CH_{ar}). ¹³C NMR (CDCl₃) δ 21.3, 21.5, 21.6 (3 OAc), 23.5 (NHAc), 38.3 (C-3), 38.9 (C-9), 49.9 (C-5), 53.2 (OMe), 60.8 (CH₂Ar), 68.3 (C-8), 68.7 (C-7), 69.4 (C-4), 72.7 (C-6), 98.0 (C-2), 117.3, 117.4 (*J* = 17.0 Hz), 125.7, 128.8, 129.2, 132.4, 132.5 (*J* = 9.0 Hz), 133.0, 138.1 (12 C-Ar), 166.7, 168.4, 170.7, 170.9, 171.6, 172.9 (6 CO). ESI-MS calcd for C₃₂H₃₅ClF₂N₂O₁₂ [M + Na]⁺ 735.18; found *m/z* 735.15.

Sodium (4-Chlorobenzyl 5-Acetamido-9-(4-chlorobenzamido)-3,5,9-trideoxy- β -glycero- α -*D*-galacto-2-nonulopyranosid)onate (13a). Compound **12a** (25.0 mg, 0.03 mmol) was treated with 10% aqueous NaOH (0.2 mL) in MeOH (1.0 mL). The crude product was purified by chromatography on RP-18 (5% gradient of MeOH in H₂O) to yield **13a** as a white solid (15.0 mg, 50%). [α]_D²⁰ -0.25 (c 0.41, H₂O). ¹H NMR (500 MHz, CD₃OD) δ 1.55 (dd, *J* = 3.3, 11.9 Hz, 1H, H-3a), 1.90 (s, 3H, NHAc), 2.81 (dd, *J* = 2.0, 12.2 Hz, 1H, H-3b), 3.34 (dd, *J* = 1.8, 9.0 Hz, 1H, H-7), 3.41 (dd, *J* = 7.8, 13.6 Hz, 1H, H-9a), 3.55–3.63 (m, 3H, H-4, H-5, H-6), 3.67 (dd, *J* = 3.1 Hz, 13.6 Hz, 1H, H-9b), 3.94 (m, 1H, H-8), 4.40, 4.70 (A, B of AB, *J* = 11.6 Hz, 2H, CH₂Ar), 7.18, 7.25 (AA', BB' of AA'BB', *J* = 8.4 Hz, 4H, CH_{ar}), 7.36, 7.72 (AA', BB' of AA'BB', *J* = 8.6 Hz, 4H, CH_{ar}). ¹³C NMR (CD₃OD) δ 22.6 (NHAc), 42.7 (C-3), 44.6 (C-9), 54.2 (C-5), 66.5 (CH₂Ar), 69.6 (C-4), 71.2 (C-8), 72.5 (C-7), 74.4 (C-6), 102.1 (C-2), 129.2, 129.7, 130.1, 130.6, 134.0, 134.5, 138.6, 138.8 (12 C-Ar), 169.2, 174.3, 175.5 (3 CO). HRMS calcd for C₂₅H₂₈Cl₂N₂O₉ [M - H]⁻ 615.0891; found 615.0888.

Sodium (4-Fluorobenzyl 5-Acetamido-9-(4-chlorobenzamido)-3,5,9-trideoxy- β -glycero- α -*D*-galacto-2-nonulopyranosid)onate (13b). Compound **12b** (37.0 mg, 0.05 mmol) was treated with 10% aqueous NaOH (0.3 mL) in MeOH (1.2 mL). The crude product was purified by chromatography on RP-18 (5% gradient of MeOH in H₂O) to yield **13b** as a white solid (21.1 mg, 70%). [α]_D²⁰ -0.22 (c 0.33, H₂O). ¹H NMR (500 MHz, CD₃OD) δ 1.54 (m, 1H, H-3a), 1.90 (s, 3H, NHAc), 2.80 (m, 1H, H-3b), 3.35 (m, 1H, H-7), 3.42 (m, 1H, H-9a), 3.58–3.69 (m, 4H, H-4, H-5, H-6, H-9b), 3.96 (m, 1H, H-8), 4.39, 4.69 (A, B of AB, *J* = 11.2 Hz, 2H, CH₂Ar), 6.90 (t, *J* = 8.8 Hz, 2H, CH_{ar}), 7.27 (m, 2H, CH_{ar}), 7.35 (m, 2H, CH_{ar}), 7.72 (BB' of AA'BB', *J* = 8.5 Hz, 2H, CH_{ar}). ¹³C NMR (CD₃OD) δ 22.7 (NHAc), 42.7 (C-3), 44.5 (C-9), 54.2 (C-5), 66.7 (CH₂Ar), 69.6 (C-4), 71.4 (C-8), 72.5 (C-7), 74.4 (C-6), 102.1 (C-2), 115.8 (*J* = 12.5 Hz), 130.1, 129.7, 131.1 (*J* = 21.3 Hz), 138.6, 162.0 (12 C-Ar), 164.6, 169.3, 174.4 (3 CO). HRMS calcd for C₂₅H₂₈ClFN₂O₉ [M - H]⁻ 577.1367; found 577.1369.

Sodium (Pentafluorobenzyl 5-Acetamido-9-(4-chlorobenzamido)-3,5,9-trideoxy- β -glycero- α -*D*-galacto-2-nonulopyranosid)onate (13c). Compound **12c** (25.0 mg, 0.03 mmol) was treated with 10% aqueous NaOH (0.2 mL) in MeOH (1.0 mL). The crude product was purified by chromatography on RP-18 (5% gradient of MeOH in H₂O) to yield **13c** as a white solid (8.0 mg, 39%). [α]_D²⁰ -0.02 (c 0.32, H₂O). ¹H NMR (500 MHz, D₂O) δ 1.63 (t, *J* = 12.1 Hz, 1H, H-3a), 1.97 (s, 3H, NHAc), 2.71 (dd, *J* = 4.7, 12.4 Hz, 1H, H-3b), 3.50 (m, 2H, H-7, H-9a), 3.65 (ddd, *J* = 4.7, 9.5, 11.9 Hz, 1H, H-4), 3.74–3.79 (m, 3H, H-5, H-6, H-9b), 3.88 (ddd, *J* = 2.9, 7.8, 8.8 Hz, 1H, H-8), 4.66, 4.86 (A, B of AB, *J* = 11.7 Hz, 2H, CH₂Ar), 7.50, 7.73 (AA', BB' of AA'BB', *J* = 8.6 Hz, 4H, CH_{ar}). ¹³C NMR (D₂O) δ 21.9 (NHAc), 40.3 (C-3), 42.6 (C-9), 51.8 (C-5), 54.1 (CH₂Ar), 68.1 (C-4), 69.8 (C-7), 70.3 (C-8), 72.8 (C-6), 101.0 (C-2), 128.7, 128.7, 132.2, 136.2, 137.5, 139.1

3.3 Pharmacokinetic behavior of MAG antagonists

(12 C-Ar), 170.1, 172.8, 175.0 (3 CO). HRMS calcd for $C_{25}H_{23}ClF_5N_2NaO_9 [M - H]^-$ 625.1018; found 625.1015.

Sodium (2-Naphthyl 5-Acetamido-9-(4-chlorobenzamido)-3,5,9-trideoxy- β -glycero- α - β -galacto-2-nonulopyranosid)onate (13d). Compound **12d** (25.0 mg, 0.03 mmol) was treated with 10% aqueous NaOH (0.2 mL) in MeOH (1.0 mL). The crude product was purified by chromatography on RP-18 (5% gradient of MeOH in H₂O) to yield **13d** as a white solid (14.0 mg, 70%). $[\alpha]_D^{20}$ -0.37 (c 0.46, H₂O). ¹H NMR (500 MHz, CD₃OD) δ 1.60 (m, 1H, H-3a), 1.90 (s, 3H, NHAc), 2.84 (d, J = 11.8 Hz, H-3b), 3.35 (d, J = 8.9 Hz, H-7), 3.42 (dd, J = 7.7, 13.7 Hz, H-9a), 3.60–3.68 (m, 4H, H-4, H-5, H-6, H-9b), 4.60 (A of AB, J = 11.5 Hz, 1H, CH₂Ar), 3.96 (m, 1H, H-8), 4.89 (B of AB, J = 11.5 Hz, 1H, CH₂Ar), 7.31–7.36 (m, 4H, CH_{ar}), 7.40 (dd, J = 1.5, 8.4 Hz, 1H, CH_{ar}), 7.67–7.72 (m, 6H, CH_{ar}). ¹³C NMR (CD₃OD) δ 21.7 (NHAc), 43.3 (C-3), 43.4 (C-9), 53.1 (C-5), 68.6 (CH₂Ar), 71.3 (C-7), 72.0 (C-4), 73.3 (C-6), 110.0 (B of AB, J = 12.5 Hz, 126.3, 126.4, 127.6, 127.7, 127.9, 128.6, 129.1 (16 C-Ar), 174.6, 175.3 (3C, CO). HRMS calcd for $C_{29}H_{30}ClN_2NaO_9 [M + Na]^+$ 631.1438; found 631.1435.

Sodium (2,3-Dichlorobenzyl 5-Acetamido-9-(4-chlorobenzamido)-3,5,9-trideoxy- β -glycero- α - β -galacto-2-nonulopyranosid)onate (13e). Compound **12e** (25.0 mg, 0.03 mmol) was treated with 10% aqueous NaOH (0.2 mL) in MeOH (1.0 mL). The crude product was purified by chromatography on RP-18 (5% gradient of MeOH in H₂O) to yield **13e** as a white solid (10.0 mg, 50%). $[\alpha]_D^{20}$ -0.19 (c 0.53, H₂O). ¹H NMR (500 MHz, CD₃OD) δ 1.69 (t, J = 11.8 Hz, 1H, H-3a), 1.93 (s, 3H, NHAc), 2.01 (dd, J = 9.1, 11.8 Hz, 1H, H-3b), 3.36 (dd, J = 1.7, 9.0 Hz, 1H, H-7), 3.45 (dd, J = 7.6, 13.6 Hz, 1H, H-9a), 3.59 (m, 1H, H-6), 3.65–3.70 (m, 3H, H-4, H-5, H-9b), 3.92 (m, 1H, H-8), 4.65, 4.89 (A, B of AB, J = 13.6 Hz, 2H, CH₂Ar), 7.18 (t, J = 7.9 Hz, 1H, CH_{ar}), 7.32 (dd, J = 1.5, 8.0 Hz, 1H, CH_{ar}), 7.39 (AA' of AA'BB', J = 8.5 Hz, 2H, CH_{ar}), 7.49 (dd, J = 1.1, 7.7 Hz, 1H, CH_{ar}), 7.74 (BB' of AA'BB', J = 8.5 Hz, 2H, CH_{ar}). ¹³C NMR (CD₃OD) δ 21.6 (NHAc), 41.5 (C-3), 43.4 (C-9), 53.1 (C-5), 63.5 (CH₂Ar), 68.6 (C-4), 70.2 (C-8), 71.5 (C-7), 73.4 (C-6), 102.5 (C-2), 113.3, 117.0, 118.4, 127.4, 127.5, 128.6, 128.9, 129.0, 139.6 (12 C-Ar), 163.8, 174.5 (3C, 3 CO). HRMS calcd for $C_{25}H_{27}Cl_2N_2O_9 [M + Na]^+$ 627.0682; found 627.0683.

Sodium (2,3-Difluorobenzyl 5-Acetamido-9-(4-chlorobenzamido)-3,5,9-trideoxy- β -glycero- α - β -galacto-2-nonulopyranosid)onate (13f). Compound **12f** (44.0 mg, 0.06 mmol) was treated with 10% aqueous NaOH (0.3 mL) in MeOH (1.5 mL). The crude product was purified by chromatography on RP-18 (5% gradient of MeOH in H₂O) to yield **13f** as a white solid (23.0 mg, 64%). $[\alpha]_D^{20}$ -0.18 (c 1.13, H₂O). ¹H NMR (500 MHz, CD₃OD) δ 1.56 (m, 1H, H-3a), 1.90 (s, 3H, NHAc), 2.84 (dd, J = 3.0, 12.2 Hz, 1H, H-3b), 3.37 (d, J = 9.0 Hz, 1H, H-7), 3.46 (dd, J = 7.7, 13.6 Hz, 1H, H-9a), 3.59 (m, 1H, H-6), 3.63–3.70 (m, 3H, H-4, H-5, H-9b), 3.96 (m, 1H, H-8), 4.60, 4.85 (A, B of AB, J = 12.2 Hz, 2H, CH₂Ar), 7.04 (m, 2H, CH_{ar}), 7.24 (t, J = 6.5 Hz, 1H, CH_{ar}), 7.38, 7.75 (AA', BB' of AA'BB', J = 8.5 Hz, 4H, CH_{ar}). ¹³C NMR (CD₃OD) δ 21.6 (NHAc), 41.5 (C-3), 43.5 (C-9), 53.1 (C-5), 59.2 (CH₂Ar), 68.6 (C-4), 70.3 (C-8), 71.4 (C-7), 73.4 (C-6), 101.0 (C-2), 115.9, 116.1 (J = 17.3 Hz), 124.2, 125.3, 128.6, 129.1, 133.5, 137.6 (12 C-Ar), 168.3, 173.0, 174.5 (3 CO). HRMS calcd for $C_{25}H_{27}ClF_2N_2O_9 [M + Na]^+$ 595.1273; found 595.1272.

Methyl (Methyl 5-tert-Butyloxycarbonylamino-4,7,8-tri-O-acetyl-9-azido-3,5,9-trideoxy-2-thio- β -glycero- α - β -galacto-2-nonulopyranosid)onate (14). Compound **10** (85.0 mg, 0.17 mmol) was dissolved in dry THF (0.7 mL) under argon. Boc₂O (74.0 mg, 0.34 mmol) was added to the reaction mixture, followed by DMAP (4.50 mg, 0.02 mmol). The reaction mixture was heated up to 60 °C for 5 h. After cooling to rt, MeOH (0.7 mL) and N₂H₄·H₂O (52 μ L, 1.1 mmol) were added and stirring was continued for 16 h. The reaction mixture was washed successively with 0.1 M HCl (1 \times 5 mL), 0.5 M CuSO₄ (1 \times 5 mL), saturated aqueous NaHCO₃ (2 \times 5 mL), and H₂O (1 \times 5 mL). The organic layer was dried over Na₂SO₄, filtered, and concentrated under

reduced pressure to give a yellow oil. The crude product was reacted with acetic anhydride (0.9 mL) in dry pyridine (1.7 mL). A catalytic amount of DMAP was added, and stirring was continued at rt. After 18 h, the reaction mixture was washed with CuSO₄ (0.5 M, 4 \times 5 mL), saturated aqueous NaHCO₃ (1 \times 5 mL), and H₂O (1 \times 5 mL). The organic layer was dried over Na₂SO₄, filtered, and the solvent was evaporated. The crude product was purified by chromatography on silica gel (EA:PE, gradient 1:1 to 2:1) to yield **14** (72 mg, 76%) as a white foam. $[\alpha]_D^{20}$ 0.31 (c 1.68, CH₂Cl₂). ¹H NMR (500 MHz, CDCl₃) δ 1.37 (s, 9H, *t*-Butyl), 1.95 (m, 1H, H-3a), 2.02 (s, 3H, SMe), 2.10, 2.14, 2.17 (3 s, 9H, 3 OAc), 2.73 (dd, J = 4.6, 12.7 Hz, 1H, H-3b), 3.25 (dd, J = 6.0, 13.5 Hz, 1H, H-9a), 3.61 (dd, J = 3.2, 13.5 Hz, 1H, H-9b), 3.73 (m, 1H, H-6), 3.80 (m, 4H, OMe, H-5), 4.25 (d, J = 10.4 Hz, 1H, NH), 4.78 (m, 1H, H-4), 5.29 (m, 1H, H-8), 5.41 (m, 1H, H-7). ¹³C NMR (CDCl₃) δ 12.1 (SMe), 20.8, 21.0, 21.3 (3 OAc), 27.9 (3C, C-(CH₃)₃), 38.0 (C-3), 50.4 (C-9), 50.6 (C-9), 52.9 (OMe), 67.6 (C-7), 68.1 (C-8), 70.0 (C-4), 73.7 (C-6), 80.2 (C-2), 83.0 (C(CH₃)₃), 155.2 (CONH), 168.2, 170.0, 170.6, 174.0 (4 CO). ESI-MS calcd for $C_{22}H_{34}N_4O_{11}S [M + Na]^+$ 585.19; found *m/z* 585.15.

Methyl (Methyl 5-Amino-4,7,8-tri-O-acetyl-9-azido-3,5,9-trideoxy-2-thio- β -glycero- α - β -galacto-2-nonulopyranosid)onate (15). Compound **14** (120 mg, 0.21 mmol) was dissolved in 4 M PhOH (in abs DCM; 7.5 mL) and 4 M TMSCl (in abs DCM; 1.5 mL). The reaction mixture was stirred at rt for 2 h. The reaction mixture was washed with saturated aqueous NaHCO₃ (2 \times 5 mL) and H₂O (1 \times 5 mL). The organic layer was dried over Na₂SO₄, filtered, and the solvent was evaporated. The crude product was purified by chromatography on silica gel (EA:PE, gradient 1:1 to 8:1) to yield **15** as a white foam (74 mg, 70%). ¹H NMR (500 MHz, CDCl₃) δ 2.01 (s, 3H, SMe), 2.04 (m, 1H, H-3a), 2.10, 2.11, 2.19 (3 s, 9H, 3 OAc), 2.71 (dd, J = 4.7, 12.8 Hz, 1H, H-3b), 3.38 (d, J = 10.5 Hz, 1H, H-6), 3.66 (dd, J = 3.3, 13.3 Hz, 1H, H-9a), 3.70 (dd, J = 2.8, 13.3 Hz, 1H, H-9b), 3.76 (dd, J = 1.3, 9.4 Hz, 1H, H-7), 3.78 (s, 3H, OMe), 3.98 (dt, J = 8.0, 10.5 Hz, 1H, H-5), 4.93 (dd, J = 6.9, 10.7 Hz, 1H, H-4), 5.26 (t, J = 3.9, 9.4 Hz, 1H, H-8), 5.94 (d, J = 7.8 Hz, 2H, NH₂). ¹³C NMR (CDCl₃) δ 12.0 (SMe), 21.1, 21.2, 23.2 (3 OAc), 37.7 (C-3), 51.2, 52.1, 52.9 (3C, C-5 C-9, OMe), 66.8, 69.3, 70.0 (3C, C-4, C-7, C-8), 75.3 (C-6), 82.2 (C-2), 167.9, 170.2, 172.4, 172.9 (4 CO). ESI-MS calcd for $C_{17}H_{26}N_4O_9S [M + Na]^+$ 485.14; found *m/z* 485.13.

Methyl (Methyl 5-Fluoroacetamido-4,7,8-tri-O-acetyl-9-azido-3,5,9-trideoxy-2-thio- β -glycero- α - β -galacto-2-nonulopyranosid)onate (16a). Compound **15** (74.0 mg, 0.16 mmol) was dissolved in dry DCM (1.8 mL) and cooled to 0 °C. Then, monofluoroacetic chloride was added dropwise (30.0 mg, 31.0 μ L, 0.32 mmol), followed by the addition of NEt₃ (324 mg, 0.45 mL, 3.2 mmol) and DMAP (9.8 mg, 0.08 mmol). Stirring was continued overnight, and the reaction mixture was allowed to come to rt. The brown solution was washed with saturated aqueous NaHCO₃ (3 \times 5 mL), saturated aqueous NaCl (1 \times 5 mL), and H₂O (1 \times 5 mL). The organic phase was dried over Na₂SO₄, filtered, and concentrated under reduced pressure. The crude product was purified by chromatography on silica gel (EA:PE, gradient 1:1 to 2:1) to yield **16a** (71 mg, 85%). $[\alpha]_D^{20}$ 0.34 (c 1.2, CH₂Cl₂). ¹H NMR (500 MHz, CDCl₃) δ 1.98 (m, 1H, H-3a), 2.03 (s, 3H, SMe), 2.12, 2.15, 2.21 (3 s, 9H, 3 OAc), 2.79 (dd, J = 4.7, 12.8 Hz, 1H, H-3b), 3.24 (dd, J = 4.8, 13.6 Hz, 1H, H-9a), 3.64 (dd, J = 2.8, 13.6 Hz, 1H, H-9b), 3.84 (s, 3H, OMe), 3.90 (dd, J = 1.9, 10.7 Hz, 1H, H-6), 4.14 (m, 1H, H-5), 4.71 (m, 2H, CH₂F), 4.92 (td, J = 4.7, 11.6 Hz, 1H, H-4), 5.32 (m, 2H, H-7, H-8), 6.09 (dd, J = 3.3, 10.3 Hz, 1H, NH). ¹³C NMR (CDCl₃) δ 12.2 (SMe), 20.9 (3C, OAc), 37.8 (C-3), 48.6 (C-5), 50.6 (C-9), 53.1 (OMe), 67.8 (C-7), 69.4, 69.6 (2C, C-4, C-8), 74.1 (C-6), 80.8 (J = 186.1 Hz, CH₂F), 83.1 (C-2), 168.2, 170.2, 170.6 (5C, CO). ESI-MS calcd for $C_{19}H_{27}FN_4O_{10}S [M + Na]^+$ 545.14; found *m/z* 545.15.

Methyl (Methyl 5-Chloroacetamido-4,7,8-tri-O-acetyl-9-azido-3,5,9-trideoxy-2-thio- β -glycero- α - β -galacto-2-nonulopyranosid)onate (16b). Compound **15** (55.0 mg, 0.12 mmol) was dissolved in dioxane/water (0.5 mL/0.1 mL), treated with triethylamine

(48.6 mg, 34 μ L, 0.48 mmol), and cooled to 0 °C. Then, chloroacetic anhydride (41.0 mg, 0.48 mmol) was added, and stirring was continued at rt for 3 h. The reaction mixture was diluted with CHCl_3 (10.0 mL) and washed successively with saturated aqueous NaHCO_3 (3 \times 5 mL) and H_2O (1 \times 5 mL). The organic layer was dried over Na_2SO_4 , filtered, and concentrated under reduced pressure. The crude product was purified by chromatography on silica gel (gradient, PE:EA; 1:1 to 1:2) to yield **16b** as a white foam (42 mg, 66%). $[\alpha]_{\text{D}}^{20}$ 0.33 (*c* 0.95, CH_2Cl_2). ^1H NMR (500 MHz, CDCl_3) δ 1.91 (t, *J* = 12.2 Hz, 1H, H-3a), 1.96 (s, 3H, SMe), 2.06, 2.08, 2.13 (3 s, 9H, 3 OAc), 2.72 (dd, *J* = 4.7 Hz, 12.8 Hz, 1H, H-3b), 3.18 (m, 1H, H-9a), 3.59 (m, 1H, H-9b), 3.78 (s, 3H, OMe), 3.85 (A of AB, *J* = 15.0 Hz, 1H, CH_2Cl), 3.86 (m, 1H, H-6), 3.93 (B of AB, *J* = 15.0 Hz, 1H, CH_2Cl), 4.03 (m, 1H, H-5), 4.90 (dt, *J* = 4.7 Hz, 11.5 Hz, 1H, H-4), 5.24 (m, 2H, H-7, H-8), 6.28 (d, *J* = 10.1 Hz, 1H, NH). ^{13}C NMR (CDCl_3) δ 12.1 (SMe), 20.8, 20.9, 21.1 (3 OAc), 37.9 (C-3), 42.5 (CH_2Cl), 49.7 (C-9), 50.6 (C-5), 53.1 (OMe), 67.1, 67.9, 69.2 (3C, C-4, C-7, C-8), 74.2 (C-6), 83.1 (C-2), 166.6, 167.8, 170.3, 170.6 (5C, CO). ESI-MS calcd for $\text{C}_{19}\text{H}_{27}\text{Cl}_2\text{N}_4\text{O}_{10}\text{S}$ [*M* + *Na*] $^+$ 561.10; found *m/z* 561.37.

Methyl (Methyl 5-*o*-Nitrotoluenesulfonamido-4,7,8-tri-*o*-acetyl-9-azido-3,5,9-trideoxy-2-thio-*D*-glycero- α -*D*-galacto-2-nonulopyranosid)onate (16c). Compound **15** (73.0 mg, 0.16 mmol) was dissolved in dry DCM (3.0 mL), and it was cooled to 0 °C. Nonylchloride (105 mg, 0.47 mmol), NEt_3 (34.0 μ L, 48.0 mg, 0.47 mmol), and DMAP (10.0 mg, 0.08 mmol) were added successively. The reaction mixture was stirred at rt overnight. Then it was washed with saturated aqueous NaHCO_3 (2 \times 5 mL) and H_2O (1 \times 5 mL). The organic phase was dried over Na_2SO_4 , filtered, and concentrated under reduced pressure. The crude product was purified by chromatography on silica gel (EA:PE, gradient 1:1 to 2:1) to yield **16c** (81 mg, 78%). ^1H NMR (500 MHz, CDCl_3) δ 1.85 (m, 1H, H-3a), 2.02 (s, 3H, SMe), 2.10, 2.13, 2.21 (3 s, 9H, 3 OAc), 2.80 (m, 1H, H-3b), 3.32 (dd, *J* = 6.2, 13.4 Hz, 1H, H-9a), 3.57 (dd, *J* = 3.2, 13.4 Hz, 1H, H-9b), 3.80 (m, 1H, H-5), 3.82 (s, 3H, OMe), 3.91 (d, *J* = 10.5 Hz, 1H, H-6), 4.97 (td, *J* = 4.7, 11.4 Hz, 1H, H-4), 5.30 (m, 2H, H-7, H-8), 5.75 (d, *J* = 9.4 Hz, 1H, NH), 7.70 (m, 2H, CH_{ar}), 7.90 (d, *J* = 7.9, 1H, CH_{ar}), 8.10 (d, *J* = 6.5, 1H, CH_{ar}). ^{13}C NMR (CDCl_3) δ 12.1 (SMe), 20.5, 21.1, 21.1 (3 OAc), 38.1 (C-3), 50.8 (C-9), 53.2, 53.5 (2C, C-5, OMe), 68.8 (C-7), 69.7 (C-4), 70.4 (C-8), 74.7 (C-6), 82.8 (C-2), 125.5, 130.4, 133.5, 135.5, 147.5 (6C, C-Ar), 167.8, 170.4 (4C, CO). ESI-MS calcd for $\text{C}_{23}\text{H}_{29}\text{N}_5\text{O}_{13}\text{S}_2$ [*M* - *H*] $^-$ 646.12; found *m/z* 646.56.

Methyl (Methyl 5-Methylsulfonamido-4,7,8-tri-*o*-acetyl-9-azido-3,5,9-trideoxy-2-thio-*D*-glycero- α -*D*-galacto-2-nonulopyranosid)onate (16d). Compound **15** (50.0 mg, 0.11 mmol) was dissolved in dry DCM (2.0 mL) under argon atmosphere and subsequently cooled to 0 °C. Methanesulfonylchloride (25.0 μ L, 37.0 mg, 0.32 mmol), NEt_3 (45.0 μ L, 33.0 mg, 0.32 mmol), and a catalytic amount of DMAP were added successively. The reaction mixture was stirred at 0 °C overnight. Then it was washed with saturated aqueous NaHCO_3 (2 \times 5 mL) and H_2O (1 \times 5 mL). The organic phase was dried over Na_2SO_4 , filtered, and concentrated under reduced pressure. The crude product was purified by chromatography on silica gel (EA:PE, gradient 1:1 to 2:1) to yield **16d** (30 mg, 66%). ^1H NMR (500 MHz, CDCl_3) δ 1.98 (t, *J* = 12.3 Hz, 1H, H-3a), 2.03 (s, 3H, SMe), 2.13, 2.17 (3 s, 9H, 3 OAc), 2.68 (dd, *J* = 4.7, 12.7 Hz, 1H, H-3b), 3.14 (s, 3H, CH_3), 3.29 (dd, *J* = 6.1, 13.4 Hz, 1H, H-9a), 3.66 (m, 2H, H-5, H-9b), 3.77 (s, 3H, OMe), 3.88 (dd, *J* = 1.6, 10.6 Hz, 1H, H-6), 4.55 (d, *J* = 9.8 Hz, 1H, NH), 5.16 (td, *J* = 4.7, 11.5 Hz, 1H, H-4), 5.26 (m, 1H, H-8), 5.48 (dd, *J* = 1.6, 7.2 Hz, 1H, H-7). ^{13}C NMR (CDCl_3) δ 14.3 (SMe), 20.9, 21.1, 21.4 (3 OAc), 31.7 (CH_3), 38.2 (C-3), 50.7 (C-9), 52.5 (C-5), 53.0 (OMe), 68.3, 69.6 (2C, C-7, C-8), 70.4 (C-4), 74.5 (C-6), 82.8 (C-2), 167.8, 170.3, 171.7, 172.2 (4 CO). ESI-MS calcd for $\text{C}_{18}\text{H}_{28}\text{N}_4\text{O}_{11}\text{S}_2$ [*M* + *Na*] $^+$ 563.12; found *m/z* 563.18.

Methyl ((2,3-Difluorobenzyl) 5-Fluoroacetamido-4,7,8-tri-*o*-acetyl-9-azido-3,5,9-trideoxy-*D*-glycero- α -*D*-galacto-2-nonulopyranosid)onate (17a). Compound **16a** (55.0 mg, 0.16 mmol) was

dissolved in dry acetonitrile (2 mL). Powdered MS 3 Å (50 mg) and 2,3-difluorobenzyl alcohol (35.0 μ L, 42.0 mg, 0.29 mmol) were added. The reaction mixture was stirred at rt for 1.5 h. Then the suspension was cooled to -40 °C and was subsequently treated with *N*-iodosuccinimide (35.0 mg, 0.16 mmol) and triflic acid (8.00 μ L, 13.0 mg, 0.09 mmol). After 30 min, the reaction mixture was warmed to -30 °C and stirring was continued for 20 h. After warming to rt, the mixture was filtered through a pad of celite and washed with 20% $\text{Na}_2\text{S}_2\text{O}_3$ (1 \times 2 mL), saturated aqueous NaHCO_3 (3 \times 5 mL), and H_2O (1 \times 5 mL). The organic phase was dried over Na_2SO_4 , filtered, and concentrated under reduced pressure. The crude product was purified by chromatography on silica gel (1% gradient *i*PrOH in petrol ether/DCM 2:1) to yield **16a** (43 mg, 66%) as a colorless oil. $[\alpha]_{\text{D}}^{20}$ -0.04 (*c* 0.73, CH_2Cl_2). ^1H NMR (500 MHz, CDCl_3) δ 2.03 (s, 3H, OAc), 2.04 (m, 1H, H-3a), 2.16, 2.21 (2 s, 6H, 2 OAc), 2.69 (dd, *J* = 4.7, 12.9 Hz, 1H, H-3b), 3.26 (dd, *J* = 5.3, 13.5 Hz, 1H, H-9a), 3.58 (dd, *J* = 2.8, 13.5 Hz, 1H, H-9b), 3.79 (s, 3H, OMe), 4.21 (m, 2H, H-5, H-6), 4.53 (A of AB, *J* = 12.0 Hz, 1H, CH_2Ar), 4.63 (m, 2H, CH_2F), 4.83 (B of AB, *J* = 12.3 Hz, 1H, CH_2Ar), 4.95 (ddd, *J* = 4.7, 10.0, 12.1 Hz, 1H, H-4), 5.35 (m, 2H, H-7, H-8), 6.18 (dd, *J* = 3.3, 9.0 Hz, 1H, NHFAc), 7.11 (m, 3H, CH_{ar}). ^{13}C NMR (CDCl_3) δ 20.9 (3C, OAc), 37.9 (C-3), 48.6 (C-5), 50.9 (C-9), 53.0 (OMe), 60.5 (CH_2Ar), 67.8 (C-7), 68.7 (C-8), 69.3 (C-4), 72.6 (C-6), 80.1 (*J* = 186.1 Hz, CH_2F), 98.7 (C-2), 116.9, 117.1, 125.1, 126.6 (6C, C-Ar), 168.0, 170.2, 170.7 (5C, CO). ESI-MS calcd for $\text{C}_{25}\text{H}_{29}\text{F}_3\text{N}_5\text{O}_{11}$ [*M* + *Na*] $^+$ 641.17; found *m/z* 641.14.

Methyl ((2,3-Difluorobenzyl) 5-Chloroacetamido-4,7,8-tri-*o*-acetyl-9-azido-3,5,9-trideoxy-*D*-glycero- α -*D*-galacto-2-nonulopyranosid)onate (17b). Compound **16b** (63.0 mg, 0.12 mmol) was reacted with 2,3-difluorobenzyl alcohol (41.0 μ L, 0.36 mmol), *N*-iodosuccinimide (42.0 mg, 0.19 mmol), and triflic acid (8.0 μ L, 14.4 mg, 0.1 mmol). The crude product was purified by chromatography on silica gel (0.5% gradient *i*PrOH in PE:DCM, 8:4) to yield **17b** (50 mg, 68%) as a colorless oil. $[\alpha]_{\text{D}}^{20}$ -0.01, (*c* 1.05, CH_2Cl_2). ^1H NMR (500 MHz, CDCl_3) δ 2.02 (m, 1H, H-3a), 2.03, 2.16, 2.21 (3 s, 9H, 3 OAc), 2.70 (dd, *J* = 4.6, 12.9 Hz, 1H, H-3b), 3.28 (dd, *J* = 5.8, 13.5 Hz, 1H, H-9a), 3.59 (dd, *J* = 3.0, 13.5 Hz, 1H, H-9b), 3.81 (s, 3H, OMe), 3.93, 4.01 (A, B of AB, *J* = 15.0 Hz, 2H, CH_2Cl), 4.11 (m, 1H, H-5), 4.24 (dd, *J* = 2.1, 10.7 Hz, 1H, H-6), 4.54, 4.83 (A, B of AB, *J* = 12.0 Hz, 2H, CH_2Ar), 4.99 (m, 1H, H-4), 5.32 (dd, *J* = 2.1, 7.8 Hz, 1H, H-7), 5.36 (m, 1H, H-8), 6.41 (d, *J* = 10.1 Hz, 1H, NH), 7.06-7.17 (m, 3H, CH_{ar}). ^{13}C NMR (CDCl_3) δ 20.8, 20.9, 21.1 (3 OAc), 37.9 (C-3), 42.4 (CH_2Cl), 49.7 (C-5), 50.9 (C-9), 60.5 (CH_2Ar), 67.9, 68.1, 68.4 (3C, C-4, C-7, C-8), 72.6 (C-6), 98.7 (C-2), 117.0, 123.9, 125.1, 126.5, 149.5, 151.4 (6 C-Ar), 166.7, 168.0, 170.2, 170.3, 170.7 (5 CO). ESI-MS calcd for $\text{C}_{25}\text{H}_{29}\text{Cl}_2\text{FN}_5\text{O}_{11}$ [*M* + *Na*] $^+$ 657.14; found *m/z* 657.29.

Methyl ((2,3-Difluorobenzyl) 5-(*o*-Nitrotoluenesulfonamido)-4,7,8-tri-*o*-acetyl-9-azido-3,5,9-trideoxy-*D*-glycero- α -*D*-galacto-2-nonulopyranosid)onate (17c). Compound **16c** (62.0 mg, 0.10 mmol) was reacted with 2,3-difluorobenzyl alcohol (30.0 μ L, 38.0 mg, 0.29 mmol), *N*-iodosuccinimide (32.0 mg, 0.14 mmol), and triflic acid (7.00 μ L, 12.0 mg, 0.08 mmol). The crude product was purified by chromatography on silica gel (toluene/EA, gradient 1:1 to 2:1) to yield **17c** (44 mg, 61%). ^1H NMR (500 MHz, CDCl_3) δ 1.84 (t, *J* = 12.4 Hz, 1H, H-3a), 2.08, 2.17, 2.28 (3 s, 9H, 3 OAc), 2.64 (dd, *J* = 4.6, 12.8 Hz, 1H, H-3b), 3.29 (m, 1H, H-9a), 3.45 (m, 1H, H-9b), 3.73 (s, 3H, OMe), 3.79 (m, 2H, H-5, H-7), 4.12 (d, *J* = 8.8 Hz, 1H, H-6), 4.46, 4.77 (A, B of AB, *J* = 12.0 Hz, 2H, CH_2Ar), 4.91 (td, *J* = 4.6, 11.5 Hz, 1H, H-4), 5.25 (d, *J* = 7.8 Hz, 1H, H-8), 5.60 (d, *J* = 9.4 Hz, 1H, NH), 7.09 (m, 3H, CH_{ar}), 7.69 (m, 2H, CH_{ar}), 7.85 (d, *J* = 7.9 Hz, 1H, CH_{ar}), 8.07 (d, *J* = 7.8 Hz, 1H, CH_{ar}). ^{13}C NMR (CDCl_3) δ 21.1 (3C, OAc), 38.1 (C-3), 51.1 (C-5), 53.1 (C-9), 53.6 (OMe), 60.5 (CH_2Ar), 68.7, 68.8 (2C, C-4, C-7), 69.8 (C-8), 73.2 (C-6), 125.5, 130.4, 133.5, 147.6 (12C, C-Ar), 168.0, 170.1, 170.3, 170.5 (4 CO). ESI-MS calcd for $\text{C}_{29}\text{H}_{31}\text{F}_2\text{N}_5\text{O}_{14}\text{S}$ [*M* + *Na*] $^+$ 766.16; found *m/z* 766.14.

Methyl ((2,3-Difluorobenzyl) 5-Methylsulfonamido-4,7,8-tri-O-acetyl-9-azido-3,5,9-trideoxy-D-glycero- α -D-galacto-2-nonulopyranosid)onate (17d). Compound 16d (56.0 mg, 0.10 mmol) was reacted with 2,3-difluorobenzyl alcohol (33.0 μ L, 42.0 mg, 0.29 mmol), *N*-iodosuccinimide (35.0 mg, 0.16 mmol), and triflic acid (8.00 μ L, 13.0 mg, 0.09 mmol). The crude product was purified by chromatography on silica gel (1% gradient *i*PrOH in petrol ether/DCM 2:1) to yield 17d (37 mg, 56%). ¹H NMR (500 MHz, CDCl₃) δ 1.95 (t, *J* = 12.5, 1H, H-3a), 2.13, 2.18 (2 s, 9H, 3 OAc), 2.61 (dd, *J* = 4.6, 12.7 Hz, 1H, H-3b), 3.02 (s, 3H, CH₃), 3.31 (dd, *J* = 6.3, 13.5 Hz, 1H, H-9a), 3.60 (dd, *J* = 3.3, 13.5 Hz, 1H, H-9b), 3.71 (m, 4H, H-5, OMe), 4.12 (dd, *J* = 1.7, 10.7 Hz, 1H, H-6), 4.54, 4.81 (A, B of AB, *J* = 11.8 Hz, 2H, CH₂Ar), 5.09 (m, 1H, H-4), 5.31 (m, 1H, H-8), 5.49 (dd, *J* = 1.7, 7.5 Hz, 1H, H-7), 7.11 (m, 3H, CH₂Ar). ¹³C NMR (CDCl₃) δ 20.9, 21.1, 21.4 (3 OAc), 38.1 (C-3), 42.3 (CH₃), 50.8 (C-9), 52.6, 53.0 (2C, OMe, C-5), 60.4 (CH₂Ar), 68.1 (C-4), 68.8 (C-7), 70.0 (C-8), 72.8 (C-6), 98.5 (C-2), 116.9, 117.0, 124.0, 125.1 (6C, C-Ar), 167.7, 170.1, 170.7, 172.1 (4 CO). ESI-MS calcd for C₂₄H₃₀F₂N₄O₁₂S [M + Na]⁺ 659.15; found *m/z* 659.24.

Methyl ((2,3-Difluorobenzyl) 5-Fluoroacetamido-4,7,8-tri-O-acetyl-9-(4-chlorobenzamido)-3,5,9-trideoxy-D-glycero- α -D-galacto-2-nonulopyranosid)onate (18a). Compound 17a (55.0 mg, 0.09 mmol) was dissolved in dry DCM (2 mL). *p*-Chlorobenzoyl chloride (45.0 μ L, 62.0 mg, 0.36 mmol) and triphenylphosphine (47.0 mg, 0.18 mmol) were added. The reaction mixture was stirred at rt overnight. Afterward, the reaction mixture was washed with saturated aqueous NaHCO₃ (3 \times 5 mL) and H₂O (1 \times 5 mL). The organic phase was dried over Na₂SO₄, filtered, and concentrated under reduced pressure. The crude product was purified by chromatography on silica gel (EA:PE, gradient 1:1 to 2:1) to yield 18a (31 mg, 48%) as a white foam. ¹H NMR (500 MHz, CDCl₃) δ 1.97 (m, 1H, H-3a), 1.97, 2.09, 2.18 (3 s, 9H, 3 OAc), 2.64 (dd, *J* = 4.6, 12.8 Hz, 1H, H-3b), 2.94 (dd, *J* = 3.9, 15.0 Hz, 1H, H-9a), 3.69 (s, 3H, OMe), 4.09 (m, 1H, H-6), 4.22 (m, 2H, H-5, H-9b), 4.46 (A of AB, *J* = 12.0 Hz, 1H, CH₂Ar), 4.64 (m, 2H, CH₂F), 4.78 (B of AB, *J* = 12.0 Hz, 1H, CH₂Ar), 4.86 (m, 1H, H-4), 5.11 (dd, *J* = 2.0, 9.8 Hz, 1H, H-7), 5.27 (m, 1H, H-8), 6.12 (dd, *J* = 3.3, 10.0 Hz, 1H, NHAc), 6.89 (dd, *J* = 4.3, 7.9 Hz, 1H, NH), 7.03 (m, 3H, CH₂Ar), 7.34, 7.67 (AA', BB' of AA'BB', *J* = 8.5 Hz, 4H, CH₂Ar). ¹³C NMR (CDCl₃) δ 20.8, 21.1 (3C, OAc), 37.9 (C-3), 38.7 (C-9), 48.7 (C-5), 52.9 (OMe), 60.5 (CH₂Ar), 67.8 (C-7), 68.2 (C-8), 68.7 (C-4), 72.0 (C-6), 80.0 (*J* = 186.0 Hz, CH₂F), 98.6 (C-2), 117.1, 124.0, 125.3, 126.6, 128.4, 128.8, 131.5, 132.6, 137.8 (12C, C-Ar), 166.4, 167.8, 168.3, 170.5, 170.7, 172.3 (6 CO). ESI-MS calcd for C₃₂H₃₄ClF₃N₂O₁₂ [M + Na]⁺ 753.18; found *m/z* 753.19.

Methyl ((2,3-Difluorobenzyl) 5-Chloroacetamido-4,7,8-tri-O-acetyl-9-(4-chlorobenzamido)-3,5,9-trideoxy-D-glycero- α -D-galacto-2-nonulopyranosid)onate (18b). Compound 17b (52.2 mg, 0.08 mmol) was reacted with *p*-chlorobenzoyl chloride (23.0 μ L, 31.0 mg, 0.18 mmol) and triphenylphosphine (47.0 mg, 0.18 mmol). The crude product was purified by chromatography on silica gel (0.5% gradient of MeOH in DCM) to yield in 18b (25.0 mg, 48%). [α]_D²⁰ 0.04 (*c* 1.06, CH₂Cl₂). ¹H NMR (500 MHz, CDCl₃) δ 2.00 (m, 1H, H-3a), 2.03, 2.16, 2.25 (3 s, 9H, 3 OAc), 2.71 (m, 1H, H-3b), 3.01 (m, 1H, H-9a), 3.77 (s, 3H, OMe), 3.97 (m, 2H, CH₂Cl), 4.11 (m, 1H, H-6), 4.20 (m, 1H, H-5), 4.29 (m, 1H, H-9b), 4.54, 4.85 (A, B of AB, *J* = 11.9 Hz, 2H, CH₂Ar), 4.95 (m, 1H, H-4), 5.18 (m, 1H, H-7), 5.31 (m, 1H, H-8), 6.39 (m, 1H, NHAc), 6.97 (m, 1H, NH), 7.06–7.15 (m, 3H, CH₂Ar), 7.40 (m, 2H, CH₂Ar), 7.74 (m, 2H, CH₂Ar). ¹³C NMR (CDCl₃) δ 20.8, 21.2 (3C, OAc), 38.0 (C-3), 38.6 (C-9), 42.4 (CH₂Cl), 49.8 (C-5), 52.9 (OMe), 60.4 (CH₂Ar), 67.8, 68.3, 68.5 (3C, C-4, C-7, C-8), 72.1 (C-6), 98.6 (C-2), 117.0 (*J* = 17.5 Hz), 124.0, 125.3, 126.5, 128.4, 128.9, 132.7, 137.8 (12C-Ar), 166.4, 166.7, 167.9, 170.5, 170.7, 172.3 (6 CO). ESI-MS calcd for C₃₂H₃₄Cl₂F₂N₂O₁₂ [M + Na]⁺ 769.14; found *m/z* 769.34.

Methyl ((2,3-Difluorobenzyl) 5-(*o*-Nitrotoluenesulfonamido)-4,7,8-tri-O-acetyl-9-(4-chlorobenzamido)-3,5,9-trideoxy-D-glycero- α -D-galacto-2-nonulopyranosid)onate (18c). Compound

17c (44.0 mg, 0.06 mmol) was dissolved in dry DCE (2 mL). *p*-Chlorobenzoyl chloride (30.0 μ L, 40.0 mg, 0.23 mmol) and triphenylphosphine (31.0 mg, 0.12 mmol) were added. The reaction mixture was stirred at rt overnight. The crude product was purified by chromatography on silica gel (EA:PE, gradient 1:1 to 2:1) to yield 18c (29 mg, 58%) as a white foam. ¹H NMR (500 MHz, CDCl₃) δ 1.90 (m, 1H, H-3a), 2.04, 2.14, 2.32 (3 s, 9H, 3 OAc), 2.69 (dd, *J* = 4.5, 12.7 Hz, 1H, H-3b), 2.92 (d, *J* = 15.2 Hz, 1H, H-9a), 3.75 (s, 3H, OMe), 3.91 (m, 1H, H-5), 4.12 (m, 1H, H-6), 4.38 (m, 1H, H-9b), 4.52 (A of AB, *J* = 11.9 Hz, 1H, CH₂Ar), 4.84 (m, 2H, H-4, CH₂Ar), 5.31 (m, 2H, H-7, H-8), 5.64 (d, *J* = 9.4 Hz, 1H, NH), 7.13 (m, 4H, CH₂Ar), 7.21 (m, 1H, NH), 7.40 (m, 3H, CH₂Ar), 7.72 (m, 4H, CH₂Ar). ¹³C NMR (CDCl₃) δ 20.3, 21.2, 21.3 (3 OAc), 38.2, 38.3 (2C, C-3, C-9), 53.0 (OMe), 53.7 (C-5), 60.6 (CH₂Ar), 68.2, 68.4 (2C, C-7, C-8), 69.0 (C-4), 72.6 (C-6), 98.2 (C-2), 117.0, 123.9, 125.6, 128.8, 130.3, 131.5, 132.1, 132.8, 133.3 (18C, C-Ar), 166.6, 167.7, 169.9, 170.4, 172.4 (5 CO). ESI-MS calcd for C₃₆H₃₆ClF₂N₃O₁₅S [M + Na]⁺ 878.15; found *m/z* 878.28.

Methyl ((2,3-Difluorobenzyl) 5-Methylsulfonamido-4,7,8-tri-O-acetyl-9-(4-chlorobenzamido)-3,5,9-trideoxy-D-glycero- α -D-galacto-2-nonulopyranosid)onate (18d). Compound 17d (35.0 mg, 0.06 mmol) was dissolved in dry DCM (2 mL). *p*-Chlorobenzoyl chloride (28.0 μ L, 38.0 mg, 0.22 mmol) and triphenylphosphine (29.0 mg, 0.11 mmol) were added. The reaction mixture was stirred at rt overnight. The crude product was purified by chromatography on silica gel (EA:PE, gradient 1:1 to 2:1) to yield 18d (21 mg, 52%) as a white foam. ¹H NMR (500 MHz, CDCl₃) δ 1.98 (t, *J* = 13.6 Hz, 1H, H-3a), 2.05, 2.10, 2.13 (3 s, 9H, 3 OAc), 2.67 (dd, *J* = 4.6, 12.7 Hz, 1H, H-3b), 2.99 (s, 3H, CH₃), 3.05 (m, 1H, H-9a), 3.70 (s, 3H, OMe), 3.77 (m, 1H, H-5), 4.09 (d, *J* = 1.5 Hz, 1H, H-6), 4.30 (ddd, *J* = 3.0, 8.2, 15.1 Hz, 1H, H-9b), 4.54 (A of AB, *J* = 12.1 Hz, 1H, CH₂Ar), 4.59 (d, *J* = 9.6 Hz, 1H, NH), 4.83 (B of AB, *J* = 11.9 Hz, 1H, CH₂Ar), 4.99 (ddd, *J* = 4.6, 10.4, 12.2 Hz, 1H, H-4), 5.30 (m, 1H, H-8), 5.37 (dd, *J* = 1.7, 9.6 Hz, 1H, H-7), 7.13 (m, 4H, CH₂Ar, NH), 7.40, 7.75 (AA', BB' of AA'BB', *J* = 8.5 Hz, 4H, CH₂Ar). ¹³C NMR (CDCl₃) δ 21.2, 21.2, 21.3 (3 OAc), 29.7 (C-3), 38.2, 38.8 (2C, C-9, CH₃), 42.3 (C-5), 52.8 (OMe), 60.5 (CH₂Ar), 68.1, 68.5, 69.1 (3C, C-4, C-7, C-8), 72.4 (C-6), 98.4 (C-2), 116.9, 117.1, 125.3, 128.4, 128.9, 132.1, 132.7, 137.8 (12C, C-Ar), 166.4, 167.7, 170.5, 171.6, 172.6 (5 CO). ESI-MS calcd for C₃₁H₃₅ClF₂N₂O₁₃S [M + Na]⁺ 771.15; found *m/z* 771.29.

Sodium ((2,3-Difluorobenzyl) 5-Fluoroacetamido-9-(4-chlorobenzamido)-3,5,9-trideoxy-D-glycero- α -D-galacto-2-nonulopyranosid)onate (19a). Compound 18a (28.0 mg, 0.04 mmol) was dissolved in THF/water (2.0 mL/0.5 mL) and was reacted with LiOH (9.00 mg, 0.38 mmol). The reaction mixture was stirred at rt for 4 h. 7% HCl (aq) was added to adjust the pH to 7. The crude product was purified by reversed-phase chromatography (RP-18, 10% gradient MeOH in H₂O) followed by ion exchange chromatography (Dowex-50) and P2 size exclusion chromatography to yield 19a (7.0 mg, 30%) as a white foam. [α]_D²⁰ -0.73 (*c* 0.08, H₂O). ¹H NMR (500 MHz, D₂O) δ 1.59 (t, *J* = 12.2, 1H, H-3a), 2.65 (dd, *J* = 4.7, 12.4, 1H, H-3b), 3.31 (dd, *J* = 7.7, 14.0 Hz, 1H, H-9a), 3.41 (dd, *J* = 1.8, 8.8 Hz, 1H, H-5), 3.64 (m, 3H, H-4, H-8, H-9b), 3.77 (dd, *J* = 1.9, 10.5 Hz, 1H, H-6), 3.84 (m, 1H, H-7), 4.52 (A of AB, *J* = 11.7 Hz, 1H, CH₂Ar), 4.70 (m, 2H, CH₂Ar, CH₂F), 4.81 (d, *J* = 5.1 Hz, 1H, CH₂F), 7.02 (m, 3H, CH₂Ar), 7.39, 7.62 (AA', BB' of AA'BB', *J* = 8.7 Hz, 4H, CH₂Ar). ¹³C NMR (CDCl₃) δ 40.4, 42.6 (2C, C-3, C-9), 57.2 (C-5), 60.6 (CH₂Ar), 68.0 (C-4), 69.7 (C-7), 70.3 (C-8), 72.3 (C-6), 87.0 (CH₂F), 101.3 (C-2), 117.2, 125.8, 128.6, 128.8, 132.1, 137.5, 141.7 (12C, C-Ar), 173.1, 175.3, 189.7 (3 CO). HRMS calcd for C₂₅H₂₆ClF₃N₂O₉ [M - H]⁻ 589.1206; found 589.1191.

Sodium ((2,3-Difluorobenzyl) 5-Chloroacetamido-9-(4-chlorobenzamido)-3,5,9-trideoxy-D-glycero- α -D-galacto-2-nonulopyranosid)onate (19b). Compound 18b (21.0 mg, 0.03 mmol) was treated with LiOH (6.7 mg, 0.3 mmol) in THF/water (2.0 mL/0.5 mL). The crude product was purified by chromatography on silica gel

(0.1% gradient of H₂O in DCM/MeOH; 2:1) followed by ion exchange chromatography (Dowex 50) and P2 size exclusion chromatography to yield **19b** as a white solid (10 mg, 60%). ¹H NMR (500 MHz, MeOD) δ 1.58 (dd, *J* = 10.7, 12.1 Hz, 1H, H-3a), 2.82 (m, 1H, H-3b), 3.35 (m, 1H, H-7), 3.46 (m, 1H, H-9a), 3.68 (m, 4H, H-4, H-5, H-6, H-9b), 3.93 (m, 2H, CH₂Cl), 4.57, 4.84 (A, B of AB, *J* = 12.1 Hz, 2H, CH₂Ar), 7.01 (m, 3H, CH_{ar}), 7.35, 7.72 (AA', BB' of AA'/BB', *J* = 8.5 Hz, 4H, CH_{ar}). ¹³C NMR (MeOD) δ 43.0 (C-3), 44.8 (C-9), 45.0 (CH₂Cl), 54.0 (C-5), 63.1 (CH₂Ar), 70.5, 72.2, 72.9 (3C, C-4, C-7, C-8), 74.9 (C-6), 103.8 (C-2), 119.7, 126.9, 128.4, 128.9, 131.2, 131.3, 140.1 (10 C-Ar), 170.0, 170.5, 173.11 (3 CO). HRMS calcd for C₂₅H₂₅ClF₂N₂-NaO₉ [M + Na]⁺ 651.0701; found *m/z* 651.0700.

Sodium ((2,3-Difluorobenzyl) 5-(*o*-Nitrotoluenesulfonamido)-9-(4-chlorobenzamido)-3,5,9-trideoxy- α -D-galacto-2-nonulopyranosid)onate (19c). Compound **18c** (29.0 mg, 0.03 mmol) was dissolved in THF/H₂O (2 mL/0.5 mL) and was reacted with LiOH (8.00 mg, 0.33 mmol). The crude product was purified on RP-18 (10% gradient MeOH in water) followed by ion exchange chromatography (Dowex-50) and P2 size exclusion chromatography to yield **19c** (10 mg, 40%). [α]_D²⁰ -0.35 (c 0.10, H₂O). ¹H NMR (500 MHz, D₂O) δ 1.45 (t, *J* = 12.2 Hz, 1H, H-3a), 2.52 (dd, *J* = 4.5, 12.3 Hz, 1H, H-3b), 3.16 (t, *J* = 9.8 Hz, 1H, H-5), 3.43 (m, 2H, H-4, H-9a), 3.60 (dd, *J* = 2.9, 14.2 Hz, 1H, H-9b), 3.67 (m, 2H, H-6, H-8), 3.74 (dd, *J* = 1.1, 8.9 Hz, 1H, H-7), 4.50 (A of AB, *J* = 11.7 Hz, 1H, CH₂Ar), 4.65 (m, 1H, CH₂Ar), 7.04 (m, 3H, CH_{ar}), 7.42 (AA' of AA'/BB', *J* = 8.5 Hz, 2H, CH_{ar}), 7.60 (m, 4H, CH_{ar}), 7.98 (BB' of AA'/BB', *J* = 7.6 Hz, 2H, CH_{ar}). ¹³C NMR (D₂O) δ 40.4 (C-3), 42.4 (C-9), 56.5 (C-5), 60.5 (CH₂Ar), 69.4 (C-7), 69.5 (C-4), 70.3 (C-8), 73.8 (C-6), 101.2 (C-2), 117.1, 124.2, 125.8, 128.7, 130.2, 132.1, 132.5, 137.5, 146.8 (18C, C-Ar), 170.0, 173.3 (2 CO). HRMS calcd for C₂₉H₂₇ClF₂N₃NaO₁₂S [M + Na]⁺ 760.0767; found *m/z* 760.0775.

Sodium ((2,3-Difluorobenzyl) 5-Methylsulfonamido-9-(4-chlorobenzamido)-3,5,9-trideoxy- α -D-galacto-2-nonulopyranosid)onate (19d). Compound **18d** (21.0 mg, 0.03 mmol) was dissolved in THF/H₂O (2 mL/0.5 mL) and was reacted with LiOH (7.00 mg, 0.28 mmol). The crude product was purified on RP-18 (10% gradient MeOH in water) followed by ion exchange chromatography (Dowex-50) and P2 size exclusion chromatography to yield **19d** (10 mg, 59%). [α]_D²⁰ -0.44 (c 0.07, H₂O). ¹H NMR (500 MHz, D₂O) δ 1.56 (t, *J* = 12.2 Hz, 1H, H-3a), 2.62 (dd, *J* = 4.6, 12.4 Hz, 1H, H-3b), 3.02 (s, 3H, CH₃), 3.23 (t, *J* = 10.1 Hz, 1H, H-5), 3.40 (dd, *J* = 7.8, 14.7 Hz, 1H, H-9a), 3.48 (td, *J* = 4.6, 11.9 Hz, 1H, H-4), 3.66 (m, 3H, H-6, H-8, H-9b), 3.75 (d, *J* = 8.7 Hz, 1H, H-7), 4.51 (A of AB, *J* = 11.8 Hz, 1H, CH₂Ar), 4.66 (m, 1H, CH₂Ar), 7.02 (m, 3H, CH_{ar}), 7.40, 7.63 (AA', BB' of AA'/BB', *J* = 8.6 Hz, 4H, CH_{ar}). ¹³C NMR (D₂O) δ 40.9, 41.3 (2C, C-3, C-9), 42.5 (CH₃), 55.5 (C-5), 60.6 (CH₂Ar), 68.6 (C-7), 69.3 (C-4), 70.3 (C-8), 73.2 (C-6), 101.2 (C-2), 112.4, 117.2, 124.4, 125.8, 128.7, 128.8, 137.5 (12C, C-Ar), 173.1, 187.7 (2 CO). HRMS calcd for C₂₄H₂₆ClF₂N₂NaO₁₀S [M + Na]⁺ 653.0760; found *m/z* 653.0759.

Sodium ((2,3-Difluorobenzyl) 5-Methoxyacetamido-9-(4-chlorobenzamido)-3,5,9-trideoxy- α -D-galacto-2-nonulopyranosid)onate (19e). Compound **18b** (10 mg, 0.01 mmol) was treated with 10% aqueous NaOH (0.3 mL) in MeOH (1.5 mL) at rt for 4 h. The crude product was purified by chromatography on RP-18 (5% gradient of MeOH in H₂O) to yield **19e** (2.3 mg, 19%) and **19b** (1.7 mg, 21%) as white solids. [α]_D²⁰ -19.1 (c 0.46, MeOH). ¹H NMR (500 MHz, D₂O) δ 1.67 (t, *J* = 12.2 Hz, 1H, H-3a), 2.73 (dd, *J* = 4.6, 12.4 Hz, 1H, H-3b), 3.28 (s, 3H, OMe), 3.41-3.56 (m, 2H, H-7, H-9a), 3.62-3.79 (m, 3H, H-4, H-8, H-9b), 3.82-3.89 (m, 2H, H-5, H-6), 3.95, 3.98 (A, B of AB, *J* = 15.6 Hz, 2H, CH₂OMe), 4.62, 4.78 (A, B of AB, *J* = 11.7 Hz, 2H, CH₂Ar), 7.00-7.22 (m, 3H, CH_{ar}), 7.49, 7.71 (AA', BB' of AA'/BB', *J* = 8.5 Hz, 4H, CH_{ar}). ¹³C NMR (D₂O) δ 40.4 (C-3), 42.4 (C-9), 51.5 (C-5), 58.9 (OMe), 60.6 (CH₂Ar), 67.9 (C-4), 69.6 (C-7), 70.2 (C-8), 70.8 (CH₂OMe), 72.4 (C-6), 101.2 (C-2), 110.0, 117.1, 117.2, 124.4, 125.9, 128.7, 128.8, 132.1 (12C, C-Ar), 173.0,

173.5 (3C, CO). HRMS calcd for C₂₆H₂₈ClF₂N₂O₁₀Na [M + Na]⁺ 647.1195; found *m/z* 647.5573.

Sodium ((2,3-Difluorobenzyl) 5-Cyclopropylamido-9-(4-chlorobenzamido)-3,5,9-trideoxy- α -D-galacto-2-nonulopyranosid)onate (19f). Compound **23f** (31.0 mg, 0.04 mmol) was dissolved in THF/water (2.0 mL/0.5 mL) and was reacted with LiOH (10.0 mg, 0.42 mmol). The crude product was purified on RP-18 (10% gradient MeOH in H₂O) followed by ion exchange chromatography (Dowex-50) and P2 size exclusion chromatography to yield **19f** (11 mg, 44%). [α]_D²⁰ -0.1 (c 0.26, H₂O). ¹H NMR (500 MHz, D₂O) δ 0.59 (m, 2H, CH₂), 0.70 (m, 2H, CH₂), 1.44 (m, 1H, CH), 1.56 (t, *J* = 11.8 Hz, 1H, H-3a), 2.64 (dd, *J* = 3.5, 11.8 Hz, 1H, H-3b), 3.37 (d, *J* = 8.2 Hz, 1H, H-7), 3.47 (m, 1H, H-9a), 3.63 (m, 4H, H-5, H-6, H-8, H-9b), 4.52, 4.69 (A, B of AB, *J* = 11.6 Hz, 2H, CH₂Ar), 7.04 (m, 3H, CH_{ar}), 7.40, 7.63 (AA', BB' of AA'/BB', *J* = 8.1 Hz, 4H, CH_{ar}). ¹³C NMR (CDCl₃) δ 6.8, 7.0 (2C, CH₂), 14.1 (CH), 40.5, 42.3 (2C, C-3, C-9), 51.9 (C-5), 60.5 (CH₂Ar), 68.0 (C-4), 69.4 (C-7), 70.1 (C-8), 72.8 (C-6), 101.2 (C-2), 117.1, 124.4, 125.9, 128.7, 132.1, 137.6 (12C, C-Ar), 170.0, 173.1, 178.3 (3 CO). HRMS calcd for C₂₇H₂₈ClF₂N₂O₉ [M - H]⁻ 597.1457; found 597.1454.

Sodium ((2,3-Difluorobenzyl) 5-Cyclobutylamido-9-(4-chlorobenzamido)-3,5,9-trideoxy- α -D-galacto-2-nonulopyranosid)onate (19g). Compound **23g** (44.0 mg, 0.06 mmol) was dissolved in THF/water (2.0 mL/0.5 mL) and was reacted with LiOH (14.0 mg, 0.58 mmol). The crude product was purified on RP-18 (10% gradient MeOH in H₂O) followed by ion exchange chromatography (Dowex-50) and P2 size exclusion chromatography to yield **19g** (17 mg, 49%). [α]_D²⁰ -0.2 (c 0.11, H₂O). ¹H NMR (500 MHz, D₂O) δ 1.55 (m, 1H, H-3a), 1.85 (m, 6H, CH₂), 2.63 (dd, *J* = 3.9, 12.2 Hz, 1H, H-3b), 2.99 (quint, *J* = 8.8 Hz, 1H, CH), 3.32 (d, *J* = 8.6 Hz, 1H, H-9a), 3.61 (m, 6H, H-4, H-5, H-6, H-7, H-8, H-9b), 4.52, 4.68 (A, B of AB, *J* = 11.4 Hz, 2H, CH₂Ar), 7.05 (m, 3H, CH_{ar}), 7.40, 7.63 (AA', BB' of AA'/BB', *J* = 7.5 Hz, 4H, CH_{ar}). ¹³C NMR (D₂O) δ 17.4, 24.5 (3C, CH₂), 39.2 (CH), 40.5 (C-3), 42.1 (C-9), 51.6 (C-5), 60.5 (CH₂Ar), 67.8 (C-4), 69.3 (C-7), 70.1 (C-8), 72.7 (C-6), 110.0 (C-2), 115.6, 123.3, 125.9, 128.8, 150.9 (12C, C-Ar), 170.0, 175.8, 179.7 (3 CO). ESI-MS calcd for C₂₈H₃₀ClF₂N₂NaO₉ [M + Na]⁺ 657.1403; found *m/z* 657.1401.

Methyl (Methyl 5-*tert*-Butyloxycarbonylamino-4,7,8-tri-*O*-acetyl-9-(4-chlorobenzamido)-3,5,9-trideoxy-2-thio- α -D-galacto-2-nonulopyranosid)onate (20). Compound **14** (167 mg, 0.30 mmol) was dissolved in dry DCE (5 mL). *p*-Chlorobenzoyl chloride (150 μ L, 210 mg, 1.19 mmol) and triphenylphosphine (156 mg, 0.59 mmol) were added. The reaction mixture was stirred at rt overnight. Afterward, the reaction mixture was washed with saturated aqueous NaHCO₃ (3 \times 5 mL) and H₂O (1 \times 5 mL). The organic phase was dried over Na₂SO₄, filtered, and concentrated under reduced pressure. The crude product was purified by chromatography on silica gel (EA:PE, gradient 1:1 to 2:1) to yield **20** (95 mg, 48%) as a white foam. ¹H NMR (500 MHz, CD₂Cl₂) δ 1.39 (s, 9H, C(CH₃)₃), 1.92 (s, 3H, SMe), 2.01 (s, 6H, 2 OAc), 2.12 (m, 1H, H-3a), 2.23 (s, 3H, OAc), 2.56 (dd, *J* = 4.7, 13.8 Hz, 1H, H-3b), 3.00 (td, *J* = 3.2, 15.2 Hz, 1H, H-9a), 3.79 (m, 4H, OMe, H-5), 4.23 (d, *J* = 10.6 Hz, 1H, H-6), 4.41 (ddd, *J* = 3.1, 8.8, 14.4 Hz, 1H, H-9b), 4.52 (dd, *J* = 2.9, 10.0 Hz, 1H, NHAc), 5.09 (m, 1H, H-8), 5.16 (td, *J* = 4.6, 11.0 Hz, 1H, H-4), 5.33 (m, 1H, H-7), 7.23 (d, *J* = 3.9 Hz, 1H, NH), 7.54, 8.08 (AA', BB' of AA'/BB', *J* = 8.5 Hz, 4H, CH_{ar}). ¹³C NMR (CD₂Cl₂) δ 11.7 (SMe), 21.2, 21.3, 21.4 (3 OAc), 28.5 (C(CH₃)₃), 37.8 (C-3), 38.4 (C-9), 51.5 (C-5), 53.3 (OMe), 68.9 (C-7), 70.0 (C-4), 70.6 (C-8), 71.5 (C-6), 80.5 (C-2), 85.3 (C(CH₃)₃), 129.3, 132.4, 138.0, 141.8 (6C, C-Ar), 155.7 (CONH), 166.7, 168.6, 170.5, 170.7, 172.4 (5 CO). ESI-MS calcd for C₂₉H₃₉ClN₂O₁₂S [M + Na]⁺ 697.18; found *m/z* 697.25.

Methyl (Methyl 5-Amino-4,7,8-tri-*O*-acetyl-9-(4-chlorobenzamido)-3,5,9-trideoxy-2-thio- α -D-galacto-2-nonulopyranosid)onate (21). Compound **20** (95.0 mg, 0.14 mmol) was dissolved in 4 M PhOH (in DCM; 4 mL) and 4 M TMSCl

3.3 Pharmacokinetic behavior of MAG antagonists

(in DCM; 2 mL). The reaction mixture was stirred at rt for 2 h. The crude product was purified by chromatography on silica gel (EA:PE, gradient 1:1 to 8:1) to yield **21** as a white foam (51 mg, 63%). ¹H NMR (500 MHz, CD₂Cl₂) δ 1.95 (s, 3H, SMe), 1.99 (dd, *J* = 5.7, 14.0 Hz, 1H, H-3a), 2.04, 2.06, 2.19 (3 s, 9H, 3 OAc), 2.57 (dd, *J* = 4.7, 13.7 Hz, 1H, H-3b), 2.62 (t, *J* = 10.0 Hz, 1H, H-5), 3.34–3.42 (m, 1H, H-9a), 3.76 (s, 3H, OMe), 4.06 (dd, *J* = 1.4, 10.0 Hz, 1H, H-6), 4.17 (ddd, *J* = 3.3, 7.0, 15.0 Hz, 1H, H-9b), 4.98 (td, *J* = 4.7, 11.4 Hz, 1H, H-4), 5.18 (dt, *J* = 3.7, 7.5 Hz, 1H, H-8), 5.61 (dd, *J* = 1.5, 7.5 Hz, 1H, H-7), 6.90 (m, 2H, NH₂), 7.43, 7.74 (AA', BB' of AA'BB', *J* = 8.6 Hz, 4H, CH_{ar}). ¹³C NMR (CD₂Cl₂) δ 11.8 (SMe), 21.3, 21.4, 21.4 (3 OAc), 37.0 (C-3), 39.4 (C-9), 52.2 (C-5), 53.3 (OMe), 69.5 (C-7), 71.3 (C-8), 73.0 (C-4), 73.8 (C-6), 84.7 (C-2), 129.1, 129.3, 130.1, 133.5 (6C, C-Ar), 166.3, 168.2, 170.3, 170.4, 171.4 (5 CO). ESI-MS calcd for C₂₄H₃₁ClN₂O₁₀S [M + Na]⁺ 597.13; found *m/z* 597.14.

Methyl (Methyl 5-Cyclopropylamido-4,7,8-tri-*O*-acetyl-9-(4-chlorobenzamido)-3,5,9-trideoxy-2-thio-*D*-glycero- α -*D*-galacto-2-nonulopyranosid)onate (22f). Compound **21** (74.0 mg, 0.16 mmol) was dissolved in dry DCM (2.0 mL) under argon atmosphere. Cyclopropanoyl chloride (24.0 μ L, 28.0 mg, 0.27 mmol), NEt₃ (37.0 μ L, 27.0 mg, 0.27 mmol), and a catalytic amount of DMAP were added successively. The reaction mixture was stirred at rt for 3.5 h. Then it was washed with saturated aqueous NaHCO₃ (3 \times 5 mL) and H₂O (1 \times 5 mL). The organic phase was dried over Na₂SO₄, filtered, and concentrated under reduced pressure. The crude product was purified by chromatography on silica gel (EA:PE, gradient 1:1 to 2:1) to yield **22f** (43 mg, 75%). [α]_D²⁰ 0.48 (*c* 2.16, CH₂Cl₂). ¹H NMR (500 MHz, CDCl₃) δ 0.70 (m, 2H, CH₂), 0.91 (m, 2H, CH₂), 1.22 (m, 1H, CH), 2.01 (m, 4H, H-3a, SMe), 2.10, 2.12, 2.20 (3 s, 9H, 3 OAc), 2.71 (dd, *J* = 4.6, 12.7 Hz, 1H, H-3b), 2.86 (m, 1H, H-9a), 3.73 (dd, *J* = 2.0, 10.7 Hz, 1H, H-6), 3.76 (s, 3H, OMe), 4.24 (q, *J* = 10.5 Hz, 1H, H-5), 4.36 (ddd, *J* = 2.9, 8.7, 11.6 Hz, 1H, H-9b), 4.84 (td, *J* = 4.6, 11.6 Hz, 1H, H-4), 5.12 (dd, *J* = 2.0, 10.1 Hz, 1H, H-7), 5.25 (dt, *J* = 2.7, 10.1 Hz, 1H, H-8), 5.42 (d, *J* = 10.3 Hz, 1H, 5-NH), 7.18 (dd, *J* = 4.0, 8.7 Hz, 1H, NH), 7.39, 7.75 (AA', BB' of AA'BB', *J* = 8.6 Hz, 4H, CH_{ar}). ¹³C NMR (CDCl₃) δ 7.4 (2C, CH₂), 12.1 (CH), 14.6 (SMe), 21.1 (3C, 3 OAc), 37.8, 38.2 (2C, C-3, C-9), 49.4 (C-5), 52.9 (OMe), 67.9, 68.2 (2C, C-7, C-8), 69.7 (C-4), 73.9 (C-6), 82.8 (C-2), 128.8, 129.4, 132.7, 137.7 (6C, C-Ar), 166.1, 167.7, 170.3, 171.2, 172.4, 173.7 (6 CO). ESI-MS calcd for C₂₈H₃₅ClN₂O₁₁S [M + Na]⁺ 665.17; found *m/z* 665.06.

Methyl (Methyl 5-Cyclobutylamido-4,7,8-tri-*O*-acetyl-9-(4-chlorobenzamido)-3,5,9-trideoxy-2-thio-*D*-glycero- α -*D*-galacto-2-nonulopyranosid)onate (22g). Compound **21** (60 mg, 0.1 mmol) was dissolved in dry DCM (2.4 mL). Cyclobutanecarbonyl chloride (36 μ L, 37 mg, 0.3 mmol), NEt₃ (44 μ L, 32 mg, 0.3 mmol), and a catalytic amount of DMAP were added successively. The reaction mixture was stirred at rt overnight. Then it was washed with saturated aqueous NaHCO₃ (3 \times 5 mL) and H₂O (1 \times 5 mL). The organic phase was dried over Na₂SO₄, filtered, and concentrated under reduced pressure. The crude product was purified by chromatography on silica gel (EA:PE, gradient 1:1 to 2:1) to yield **22g** (27 mg, 39%). ¹H NMR (500 MHz, CDCl₃) δ 2.00 (m, 4H, SMe, H-3a), 2.03 (s, 3H, OAc), 2.08 (m, 2H, CH₂), 2.13 (s, 3H, OAc), 2.18 (m, 4H, CH₂), 2.27 (s, 3H, OAc), 2.71 (dd, *J* = 4.6, 12.7 Hz, 1H, H-3b), 2.86 (m, 2H, CH, H-9a), 3.71 (dd, *J* = 2.1, 10.8 Hz, 1H, NH), 3.77 (s, 3H, OMe), 4.20 (t, *J* = 10.4 Hz, 1H, H-5), 4.37 (ddd, *J* = 2.9, 8.8, 15.2 Hz, 1H, H-9b), 4.82 (td, *J* = 4.6, 11.6 Hz, 1H, H-4), 5.08 (d, *J* = 10.3 Hz, 1H, H-6), 5.27 (m, 2H, H-7, H-8), 7.13 (dd, *J* = 4.0, 8.6 Hz, 1H, 5-NH), 7.38, 7.74 (AA', BB' of AA'BB', *J* = 8.6 Hz, 4H, CH_{ar}). ¹³C NMR (CDCl₃) δ 12.1 (SMe), 18.2 (CH₂), 20.9 (3C, OAc), 24.9 (2C, CH₂), 37.8, 38.2 (2C, C-3, C-9), 39.8 (CH), 49.2 (C-5), 53.0 (OMe), 68.0, 68.1, 69.6 (3C, C-4, C-7, C-8), 73.8 (C-4), 82.8 (C-2), 128.4, 132.7, 137.7 (6C, C-Ar), 166.1, 167.7, 170.3, 172.6, 175.0 (6C, CO). ESI-MS calcd for C₂₉H₃₇ClN₂O₁₁S [M + Na]⁺ 679.18; found *m/z* 679.11.

Methyl ((2,3-Difluorobenzyl) 5-Cyclopropylamido-4,7,8-tri-*O*-acetyl-9-(4-chlorobenzamido)-3,5,9-trideoxy-*D*-glycero- α -*D*-galacto-2-nonulopyranosid)onate (22f). Compound **22f** (37.0 mg, 0.06 mmol) was reacted with 2,3-difluorobenzyl alcohol (18.0 μ L, 23.0 mg, 0.16 mmol), *N*-iodosuccinimide (20.0 mg, 0.09 mmol), and triflic acid (4.00 μ L, 7.00 mg, 0.05 mmol). The crude product was purified by chromatography on silica gel (1% gradient *i*PrOH in petrol ether/DCM 2:1) to yield **22f** (31 mg, 72%). [α]_D²⁰ 0.23 (*c* 1.73, CH₂Cl₂). ¹H NMR (500 MHz, CDCl₃) δ 0.79 (m, 2H, CH₂), 1.00 (m, 2H, CH₂), 1.29 (m, 1H, CH), 2.08 (m, 1H, H-3a), 2.09, 2.21, 2.29 (3 s, 9H, 3 OAc), 2.72 (dd, *J* = 4.5, 12.8 Hz, 1H, H-3b), 2.98 (m, 1H, H-9a), 3.82 (s, 3H, OMe), 4.11 (m, 1H, H-6), 4.34 (m, 1H, H-5), 4.41 (m, 1H, H-9b), 4.59, 4.89 (A, B of AB, *J* = 12.0 Hz, 2H, CH₂Ar), 4.95 (m, 1H, H-4), 5.21 (dd, *J* = 1.8, 10.0 Hz, 1H, H-7), 5.36 (m, 1H, H-8), 5.49 (d, *J* = 10.2 Hz, 1H, 5-NH), 7.19 (m, 4H, NH, CH_{ar}), 7.47, 7.84 (AA', BB', *J* = 8.5 Hz, 4H, CH_{ar}). ¹³C NMR (CDCl₃) δ 7.1, 7.4 (2C, 2 CH₂), 14.6 (SMe), 20.8, 21.2, 21.3 (3 OAc), 25.4 (CH), 38.0, 38.4 (2C, C-3, C-9), 49.5 (C-5), 52.8 (OMe), 60.5 (CH₂Ar), 67.9, 68.4, 68.9 (3C, C-4, C-7, C-8), 72.5 (C-6), 98.6 (C-2), 115.8, 117.1, 123.9, 125.4, 126.7, 128.5, 132.7, 137.7 (12C, C-Ar), 166.2, 168.0, 170.3, 171.2, 172.4, 173.8 (6 CO). ESI-MS calcd for C₃₄H₃₇ClF₂N₂O₁₂ [M + Na]⁺ 761.20; found *m/z* 761.16.

Methyl ((2,3-Difluorobenzyl) 5-Cyclobutylamido-4,7,8-tri-*O*-acetyl-9-(4-chlorobenzamido)-3,5,9-trideoxy-*D*-glycero- α -*D*-galacto-2-nonulopyranosid)onate (22g). Compound **22g** (53.0 mg, 0.08 mmol) was reacted with 2,3-difluorobenzyl alcohol (25.0 μ L, 33.0 mg, 0.23 mmol), *N*-iodosuccinimide (27.0 mg, 0.12 mmol), and triflic acid (6.00 μ L, 10.0 mg, 0.07 mmol). The crude product was purified by chromatography on silica gel (1% gradient *i*PrOH in petrol ether/DCM 2:1) to yield **22g** (44 mg, 72%). [α]_D²⁰ 0.23 (*c* 1.7, CH₂Cl₂). ¹H NMR (500 MHz, CDCl₃) δ 1.85 (m, 1H, H-3a), 1.99 (s, 3H, OAc), 2.04 (m, 4H, 2 CH₂), 2.13 (s, 3H, OAc), 2.18 (m, 2H, CH₂), 2.27 (s, 3H, OAc), 2.63 (dd, *J* = 4.5, 12.7 Hz, 1H, H-3b), 2.84 (quint, *J* = 10.0 Hz, 1H, CH), 2.91 (dt, *J* = 3.5, 15.0 Hz, 1H, H-9a), 3.73 (s, 3H, OMe), 4.03 (d, *J* = 12.5 Hz, 1H, H-6), 4.22 (q, *J* = 10.4 Hz, 1H, H-5), 4.33 (ddd, *J* = 2.8, 8.6, 15.1 Hz, 1H, H-9b), 4.51 (A of AB, *J* = 11.8 Hz, 1H, CH₂Ar), 4.82 (m, 2H, H-4, CH₂Ar), 5.10 (dd, *J* = 1.7, 9.9 Hz, 1H, H-7), 5.17 (d, *J* = 10.4 Hz, 1H, 5-NH), 5.26 (m, 1H, H-8), 5.36 (d, *J* = 10.2 Hz, 1H, 5-NH), 7.09 (m, 3H, CH_{ar}), 7.19 (dd, *J* = 4.9, 8.3 Hz, 1H, NH), 7.37, 7.73 (AA', BB' of AA'BB', *J* = 8.4 Hz, 4H, CH_{ar}). ¹³C NMR (CDCl₃) δ 18.1 (2C, CH₂), 21.2 (3C, OAc), 25.3 (CH₂), 37.9 (C-3), 38.3 (C-9), 39.7 (CH), 49.1 (C-5), 52.8 (OMe), 60.3 (CH-Ar), 67.8, 68.2, 68.8 (3C, C-4, C-7, C-8), 72.3 (C-6), 98.5 (C-2), 116.4, 117.1, 123.7, 125.3, 128.7, 132.5, 137.6 (12C, C-Ar), 167.9, 171.1, 172.4, 175.0 (6C, CO). ESI-MS calcd for C₃₅H₃₉ClF₂N₂O₁₂ [M + Na]⁺ 775.22; found *m/z* 775.25.

Hapten Inhibition Assays with MAG_{d1-3}-Fc. Murine MAG_{d1-3}-Fc was affinity purified from CHO-Lec 3.2.8.1 cell culture supernatant as described before,⁴⁰ dialyzed against 10 mM phosphate buffer pH 7.4, sterile filtered, and stored at 4 °C. The purified protein is stable for several months. The protein was analyzed by an ELISA and binding assay with immobilized fetuin. Inhibition assays for MAG were performed as described previously.^{26,30,40} In brief, fetuin was immobilized in microtiter plates and binding of MAG-Fc was determined in the presence of seven to eight different concentrations for each inhibitor using alkaline phosphatase-labeled anti-Fc antibodies. The half-maximal inhibitory concentrations were determined from corresponding binding curves and used to calculate relative inhibitory concentrations (rIC₅₀).

SPR Analysis. The SPR measurements were performed on a Biacore 3000 surface plasmon resonance based optical biosensor (Biacore AB, Sweden). Sensor chips (CM5 and CM4), immobilization kits, maintenance supply and HBS-EP (10 mM HEPES pH 7.4, 150 mM NaCl, 3 mM EDTA, 0.005% v/v surfactant P20) were purchased from Biacore AB (HBS-EP ready-to-use; degassed and filtered). CM5 (CM4, respectively) chips were preconditioned prior to usage by injecting a series of

conditioning solutions. A flow rate of 50 $\mu\text{L}/\text{min}$ was used and $2 \times 20 \mu\text{L}$ of 50 mM NaOH, 10 mM HCl, 0.1% SDS, and 100 mM H_2PO_4 were injected. The carboxy groups on the CM5 (CM4) chip were activated for 10 min with a 1:1 mixture of 0.1 M *N*-hydroxysuccinimide (NHS) and 0.1 M 3-(*N,N*-dimethylamino)propyl-*N*-ethylcarbodiimide (EDC) at a flow rate of 10 $\mu\text{L}/\text{min}$. Protein A (P6031) was purchased from Sigma. A sample and a reference surface were prepared sequentially or in parallel. For immobilizing protein A, a stock solution (1 mg/mL in 50 mM phosphate buffer, pH 7.0) was diluted in 10 mM sodium acetate, pH 5.0 to obtain a concentration of 30 $\mu\text{g}/\text{mL}$. This solution was then injected over the activated surface for 10 min at a flow rate of 10 $\mu\text{L}/\text{min}$. Protein A densities around 4000 RU and 5000 RU were achieved. Flow cells were blocked with a 10 min injection of 1 M ethanolamine, pH 8.0. For capturing, $\text{MAG}_{\text{d1-3}}\text{-Fc}$ solution (expressed and purified as described⁴⁰) was diluted to a 30–40 $\mu\text{g}/\text{mL}$ concentration using HBS-EP. Afterward, $\text{MAG}_{\text{d1-3}}\text{-Fc}$ was injected at a flow rate of 1 $\mu\text{L}/\text{min}$ for 10 min. The surface was equilibrated overnight at a flow rate of 5 $\mu\text{L}/\text{min}$, achieving densities around 2000 RU. 10-fold dilution series were freshly prepared in eluent buffer immediately before use. All binding experiments were conducted at 25 $^\circ\text{C}$ (except thermodynamic measurements) at a flow rate of 20 $\mu\text{L}/\text{min}$. The samples were injected over 1 min, followed by 1 min dissociation. Each sample was measured with a duplicate of one concentration, using a randomized concentration order. Several buffer samples were injected before the first concentration, and one blank between each concentration, which were used for the double blank referencing during data processing. Double referencing was applied to correct for bulk effects and other systematic artifacts. Data processing and equilibrium binding constant determinations were accomplished with Scrubber (BioLogic Software, Version 1.1 g or 2.0a). Kinetic data were simultaneously fit using the nonlinear regression program Clamp or Scrubber 2.0a.

Stability Test. To determine the stability of a compound in the central nervous system, an artificial cerebrospinal fluid (aCSF) was prepared based on published data.⁴¹ The following concentrations (all in mM/L) were used: sodium 140, chlorine 125, hydrogen carbonate 22.5, potassium 2.9, calcium 1.15, magnesium 1, urea 4.16, and glucose 3.2. Because the composition of proteins in the CSF is comparable to the serum but at a lower concentration (the ratio of liquor protein to serum protein is 4×10^{-3}),⁵⁹ 0.4% v/v of human plasma (Sigma-Aldrich) was added and the pH was adjusted to 7.3. Then 100 μM solutions of the compound were prepared and shaken at 37 $^\circ\text{C}$ and 300 rpm on an Eppendorf-Thermomixer Comfort. Samples were withdrawn after 0, 30, 60, 120, 180 min and 20 h, respectively. The value assigned to every time point was the average of a triplicate measurement. The quantification of the samples was performed on a Agilent 1100 series HPLC instrument with a UV-DAD spectrometer using the ChemStation software.

logD_{7.3} Determination. Two similar ratios of octanol to buffer were chosen according to the expected logD value, whereas every ratio was measured as a triplicate. Phosphate buffer at pH 7.3 was prepared and shaken overnight together with octanol in order to mutually saturate the two phases. Upon separation of the two layers, the buffer phase was withdrawn and mixed with an analyte stock solution in DMSO to yield a final concentration of 10^{-4} M. Both phases were transferred to a PCR plate, which was covered with aluminum foil (Axygen PCR-AS-200) and shaken for 1 h at 1200 rpm and 25 $^\circ\text{C}$ on a PHMP-4 instrument (Grant-bio). After 2.5 h at room temperature, the aqueous phases were transferred to microvials, centrifuged for 30 s, and analyzed by HPLC (Agilent 1100 series). The values were accepted if the mean values of the two ratios did not differ by more than 0.1 unit.

BBB-PAMPA.⁴² Consumables (system solution, P/N 110151; brain sink buffer, P/N 110674; BBB-1 lipid solution, P/N 110672; preloaded PAMPA sandwich with stirring devices,

P/N 110 212) were purchased from pION. Each donor compartment of the preloaded PAMPA plate was filled with 200 μL of pION's system solution at pH 7.4, containing the analytes at a concentration of 50 μM . Then 150 μL of the same solution were transferred to an UV-plate (UV-Star, Greiner Bio-one) and UV spectra were recorded as reference on a SpectraMax instrument (Molecular Devices). The filter membranes of the acceptor compartments were impregnated with 5 μL of BBB-1 lipid solution and each compartment was filled with 200 μL of brain sink buffer. The system was assembled and individual stirring of the wells was induced by pION's GutBox to yield an unstirred water layer thickness of 40 μm . After 30 min, the UV data of the acceptor and the donor plate were acquired on a SpectraMax instrument (Molecular Devices) and analyzed by the PAMPA Evolution command software (version 3.4, pION).

NMR. Shigemi NMR tubes were used to reduce the sample volume needed for measurement to 250 μL . $\text{MAG}_{\text{d1-3}}\text{-Fc}$ protein was diluted from a stock solution of 1 mg/mL by a factor of 2 using 99.8% D_2O (Armar Chemicals). Following dilution, the 0.5 mg/mL $\text{MAG}_{\text{d1-3}}\text{-Fc}$ was in a solvent of 50% D_2O and 50% H_2O , with 0.01% NaN_3 with a buffer of 5 mM PBS. Stock solutions of **4** were prepared in D_2O at 100, 50, and 20 mM and added to the NMR samples containing $\text{MAG}_{\text{d1-3}}\text{-Fc}$ for both the titration curve and competition experiments. Stock solutions of **13f** and **25** were prepared in D_2O at 5 mM to add to the NMR samples containing $\text{MAG}_{\text{d1-3}}\text{-Fc}$ for the competition experiments. All NMR experiments were carried out at 300 K on a Bruker DRX500 spectrometer, equipped with Z-gradient SEI probe. The pulse sequence used for the selective inversion recovery experiments began with a selective 25 ms I-Burp-1⁶⁰ 180 $^\circ$ pulse applied to the *para*-hydrogen of the benzamide group of compound **4**. This proton does not overlap with any other resonances of **13f** and **25**. A further benefit of the *para*-hydrogen of the benzamide group of compound **4** was that its resonance frequency was sufficiently different from the water resonance, thus avoiding complications due to radiation damping.⁶¹ Following the selective inversion pulse, a 1 ms gradient pulse was applied to dephase any residual transverse magnetization. The gradient pulse was followed by a variable delay to allow for the recovery of longitudinal magnetization. The delay was followed by a DPFGE water suppression sequence to suppress the magnetization from the 50% H_2O .⁶¹

For each selective inversion recovery time measurement (s_{11}), 10 experiments were performed. These experiments consisted of increasing delays following the selective inversion pulse and gradient of 0.1, 0.25, 0.5, 0.75, 1, 1.5, 2, 3, 5, and 10 s. Then 32 scans, preceded by eight dummy scans, were measured for the concentrations of compound **4** of 500 μM and 1 mM. Sixteen scans, preceded by eight dummy scans, were measured for the concentrations of compound **4** of 2, 4, and 7 mM. For the competitive experiments with 25 μM of either **13f** or **25** added to 500 μM of **4**, 32 scans, preceded by eight dummy scans, were measured. A delay of 20 s following the measurement of each transient was inserted to allow the magnetization to return to equilibrium. Prior to the measurement upon addition of either **13f** or **25**, a 1 h incubation time for equilibration was allowed. The NMR data were analyzed using XWINNMR version 3.5 operating on a PC running under Linux OS. The spectra were apodized with an exponential decay function with 2 Hz line broadening. The inversion recovery data, as well as the one-site binding model, were fit using Prism 4 (GraphPad Software Inc., San Diego, CA).

Acknowledgment. We thank the Volkswagen Foundation, the Swiss National Science Foundation, the German Federal Ministry for Education and Research (BMBF, project 031632A), and the Tönjes–Vagt Foundation (project XXI) for their support of this work.

Supporting Information Available: Surface plasmon resonance assay, structure of compounds implemented additionally

in the Biacore–Hapten assay correlation, HRMS data, HPLC traces, and ^1H spectra of target compounds **13a–f**, **19a–g**. This material is available free of charge via the Internet at <http://pubs.acs.org>.

References

- Schwab, M. E.; Bandtlow, C. E. Neurobiology—Inhibitory Influences. *Nature* **1994**, *371*, 658–659.
- Ramon y Cajal, S. *Degeneration and Regeneration of the Nervous System*; Oxford University Press: London, 1928.
- Schwab, M. E.; Caroni, P. Oligodendrocytes and CNS myelin are nonpermissive substrates for neurite growth and fibroblast spreading *in vitro*. *J. Neurosci.* **1988**, *8*, 2381–2393.
- Sandvig, A.; Berry, M.; Barrett, L. B.; Butt, A.; Logan, A. Myelin-reactive glia-, and scar-derived CNS axon growth inhibitors: expression, receptor signaling, and correlation with axon regeneration. *Glia* **2004**, *46*, 225–251.
- Filbin, M. T. Myelin-associated inhibitors of axonal regeneration in the adult mammalian CNS. *Nature Rev. Neurosci.* **2003**, *4*, 703–713.
- He, Z. G.; Koprivica, V. The Nogo signaling pathway for regeneration block. *Annu. Rev. Neurosci.* **2004**, *27*, 341–368.
- Caroni, P.; Savio, T.; Schwab, M. E. Central nervous-system regeneration—oligodendrocytes and myelin as nonpermissive substrates for neurite outgrowth. *Prog. Brain Res.* **1988**, *78*, 363–370.
- Quarles, R. H. A hypothesis about the relationship of myelin-associated glycoprotein's function in myelinated axons to its capacity to inhibit neurite outgrowth. *Neurochem. Res.* **2009**, *34*, 79–86.
- Quarles, R. H. Myelin-associated glycoprotein (MAG): past, present and beyond. *J. Neurochem.* **2007**, *100*, 1431–1448.
- Crocker, P. R.; Clark, E. A.; Filbin, M.; Gordon, S.; Jones, Y.; Kehrl, J. H.; Kelm, S.; Le Douarin, N.; Powell, L.; Roder, J.; Schnaar, R. L.; Sgroi, D. C.; Stamenkovic, K.; Schauer, R.; Schachner, M.; van den Berg, T. K.; van der Merwe, P. A.; Watt, S. M.; Varki, A. Siglecs: A Family of Sialic Acid Binding Lectins. *Glycobiology* **1998**, *8*, Glycoforum 2 v–vi.
- Kelm, S.; Pelz, A.; Schauer, R.; Filbin, M. T.; Tang, S.; de Bellard, M. E.; Schnaar, R. L.; Mahoney, J. A.; Hartnell, A.; Bradford, P. Sialoadhesin, myelin-associated glycoprotein and CD22 define a new family of sialic acid-dependent adhesion molecules of the immunoglobulin superfamily. *Curr. Biol.* **1994**, *4*, 965–972.
- Lauren, J.; Hu, F.; Chin, J.; Liao, J.; Airaksinen, M. S.; Strittmatter, S. M. Characterization of Myelin Ligand Complexes with Neuronal Nogo-66 Receptor Family Members. *J. Biol. Chem.* **2007**, *282*, 5715–5725.
- Robak, L. A.; Venkatesh, K.; Lee, H.; Raiker, S. J.; Duan, Y.; Lee-Osbourne, J.; Hofer, T.; Mage, R. G.; Rader, C.; Giger, R. J. Molecular basis of the interactions of the Nogo-66 receptor and its homolog NgR2 with myelin-associated glycoprotein: development of NgR^{DMN1} Fc, a novel antagonist of CNS myelin inhibition. *J. Neurosci.* **2009**, *29*, 5766–5783.
- Yang, L. J. S.; Zeller, C. B.; Shaper, N. L.; Kiso, M.; Hasegawa, A.; Shapiro, R. E.; Schnaar, R. L. Gangliosides are neuronal ligands for myelin-associated glycoprotein. *Proc. Nat. Acad. Sci. U.S.A.* **1996**, *93*, 814–818.
- Tang, S.; Shen, Y. J.; DeBellard, M. E.; Mukhopadhyay, G.; Salzer, J. L.; Crocker, P. R.; Filbin, M. T. Myelin-associated glycoprotein interacts with neurons via a sialic acid binding site at ARG118 and a distinct neurite inhibition site. *J. Cell Biol.* **1997**, *138*, 1355–1366.
- Vinson, M.; Strijbos, P. J. L. M.; Rowles, A.; Facci, L.; Moore, S. E.; Simmons, D. L.; Walsh, F. S. Myelin-associated glycoprotein interacts with ganglioside GT1b—A mechanism for neurite outgrowth inhibition. *J. Biol. Chem.* **2001**, *276*, 20280–20285.
- Wörter, V.; Schweigreiter, R.; Kinzel, B.; Mueller, M.; Barske, C.; Böck, G.; Frenzel, S.; Bandtlow, C. E. Inhibitory Activity of Myelin-Associated Glycoprotein on Sensory Neurons Is Largely Independent of NgR1 and NgR2 and Resides within Ig-Like Domains 4 and 5. *PLoS One* **2009**, *4*, e5218; DOI:10.1371/journal.pone.0005218.
- Yang, L. J. S.; Lorenzini, I.; Vajn, K.; Mountney, A.; Schramm, L. P.; Schnaar, R. L. Sialidase enhances spinal axon outgrowth *in vivo*. *Proc. Nat. Acad. Sci. U.S.A.* **2006**, *103*, 11057–11062.
- Collins, B. E.; Kiso, M.; Hasegawa, A.; Tropak, M. B.; Roder, J. C.; Crocker, P. R.; Schnaar, R. L. Binding specificities of the sialoadhesin family of I-type lectins—sialic acid linkage and substructure requirements for binding of myelin-associated glycoprotein, Schwann cell myelin protein, and sialoadhesin. *J. Biol. Chem.* **1997**, *272*, 16889–16895.
- Vyas, A. A.; Blixt, O.; Paulson, J. C.; Schnaar, R. L. Potent glycan inhibitors of myelin-associated glycoprotein enhance axon outgrowth *in vitro*. *J. Biol. Chem.* **2005**, *280*, 16305–16310.
- Ito, H.; Ishida, H.; Collins, B.; Fromholt, S.; Schnaar, R.; Kiso, M. Systematic synthesis and MAG-binding activity of novel sulfated GM1b analogues as mimics of Chol-1 (alpha-series) gangliosides: highly active ligands for neural Siglecs. *Carbohydr. Res.* **2003**, *338*, 1621–1639.
- Schwardt, O.; Gaethje, H.; Vedani, A.; Mesch, S.; Gao, G.; Spreafico, M.; von Orelli, J.; Kelm, S.; Ernst, B. Examination of the Biological Role of the alpha(2–6)-Linked Sialic Acid in Gangliosides Binding to the Myelin-Associated Glycoprotein (MAG). *J. Med. Chem.* **2009**, *52*, 989–1004.
- Bhunia, A.; Schwardt, O.; Gaethje, H.; Gao, G.; Kelm, S.; Benie, A. J.; Hricovini, M.; Peters, T.; Ernst, B. Consistent Bioactive Conformation of the Neu5Ac alpha(2–3)Gal Epitope Upon Lectin Binding. *ChemBioChem* **2008**, *9*, 2941–2945.
- Shin, S.; Gäthje, H.; Schwardt, O.; Gao, G.; Ernst, B.; Kelm, S.; Meyer, B. Binding epitopes of gangliosides to their neuronal receptor, myelin-associated glycoprotein, from saturation transfer difference NMR. *ChemBioChem* **2008**, *9*, 2946–2949.
- Schwizer, D.; Gäthje, H.; Kelm, S.; Porro, M.; Schwardt, O.; Ernst, B. Antagonists of the myelin-associated glycoprotein: a new class of tetrasaccharide mimics. *Bioorg. Med. Chem.* **2006**, *14*, 4944–4957.
- Kelm, S.; Brossmer, R.; Isecke, R.; Gross, H. J.; Strenge, K.; Schauer, R. Functional groups of sialic acids involved in binding to Siglecs (Sialoadhesins) deduced from interactions with synthetic analogues. *Eur. J. Biochem.* **1998**, *255*, 663–672.
- Kelm, S.; Brossmer, R. Neuraminic acid derivatives for use as Siglec inhibitors. PCT Patent WO 03/000709A2, **2003**.
- Strenge, K.; Schauer, R.; Bovin, N.; Hasegawa, A.; Kiso, M.; Kelm, S. Glycan specificity of myelin-associated glycoprotein and sialoadhesin deduced from interactions with synthetic oligosaccharides. *Eur. J. Biochem.* **1998**, *258*, 677–685.
- Gao, G.; Smiesko, M.; Schwardt, O.; Gäthje, H.; Kelm, S.; Vedani, A.; Ernst, B. Mimetics of the tri- and tetrasaccharide epitope of GQ1b as myelin-associated glycoprotein (MAG) ligands. *Bioorg. Med. Chem.* **2007**, *15*, 7459–7469.
- Shelke, S. V.; Gao, G. P.; Mesch, S.; Gäthje, H.; Kelm, S.; Schwardt, O.; Ernst, B. Synthesis of sialic acid derivatives as ligands for the myelin-associated glycoprotein (MAG). *Bioorg. Med. Chem.* **2007**, *15*, 4951–4965.
- Hasegawa, A.; Ohki, H.; Nagahama, T.; Ishida, H.; Kiso, M. A facile, large-scale preparation of the methyl 2-thioglycoside of N-acetylneuraminic acid, and its usefulness for the alpha-stereoselective synthesis of sialoglycosides. *Carbohydr. Res.* **1991**, *212*, 277–281.
- Fitz, W.; Rosenthal, P. B.; Wong, C. H. Synthesis and inhibitory properties of a thiomethylmercuric sialic acid with application to the X-ray structure determination of 9-O-acetylsialic acid esterase from influenza C virus. *Bioorg. Med. Chem.* **1996**, *4*, 1349–1353.
- Hossain, N.; Zapata, A.; Wilstermann, M.; Nilsson, U. J.; Magnusson, G. Synthesis of GD3-lactam: a potential ligand for the development of an anti-melanoma vaccine. *Carbohydr. Res.* **2002**, *337*, 569–580.
- Ren, C. T.; Chen, C. S.; Wu, S. H. Synthesis of a sialic acid dimer derivative, 2'-alpha-O-benzyl Neu5Ac-alpha-(2→5)Neu5Gc. *J. Org. Chem.* **2002**, *67*, 1376–1379.
- Boullanger, P.; Maunier, V.; Lafont, D. Syntheses of amphiphilic glycosylamides from glycosyl azides without transient reduction to glycosylamines. *Carbohydr. Res.* **2000**, *324*, 97–106.
- Alzuet, G.; Ferrer, S.; Borrás, J.; Solans, X. Structure of methazolamide—an inhibitor of carbonic anhydrase. *Acta Crystallogr., Sect. C: Cryst. Struct. Commun.* **1991**, *47*, 2377–2379.
- Izumi, M.; Shen, G. J.; Wacovich-Sgarbi, S.; Nakatani, T.; Plettenburg, O.; Wong, C. H. Microbial glycosyltransferases for carbohydrate synthesis: alpha-2,3-sialyltransferase from *Neisseria gonorrhoeae*. *J. Am. Chem. Soc.* **2001**, *123*, 10909–10918.
- Grehn, L.; Gunnarsson, K.; Ragnarsson, U. Removal of formyl, acetyl, and benzoyl groups from amides with conversion into the corresponding *tert*-butyl carbamates. *J. Chem. Soc., Chem. Commun.* **1985**, 1317–1318.
- Kaiser, E.; Tam, J. P.; Kubiak, T. M.; Merrifield, R. B. Chlorotrimethylsilane-phenol as a mild deprotection reagent for the *tert*-butyl based protecting groups in peptide-synthesis. *Tetrahedron Lett.* **1988**, *29*, 303–306.
- Bock, N.; Kelm, S. Binding and Inhibition Assay for Siglecs. In *Methods Mol. Biol.*, Vol. 347; Brockhausen, I., Eds.; Humana Press Inc: Totowa, NJ, 2006; pp 359–376.
- Mitchell, R.; Herbert, D.; Carman, C. Acid-base constants and temperature coefficients for cerebrospinal fluid. *J. Appl. Physiol.* **1965**, *20*, 27–30.

3 Results and discussion

Article

Journal of Medicinal Chemistry, 2010, Vol. 53, No. 4 1615

- (42) Di, L.; Kerns, E.; Fan, K.; McConnell, O.; Carter, G. High throughput artificial membrane permeability assay for blood-brain barrier. *Eur. J. Med. Chem.* **2003**, *38*, 223–232.
- (43) Rich, R.; Myszka, D. Advances in surface plasmon resonance biosensor analysis. *Curr. Opin. Biotechnol.* **2000**, *11*, 54–61.
- (44) Morton, T.; Myszka, D. Kinetic analysis of macromolecular interactions using surface plasmon resonance biosensors. *Methods Enzymol.* **1998**, *295*, 268–294.
- (45) Nagata, K.; Handa, H. *Real-Time Analysis of Biomolecular Interactions: Applications of Biacore*; Springer Verlag: Berlin, 2000.
- (46) Mannen, T.; Yamaguchi, S.; Honda, J.; Sugimoto, S.; Kitayama, A.; Nagamune, T. Observation of charge state and conformational change in immobilized protein using surface plasmon resonance sensor. *Anal. Biochem.* **2001**, *293*, 185–193.
- (47) Gestwicki, J. E.; Hsieh, H. V.; Pitner, J. B. Using receptor conformational change to detect low molecular weight analytes by surface plasmon resonance. *Anal. Chem.* **2001**, *73*, 5732–5737.
- (48) Stokmaier, D.; Khorev, O.; Cutting, B.; Born, R.; Ricklin, D.; Ernst, T. O. G.; Böni, F.; Schwingruber, K.; Gentner, M.; Wittwer, M.; Spreafico, M.; Vedani, A.; Rabbani, S.; Schwardt, O.; Ernst, B. Design, synthesis and evaluation of monovalent ligands for the asialoglycoprotein receptor (ASGP-R). *Bioorg. Med. Chem.* **2009**, *17*, 7254–7264.
- (49) Dalvit, C.; Flocco, M.; Knapp, S.; Mostardini, M.; Perego, R.; Stockman, B. J.; Veronesi, M.; Varasi, M. High-throughput NMR-based screening with competition binding experiments. *J. Am. Chem. Soc.* **2002**, *124*, 7702–7709.
- (50) Roos, H.; Karlsson, R.; Nilshans, H.; Persson, A. Thermodynamic analysis of protein interactions with biosensor technology. *J. Mol. Recognit.* **1998**, *11*, 204–210.
- (51) Humphrey, W.; Dalke, A.; Schulten, K. VMD—Visual Molecular Dynamics. *J. Mol. Graphics* **1996**, *14*, 33–38.
- (52) May, A. P.; Robinson, R. C.; Vinson, M.; Crocker, P. R.; Jones, E. Y. Crystal structure of the N-terminal domain of sialoadhesin in complex with 3' sialyllactose at 1.85 angstrom resolution. *Mol. Cell* **1998**, *1*, 719–728.
- (53) Crocker, P. R.; Klem, S. *The Siglec Family of I-type Lectins*; Wiley-VCH: Weinheim, 2000; Vol. IV, pp 579–595.
- (54) Sinnokrot, M. O.; Sherrill, C. D. Substituent effects in pi-pi interactions: sandwich and T-shaped configurations. *J. Am. Chem. Soc.* **2004**, *126*, 7690–7697.
- (55) Mehta, P.; Cummings, R. D.; McEver, R. P. Affinity and kinetic analysis of P-selectin binding to P-selectin glycoprotein ligand-1. *J. Biol. Chem.* **1998**, *273*, 32506–32513.
- (56) Wild, M. K.; Huang, M.-C.; Schulze-Horsel, U.; van der Merwe, P. A.; Vestweber, D. Affinity, kinetics and thermodynamics of E-selectin binding to E-selectin ligand-1. *J. Biol. Chem.* **2001**, *276*, 31602–31612.
- (57) Nicholson, M. W.; Barclay, A. N.; Singer, M. S.; Rosen, S. D.; van der Merwe, P. A. Affinity and kinetic analysis of L-selectin (CD62L) binding to glycosylation-dependent cell-adhesion molecule-1. *J. Biol. Chem.* **1998**, *273*, 763–770.
- (58) Herfurth, L.; Ernst, B.; Wagner, B.; Ricklin, D.; Strasser, D. S.; Magnani, J. L.; Benie, A. J.; Peters, T. Comparative epitope mapping with saturation transfer difference NMR of sialyl Lewis^x compounds and derivatives bound to a monoclonal antibody. *J. Med. Chem.* **2005**, *48*, 6879–6886.
- (59) Wissenschaftliche Tabellen Geigy, 8th ed.; Ciba Geigy: Basel, 1977; Vol. Teilband Körperflüssigkeiten, pp 161–173.
- (60) Geen, H.; Freeman, R. Band-selective radiofrequency pulses. *J. Magn. Reson.* **1991**, *93*, 93–141.
- (61) Cutting, B.; Chen, J. H.; Moskau, D.; Bodenhausen, G. Radiation damping compensation of selective pulses in water-protein exchange spectroscopy. *J. Biomol. NMR* **2000**, *17*, 323–330.

4. Summary and outlook

4 Summary and outlook

During the past decades, pharmacokinetic characterization has been increasingly implemented already at early stages of the drug discovery and development process. Even though the study that sparked this development has been shown to be biased by a high percentage of antibiotics,² the importance of such assays in avoiding preventable attritions has been recognized.¹⁰⁷ As a result, a wealth of new assays has been developed and the existing procedures were continuously adapted to high-throughput requirements thus yielding a plethora of pharmacokinetic information.⁶ This provides project teams already at early stages with a basis for informed decisions and enables them to continue the development of the most promising compounds while abandoning less promising, especially pharmacokinetically questionable molecules.

During this doctoral thesis, various assays have been established to determine pharmacokinetic properties of carbohydrate mimetics. Regarding their physicochemical properties, procedures to determine $\log D_{7.4}$, pK_a , and solubility have been implemented. Furthermore, absorption is assessed by PAMPA and Caco-2 experiments and plasma protein binding is measured. These assays were combined to form the PADMET platform, with PADMET standing for **p**hysicochemical properties, **a**bsorption, **d**istribution, **m**etabolism, **e**limination, and **t**oxicity. The rationale behind the platform was the elucidation of the pharmacokinetic behavior of carbohydrates and mimetics thereof as well as the development of compounds with ameliorated drug-likeness.

During the development of the PADMET platform the need for a fast and simple pK_a determination method became apparent. NMR spectroscopy offers an inexpensive, uncomplicated, and relatively fast approach that does not require special instrumentation. Furthermore, by the use of ^1H -NMR spectroscopy both sample consumption and measuring time are drastically reduced. Additional advantages include the possible use of DMSO stock solutions as starting point and information about the site of protonation in multiprotic compounds. In brief, the assay is performed by gradually changing the pH of a sample solution and monitoring the chemical shift of protons adjacent to ionizable centers by ^1H -NMR spectroscopy. The shift is then plotted against the pH of the respective sample and the pK_a is read out from the inflection point of the resulting sigmoidal curve. Even though this approach has been used before, the scope and limitations of it were never extensively studied.

4 Summary and outlook

Therefore, a methodology was developed and validated with a diverse set of compounds with pK_a values between 1 and 14. Indeed, excellent correlations to literature values stemming from potentiometric titration and to values determined by spectral gradient analysis (UV-based) methods could be observed. Furthermore, pK_a values determined by the $^1\text{H-NMR}$ methodology were closer to reference values compared to calculated values.

To date, 93 carbohydrate mimetics have been characterized concerning their pharmacokinetic behavior. Thereof, 62 compounds were FimH antagonists for which PAMPA, $\log D_{7.4}$, pK_a , and solubility values were determined. Additionally, permeation in the Caco-2 assay, plasma protein binding, and critical micelle concentration were measured for selected compounds. The remaining 31 carbohydrate mimetics consist of 16 selectine antagonists, 11 MAG antagonists, and 4 CD 22 antagonists of which only the MAG antagonists were further discussed in this thesis. Additional publications in the near future will reveal the corresponding pharmacokinetic properties of the other two compound classes.

From the pharmacokinetic point of view, the aim of the FimH antagonist program was to develop orally available compounds with fast renal excretion. For this purpose, the components of the PADMET platform were used in order to predict the expected pharmacokinetic behavior and to select the most suitable compounds for *in vivo* testing. The desired profile included permeation in the PAMPA, suggesting oral bioavailability, and at the same time low $\log D_{7.4}$ values, sufficient solubility as well as low plasma protein binding, leading to fast renal excretion. Since compounds with low lipophilicity that are concomitantly permeating through membranes by passive diffusion are rarely achievable, a prodrug approach was chosen. Indeed, this allowed the synthesis of compounds that fulfilled the desired criteria. Finally, the predicted behavior based on *in vitro* results could be confirmed by *in vivo* studies in a UTI mouse model which highlights the usefulness of early pharmacokinetic assays. This strategy led to the first and up to date only orally available FimH antagonist.

Both PAMPA and $\log D_{7.4}$ values of the FimH antagonist dataset were used for a thorough analysis of the underlying causes for membrane permeation of carbohydrate mimetics. For this purpose experimental and computational parameters were tested for their predictive power regarding passive membrane permeation of this compound class. To the best of our knowledge, it is the first time that such a study has been performed with carbohydrate

4. Summary and outlook

mimetics. Interestingly, the results of this study suggest that calculated logP values are the best descriptor for passive permeation of this compound class and other descriptors for surface area, polarizability or hydrogen bonding are less important. Furthermore, calculated logP values were more suited to explain the permeation behavior than experimental logD_{7.4} values. Finally, a combination of descriptors did not markedly improve the predictive power compared to calculated logP as single descriptor. These findings are in contrast to previously published studies with other compound classes where combinations of descriptors yielded better prediction of permeation behavior than single descriptor models. In conclusion, the permeation behavior of carbohydrate mimetics is probably differing from other compound classes.

For the MAG project the requirements for antagonists were defined differently. Oral availability was not required, since the compounds are planned to be injected directly to the site of action, *i.e.*, the central nervous system (CNS). Instead, maintenance of a sufficiently high local concentration is critical and therefore permeation through the blood-brain barrier and degradation in the cerebrospinal fluid (CSF) were studied. For these purposes, a blood brain-barrier PAMPA was performed and the stability of the compounds was assessed in artificial cerebrospinal fluid. Neither permeation nor degradation were observed, thus yielding the desired properties. Therefore, the local concentration is probably maintained over a sufficiently long time period unless the compounds are removed during physiological CSF turnover processes. Nevertheless, active efflux (*e.g.*, by P-gp) and unspecific binding to CNS tissue remains to be determined to draw final conclusions.

The platform will be expanded in the near future. Assays for metabolic stability questions will be established by Simon Kleeb. A first step into this direction has been taken by building up an assay for the determination of ester cleavage, as exemplified in the FimH publication. Further developments will include the introduction of metabolic stability assays with microsomes (oxidative metabolism by cytochromes) and deepened understanding of glucuronidation. Moreover, the identification of metabolic soft spots in order to introduce stabilizing moieties and decrease metabolic degradation will be an important task. Additionally, more needs to be learned about the toxicity of the carbohydrate mimetics. Especially the incorporation of the Ames test¹⁹⁶ or the GADD45a-GFP¹⁰² (human cells) genotoxicity assay into the PADMET platform seems promising. Furthermore, cytotoxicity assays, such as the MTT assay,¹⁰³ should be established to enrich the early-toxicity profiling.

5 Curriculum vitae

5 Curriculum vitae

Name, Address: Matthias Wittwer
Marktgasse 10
3177 Laupen
Phone: +41 (0)31 747 81 82
matthias.wittwer@gmail.com



Date of birth: June 7, 1982

Native place: Trub, Switzerland

Nationality: Swiss

Marital status: Single

Education

Since March 2011 Postdoctoral scholar at the University of California, San Francisco (Prof. K. Giacomini).

Sept.-Dec. 2010 Postdoctoral Scholar at the Institute of Molecular Pharmacy, University of Basel (Prof. Beat Ernst).

May 2007-Sept. 2010 PhD student at the Institute of Molecular Pharmacy, University of Basel (Prof. Beat Ernst).

Thesis topic: *The PADMET Platform – Pharmacokinetic Characterization of Carbohydrate Mimetics*

October 2006 Eidgenössisches Staatsexamen (Federal State Examination) in Pharmacy equivalent to Master of Pharmacy, GPA: 5.4 (max. grade 6)

2005-2006 Practical year at the Rathaus Pharmacy, Bern

March-October 2005 Diploma thesis in Pharmaceutical Chemistry, Institute of Molecular Pharmacy, University of Basel, (grade: 6, max. grade 6)

Synthesis of monosaccharide mimics for increasing the affinity of trivalent glycoside carriers for the asialoglycoprotein receptor (ASGP-R)

2003-2005 Third and fourth year of studies in Pharmacy at the University of Basel, Switzerland, GPA: 6 (max. grade 6)

2001-2003 First two years of studies in Pharmacy at the University of Bern, Switzerland

2001 Matura with biology and chemistry as major subjects, Bern, Switzerland

5. Curriculum vitae

Professional experience

- 2007-2009 Working as a pharmacist in Liestal (Adler Apotheke) and Bubendorf (Apotheke Studer AG)
- 2007-2010 Teaching of courses for pharmacy assistant pupils regarding GMP for pharmaceuticals in small quantities at the Berufsschule des Detailhandels in Bern
- 2007-2010 Teaching of pharmacology courses for nurses at the Bethesda hospital in Basel
- November 2006 - January 2007 Working as a pharmacist in the Schlossapotheke Laupen (BE)
- 2005-2006 Working as assistant pharmacist at the Rathaus Apotheke Bern
- 2003-2006 Official student's delegate of the aseph (Swiss Pharmacy Student's Association) in various task forces (Arbeitsgruppe für Assistenzjahr und Famulatur, Regionale Aufsichtskommission Basel)

Skills

Professional skills: Experience with various pharmacokinetic assays (establishment or development, validation and application), including PAMPA, Caco-2, pK_a and log D/P determination, plasma protein binding and various stability assays (GIT, CNS, plasma, microsomes, cytochromes). Good general knowledge about pharmacokinetics regarding in vivo as well as in vitro settings.
Knowledge of the relevant softwares (e.g. PAMPA Explorer), cell culture and analytical methods (NMR, LC-MS, UV and fluorescence spectroscopy).

Computational skills: Good knowledge of Microsoft Word, Excel and PowerPoint.

Languages: German: native language.
English: fluent in written and spoken usage (Cambridge Advanced Exam passed with grade A). Language stay in New Zealand for two months (February and March 2007), one thereof at the Nelson English Centre.
French: fluent in written and spoken usage.
Italian: intermediate level.

5 Curriculum vitae

Scientific qualifications

- Publications
- Stokmaier, D.; Khorev, O.; Cutting, B.; Born, R.; Ricklin, D.; Ernst, T. O. G.; Böni, F.; Schwingruber, K.; Gentner, M.; Wittwer, M.; Spreafico, M.; Vedani, A.; Rabbani, S.; Schwarzt, O.; Ernst, B. Design, synthesis, and evaluation of monovalent ligands for the asialoglycoprotein receptor (ASGP-R), *Bioorg. Med. Chem.*, **2009**, *17*, 7254-7264.
- Mesch, S.; Moser, D.; Strasser, D. S.; Kelm, A.; Cutting, B.; Rossato, G.; Vedani, A.; Koliwer-Brandl, H.; Wittwer, M.; Rabbani, S.; Schwarzt, O.; Kelm, S.; Ernst, B. Low Molecular Weight Antagonists of the Myelin-Associated Glycoprotein: Synthesis, Docking, and Biological Evaluation *J. Med. Chem.* **2010**, *53*, 1597-1615.
- Klein, T.*; Abgottspon, D.*; Wittwer, M.*; Rabbani, S.*; Herold, J.*; Jiang, X.; Kleeb, S.; Lüthi, C.; Scharenberg, M.; Bezençon, J.; Gubler, E.; Pang, L.; Smiesko, M.; Cutting, B.; Schwarzt, O.; Ernst, B. FimH Antagonists for the Oral Treatment of Urinary Tract Infections: From Design and Synthesis to *In Vitro* and *In Vivo* Evaluation *J. Med. Chem.* **2010**, *53*, 8627-8641.
- Ernst, B.; Schwarzt, O.; Mesch, S.; Wittwer, M.; Rossato, G.; Vedani, A. From the ganglioside GQ1b α to glycomimetic antagonists of the myelin-associated glycoprotein (MAG) *Chimia*, **2010**, *64*, 17-22.
- Schwarzt, O.; Rabbani, S.; Hartmann, M.; Abgottspon, D.; Wittwer, M.; Kleeb, S.; Zalewski, A.; Smiesko, M.; Cutting, B.; Ernst, B. Design, synthesis and biological evaluation of mannosyl traizoles as FimH antagonists *Bioorg. Med. Chem.*, **2011**, *19*, 6454-6473.
- Mesch, S.; Lemme, K.; Wittwer, M.; Koliwer-Brandl, H.; Schwarzt, O.; Kelm, S.; Ernst, B. From a Library of MAG Antagonists to Nanomolar CD22 Ligands *ChemMedChem*, **2012**, *7*, 134-143.
- Jiang, X.; Abgottspon, D.; Kleeb, S.; Rabbani, S.; Scharenberg, M.; Wittwer, M.; Haug, M.; Schwarzt, O.; Ernst, B. Antiadhesion therapy for urinary tract infections – a balanced PK/PD profile proved to be key for success *J. Med. Chem.*, **2012**, *55*, 4700-4713.
- Wittwer, M.; Bezençon, J.; Cutting, B.; Wagner, B.; Kansy, M.; Ernst, B. pK_a determination by ¹H-NMR spectroscopy – An old methodology revisited *ChemMedChem*, *in preparation*.
- Wittwer, M.; Kleeb, S.; Bezençon, J.; Gubler, E.; Cutting, B.; Ernst, B. The PADMET Platform – Early Pharmacokinetic Characterization in Academia *Bioorg. Med. Chem.*, *in preparation*.
- Wittwer, M.; Smiesko, M.; Ernst, B. Sweet previsions: Modeling the permeation of carbohydrate mimetics *J. Med. Chem.*, *in preparation*.

5. Curriculum vitae

- Posters
- Wittwer, M.; Mesch, S.; Gubler, E.; Cutting, B.; Ernst, B. The PADMET Platform – Pharmacokinetic Profiling of Glycomimetics. *logP2009 Symposium*, **2009**, Zurich, Switzerland.
- Wittwer, M.; Bezençon, J.; Cutting, B.; Wagner, B.; Kansy, M.; Ernst, B. pK_a determination by $^1\text{H-NMR}$ spectroscopy – An old methodology revisited. *Swiss Pharma Science Day*, September 9th **2010**, Bern, Switzerland.
- Wittwer, M.; Kleeb, S.; Bezençon, J.; Gubler, E.; Cutting, B.; Ernst, B. PADMET Platform: Pharmacokinetic Profiling of Glycomimetics. *Swiss Pharma Science Day*, September 9th **2010**, Bern, Switzerland.
- Wittwer, M.; Smiesko, M.; Ernst, B. Sweet Previsions: Modeling the Permeation of Carbohydrate Antagonists. *Fall Meeting of the Swiss Chemical Society*, September 16th **2010**, Zurich, Switzerland
- Presentation
- Wittwer, M.; Mesch, S.; Gubler, E.; Cutting, B.; Ernst, B. The PADMET Platform. *Annual Research Meeting of the Department of Pharmaceutical Sciences*, February 13th **2009**, Basel, Switzerland
- Teaching
- Supervisor of several practical courses for pharmacy students
- Supervision of two master theses (*Simulation der intestinalen Permeation von FimH- und E-Selektin-Antagonisten mittels PAMPA und Caco-2-Assay* and *Determination of Pharmacokinetic Properties of FimH Antagonists*)
- Numerous group-internal lectures (drug discovery, analytics)
- Writing
- Course on Scientific Writing with Dr. Silvia Rogers (Mediwrite, Basel), spring semester 2009.

Awards/Fellowships

- March 2012
- Appointment for the Research Participation Program at the Center for Drug Evaluation and Research (CDER), U.S. Food and Drug Administration.
- June 2010
- Fellowship for prospective researchers (1 year), Swiss National Science Foundation.
- October 2008
- toppharm award for the best federal state examination in 2006 at the University of Basel.

6 References

6 References

1. Kerns, E. H.; Di, L. Pharmaceutical profiling in drug discovery. *Drug Discovery Today* **2003**, *8*, 316-323.
2. Prentis, R. A.; Lis, Y.; Walker, S. R. PHARMACEUTICAL INNOVATION BY THE 7 UK-OWNED PHARMACEUTICAL COMPANIES (1964-1985). *British Journal of Clinical Pharmacology* **1988**, *25*, 387-396.
3. Kennedy, T. Managing the drug discovery/development interface. *Drug Discovery Today* **1997**, *2*, 436-444.
4. van de Waterbeemd, H.; Smith, D. A.; Beaumont, K.; Walker, D. K. Property-based design: Optimization of drug absorption and pharmacokinetics. *Journal of Medicinal Chemistry* **2001**, *44*, 1313-1333.
5. Ruiz-Garcia, A.; Bermejo, M.; Moss, A.; Casabo, V. G. Pharmacokinetics in drug discovery. *J. Pharm. Sci.* **2008**, *97*, 654-690.
6. Kerns, E. H.; Di, L. *Drug-like properties : concepts, structure design and methods : from ADME to toxicity optimization*. Academic Press: Amsterdam ; London, 2008; p xix, 526 p., [2] p. of plates.
7. Horter, D.; Dressman, J. B. Influence of physicochemical properties on dissolution of drugs in the gastrointestinal tract. *Advanced Drug Delivery Reviews* **1997**, *25*, 3-14.
8. Box, K.; Bevan, C.; Comer, J.; Hill, A.; Allen, R.; Reynolds, D. High-throughput measurement of pK(a) values in a mixed-buffer linear pH gradient system. *Analyt. Chem.* **2003**, *75*, 883-892.
9. Avdeef, A. pH-metric log P. II: Refinement of partition coefficients and ionization constants of multiprotic substances. *J Pharm Sci* **1993**, *82*, 183-90.
10. Ishihama, Y.; Nakamura, M.; Miwa, T.; Kajima, T.; Asakawa, N. A rapid method for pKa determination of drugs using pressure-assisted capillary electrophoresis with photodiode array detection in drug discovery. *J Pharm Sci* **2002**, *91*, 933-42.
11. Beckers, J. L.; Everaerts, F. M.; Ackermans, M. T. Determination of absolute mobilities, PK values and separation numbers by capillary zone electrophoresis - effective mobility as a parameter for screening. *Journal of Chromatography* **1991**, *537*, 407-428.
12. Berger, S.; Braun, S.; Braun, S. a. m. b. N. M. R. e. *200 and more NMR experiments : a practical course*. [New ed.]. ed.; Wiley-VCH: Weinheim ; [Great Britain], 2004; p xv, 838 p.
13. Handloser, C. S.; Chakrabarty, M. R.; Mosher, M. W. Experimental determination of pK_a values by use of NMR chemical shift. *Journal of Chemical Education* **1973**, *50*, 510-511.
14. Szakacs, Z.; Hagele, G. Accurate determination of low pK values by H-1 NMR titration. *Talanta* **2004**, *62*, 819-825.
15. Waring, M. J. Lipophilicity in drug discovery. *Expert Opinion on Drug Discovery* **2010**, *5*, 235-248.
16. Dearden, J. C.; Bresnen, G. M. THE MEASUREMENT OF PARTITION-COEFFICIENTS. *Quantitative Structure-Activity Relationships* **1988**, *7*, 133-144.
17. Andersson, J. T.; Schrader, W. A method for measuring 1-octanol - Water partition coefficients. *Analyt. Chem.* **1999**, *71*, 3610-3614.
18. Minick, D. J.; Frenz, J. H.; Patrick, M. A.; Brent, D. A. A COMPREHENSIVE METHOD FOR DETERMINING HYDROPHOBICITY CONSTANTS BY REVERSED-PHASE HIGH-PERFORMANCE LIQUID-CHROMATOGRAPHY. *Journal of Medicinal Chemistry* **1988**, *31*, 1923-1933.
19. Plass, M.; Valko, K.; Abraham, M. H. Determination of solute descriptors of tripeptide derivatives based on high-throughput gradient high-performance liquid chromatography retention data. *Journal of Chromatography A* **1998**, *803*, 51-60.

6. References

20. Valko, K.; Plass, M.; Bevan, C.; Reynolds, D.; Abraham, M. H. Relationships between the chromatographic hydrophobicity indices and solute descriptors obtained by using several reversed-phase, diol, nitrile, cyclodextrin and immobilised artificial membrane-bonded high-performance liquid chromatography columns. *Journal of Chromatography A* **1998**, 797, 41-55.
21. Kerns, E. H.; Di, L.; Petusky, S.; Kleintop, T.; Huryn, D.; McConnell, O.; Carter, G. Pharmaceutical profiling method for lipophilicity and integrity using liquid chromatography-mass spectrometry. *Journal of Chromatography B-Analytical Technologies in the Biomedical and Life Sciences* **2003**, 791, 381-388.
22. Poole, S. K.; Durham, D.; Kibbey, C. Rapid method for estimating the octanol-water partition coefficient (log P_{ow}) by microemulsion electrokinetic chromatography. *Journal of Chromatography B-Analytical Technologies in the Biomedical and Life Sciences* **2000**, 745, 117-126.
23. Slater, B.; McCormack, A.; Avdeef, A.; Comer, J. E. A. pH-metric logP 4. Comparison of partition-coefficients determined by HPLC and potentiometric methods to literature values. *Journal of Pharmaceutical Sciences* **1994**, 83, 1280-1283.
24. Lipinski, C. A.; Lombardo, F.; Dominy, B. W.; Feeney, P. J. Experimental and computational approaches to estimate solubility and permeability in drug discovery and development settings. *Advanced Drug Delivery Reviews* **1997**, 23, 3-25.
25. Lipinski, C. A. Drug-like properties and the causes of poor solubility and poor permeability. *Journal of Pharmacological and Toxicological Methods* **2000**, 44, 235-249.
26. Kerns, E. High throughput physicochemical profiling for drug discovery. *J Pharm Sci* **2001**, 90, 1838-58.
27. Stuart, M.; Box, K. Chasing equilibrium: Measuring the intrinsic solubility of weak acids and bases. *Analytical Chemistry* **2005**, 77, 983-990.
28. Avdeef, A. High-throughput measurements of solubility profiles. *Pharmacokinetic Optimization in Drug Research* **2001**, 305-325.
29. Bevan, C. D.; Lloyd, R. S. A high-throughput screening method for the determination of aqueous drug solubility using laser nephelometry in microtiter plates. *Analytical Chemistry* **2000**, 72, 1781-1787.
30. Suomalainen, P.; Johans, C.; Soderlund, T.; Kinnunen, P. K. J. Surface activity profiling of drugs applied to the prediction of blood-brain barrier permeability. *J. Med. Chem.* **2004**, 47, 1783-1788.
31. Fischer, H.; Gottschlich, R.; Seelig, A. Blood-brain barrier permeation: Molecular parameters governing passive diffusion. *Journal of Membrane Biology* **1998**, 165, 201-211.
32. Seelig, A.; Gottschlich, R.; Devant, R. M. A METHOD TO DETERMINE THE ABILITY OF DRUGS TO DIFFUSE THROUGH THE BLOOD-BRAIN-BARRIER. *Proceedings of the National Academy of Sciences of the United States of America* **1994**, 91, 68-72.
33. Vitovic, P.; Alakoskela, J. M.; Kinnunen, P. K. J. Assessment of drug-lipid complex formation by a high-throughput Langmuir-balance and correlation to phospholipidosis. *Journal of Medicinal Chemistry* **2008**, 51, 1842-1848.
34. Lavasanifar, A.; Samuel, J.; Kwon, G. S. Poly(ethylene oxide)-block-poly(L-amino acid) micelles for drug delivery. *Advanced Drug Delivery Reviews* **2002**, 54, 169-190.
35. Wang, J.; Mongayt, D.; Torchilin, V. P. Polymeric micelles for delivery of poorly soluble drugs: Preparation and anticancer activity in vitro of paclitaxel incorporated into mixed micelles based on poly(ethylene glycol)-lipid conjugate and positively charged lipids. *Journal of Drug Targeting* **2005**, 13, 73-80.
36. Padday, J. F. TABLES OF PROFILES OF AXISYMMETRIC MENISCI. *Journal of Electroanalytical Chemistry* **1972**, 37, 313-&.

6 References

37. Padday, J. F.; Pitt, A. R.; Pashley, R. M. MENISCI AT A FREE LIQUID SURFACE - SURFACE-TENSION FROM MAXIMUM PULL ON A ROD. *Journal of the Chemical Society-Faraday Transactions I* **1975**, 71, 1919-1931.
38. Johans, C.; Palonen, I.; Suomalainen, P.; Kinnunen, P. K. J. Making surface tension measurement a practical utility for modern industrial R&D. *American Laboratory* **2005**, 37, 14-+.
39. Freud, B. B.; Freud, H. Z. A theory of the ring method for the determination of surface tension. *Science* **1930**, 71, 345-346.
40. Freud, B. B.; Freud, H. Z. A theory of the ring method for the determination of surface tension. *Journal of the American Chemical Society* **1930**, 52, 1772-1782.
41. Dominguez, A.; Fernandez, A.; Gonzalez, N.; Iglesias, E.; Montenegro, L. Determination of critical micelle concentration of some surfactants by three techniques. *Journal of Chemical Education* **1997**, 74, 1227-1231.
42. Ananthapadmanabhan, K. P.; Goddard, E. D.; Turro, N. J.; Kuo, P. L. Fluorescence probes for critical micelle concentration. *Langmuir* **1985**, 1, 352-355.
43. Posa, M.; Guzsvany, V.; Csanadi, J. Determination of critical micellar concentrations of two monoketo derivatives of cholic acid. *Colloids and Surfaces B-Biointerfaces* **2009**, 74, 84-90.
44. Giomini, M.; Giuliani, A. M.; Trotta, E.; Boicelli, C. A. The use of NMR parameters for the evaluation of the critical micelle concentration of lecithin in reverse micellar systems. *Chemical Physics Letters* **1989**, 158, 334-340.
45. Ohta, A.; Toda, K.; Morimoto, Y.; Asakawa, T.; Miyagishi, S. Effect of the side chain of N-acyl amino, acid surfactants on micelle formation: An isothermal titration calorimetry study. *Colloids and Surfaces a-Physicochemical and Engineering Aspects* **2008**, 317, 316-322.
46. Bai, G. Y.; Lopes, A.; Bastos, M. Thermodynamics of micellization of alkylimidazolium surfactants in aqueous solution. *Journal of Chemical Thermodynamics* **2008**, 40, 1509-1516.
47. Heerklotz, H.; Seelig, J. Correlation of membrane/water partition coefficients of detergents with the critical micelle concentration. *Biophysical Journal* **2000**, 78, 2435-2440.
48. Heerklotz, H.; Seelig, J. Titration calorimetry of surfactant-membrane partitioning and membrane solubilization. *Biochimica Et Biophysica Acta-Biomembranes* **2000**, 1508, 69-85.
49. Cifuentes, A.; Bernal, J. L.; DiezMasa, J. C. Determination of critical micelle concentration values using capillary electrophoresis instrumentation. *Analytical Chemistry* **1997**, 69, 4271-4274.
50. Dressman, J. B.; Thelen, K.; Jantratid, E. Towards quantitative prediction of oral drug absorption. *Clinical Pharmacokinetics* **2008**, 47, 655-667.
51. Ong, S. W.; Liu, H. L.; Qiu, X. X.; Bhat, G.; Pidgeon, C. MEMBRANE PARTITION-COEFFICIENTS CHROMATOGRAPHICALLY MEASURED USING IMMOBILIZED ARTIFICIAL MEMBRANE SURFACES. *Analytical Chemistry* **1995**, 67, 755-762.
52. Ong, S. W.; Liu, H. L.; Pidgeon, C. Immobilized-artificial-membrane chromatography: Measurements of membrane partition coefficient and predicting drug membrane permeability. *Journal of Chromatography A* **1996**, 728, 113-128.
53. Pidgeon, C.; Ong, S. W.; Liu, H. L.; Qiu, X. X.; Pidgeon, M.; Dantzig, A. H.; Munroe, J.; Hornback, W. J.; Kasher, J. S.; Glunz, L.; Szczerba, T. IAM CHROMATOGRAPHY - AN IN-VITRO SCREEN FOR PREDICTING DRUG MEMBRANE-PERMEABILITY. *Journal of Medicinal Chemistry* **1995**, 38, 590-594.
54. Pidgeon, C.; Ong, S. W. PREDICTING DRUG MEMBRANE INTERACTIONS. *Chemtech* **1995**, 25, 38-48.

6. References

55. Valko, K.; Du, C. M.; Bevan, C. D.; Reynolds, D. P.; Abraham, M. H. Rapid-gradient HPLC method for measuring drug interactions with immobilized artificial membrane: Comparison with other lipophilicity measures. *Journal of Pharmaceutical Sciences* **2000**, *89*, 1085-1096.
56. Kansy, M.; Senner, F.; Gubernator, K. Physicochemical high throughput screening: Parallel artificial membrane permeation assay in the description of passive absorption processes. *J. Med. Chem.* **1998**, *41*, 1007-1010.
57. Avdeef, A. *Absorption and drug development : solubility, permeability, and charge state*. Wiley-Interscience: Hoboken, N.J. ; [Great Britain], 2003; p xxiv, 287 p.
58. Avdeef, A.; Bendels, S.; Di, L.; Faller, B.; Kansy, M.; Sugano, K.; Yamauchi, Y. PAMPA - Critical factors for better predictions of absorption. *J. Pharm. Sci.* **2007**, *96*, 2893-2909.
59. Kansy, M.; Avdeef, A.; Fischer, H. Advances in screening for membrane permeability: high-resolution PAMPA for medicinal chemists. *Drug. Discov. Today*. **2004**, *1*, 349-355.
60. Gan, L. S. L.; Thakker, D. R. Applications of the Caco-2 model in the design and development of orally active drugs: Elucidation of biochemical and physical barriers posed by the intestinal epithelium. *Advanced Drug Delivery Reviews* **1997**, *23*, 77-98.
61. Artursson, P.; Karlsson, J. CORRELATION BETWEEN ORAL-DRUG ABSORPTION IN HUMANS AND APPARENT DRUG PERMEABILITY COEFFICIENTS IN HUMAN INTESTINAL EPITHELIAL (CACO-2) CELLS. *Biochem. Biophys. Res. Commun.* **1991**, *175*, 880-885.
62. Hubatsch, I.; Ragnarsson, E. G. E.; Artursson, P. Determination of drug permeability and prediction of drug absorption in Caco-2 monolayers. *Nat. Protoc.* **2007**, *2*, 2111-2119.
63. Hidalgo, I. J. Assessing the absorption of new pharmaceuticals. *Current Topics in Medicinal Chemistry* **2001**, *1*, 385-401.
64. Irvine, J. D.; Takahashi, L.; Lockhart, K.; Cheong, J.; Tolan, J. W.; Selick, H. E.; Grove, J. R. MDCK (Madin-Darby canine kidney) cells: A tool for membrane permeability screening. *Journal of Pharmaceutical Sciences* **1999**, *88*, 28-33.
65. Kerns, E.; Di, L.; Petusky, S.; Farris, M.; Ley, R.; Jupp, P. Combined application of parallel artificial membrane permeability assay and Caco-2 permeability assays in drug discovery. *J Pharm Sci* **2004**, *93*, 1440-53.
66. Tetko, I. V.; Poda, G. I. Application of ALOGPS 2.1 to predict log D distribution coefficient for Pfizer proprietary compounds. *Journal of Medicinal Chemistry* **2004**, *47*, 5601-5604.
67. Lobell, M.; Sivarajah, V. In silico prediction of aqueous solubility, human plasma protein binding and volume of distribution of compounds from calculated pK(a) and AlogP98 values. *Molecular Diversity* **2003**, *7*, 69-87.
68. Lombardo, F.; Obach, R. S.; Shalaeva, M. Y.; Gao, F. Prediction of volume of distribution values in humans for neutral and basic drugs using physicochemical measurements and plasma protein binding data. *Journal of Medicinal Chemistry* **2002**, *45*, 2867-2876.
69. Trainor, G. L. Plasma Protein Binding and the Free Drug Principle: Recent Developments and Applications. *Annual Reports in Medicinal Chemistry, Vol 42* **2007**, *42*, 489-502.
70. Trainor, G. L. The importance of plasma protein binding in drug discovery. *Expert Opinion on Drug Discovery* **2007**, *2*, 51-64.
71. Banker, M. J.; Clark, T. H.; Williams, J. A. Development and validation of a 96-well equilibrium dialysis apparatus for measuring plasma protein binding. *Journal of Pharmaceutical Sciences* **2003**, *92*, 967-974.
72. Kariv, I.; Cao, H.; Oldenburg, K. R. Development of a high throughput equilibrium dialysis method. *Journal of Pharmaceutical Sciences* **2001**, *90*, 580-587.

6 References

73. Talbert, A. M.; Tranter, G. E.; Holmes, E.; Francis, P. L. Determination of drug-plasma protein binding kinetics and equilibria by chromatographic profiling: Exemplification of the method using L-tryptophan and albumin. *Analytical Chemistry* **2002**, 74, 446-452.
74. Weisiger, R. A. DISSOCIATION FROM ALBUMIN - A POTENTIALLY RATE-LIMITING STEP IN THE CLEARANCE OF SUBSTANCES BY THE LIVER. *Proceedings of the National Academy of Sciences of the United States of America* **1985**, 82, 1563-1567.
75. Robinson, P. J.; Rapoport, S. I. KINETICS OF PROTEIN-BINDING DETERMINE RATES OF UPTAKE OF DRUGS BY BRAIN. *American Journal of Physiology* **1986**, 251, R1212-R1220.
76. Venkatakrishnan, K.; von Moltke, L. L.; Obach, R. S.; Greenblatt, D. J. Drug metabolism and drug interactions: Application and clinical value of in vitro models. *Current Drug Metabolism* **2003**, 4, 423-459.
77. Wermuth, C. G. *The practice of medicinal chemistry*. 2nd ed. ed.; Academic: Amsterdam ; London, 2003; p xiv, 768 p., [8] p. of plates.
78. Obach, R. S.; Baxter, J. G.; Liston, T. E.; Silber, B. M.; Jones, B. C.; MacIntyre, F.; Rance, D. J.; Wastall, P. The prediction of human pharmacokinetic parameters from preclinical and in vitro metabolism data. *Journal of Pharmacology and Experimental Therapeutics* **1997**, 283, 46-58.
79. Mohutsky, M. A.; Chien, J. Y.; Ring, B. J.; Wrighton, S. A. Predictions of the in vivo clearance of drugs from rate of loss using human liver microsomes for phase I and phase II biotransformations. *Pharmaceutical Research* **2006**, 23, 654-662.
80. Li, A. P. Screening for human ADME/Tox drug properties in drug discovery. *Drug Discovery Today* **2001**, 6, 357-366.
81. Gomez-Lechon, M. J.; Donato, M. T.; Castell, J. V.; Jover, R. Human Hepatocytes in primary culture: The choice to investigate drug metabolism in man. *Current Drug Metabolism* **2004**, 5, 443-462.
82. Gebhardt, R.; Hengstler, J. G.; Muller, D.; Glockner, R.; Buenning, P.; Laube, B.; Schmelzer, E.; Ullrich, M.; Utesch, D.; Hewitt, N.; Ringel, M.; Hilz, B. R.; Bader, A.; Langsch, A.; Koose, T.; Burger, H. J.; Maas, J.; Oesch, F. New hepatocyte in vitro systems for drug metabolism: Metabolic capacity and recommendations for application in basic research and drug development, standard operation procedures. *Drug Metabolism Reviews* **2003**, 35, 145-213.
83. Lu, C.; Miwa, G. T.; Prakash, S.; Balani, S. K. A novel model for the prediction of drug-drug interactions in humans based on in vitro CYP phenotypic data. *Drug Metabolism Reviews* **2006**, 38, 157.
84. Haraldsson, B.; Jeansson, M. Glomerular filtration barrier. *Current Opinion in Nephrology and Hypertension* **2009**, 18, 331-335.
85. Zhang, Y.; Bachmeier, C.; Miller, D. In vitro and in vivo models for assessing drug efflux transporter activity. *Adv Drug Deliv Rev* **2003**, 55, 31-51.
86. Kerns, E.; Hill, S.; Detlefsen, D.; Volk, K.; Long, B.; Carboni, J.; Lee, M. Cellular uptake profile of paclitaxel using liquid chromatography tandem mass spectrometry. *Rapid Commun Mass Spectrom* **1998**, 12, 620-4.
87. Tamai, I.; Tomizawa, N.; Kadowaki, A.; Terasaki, T.; Nakayama, K.; Higashida, H.; Tsuji, A. Functional expression of intestinal dipeptide/beta-lactam antibiotic transporter in *Xenopus laevis* oocytes. *Biochem Pharmacol* **1994**, 48, 881-8.
88. Glavinas, H.; Krajcsi, P.; Cserepes, J.; Sarkadi, B. The role of ABC transporters in drug resistance, metabolism and toxicity. *Curr Drug Deliv* **2004**, 1, 27-42.
89. Polli, J.; Wring, S.; Humphreys, J.; Huang, L.; Morgan, J.; Webster, L.; Serabjit-Singh, C. Rational use of in vitro P-glycoprotein assays in drug discovery. *J Pharmacol Exp Ther* **2001**, 299, 620-8.

6. References

90. Schuster, D.; Laggner, C.; Langer, T. Why drugs fail--a study on side effects in new chemical entities. *Curr Pharm Des* **2005**, *11*, 3545-59.
91. Sanguinetti, M.; Mitcheson, J. Predicting drug-hERG channel interactions that cause acquired long QT syndrome. *Trends Pharmacol Sci* **2005**, *26*, 119-24.
92. Honig, P.; Wortham, D.; Zamani, K.; Conner, D.; Mullin, J.; Cantilena, L. Terfenadine-ketoconazole interaction. Pharmacokinetic and electrocardiographic consequences. *JAMA* **1993**, *269*, 1513-8.
93. Dorn, A.; Hermann, F.; Ebneith, A.; Bothmann, H.; Trube, G.; Christensen, K.; Apfel, C. Evaluation of a high-throughput fluorescence assay method for HERG potassium channel inhibition. *J Biomol Screen* **2005**, *10*, 339-47.
94. Finlayson, K.; Turnbull, L.; January, C.; Sharkey, J.; Kelly, J. [3H]dofetilide binding to HERG transfected membranes: a potential high throughput preclinical screen. *Eur J Pharmacol* **2001**, *430*, 147-8.
95. Rezazadeh, S.; Hesketh, J.; Fedida, D. Rb⁺ flux through hERG channels affects the potency of channel blocking drugs: correlation with data obtained using a high-throughput Rb⁺ efflux assay. *J Biomol Screen* **2004**, *9*, 588-97.
96. Wood, C.; Williams, C.; Waldron, G. Patch clamping by numbers. *Drug Discov Today* **2004**, *9*, 434-41.
97. Fenech, M. The cytokinesis-block micronucleus technique and its application to genotoxicity studies in human populations. *Environ Health Perspect* **1993**, *101* Suppl 3, 101-7.
98. Tice, R.; Hayashi, M.; MacGregor, J.; Anderson, D.; Blakey, D.; Holden, H.; Kirsch-Volders, M.; Oleson, F. J.; Pacchierotti, F.; Preston, R. Report from the working group on the in vivo mammalian bone marrow chromosomal aberration test. *Mutat Res* **1994**, *312*, 305-12.
99. Tice, R.; Agurell, E.; Anderson, D.; Burlinson, B.; Hartmann, A.; Kobayashi, H.; Miyamae, Y.; Rojas, E.; Ryu, J.; Sasaki, Y. Single cell gel/comet assay: guidelines for in vitro and in vivo genetic toxicology testing. *Environ Mol Mutagen* **2000**, *35*, 206-21.
100. Ames, B. N.; Lee, F. D.; Durston, W. E. IMPROVED BACTERIAL TEST SYSTEM FOR DETECTION AND CLASSIFICATION OF MUTAGENS AND CARCINOGENS. *Proceedings of the National Academy of Sciences of the United States of America* **1973**, *70*, 782-786.
101. Clive, D.; Spector, J. Laboratory procedure for assessing specific locus mutations at the TK locus in cultured L5178Y mouse lymphoma cells. *Mutat Res* **1975**, *31*, 17-29.
102. Hastwell, P.; Chai, L.; Roberts, K.; Webster, T.; Harvey, J.; Rees, R.; Walmsley, R. High-specificity and high-sensitivity genotoxicity assessment in a human cell line: validation of the GreenScreen HC GADD45a-GFP genotoxicity assay. *Mutat Res* **2006**, *607*, 160-75.
103. Mosmann, T. Rapid colorimetric assay for cellular growth and survival: application to proliferation and cytotoxicity assays. *J Immunol Methods* **1983**, *65*, 55-63.
104. Zhang, S.; Lipsky, M.; Trump, B.; Hsu, I. Neutral red (NR) assay for cell viability and xenobiotic-induced cytotoxicity in primary cultures of human and rat hepatocytes. *Cell Biol Toxicol* **1990**, *6*, 219-34.
105. Decker, T.; Lohmann-Matthes, M. A quick and simple method for the quantitation of lactate dehydrogenase release in measurements of cellular cytotoxicity and tumor necrosis factor (TNF) activity. *J Immunol Methods* **1988**, *115*, 61-9.
106. Chen, W.; Zhang, C.; Avery, M.; Fouda, H. Reactive metabolite screen for reducing candidate attrition in drug discovery. *Adv Exp Med Biol* **2001**, *500*, 521-4.
107. Kola, I.; Landis, J. Can the pharmaceutical industry reduce attrition rates? *Nature Reviews Drug Discovery* **2004**, *3*, 711-715.
108. Balbach, S.; Korn, C. Pharmaceutical evaluation of early development candidates "the 100 mg-approach". *International Journal of Pharmaceutics* **2004**, *275*, 1-12.

6 References

109. van de Waterbeemd, H. Improving Compound Quality through in vitro and in silico Physicochemical Profiling. *Chemistry & Biodiversity* **2009**, 6, 1760-1766.
110. van de Waterbeemd, H.; Smith, D. A.; Beaumont, K.; Walker, D. K. Property-based design: Optimization of drug absorption and pharmacokinetics. *J. Med. Chem.* **2001**, 44, 1313-1333.
111. Yu, H. S.; Adedoyin, A. ADME-Tox in drug discovery: integration of experimental and computational technologies. *Drug Discovery Today* **2003**, 8, 852-861.
112. Ernst, B.; Magnani, J. L. From carbohydrate leads to glycomimetic drugs. *Nature Reviews Drug Discovery* **2009**, 8, 661-677.
113. VanTeeffelen, J. W.; Brands, J.; Stroes, E. S.; Vink, H. Endothelial glycocalyx: Sweet shield of blood vessels. *Trends in Cardiovascular Medicine* **2007**, 17, 101-105.
114. Petitou, M.; van Boeckel, C. A. A. A synthetic antithrombin III binding pentasaccharide is now a drug! What comes next? *Angewandte Chemie-International Edition* **2004**, 43, 3118-3133.
115. Weitz, J. Low-molecular-weight heparins. *N Engl J Med* **1997**, 337, 688-98.
116. Chen, X.; Zheng, Y.; Shen, Y. Voglibose (Basen, AO-128), one of the most important alpha-glucosidase inhibitors. *Curr Med Chem* **2006**, 13, 109-16.
117. Campbell, L.; Baker, D.; Campbell, R. Miglitol: assessment of its role in the treatment of patients with diabetes mellitus. *Ann Pharmacother* **2000**, 34, 1291-301.
118. Truscheit, E.; Frommer, W.; Junge, B.; Muller, L.; Schmidt, D. D.; Wingender, W. CHEMISTRY AND BIOCHEMISTRY OF MICROBIAL ALPHA-GLUCOSIDASE INHIBITORS. *Angewandte Chemie-International Edition in English* **1981**, 20, 744-761.
119. Maryanoff, B.; Nortey, S.; Gardocki, J.; Shank, R.; Dodgson, S. Anticonvulsant O-alkyl sulfamates. 2,3:4,5-Bis-O-(1-methylethylidene)-beta-D-fructopyranose sulfamate and related compounds. *J Med Chem* **1987**, 30, 880-7.
120. Li, X.; Shah, A.; Franklin, P.; Merolli, R.; Bradley, J.; Busconi, B. Arthroscopic debridement of the osteoarthritic knee combined with hyaluronic acid (Orthovisc) treatment: a case series and review of the literature. *J Orthop Surg Res* **2008**, 3, 43.
121. Weinreb, N.; Barranger, J.; Charrow, J.; Grabowski, G.; Mankin, H.; Mistry, P. Guidance on the use of miglustat for treating patients with type 1 Gaucher disease. *Am J Hematol* **2005**, 80, 223-9.
122. Vonitzstein, M.; Wu, W. Y.; Kok, G. B.; Pegg, M. S.; Dyason, J. C.; Jin, B.; Phan, T. V.; Smythe, M. L.; White, H. F.; Oliver, S. W.; Colman, P. M.; Varghese, J. N.; Ryan, D. M.; Woods, J. M.; Bethell, R. C.; Hotham, V. J.; Cameron, J. M.; Penn, C. R. RATIONAL DESIGN OF POTENT SIALIDASE-BASED INHIBITORS OF INFLUENZA-VIRUS REPLICATION. *Nature* **1993**, 363, 418-423.
123. Kim, C.; Lew, W.; Williams, M.; Liu, H.; Zhang, L.; Swaminathan, S.; Bischofberger, N.; Chen, M.; Mendel, D.; Tai, C.; Laver, W.; Stevens, R. Influenza neuraminidase inhibitors possessing a novel hydrophobic interaction in the enzyme active site: design, synthesis, and structural analysis of carbocyclic sialic acid analogues with potent anti-influenza activity. *J Am Chem Soc* **1997**, 119, 681-90.
124. Mulloy, B.; Linhardt, R. Order out of complexity--protein structures that interact with heparin. *Curr Opin Struct Biol* **2001**, 11, 623-8.
125. Esko, J.; Selleck, S. Order out of chaos: assembly of ligand binding sites in heparan sulfate. *Annu Rev Biochem* **2002**, 71, 435-71.
126. Bevilacqua, M. P.; Stengelin, S.; Gimbrone, M. A.; Seed, B. ENDOTHELIAL LEUKOCYTE ADHESION MOLECULE-1 - AN INDUCIBLE RECEPTOR FOR NEUTROPHILS RELATED TO COMPLEMENT REGULATORY PROTEINS AND LECTINS. *Science* **1989**, 243, 1160-1165.
127. Tedder, T. F.; Isaacs, C. M.; Ernst, T. J.; Demetri, G. D.; Adler, D. A.; Distech, C. M. ISOLATION AND CHROMOSOMAL LOCALIZATION OF CDNAS ENCODING A

6. References

- NOVEL HUMAN-LYMPHOCYTE CELL-SURFACE MOLECULE, LAM-1 - HOMOLGY WITH THE MOUSE LYMPHOCYTE HOMING RECEPTOR AND OTHER HUMAN ADHESION PROTEINS. *Journal of Experimental Medicine* **1989**, 170, 123-133.
128. Johnston, G. I.; Cook, R. G.; McEver, R. P. CLONING OF GMP-140, A GRANULE MEMBRANE-PROTEIN OF PLATELETS AND ENDOTHELIUM - SEQUENCE SIMILARITY TO PROTEINS INVOLVED IN CELL-ADHESION AND INFLAMMATION. *Cell* **1989**, 56, 1033-1044.
129. Barthel, S. R.; Gavino, J. D.; Descheny, L.; Dimitroff, C. J. Targeting selectins and selectin ligands in inflammation and cancer. *Expert Opinion on Therapeutic Targets* **2007**, 11, 1473-1491.
130. Berg, E. L.; Robinson, M. K.; Mansson, O.; Butcher, E. C.; Magnani, J. L. A CARBOHYDRATE DOMAIN COMMON TO BOTH SIALYL LE(A) AND SIALYL LE(X) IS RECOGNIZED BY THE ENDOTHELIAL-CELL LEUKOCYTE ADHESION MOLECULE ELAM-1. *Journal of Biological Chemistry* **1991**, 266, 14869-14872.
131. Hidalgo, A.; Chang, J. S.; Jang, J. E.; Peired, A. J.; Chiang, E. Y.; Frenette, P. S. Heterotypic interactions enabled by polarized neutrophil microdomains mediate thromboinflammatory injury. *Nature Medicine* **2009**, 15, 384-391.
132. Turhan, A.; Weiss, L. A.; Mohandas, N.; Collier, B. S.; Frenette, P. S. Primary role for adherent leukocytes in sickle cell vascular occlusion: A new paradigm. *Proceedings of the National Academy of Sciences of the United States of America* **2002**, 99, 3047-3051.
133. Hanley, W. D.; Burdick, M. M.; Konstantopoulos, K.; Sackstein, R. CD44 on LS174T colon carcinoma cells possesses E-selectin ligand activity. *Cancer Research* **2005**, 65, 5812-5817.
134. Iwai, K.; Ishikura, H.; Kaji, M.; Sugiura, H.; Ishizu, A.; Takahashi, C.; Kato, H.; Tanabe, T.; Yoshiki, T. IMPORTANCE OF E-SELECTIN (ELAM-1) AND SIALYL LEWIS(A) IN THE ADHESION OF PANCREATIC-CARCINOMA CELLS TO ACTIVATED ENDOTHELIUM. *International Journal of Cancer* **1993**, 54, 972-977.
135. Jeschke, U.; Mylonas, I.; Shabani, N.; Kunert-Keil, C.; Schindlbeck, C.; Gerber, B.; Friese, K. Expression of Sialyl Lewis X, Sialyl Lewis a, E-cadherin and cathepsin-D in human breast cancer: Immunohistochemical analysis in mammary carcinoma in situ, invasive carcinomas and their lymph node metastasis. *Anticancer Research* **2005**, 25, 1615-1622.
136. Inata, J.; Hattori, N.; Yokoyama, A.; Ohshimo, S.; Doi, M.; Ishikawa, N.; Hamada, H.; Kohno, N. Circulating KL-6/MUC1 mucin carrying sialyl Lewis(a) oligosaccharide is an independent prognostic factor in patients with lung adenocarcinoma. *International Journal of Cancer* **2007**, 120, 2643-2649.
137. Dimitroff, C. J.; Descheny, L.; Trujillo, N.; Kim, R.; Nguyen, V.; Huang, W.; Pienta, K. J.; Kutok, J. L.; Rubin, M. A. Identification of leukocyte E-selectin ligands, P-selectin glycoprotein ligand-1 and E-selectin ligand-1, on human metastatic prostate tumor cells. *Cancer Research* **2005**, 65, 5750-5760.
138. Magnani, J. L.; Nilsson, B.; Brockhaus, M.; Zopf, D.; Steplewski, Z.; Koprowski, H.; Ginsburg, V. A MONOCLONAL-ANTIBODY DEFINED ANTIGEN ASSOCIATED WITH GASTROINTESTINAL CANCER IS A GANGLIOSIDE CONTAINING SIALYLATED LACTO-N-FUCOPENTAPOSE-II. *Journal of Biological Chemistry* **1982**, 257, 4365-4369.
139. Ziske, C.; Schlie, C.; Gorschluter, M.; Glasmacher, A.; Mey, U.; Strehl, J.; Sauerbruch, T.; Schmidt-Wolf, I. G. H. Prognostic value of CA 19-9 levels in patients with inoperable adenocarcinoma of the pancreas treated with gemcitabine. *British Journal of Cancer* **2003**, 89, 1413-1417.

6 References

140. Noguchi, M.; Sato, N.; Sugimori, H.; Mori, K.; Oshimi, K. A minor E-selectin ligand, CD65, is critical for extravascular infiltration of acute myeloid leukemia cells. *Leukemia Research* **2001**, *25*, 847-853.
141. Krause, D. S.; Lazarides, K.; von Andrian, U. H.; Van Etten, R. A. Requirement for CD44 in homing and engraftment of BCR-ABL-expressing leukemic stem cells. *Nature Medicine* **2006**, *12*, 1175-1180.
142. Kogan, T. P.; Dupre, B.; Bui, H.; McAbee, K. L.; Kassir, J. M.; Scott, I. L.; Hu, X.; Vanderslice, P.; Beck, P. J.; Dixon, R. A. F. Novel synthetic inhibitors of selectin-mediated cell adhesion: Synthesis of 1,6-bis 3-(3-carboxymethylphenyl)-4-(2- α -D-mannopyranosyloxy)phenyl hexane (TBC1269). *Journal of Medicinal Chemistry* **1998**, *41*, 1099-1111.
143. Magnani, J. L.; Patton, J. T.; Sarkar, A. K.; Svarovsky, S. A.; Ernst, B. Heterobifunctional panselectin inhibitors. 2006.
144. Kaila, N.; Janz, K.; Huang, A.; Moretto, A.; DeBernardo, S.; Bedard, P. W.; Tam, S.; Clerin, V.; Keith, J. C.; Tsao, D. H. H.; Sushkova, N.; Shaw, G. D.; Camphausen, R. T.; Schaub, R. G.; Wang, Q. 2-(4-chlorobenzyl)-3-hydroxy-7,8,9,10-tetrahydrobenzo H quinoline-4-carb oxylic acid (PSI-697): Identification of a clinical candidate from the quinoline salicylic acid series of P-selectin antagonists. *Journal of Medicinal Chemistry* **2007**, *50*, 40-64.
145. Crocker, P. R.; Paulson, J. C.; Varki, A. Siglecs and their roles in the immune system. *Nature Reviews Immunology* **2007**, *7*, 255-266.
146. Kelm, S.; Pelz, A.; Schauer, R.; Filbin, M. T.; Tang, S.; Debellard, M. E.; Schnaar, R. L.; Mahoney, J. A.; Hartnell, A.; Bradfield, P.; Crocker, P. R. SIALOADHESIN, MYELIN-ASSOCIATED GLYCOPROTEIN AND CD22 DEFINE A NEW FAMILY OF SIALIC ACID-DEPENDENT ADHESION MOLECULES OF THE IMMUNOGLOBULIN SUPERFAMILY. *Current Biology* **1994**, *4*, 965-972.
147. Chen, M. S.; Huber, A. B.; van der Haar, M. E.; Frank, M.; Schnell, L.; Spillmann, A. A.; Christ, F.; Schwab, M. E. Nogo-A is a myelin-associated neurite outgrowth inhibitor and an antigen for monoclonal antibody IN-1. *Nature* **2000**, *403*, 434-439.
148. Wang, K. C.; Koprivica, V.; Kim, J. A.; Sivasankaran, R.; Guo, Y.; Neve, R. L.; He, Z. G. Oligodendrocyte-myelin glycoprotein is a Nogo receptor ligand that inhibits neurite outgrowth. *Nature* **2002**, *417*, 941-944.
149. Mukhopadhyay, G.; Doherty, P.; Walsh, F. S.; Crocker, P. R.; Filbin, M. T. A NOVEL ROLE FOR MYELIN-ASSOCIATED GLYCOPROTEIN AS AN INHIBITOR OF AXONAL REGENERATION. *Neuron* **1994**, *13*, 757-767.
150. Filbin, M. T. Myelin-associated inhibitors of axonal regeneration in the adult mammalian CNS. *Nature Reviews Neuroscience* **2003**, *4*, 703-713.
151. Vyas, A. A.; Blixt, O.; Paulson, J. C.; Schnaar, R. L. Potent glycan inhibitors of myelin-associated glycoprotein enhance axon outgrowth in vitro. *Journal of Biological Chemistry* **2005**, *280*, 16305-16310.
152. Ito, H.; Ishida, H.; Collins, B. E.; Fromholt, S. E.; Schnaar, R. L.; Kiso, M. Synthetic studies on sialoglycoconjugates, part 130. Systematic synthesis and MAG-binding activity of novel sulfated GM1b analogues as mimics of Chol-1 (α -series) gangliosides: highly active ligands for neural siglecs. *Carbohydrate Research* **2003**, *338*, 1621-1639.
153. Schwizer, D.; Gathje, H.; Kelm, S.; Porro, M.; Schwardt, O.; Ernst, B. Antagonists of the myelin-associated glycoprotein: A new class of tetrasaccharide mimics. *Bioorganic & Medicinal Chemistry* **2006**, *14*, 4944-4957.
154. Kelm, S.; Brossmer, R.; Isecke, R.; Gross, H. J.; Streng, K.; Schauer, R. Functional groups of sialic acids involved in binding to siglecs (sialoadhesins) deduced from

6. References

- interactions with synthetic analogues. *European Journal of Biochemistry* **1998**, 255, 663-672.
155. Shelke, S. V.; Gao, G. P.; Mesch, S.; Gathje, H.; Kelm, S.; Schwardt, O.; Ernst, B. Synthesis of sialic acid derivatives as ligands for the myelin-associated glycoprotein (MAG). *Bioorganic & Medicinal Chemistry* **2007**, 15, 4951-4965.
156. Gao, G.; Smiesko, M.; Schwardt, O.; Gathje, H.; Kelm, S.; Vedani, A.; Ernst, B. Mimetics of the tri- and tetrasaccharide epitope of GQ1b alpha as myelin-associated glycoprotein (MAG) ligands. *Bioorganic & Medicinal Chemistry* **2007**, 15, 7459-7469.
157. Mesch, S.; Moser, D.; Strasser, D. S.; Kelm, A.; Cutting, B.; Rossato, G.; Vedani, A.; Koliwer-Brandl, H.; Wittwer, M.; Rabbani, S.; Schwardt, O.; Kelm, S.; Ernst, B. Low Molecular Weight Antagonists of the Myelin-Associated Glycoprotein: Synthesis, Docking, and Biological Evaluation. *Journal of Medicinal Chemistry* **2010**, 53, 1597-1615.
158. Ofek, I.; Hasy, D. L.; Sharon, N. Anti-adhesion therapy of bacterial diseases: prospects and problems. *Fems Immunology and Medical Microbiology* **2003**, 38, 181-191.
159. Levy, S. B. Antibiotic resistance - the problem intensifies. *Advanced Drug Delivery Reviews* **2005**, 57, 1446-1450.
160. Fihn, S. D. Acute uncomplicated urinary tract infection in women (vol 349, pg 259, 2003). *New England Journal of Medicine* **2003**, 349, 1675-1676.
161. Mak, R. H.; Kuo, H. J. Pathogenesis of urinary tract infection: An update. *Current Opinion in Pediatrics* **2006**, 18, 148-152.
162. Palmer, L. M.; Reilly, T. J.; Utsalo, S. J.; Donnenberg, M. S. Internalization of Escherichia coli by human renal epithelial cells is associated with tyrosine phosphorylation of specific host cell proteins. *Infection and Immunity* **1997**, 65, 2570-2575.
163. Sharon, N. Carbohydrates as future anti-adhesion drugs for infectious diseases. *Biochimica Et Biophysica Acta-General Subjects* **2006**, 1760, 527-537.
164. Hung, C. S.; Bouckaert, J.; Hung, D.; Pinkner, J.; Widberg, C.; DeFusco, A.; Auguste, C. G.; Strouse, R.; Langermann, S.; Waksman, G.; Hultgren, S. J. Structural basis of tropism of Escherichia coli to the bladder during urinary tract infection. *Mol. Microbiol.* **2002**, 44, 903-915.
165. Firon, N.; Ofek, I.; Sharon, N. INTERACTION OF MANNOSE-CONTAINING OLIGOSACCHARIDES WITH THE FIMBRIAL LECTIN OF ESCHERICHIA-COLI. *Biochemical and Biophysical Research Communications* **1982**, 105, 1426-1432.
166. Firon, N.; Ashkenazi, S.; Mirelman, D.; Ofek, I.; Sharon, N. AROMATIC ALPHA-GLYCOSIDES OF MANNOSE ARE POWERFUL INHIBITORS OF THE ADHERENCE OF TYPE-1 FIMBRIATED ESCHERICHIA-COLI TO YEAST AND INTESTINAL EPITHELIAL-CELLS. *Infection and Immunity* **1987**, 55, 472-476.
167. Choudhury, D.; Thompson, A.; Stojanoff, V.; Langermann, S.; Pinkner, J.; Hultgren, S. J.; Knight, S. D. X-ray structure of the FimC-FimH chaperone-adhesin complex from uropathogenic Escherichia coli. *Science* **1999**, 285, 1061-1066.
168. Wellens, A.; Garofalo, C.; Nguyen, H.; Van Gerven, N.; Slattegard, R.; Hernalsteens, J. P.; Wyns, L.; Oscarson, S.; De Greve, H.; Hultgren, S.; Bouckaert, J. Intervening with Urinary Tract Infections Using Anti-Adhesives Based on the Crystal Structure of the FimH-Oligomannose-3 Complex. *Plos One* **2008**, 3.
169. Imberty, A.; Chabre, Y. M.; Roy, R. Glycomimetics and glycodendrimers as high affinity microbial anti-adhesins. *Chemistry-a European Journal* **2008**, 14, 7490-7499.
170. Sperling, O.; Fuchs, A.; Lindhorst, T. K. Evaluation of the carbohydrate recognition domain of the bacterial adhesin FimH: design, synthesis and binding properties of mannoside ligands. *Organic & Biomolecular Chemistry* **2006**, 4, 3913-3922.

6 References

171. Bouckaert, J.; Berglund, J.; Schembri, M.; De Genst, E.; Cools, L.; Wuhrer, M.; Hung, C. S.; Pinkner, J.; Slattegard, R.; Zavialov, A.; Choudhury, D.; Langermann, S.; Hultgren, S. J.; Wyns, L.; Klemm, P.; Oscarson, S.; Knight, S. D.; De Greve, H. Receptor binding studies disclose a novel class of high-affinity inhibitors of the Escherichia coli FimH adhesin. *Molecular Microbiology* **2005**, *55*, 441-455.
172. Thoma, G.; Magnani, J. L.; Patton, J. T.; Ernst, B.; Jahnke, W. Preorganization of the bioactive conformation of sialyl Lewis(X) analogues correlates with their affinity to E-selectin. *Angewandte Chemie-International Edition* **2001**, *40*, 1941-1945.
173. Mayer, M.; Meyer, B. Characterization of ligand binding by saturation transfer difference NMR spectroscopy. *Angewandte Chemie-International Edition* **1999**, *38*, 1784-1788.
174. Somers, W. S.; Tang, J.; Shaw, G. D.; Camphausen, R. T. Insights into the molecular basis of leukocyte tethering and rolling revealed by structures of P- and E-selectin bound to SLe(X) and PSGL-1. *Cell* **2000**, *103*, 467-479.
175. Haselhorst, T.; Blanchard, H.; Frank, M.; Kraschnefski, M. J.; Kiefel, M. J.; Szyzew, A. J.; Dyason, J. C.; Fleming, F.; Holloway, G.; Coulson, B. S.; von Itzstein, M. STD NMR spectroscopy and molecular modeling investigation of the binding of N-acetylneuraminic acid derivatives to rhesus rotavirus VP8*core. *Glycobiology* **2007**, *17*, 68-81.
176. Herfurth, L.; Ernst, B.; Wagner, B.; Ricklin, D.; Strasser, D. S.; Magnani, J. L.; Benie, A. J.; Peters, T. Comparative epitope mapping with saturation transfer difference NMR of sialyl Lewis(a) compounds and derivatives bound to a monoclonal antibody. *Journal of Medicinal Chemistry* **2005**, *48*, 6879-6886.
177. Rinnbauer, M.; Ernst, B.; Wagner, B.; Magnani, J.; Benie, A. J.; Peters, T. Epitope mapping of sialyl Lewis(x) bound to E-selectin using saturation transfer difference NMR experiments. *Glycobiology* **2003**, *13*, 435-443.
178. Schwardt, O.; Gathje, H.; Vedani, A.; Mesch, S.; Gao, G. P.; Spreafico, M.; von Orelli, J.; Kelm, S.; Ernst, B. Examination of the Biological Role of the alpha(2 -> 6)-Linked Sialic Acid in Gangliosides Binding to the Myelin-Associated Glycoprotein (MAG). *Journal of Medicinal Chemistry* **2009**, *52*, 989-1004.
179. Egan, W. J.; Lauri, G. Prediction of intestinal permeability. *Advanced Drug Delivery Reviews* **2002**, *54*, 273-289.
180. Winiwarter, S.; Ax, F.; Lennernas, H.; Hallberg, A.; Pettersson, C.; Karlen, A. Hydrogen bonding descriptors in the prediction of human in vivo intestinal permeability. *Journal of Molecular Graphics & Modelling* **2003**, *21*, 273-287.
181. Du Plessis, J.; Pugh, W. J.; Judefeind, A.; Hadgraft, J. The effect of hydrogen bonding on diffusion across model membranes: consideration of the number of H-bonding groups. *European Journal of Pharmaceutical Sciences* **2001**, *13*, 135-141.
182. Tulp, I.; Sild, S.; Maran, U. Relationship Between Structure and Permeability in Artificial Membranes: Theoretical Whole Molecule Descriptors in Development of QSAR Models. *Qsar & Combinatorial Science* **2009**, *28*, 811-814.
183. Ano, R.; Kimura, Y.; Shima, M.; Matsuno, R.; Ueno, T.; Akamatsu, M. Relationships between structure and high-throughput screening permeability of peptide derivatives and related compounds with artificial membranes: application to prediction of Caco-2 cell permeability. *Bioorganic & Medicinal Chemistry* **2004**, *12*, 257-264.
184. Winiwarter, S.; Bonham, N. M.; Ax, F.; Hallberg, A.; Lennernas, H.; Karlen, A. Correlation of human jejunal permeability (in vivo) of drugs with experimentally and theoretically derived parameters. A multivariate data analysis approach. *Journal of Medicinal Chemistry* **1998**, *41*, 4939-4949.
185. Palm, K.; Stenberg, P.; Luthman, K.; Artursson, P. Polar molecular surface properties predict the intestinal absorption of drugs in humans. *Pharmaceutical Research* **1997**, *14*, 568-571.

6. References

186. Ertl, P.; Rohde, B.; Selzer, P. Fast calculation of molecular polar surface area as a sum of fragment-based contributions and its application to the prediction of drug transport properties. *Journal of Medicinal Chemistry* **2000**, *43*, 3714-3717.
187. Varma, M. V. S.; Feng, B.; Obach, R. S.; Troutman, M. D.; Chupka, J.; Miller, H. R.; El-Kattan, A. Physicochemical Determinants of Human Renal Clearance. *Journal of Medicinal Chemistry* **2009**, *52*, 4844-4852.
188. Rautio, J.; Kumpulainen, H.; Heimbach, T.; Oliyai, R.; Oh, D.; Jarvinen, T.; Savolainen, J. Prodrugs: design and clinical applications. *Nature Reviews Drug Discovery* **2008**, *7*, 255-270.
189. Lima, M. L.; Barreiro, E. J. Bioisosterism: A Useful Strategy for Molecular Modification and Drug Design. *Current Medicinal Chemistry* **2005**, *12*, 23-49.
190. Taylor, N. R.; Vonitzstein, M. MOLECULAR MODELING STUDIES ON LIGAND-BINDING TO SIALIDASE FROM INFLUENZA-VIRUS AND THE MECHANISM OF CATALYSIS. *Journal of Medicinal Chemistry* **1994**, *37*, 616-624.
191. He, G.; Massarella, J.; Ward, P. Clinical pharmacokinetics of the prodrug oseltamivir and its active metabolite Ro 64-0802. *Clinical Pharmacokinetics* **1999**, *37*, 471-484.
192. Inui, K.; Terada, T.; Masuda, S.; Saito, H. Physiological and pharmacological implications of peptide transporters, PEPT1 and PEPT2. *Nephrology Dialysis Transplantation* **2000**, *15*, 11-13.
193. Bailey, P. D.; Boyd, C. A. R.; Collier, I. D.; George, J. P.; Kellett, G. L.; Meredith, D.; Morgan, K. M.; Pettecrew, R.; Price, R. A. Affinity prediction for substrates of the peptide transporter PepT1. *Chemical Communications* **2006**, 323-325.
194. Shitara, Y.; Horie, T.; Sugiyama, Y. Transporters as a determinant of drug clearance and tissue distribution. *European Journal of Pharmaceutical Sciences* **2006**, *27*, 425-446.
195. Holodniy, M.; Penzak, S. R.; Straight, T. M.; Davey, R. T.; Lee, K. K.; Goetz, M. B.; Raisch, D. W.; Cunningham, F.; Lin, E. T.; Olivo, N.; Deyton, L. R. Pharmacokinetics and tolerability of oseltamivir combined with probenecid. *Antimicrobial Agents and Chemotherapy* **2008**, *52*, 3013-3021.
196. Ames, B. N.; Durston, W. E.; Yamasaki, E.; Lee, F. D. CARCINOGENS ARE MUTAGENS - SIMPLE TEST SYSTEM COMBINING LIVER HOMOGENATES FOR ACTIVATION AND BACTERIA FOR DETECTION. *Proceedings of the National Academy of Sciences of the United States of America* **1973**, *70*, 2281-2285.